Redox Sensor and Effector Functions of Tetrahydrobiopterin and the Mitochondria in Molecular Models of Cardiovascular Disease

Jade Bailey

Division of Cardiovascular Medicine,
Radcliffe Department of Medicine
&
Jesus College



A thesis submitted for the degree of Doctor of Philosophy in Cardiovascular Science

University of Oxford

Trinity Term 2018

Abstract

Redox Sensor and Effector Functions of Tetrahydrobiopterin and the Mitochondria in Molecular Models of Cardiovascular Disease

Jade Bailey

Jesus College, University of Oxford

Submitted for the degree of D.Phil in Cardiovascular Science

Trinity Term 2018

Tetrahydrobiopterin (BH_4) is a redox active molecule that is essential for the production of nitric oxide (NO) by the NO synthase (NOS) enzymes. Loss of endothelial BH_4 leads to decreased NO and increased superoxide generation by endothelial NOS (eNOS) uncoupling, and the resulting endothelial dysfunction is involved in the pathogenesis of vascular diseases. Although genetic augmentation of endothelial BH_4 synthesis has proven successful at normalising dysfunction in murine studies, clinical trials of BH_4 supplementation have been limited by systemic oxidation. This highlights the need to explore the wider roles of BH_4 signalling to allow alternate therapeutic approaches. Thus the aims of this thesis were to identify novel pathways modulated by BH_4, both independent from and via NO signalling.

Our laboratory has previously reported a major NOS-independent but unidentified source of superoxide in BH_4-deficient endothelial cells. In this thesis, RNA interference targeting *Gch1* was used to knock down synthesis of the BH_4 synthetic enzyme, GTPCH, to deplete murine endothelial cells of BH_4. This model was used to reveal that mitochondria were the main site of superoxide generation in BH_4-deficient cells, and that this occurred independent from the NOS cofactor function of BH_4. Due to the localised nature of ROS signalling, the effects of BH_4 depletion on mitochondrial structure and function were subsequently investigated. BH_4-deficient endothelial cells contained larger mitochondria, elevated succinate and decreased isocitrate accumulations indicating altered tricarboxylic acid (TCA) cycle metabolism. Overall, this study shows that targeting mitochondrial superoxide generated by BH_4-deficient endothelium may present a potential therapeutic target.

In addition, inflammatory macrophages synthesise BH_4 and NO (by iNOS) to fight pathogens, however these cells are also implicated in the development of atherosclerosis. Inflammatory polarisation of macrophages involves dramatic metabolic remodelling, including NO-dependent repression of respiration, up-regulation of glycolysis and accumulation of specific TCA cycle metabolites. These changes support cytokine production and the pro-inflammatory phenotype, but mechanisms regulating this metabolic remodelling are still being elucidated and the roles of BH_4 and NO beyond modulation of respiration are unknown. In this thesis, whole cell proteomic and metabolomic analyses were carried out on inflammatory *Gch1* knockout (KO) bone marrow derived macrophages from $Gch^{fl/fl}$Tie2cre mice. This revealed that BH_4 modulated aspects of mitochondrial and metabolic pathways in inflammatory macrophages, and $Nos2^{-/-}$ (iNOS KO) macrophages were used to investigate whether changes occurred due to loss of NO signalling. BH_4 was shown to modulate the abundance of subunits making up the catalytic N-module of Complex I, HIF1α-mediated glycolytic remodelling and levels of key inflammatory mediators and TCA cycle metabolites: succinate, citrate and itaconate, via NO signalling. This study shows that NO-signalling directs critical aspects of immuno-metabolism in macrophages.

Table of Contents

List of Figures *9*

List of Tables *11*

List of Abbreviations *12*

Chapter 1. Introduction *16*

1.1 NO-redox balance in vascular disease *16*

1.1.1 Cardiovascular disease **16**

1.1.2 The endothelium and macrophages in vascular disease **16**

1.1.2.1 Endothelial dysfunction 16

1.1.2.2 Macrophage polarisation in disease 17

1.1.2.3 The endothelium and macrophages in atherogenesis 19

1.1.3 NO-redox signalling and homeostasis **21**

1.1.3.1 ROS signalling 22

1.1.3.2 RNS signalling 23

1.1.3.3 Therapeutically targeting NO-redox imbalance in vascular disease 25

1.2 NO and ROS signalling in mitochondria and metabolism *27*

1.2.1 Mitochondria and metabolism **27**

1.2.1.1 Oxidative phosphorylation 30

1.2.2 Mitochondrial ROS generation **31**

1.2.2.1 Therapeutically targeting mitochondrial ROS 32

1.2.3 Regulation of mitochondrial function and metabolism by NO **33**

1.2.3.1 Mitochondrial respiration 33

1.2.3.2 Mitochondrial morphology 33

1.2.3.3 Metabolic pathways 34

1.2.4 Endothelial mitochondria and metabolism **35**

1.2.4.1 Endothelial mitochondrial ROS in vascular disease 35

1.2.5 Macrophage metabolic remodelling in inflammation **36**

1.3 Nitric oxide synthase enzymes *38*

1.3.1 NOS isoforms **38**

1.3.2 NOS catalysis **39**

1.3.3 Endothelial NOS in vascular disease **40**

1.3.3.1 Superoxide generation by uncoupled eNOS 41

1.3.4 Inducible NOS in macrophages **42**

1.3.4.1 iNOS in human vs murine macrophages 43

1.3.4.2 Superoxide generation by iNOS 44
1.3.5 Mitochondrial NOS 45
1.4 Tetrahydrobiopterin 45
1.4.1 An essential enzyme cofactor 45
1.4.2 Synthesis of tetrahydrobiopterin 46
1.4.3 BH_4 oxidation, recycling, and the salvage pathway 47
1.4.4 BH_4 in the mitochondria 49
1.4.5 BH_4 deficiency in disease 50
1.4.6 Therapeutically augmenting BH_4 levels 51
1.4.7 Evidence of non-cofactor roles for BH_4 52
1.5 Hypotheses and aims 53
1.5.1 Hypothesis 53
1.5.2 Aims 53
Chapter 2: Materials and methods 55
2.1 Cell culture 55
2.1.1 Culture conditions 55
2.1.2 Cell lines 55
2.1.2.1 sEnd.1 cells 55
2.1.2.2 TET and GCH cells 55
2.1.2.3 Maintenance of cell lines 56
2.1.3 Primary cells 56
2.1.3.1 Bone marrow derived macrophages 56
2.2 Animals 57
2.2.1 Housing and diet 57
2.2.2 Generation of $Gch^{fl/fl}$Tie2cre mice 57
2.2.3 iNOS KO mice 58
2.3 DNA techniques 58
2.3.1 DNA extraction from cell pellets 58
2.3.2 DNA extraction from ear notches 58
2.3.3 Genotyping PCR 58
2.3.3.1 $Gch^{fl/fl}$Tie2cre mice 60
2.3.3.2 iNOS KO mice 61
2.3.4 Gel electrophoresis 62
2.4 RNA techniques 62

2.4.1 RNA extraction and quantification **63**
2.4.2 Generation of cDNA by RT-PCR **63**
2.4.3 qRT-PCR primers **64**
2.4.4 Quantitative real-time RT-PCR **64**
2.5 Protein detection ***65***
2.5.1 Preparation of protein lysates **65**
2.5.2 Measuring protein content **66**
2.5.3 Western blotting **66**
2.6 Biopterin quantification by HPLC ***69***
2.7 Quantification of superoxide by HPLC ***70***
2.8 Measurement of NO_x accumulation using the NO analyser ***71***
2.9 Measurement of nitrite accumulation using the NO analyser ***71***
2.10 Measurement of nitrite accumulation using the Griess assay ***71***
2.11 NOS activity assay ***72***
2.12 Seahorse XF^e96 extracellular flux assays ***73***
2.12.1 Preparation for Seahorse extracellular flux assays **73**
2.12.2 Seahorse MitoStress Test to analyse mitochondrial respiration **73**
2.12.2.3 Seahorse MitoStress Test calculations 75
2.12.3 Glycolytic activity using ECAR **77**
2.13 Mitochondrial isolation ***77***
2.13.1 Qproteome kit isolation **77**
2.13.2 Frezza et al. isolation **78**
2.13.3 Comparison of methods **78**
2.13.4 Yield of isolated mitochondria **79**
2.14 Statistical Analysis ***81***
2.15 Acknowledgement of collaborations ***81***
Chapter 3: Investigating the effects of BH_4 deficiency on mitochondrial function and redox signalling in endothelial cells ***84***
3.1 Introduction ***84***
3.2 Aims and hypotheses ***86***
3.2.1 Hypotheses **86**
3.2.1 Aims **86**
3.3 Methods ***87***
3.3.1 Gch1 targeted RNA interference **87**

3.3.2 Superoxide measurements using DHE **88**
3.3.3 Imaging ROS production **90**
3.3.4 Transmission electron microscopy and mitochondrial measurements **90**
3.3.5 Mitochondrial DNA content **92**
3.3.6 Seahorse XF^{e}96 analysis **93**
3.3.7 Metabolomics **94**
3.4 Results ***96***
3.4.1 Characterisation of Gch1 knock down induced BH_4 deficiency in sEnd.1 cells **96**
3.4.2 Characterisation of doxycycline induced BH_4 deficiency in 3T3 fibroblasts stably transfected with tet-off GCH1 ..... **98**
3.4.3 Elevated mitochondrial superoxide generation in BH_4-deficient cells **100**
3.4.4 Mitochondrial biopterins are depleted in BH_4-deficient cells **104**
3.4.5 Decreased phosphorylation of DRP1 at serine 616 leads to enlarged mitochondria in BH_4-deficient cells **108**
3.4.6 Mitochondrial respiratory function remains unaffected by BH_4 depletion **111**
3.4.7 BH_4 depletion increases the OCR:ECAR ratio **112**
3.4.8 BH_4 deficiency leads to changes in glycolytic and TCA cycle metabolites **114**
3.5 Discussion ***117***
3.5.1 Overview **117**
3.5.2 BH_4 as a regulator of mitochondrial redox state **117**
3.5.3 How does BH_4 enter mitochondria? **119**
3.5.4 BH_4 and NO signalling regulate mitochondrial fission **119**
3.5.5 BH_4 and mitochondrial respiratory function **120**
3.5.6 BH_4 modulates the TCA cycle and glycolysis **121**
3.5.7 Mitochondria as a therapeutic target in BH_4-deficient endothelium **123**
3.5.8 Conclusions **124**
Chapter 4: Optimising culture of bone marrow derived macrophages ***126***
4.1 Introduction ***126***
4.1.1 Macrophage heterogeneity and polarisation **126**
4.1.2 Studying macrophage function in vitro **127**
4.2 Aims and hypotheses ***128***
4.3 Methods ***129***
4.3.1 Bone marrow extraction **129**
4.3.2 Established protocol for growing bone marrow derived macrophages **129**
4.3.3 Optimised protocol for growing bone marrow derived macrophages **130**

4.3.4 Imaging of cells **131**

4.3.5 FACS **132**

4.3.6 Cytokine array **132**

4.4 Results ***133***

4.4.1 Characterising Gch$^{fl/fl}$Tie2cre bone marrow derived macrophages grown using the established protocol **133**

4.4.2 Macrophages grown in very low serum media overnight are unhealthy **135**

4.4.3 FBS and L-cell conditioned media contain BH_4 and BH_2 ..... **137**

4.4.4 Optimising BMDM cell culture in low biopterin conditions **141**

4.4.5 Treating macrophages with GMCSF leads to increased LPS/IFNγ induced production of NO **144**

4.4.6 Characterising macrophages grown in MCSF media and treated with GMCSF **149**

4.4.7 Defining the composition of cytokines in L-cell conditioned media **152**

4.4.8 Characterising Gch$^{fl/fl}$Tie2cre BMDMs grown in MCSF media and treated with GMCSF **153**

4.4.9 Characterising iNOS$^{-/-}$ BMDMs grown in MCSF media and treated with GMCSF **155**

4.5 Discussion ***157***

4.5.1 Overview **157**

4.5.2 Serum starvation and cell culture **157**

4.5.3 Replacing L-cell conditioned media with recombinant MCSF **159**

4.5.4 MCSF and GMCSF in BMDM culture **160**

4.5.5 Measurement of cytokines in GMCSF treated BMDMs **160**

4.5.6 GMCSF treatment increases NO production in stimulated BMDMs **161**

4.5.7 Advantages and disadvantages of the new BMDM cell culture protocol **162**

4.5.8 Conclusions **163**

Chapter 5: Investigating the role of BH_4 in mitochondrial function and metabolism in inflammatory macrophages ***165***

5.1 Introduction ***165***

5.2 Aims and hypotheses ***167***

5.2.1 Hypotheses **167**

5.2.2 Aims **167**

5.3 Methods ***168***

5.3.1 ROS measurements using DHE and HPLC with UV detection **168**

5.3.2 Hydrogen peroxide measurements **173**

5.3.3 Proteomics **173**

5.3.3.1 Protein extraction and digestion 173
5.3.3.2 Tandem Mass Tag (TMT)-labelling of peptides 174
5.3.3.3 Mass spectrometric analysis of proteins 174
5.3.3.4 Proteomic data analysis 176
5.3.4 Cytokine measurements by ELISA 177
5.3.5 Metabolomics 178
5.3.5.1 Sample Preparation 178
5.3.5.2 Ultrahigh-Performance Liquid Chromatography-Tandem Mass Spectroscopy (UPLC-MS/MS) 178
5.3.5.3 Bioinformatics: 179
5.3.6 Complex I activity assay 180
5.3.7 Seahorse extracellular flux assays 181
5.3.7.1 MitoStress test 181
5.3.7.2 Glycolysis rate assay 181
5.3.8 Isocitrate dehydrogenase activity assay 182
5.3.9 Aconitase activity assay 183
5.4 Results 184
5.4.1 Characterisation of Gch$^{fl/fl}$Tie2cre and iNOS KO BMDMs 184
5.4.2 Measuring ROS produced by BMDMs 186
5.4.3 Proteomic analysis of Gch$^{fl/fl}$Tie2cre macrophages 191
5.4.3.1 Proteomic analysis reveals BH_4-mediated modulation of glycolysis, macrophage activation, DNA binding and protein folding in unstimulated macrophages 196
5.4.3.2 Proteomic analysis reveals BH_4-mediated modulation of inflammation, mitochondrial function, and metabolism in stimulated macrophages 199
5.4.4 IL-1β secretion is elevated due to loss of NO signalling 202
5.4.5 NO regulates levels of Complex I subunits and function 204
5.4.6 NO regulates mitochondrial respiration 206
5.4.7 Metabolomic analysis of Gch$^{fl/fl}$Tie2cre and iNOS KO macrophages 209
5.4.8 NO modulates HIF1α-mediated regulation of glycolysis 214
5.4.9 NO regulates levels of critical TCA cycle metabolites 221
5.5 Discussion 228
5.5.1 Overview 228
5.5.2 BH_4-deficient macrophages produce less ROS? 228
5.5.3 NO regulates oxidative phosphorylation and the abundance of Complex I subunits 230
5.5.4 NO regulates glycolytic remodelling 232

5.5.5 NO regulates levels of TCA cycle metabolites 234
5.5.6 NO limits production of IL-1β 235
5.5.7 NOS-independent role for BH_4 in macrophages 236
Chapter 6: Final Discussion 239
6.1 Original hypotheses and aims 239
6.2 Key findings and future directions 239
6.2.1 Investigating the role of BH_4 in different cell types 241
6.2.2 Future studies into the role of BH_4 in endothelial cells 242
6.2.3 Future studies into the role of BH_4 and NO in macrophages 243
References 248
Appendices 279
Timing and Venue of Research 279
Research Funding 279
Other Publications 280
Presentations at International Meetings 280
Acknowledgements 281

List of Figures

Figure 1.1 The endothelium and macrophages in the initial stages of atherogenesis 21
Figure 1.2 The glycolysis pathway 28
Figure 1.3 The tricarboxylic acid cycle 29
Figure 1.4 Oxidative phosphorylation 31
Figure 1.5 eNOS catalysis and uncoupling 40
Figure 1.6 BH_4 synthesis 48
Figure 2.1 Genotyping $Gch^{fl/fl}$Tie2cre and iNOS KO mice 59
Figure 2.2 Representative MitoStress test trace and calculated parameters 76
Figure 2.2 Comparison of mitochondria isolation protocols 80
Figure 3.1 Dose response of rotenone inhibitable superoxide 89
Figure 3.2 Analysis of mitochondria in electron micrographs 91
Figure 3.3 Optimisation of cell density for analysis of OCR in sEnd.1 cells 94
Figure 3.4 *Gch1* siRNA diminished GTPCH, biopterins and NOS activity in sEnd.1 cells 97
Figure 3.5 Doxycycline decreased GTPCH and biopterins in 3T3 fibroblasts stably transfected with TET off GCH1 plasmids 99
Figure 3.6 BH_4 depletion leads to increased mitochondrial superoxide generation 102
Figure 3.7 Mitochondrial localisation of elevated superoxide in BH_4 deficient endothelial cells 103
Figure 3.8 Mitochondria contained BH_4 and a greater proportion was oxidised in this fraction than in whole cell preparations 105
Figure 3.9 Artefactual oxidation of biopterins during mitochondrial isolation 106
Figure 3.10 Mitochondrial biopterins were decreased in *Gch1* knock down sEnd.1 cells 107
Figure 3.11 Mitochondria were larger in BH_4-deficient cells 109
Figure 3.12 Phosphorylation of DRP1 at serine 616 was decreased in BH_4-deficient cells 110
Figure 3.13 Mitochondria respiratory function was unaffected by BH_4 deficiency 111
Figure 3.14 OCR:ECAR increased in BH_4 deficient cells 113
Figure 3.15 Metabolomics revealed BH_4-dependent changes in glycolysis and TCA cycle metabolites 114
Figure 3.16 Glycolytic intermediate fructose-1,6-bisphosphate was elevated in BH_4-deficient cells 115
Figure 3.17 TCA cycle intermediate succinate was elevated and isocitrate was decreased in BH_4-deficient cells 116
Figure 4.1 Established laboratory protocol for BMDM culture in L-cell conditioned media 130
Figure 4.2 Optimised protocol for growing BMDMs in recombinant MCSF and GMCSF 131
Figure 4.3 Characterisation of $Gch^{fl/fl}$Tie2cre BMDMs grown in media containing L-cell conditioned media 134
Figure 4.4 Macrophages grown in very low serum media overnight detach 136
Figure 4.5 $Gch^{fl/fl}$Tie2cre macrophages stimulated with LPS/IFNγ in DMEM F12 media containing 10% FBS produce NO 139
Figure 4.6 FBS and L-cell conditioned media contain substantial amounts of biopterins 140
Figure 4.7 Bone marrow derived macrophages can be cultured in 5% FBS 141
Figure 4.8 Protocol for culturing bone marrow derived macrophages using recombinant MCSF and low FBS concentrations 143
Figure 4.9 Protocols designed to compare LCM, MCSF and MCSF+GMCSF culture of bone marrow derived macrophages 146

Figure 4.10 Macrophages cultured in MCSF and primed with GMCSF produce more nitric oxide upon stimulation with LPS/IFNγ 147
Figure 4.11 Biopterin measurements in macrophages cultured in LCM, MCSF and MCSF+GMCSF media 148
Figure 4.12 Characterisation of bone marrow derived macrophage markers on Day 7 of culture 150
Figure 4.13 Measurement of cytokines secreted by LPS/IFNγ stimulated macrophages grown in LCM, MCSF and MCSF+GMCSF media 151
Figure 4.14 Measurement of cytokines in L-cell conditioned media 152
Figure 4.15 Characterisation of $Gch^{fl/fl}$Tie2cre bone marrow derived macrophages grown in media containing recombinant MCSF and primed with GMCSF 154
Figure 4.16 Characterisation of iNOS knock out bone marrow derived macrophages grown in media containing recombinant MCSF and primed with GMCSF 156
Figure 5.1 Detection of DHE using HPLC and a UV detector set to various wavelengths 170
Figure 5.2 Detection of DHE in sEnd.1 cells using a UV detector set to 245 and 350 nm 171
Figure 5.3 DHE standard curve and oxidation by potassium superoxide 172
Figure 5.4 Characterisation of $Gch^{fl/fl}$Tie2cre and iNOS KO BMDMs 185
Figure 5.5 ROS measurements in $Gch^{fl/fl}$Tie2cre macrophages using DHE 188
Figure 5.6 ROS measurements in iNOS KO macrophages using DHE 189
Figure 5.7 H_2O_2 secreted from $Gch^{fl/fl}$Tie2cre and iNOS KO macrophages 190
Figure 5.8 GTPCH and iNOS protein abundance 192
Figure 5.9 Scaled abundance of selected proteins with the greatest fold change between $Gch^{fl/fl}$Tie2cre and $Gch^{fl/fl}$ macrophages 195
Figure 5.10 Enrichment analysis of proteins elevated in unstimulated $Gch^{fl/fl}$Tie2cre macrophages 197
Figure 5.11 Enrichment analysis of proteins decreased in unstimulated $Gch^{fl/fl}$Tie2cre macrophages 198
Figure 5.12 Enrichment analysis of proteins elevated in $Gch^{fl/fl}$Tie2cre macrophages stimulated with LPS/IFNγ 200
Figure 5.13 Enrichment analysis of proteins decreased in $Gch^{fl/fl}$Tie2cre macrophages stimulated with LPS/IFNγ 201
Figure 5.14 Cytokine measurements in $Gch^{fl/fl}$Tie2cre and iNOS KO macrophages 203
Figure 5.15 NO-dependent regulation of Complex I N-module subunits and activity 205
Figure 5.16 BH_4-dependent inhibition of mitochondrial respiration 207
Figure 5.17 NO-dependent inhibition of mitochondrial respiration 208
Figure 5.18 Metabolomics analysis of $Gch^{fl/fl}$Tie2cre macrophages 211
Figure 5.19 Metabolomics analysis of iNOS KO macrophages 212
Figure 5.20 Abundance of metabolites involved in arginine and biopterin metabolism 213
Figure 5.21 BH_4 and NO modulate levels of glycolytic proteins and metabolites 217
Figure 5.22 Abundance of glycerol-3-phosphate 218
Figure 5.23 Glycolytic rate is unaffected by loss of BH_4 and NO 219
Figure 5.24 NO-signalling disrupts HIF1α mediated up-regulation of proteins 220
Figure 5.25 NO modulates levels of TCA cycle metabolites 223
Figure 5.26 NO modulates itaconate production 224
Figure 5.27 NO modulates IDH activity in macrophages stimulated with LPS/IFNγ 225
Figure 5.28 Abundance of TCA cycle enzymes in $Gch^{fl/fl}$Tie2cre macrophages 226
Figure 5.29 Aconitase activity is decreased in LPS/IFNγ stimulated macrophages 227

List of Tables

Table 2.1 Thermocycler settings for *Gch1* genotyping PCR....60
Table 2.2 Thermocycler settings for Tie2cre genotyping PCR....61
Table 2.3 Thermocycler settings for iNOS KO genotyping PCR....62
Table 2.4 Details of TaqMan assays used in qRT-PCR reactions....64
Table 2.5 Thermocycler settings for qRT-PCR....65
Table 2.6 Antibodies used for Western blot analysis of proteins....68
Table 2.7 Settings used to carryout Seahorse XF^{e}96 MitoStress Test....74
Table 2.8 Calculations to determine respiratory function....76
Table 3.1 Composition of Solutions A and B for transfection of sEnd.1 cells with siRNA88
Table 3.2 Thermocycler settings for real-time PCR quantifying nDNA and mtDNA....93
Table 5.1 Mass spectrometry settings used for proteomic analysis....175
Table 5.2 The 20 significantly altered proteins with the greatest fold change between unstimulated Gch$^{fl/fl}$Tie2cre versus Gch$^{fl/fl}$ macrophages measured using mass spectrometry....193
Table 5.3 The 20 significantly altered proteins with the greatest fold change between LPS/IFNγ stimulated Gch$^{fl/fl}$Tie2cre versus Gch$^{fl/fl}$ macrophages measured using mass spectrometry....194
Table 5.4 Number of proteins significantly changed in abundance between Gch$^{fl/fl}$Tie2cre and Gch$^{fl/fl}$ macrophages as determined by mass spectrometric analysis....196
Table 5.5 Number of metabolites significantly changed in abundance between Gch$^{fl/fl}$Tie2cre and Gch$^{fl/fl}$, and LPS/IFNγ and Unstimulated macrophages as determined by mass spectrometric analysis....210
Table 5.6 Number of proteins significantly changed in abundance between iNOS KO and WT, and LPS/IFNγ and Unstimulated macrophages as determined by mass spectrometric analysis....210
Table 5.7 Glycolytic and glycogen metabolising proteins encoded by genes transcriptionally regulated by HIF1α....216

List of Abbreviations

2-OHE	2-Hydroxyethidium
AAH	Amino acid hydroxylase
ADP	Adenine diphosphate
AGMO	Alkylglycerol mono-oxygenase
ANOVA	Analysis of variance
ApoE	Apolipoprotein E
ATP	Adenosine triphosphate
AU	Arbitrary units
BCA	Bicinchoninic acid
BH_4	Tetrahydrobiopterin
BH_2	7,8-dihydrobiopterin
BMDM	Bone marrow derived macrophage
BSA	Bovine serum albumin
cGMP	Cyclic guanosine monophosphate
Complex I	NADH dehydrogenase
Complex II	Succinate dehydrogenase
Complex III	Cytochrome b-c_1 complex
Complex IV	Cytochrome C oxidase
CoQ	Coenzyme Q
DDM	n-Dodecyl-β-maltoside
DHE	Dihydroethidium
DHFR	Dihydrofolate reductase
DHPR	Dihydropteridine reductase
DMEM	Dulbecco's modified eagle medium
DMSO	Dimethyl sulfoxide
DNTP	Dihydroneopterin triphosphate
DRP1	Dynamin related protein 1
DTE	Dithioerythritol
ECAR	Extracellular acidification rate
ECL	Enhanced chemiluminescence
ELISA	Enzyme-linked immunosorbent assay
eNOS	Endothelial nitric oxide synthase
ESI	Electron spray ionisation
ETC	Electron transport chain
FA	Formic acid
FACS	Fluorescence-activated cell sorting
$FADH_2$	Reduced flavin adenine dinucleotide
FBS	Foetal bovine serum
FCCP	Carbonyl cyanide-p-trifluoromethoxyphenylhydrazone
[Fe-S]	Iron-sulfur center
FMN	Flavin mononucleotide
GAPDH	Glyceraldehyde 3-phosphate dehydrogenase
GFRP	Guanosine triphosphate cyclohydrolase feedback regulatory protein
GLUT-1	Solute carrier family 2, facilitated glucose transporter member 1
GMCSF	Granulocyte-macrophage colony stimulating factor
glycoPER	Proton efflux rate attributes to glycolysis
GO term	Gene ontology term
GTP	Guanosine triphosphate
GTPCH	Guanosine triphosphate cyclohydrolase

HIF1α	Hypoxia-inducible factor 1-alpha
HILIC	Hydrophilic interaction liquid chromatography
HPLC	High performance liquid chromatography
HRP	Horseradish peroxidase
ICAM-1	Intracellular adhesion molecule-1
IDH	Isocitrate dehydrogenase
IFN	Interferon
IL	Interleukin
iNOS	Inducible nitric oxide synthase
KEAP1	Kelch-like ECH-associated protein 1
KO	Knockout
LCM	L929-cell conditioned media
LDL	Low-density lipoprotein
L-NAME	N(G)-Nitro-L-arginine methyl ester
LPS	Lipopolysaccharide
MCSF	Macrophage colony stimulating factor
MI	Myocardial infarction
mitoPER	Proton efflux rate attributed to mitochondrial acidification
MitoQ	Mitochondria-targeted coenzyme Q
$M^{(LPS/IFN\gamma)}$	Macrophages stimulated with lipopolysaccharide and interferon-γ
mnSOD	Manganese superoxide dismutase
MPC	Mitochondrial pyruvate carrier protein
MS/MS	Tandem mass spectrometry
mtDNA	Mitochondrial deoxyribonucleic acid
NAD^+	Oxidised nicotinamide adenine dinucleotide
NADH	Reduced nicotinamide adenine dinucleotide
$NADP^+$	Oxidised nicotinamide adenine dinucleotide phosphate
NADPH	Reduced nicotinamide adenine dinucleotide phosphate
nDNA	Nuclear deoxyribonucleic acid
NF-κB	Nuclear factor kappa-B
nNOS	Neuronal nitric oxide synthase
NO	Nitric oxide
NOS	Nitric oxide synthase
NOX	Nicotinamide adenine dinucleotide phosphate oxidase
NRF2	Nuclear factor erythroid 2-related factor 2
OCR	Oxygen consumption rate
OD	Optical density
OPA1	Optic atrophy protein 1
oxLDL	Oxidised LDL
PBS	Phosphate buffered saline
PCD	Pterin-4a-carbinolamine
PCR	Polymerase chain reaction
PER	Proton efflux rate
PFA	Paraformaldehyde
PFK1	6-phosphofructokinase
PFK2	6-phosphofructo-2-kinase
PFKFB3	6-phosphofructo-2-kinase/fructose-2,6-biphosphatase 3
PPP	Pentose phosphate pathway
PTM	Post-translational modification
PTPS	6-pyruvoly tetrahydropterin synthase
qBH_2	Quinoid dihydrobiopterin

qRT-PCR	Quantitative real time reverse transcriptase-polymerase chain reaction
RET	Reverse electron transport
RNAi	Ribonucleic acid interference
RNS	Reactive nitrogen species
ROS	Reactive oxygen species
RT-PCR	Reverse transcriptase-polymerase chain reaction
SD	Standard deviation
SDH	Succinate dehydrogenase
SDS-PAGE	Sodium dodecyl sulphate-polyacrylamide gel electrophoresis
SEM	Standard error of the mean
siRNA	Small interfering ribonucleic acid
SOD	Superoxide dismutase
SR	Sepiapterin reductase
TCA	Tricarboxylic acid
TFA	Trifluoroacetic acid
TIMP1	Tissue inhibitor of metalloproteinases-1
TLR	Toll-like receptor
TMT	Tandem mass tag
TNF	Tumour necrosis factor
TPP^+	Triphenylphosphonium cation
TRE	Tetracycline-response element
UPLC	Ultra-high performance liquid chromatography
UV	Ultra violet
VCAM-1	Vascular adhesion molecule-1
VDAC	Voltage-dependent anion channel
VLCAD	Very long-chain acyl CoA dehydrogenase
WT	Wild-type

Chapter 1:
Introduction

Chapter 1. Introduction

1.1 NO-redox balance in vascular disease

1.1.1 Cardiovascular disease

Cardiovascular disease is a leading cause of mortality worldwide and accounts for 25% of total deaths in the United Kingdom (UK) (BHF fact sheet November 2018). Over recent decades, advances in our understanding of the risk factors, causes, and mechanisms leading to heart and circulatory diseases have improved the treatment and prognosis of patients. Around 7 million people are living with cardiovascular pathologies in the UK alone and furthering our knowledge of these diseases will lead to more targeted therapies, improvements in the quality of life, and increased survival rates in a growing and increasingly aging population.

1.1.2 The endothelium and macrophages in vascular disease

The risk of experiencing a potentially fatal cardiovascular event, such as a myocardial infarction (MI) or stroke, is greatly elevated in people with vascular diseases, including coronary artery disease, hypertension, and atherosclerosis. Endothelial dysfunction is a hallmark of vascular pathologies and leads to the development of atherosclerotic plaques in blood vessel walls following leukocyte and lipid infiltration. Plaque rupture promotes thrombus formation, which may occlude coronary or cerebral arteries leading to an MI or stroke.

1.1.2.1 Endothelial dysfunction

Endothelial cells form a monolayer lining blood vessels throughout the body, facilitating smooth blood flow and acting as a barrier between blood in the vessel lumen and the surrounding tissues. This semi permeable barrier allows diffusion of ions and gases,

regulates permeability to larger macromolecules and immune cells, and modulates vasodilation, making the endothelium vital for the maintenance of vascular homeostasis.

The importance of the endothelium in regulating vasomotor function was highlighted by Furchgott and Zawadski in experiments demonstrating impaired vasorelaxation in denuded vessels (Furchgott and Zawadzki, 1980). These studies led to the discovery of nitric oxide (NO) as the 'endothelial derived relaxing factor'(Ignarro et al., 1987; Palmer et al., 1987) and its production by an endothelial isoform of NO synthase (eNOS) (Janssens et al., 1992). eNOS derived NO diffuses into vascular smooth muscle cells, causing their relaxation by stimulating guanylate cyclase to increase cyclic guanosine monophosphate (cGMP) levels (Rapoport et al., 1983). In addition, endothelial NO maintains vascular health by inhibiting smooth muscle cell proliferation (Garg and Hassid, 1989) and adhesion of platelets and monocytes to the endothelium (Khan et al., 1996; Radomski et al., 1987). Loss of NO is observed in endothelial dysfunction and causes vascular diseases, with impaired vasodilation causing hypertension (Huang et al., 1995) and increased monocyte adhesion and infiltration leading to atherogenesis (Cybulsky and Gimbrone, 1991). Elevated reactive oxygen species (ROS) generation also characterises endothelial dysfunction and oxidises atherogenic low-density lipoproteins (LDL), or damages cellular components (van Hinsbergh et al., 1986). Thus, mechanisms regulating NO and ROS levels determine vascular health and pathogenesis.

1.1.2.2 Macrophage polarisation in disease

Macrophages are leukocytes derived from myeloid haematopoietic progenitors (Sheng et al., 2015) and are a vital part of the immune system. Monocytes are recruited to sites of damage or infection by cytokines, where they mature into macrophages; alternatively tissue-resident macrophages, established during development, are maintained and self-renew throughout adult life (Hashimoto et al., 2013; Yona et al., 2013). Cell surface receptors allow

macrophages to recognise and respond to a range of stimuli including pathogens. As an integral part of the innate immune response to infections, pro-inflammatory macrophages phagocytose and eliminate pathogens, and produce a range of lipid mediators and cytokines to potentiate inflammation and recruit other leukocytes. They also activate the adaptive immune response by presenting antigens on major histocompatibility complex (MHC) molecules on the cell surface, where they are recognised by T cells. Furthermore, macrophages are involved in removing dead cells, the resolution of inflammation and tissue repair. Environmental cues stimulate remodelling of gene expression, protein synthesis, enzyme activity and metabolism to form macrophages with a spectrum of activation states adapted to particular functions.

Pro-inflammatory macrophages (also referred to as inflammatory, classically activated or M1) are induced by Toll-like receptor (TLR) ligands such as lipopolysaccharide (LPS), and cytokines that include interferon-γ (IFNγ) (Nathan et al., 1983). Inflammatory macrophages are characterised by enhanced ROS and NO generation – which combine to eliminate pathogens – and secrete inflammatory cytokines such as tumour necrosis factor-α (TNFα), interleukin-6 (IL-6) and IL-1β. In addition, striking metabolic remodelling through enhanced glycolysis, inhibited mitochondrial respiration and accumulation of specific metabolites, support macrophage inflammatory function and will be discussed in **Section 1.2.5**.

Macrophages are also activated by a range of non-inflammatory molecules that polarise their functions toward anti-inflammatory and reparative phenotypes. These cells are referred to as anti-inflammatory, alternatively activated or M2 macrophages and stimuli include IL-4, IL-13 and peroxisome proliferator-activated receptors (Odegaard et al., 2007; Stein et al., 1992). However, it is now appreciated that macrophages are present in a wide range of

activation states – outside of 'M1' and 'M2' categorisation – depending upon the combination of stimuli present (Xue et al., 2014).

In addition to their vital roles in the immune response to infection and injury, inflammatory macrophages are implicated in the pathogenesis of several diseases. Sepsis is potentially fatal and involves overproduction of NO and inflammatory cytokines, of which macrophages are likely to be major contributors (Bozza et al., 2007; MacMicking et al., 1995). Obesity induced inflammation and development of inflammatory macrophages contribute to insulin resistance (Nishimura et al., 2009; Xu et al., 2003) and the role of inflammatory macrophages in atherogenesis is well described (**Section 1.1.2.3**) (Quinn et al., 1987; Rahaman et al., 2006). On the other hand anti-inflammatory properties of tumour associated macrophages are suggested to support tumour development in a range of cancers (Kurahara et al., 2011; Shen et al., 2016). The idea of repolarising macrophages is an attractive therapeutic aim, and attempts to convert tumour associated macrophages towards pro-inflammatory phenotypes more effective at killing cancerous cells are underway (Guiducci et al., 2005). Furthermore, the possibility of repolarising inflammatory macrophages to improve atherosclerosis has been proposed (Khallou-Laschet et al., 2010) – although NO generating macrophages were recently reported to have more limited plasticity (Van den Bossche et al., 2016).

1.1.2.3 The endothelium and macrophages in atherogenesis

Atherosclerosis is the build-up of lipid, leukocyte, and smooth muscle cell rich plaques in the sub-endothelial intima of the artery wall. The first stages of atherogenesis are endothelial dysfunction (Celermajer et al., 1994) and retention of LDL beneath the endothelium (Skålén et al., 2002), where they are oxidised by ROS, including superoxide produced by the endothelium (van Hinsbergh et al., 1986) (Figure 1.1). In addition, increased expression of the adhesion receptors vascular adhesion molecule-1 (VCAM-1) and intercellular adhesion

molecule-1 (ICAM-1) on dysfunctional endothelium (Nakashima et al., 1998) leads to increased monocyte binding (Cybulsky and Gimbrone, 1991). Cytokines are produced in the intima in response to accumulated oxidised LDL (oxLDL) and signal sub-endothelial migration of monocytes and their differentiation into macrophages (Boring et al., 1998; Gu et al., 1998; Quinn et al., 1987). Scavenger receptors on the macrophages bind and internalise oxLDL (Endemann et al., 1993; Febbraio et al., 2000; Suzuki et al., 1997), leading to formation of cholesterol and lipid laden foam cells (Rahaman et al., 2006), which apoptose forming a highly inflammatory environment and the necrotic core of advanced plaques (Hegyi et al., 1996). Macrophages are also activated by scavenger receptors bound to oxLDL and subsequently produce inflammatory cytokines (Chávez-Sánchez et al., 2014). Macrophages activated to a pro-inflammatory state generate ROS through nicotinamide adenine dinucleotide phosphate (NADPH) oxidase (NOX) enzymes and NO through an inducible isoform of NOS (iNOS), and both have been detected in human atherosclerotic plaques (Buttery et al., 1996; Sorescu et al., 2002). Generation of ROS and NO by inflammatory macrophages were further implicated in atherogenesis upon observations of reduced atherosclerosis in apolipoprotein E (ApoE) knockout mice deficient in NOX2 or iNOS (Detmers et al., 2000; Judkins et al., 2010).

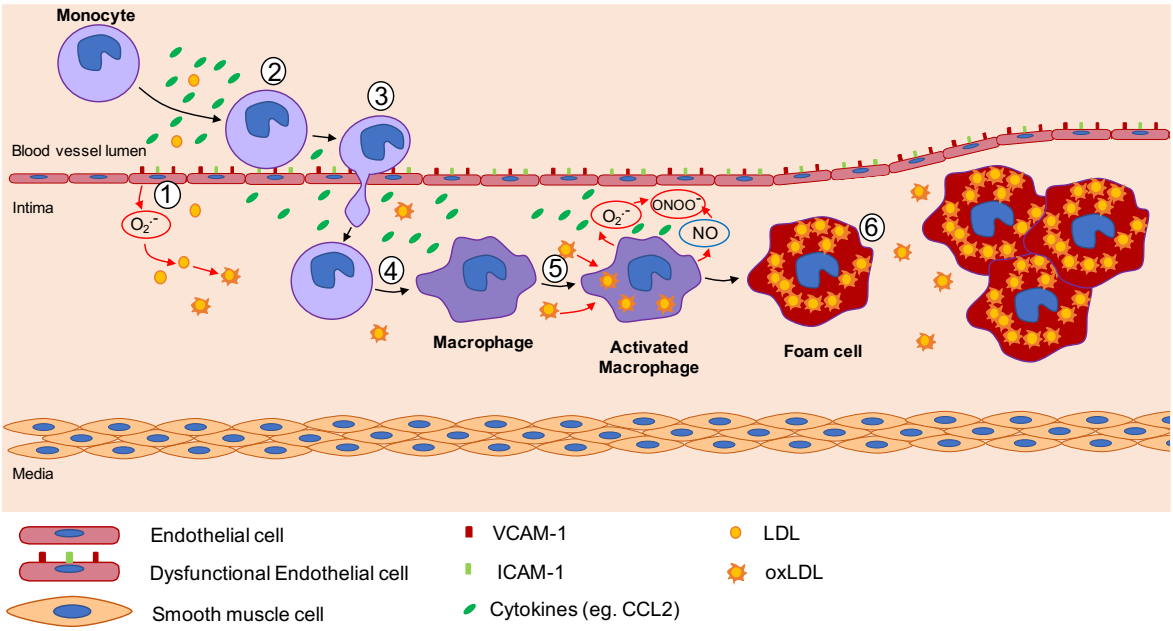


Figure 1.1 The endothelium and macrophages in the initial stages of atherogenesis

1. Dysfunctional endothelial cells display increased levels of the adhesion molecules VCAM-1 and ICAM-1 and produce increased superoxide ($O_2^{\cdot-}$) which oxidise LDL (to oxLDL) in the intima. 2. Production of cytokines attracts monocytes, which adhere to the endothelium. 3. Monocytes migrate into the intima. 4. Cytokines promote differentiation of monocytes into macrophages. 5. Macrophages phagocytose oxLDL and become activated. Activated macrophages produce superoxide and NO (which react to form peroxynitrite ($ONOO^-$)) as well as more cytokines to attract inflammatory cells. 6. Lipid laden macrophages become foam cells.

1.1.3 NO-redox signalling and homeostasis

The transfer of electrons between two molecules forms an oxidation-reduction ('redox') reaction, which is a highly conserved form of signalling in nature, whereby the electron acceptor is reduced and the electron donor is oxidised. Reactive oxygen (ROS) and nitrogen (RNS) species are key redox signalling mediators and, as discussed, perturbed levels produced by endothelial cells and macrophages are implicated in the pathogenesis of vascular disease as well as various other diseases including neurodegeneration and cancer. For these reasons, ROS/RNS levels are tightly controlled and production sites

compartmentalised, via highly regulated synthesis together with complex enzymatic and molecular antioxidant defence mechanisms.

1.1.3.1 ROS signalling

ROS are generated in response to various stimuli including cytokines and growth factors (Sundaresan et al., 1995; West et al., 2011). Superoxide ($O_2^{\cdot -}$) is a free radical anion and primary ROS formed from molecular dioxygen (O_2) by NADPH oxidase, xanthine oxidase, uncoupled NOS, and mitochondria. The unpaired electrons of free radicals leads to their highly reactive nature and superoxide reacts rapidly with other molecules. It dismutates to the more stable ROS molecule hydrogen peroxide (H_2O_2), either spontaneously or catalysed by superoxide dismutase (SOD) (McCord and Fridovich, 1969) :

$$O_2^{\cdot -} + O_2^{\cdot -} + 2H^+ \rightarrow H_2O_2 + O_2$$

Many enzymes contain iron-sulfur [Fe-S] centres and reaction of superoxide with these centres causes release of iron, which is then available to react with H_2O_2 to produce hydroxyl radicals ($^{\cdot}OH$) using Fenton chemistry (Liochev and Fridovich, 1994) :

$$Fe^{3+} + O_2^{\cdot -} \rightarrow Fe^{2+} + O_2$$

$$Fe^{2+} + H_2O_2 \rightarrow Fe^{3+} + {}^{\cdot}OH + OH^-$$

Superoxide, H_2O_2 and $^{\cdot}OH$ are major ROS signalling mediators, known to oxidise proteins, DNA and lipids. The capacity to irreversibly damage cellular components has led to the historic notion of ROS as harmful molecules that cause ‘oxidative stress’, and elevated levels have been linked with cardiovascular disease, neurodegeneration, cancers, and aging. However, it is now appreciated that ROS have physiological signalling roles, forming an important part of the immune response and oxygen sensing (Brunelle et al., 2005; West et al., 2011). Signals transmitted through reversible post-translational modification (PTM) of proteins at sulfur containing cysteine and methionine residues are the most well studied.

Cysteine thiols with low pKa values become deprotonated at cytosolic pH and the resulting thiolate anions ($R\text{-}S^-$) are readily oxidised to sulfenic acids (R-SOH) by ROS. These are prone to further oxidation to sulfinic ($R\text{-}SO_2H$) and sulfonic acids ($R\text{-}SO_3H$) or form intra and inter molecular disulfides, and are reversed by thiol containing antioxidants systems or sulfiredoxin (Biteau et al., 2003). PTMs lead to conformational changes with consequences for protein-protein interactions, localisation and enzyme activity; and redox sensitive cysteines have been identified in many protein families, leading to consequences for redox signalling in a wide range of cellular processes. The timing and location of these modifications are key to the specificity of redox signalling and are often determined by the proximity of targets to the source of ROS. The reactivity of ROS – particularly superoxide – leads to their direct signalling effects being localised close to their site of production; however, the higher stability of H_2O_2 allows wider signal transduction across cellular compartments and between cells.

1.1.3.2 RNS signalling

NO is a small gaseous signalling molecule acting as an autocrine and paracrine mediator with roles in neurotransmission, vasodilation and fighting pathogens (Bult et al., 1990; Hibbs et al., 1987; Palmer et al., 1987). It is produced intracellularly by the NOS enzymes in an oxygen dependent reaction, and with one unpaired electron NO is highly reactive and may be autoxidised to nitrite which is stored inside cells and tissues (Zweier et al., 1995). Dietary nitrite and bacterially converted nitrate contribute to these stores and are reduced to NO by nitrite reductases such as xanthine oxidoreductase and deoxyhaemoglobin (Benjamin et al., 1994; Cosby et al., 2003; Lundberg et al., 1994; Webb et al., 2004). The conversion of nitrite into NO occurs independent of oxygen concentrations and has proved a beneficial source of NO during hypoxic conditions and ischemia reperfusion injury (Totzeck et al., 2012; Webb et al., 2004).

NO modulates protein activity through direct nitrosylation of catalytic iron-haem centres (Craven and DeRubertis, 1978). Endothelial derived NO signals via this mechanism to activate guanylate cyclase, thus stimulating cGMP production and subsequent relaxation of smooth muscle cells following phosphorylation of myosin light chains (Craven and DeRubertis, 1978; Rapoport et al., 1983). NO also regulates protein functions through PTM of amino acid side chains via RNS produced after reactions with oxygen to form nitrogen dioxide radicals ($NO_2^{\cdot}$) and dinitrogen tetroxide (N_2O_3) (Kharitonov et al., 1995) :

$$2NO + O_2 \rightarrow 2NO_2^{\cdot}$$

$$NO + 2NO_2^{\cdot} \rightarrow N_2O_3$$

These products nitrosate local cysteine residues in a range of proteins (Iwakiri et al., 2006; Jaffrey et al., 2001; Stamler et al., 1992), including those involved in calcium release, respiratory function, and metabolism (Clementi et al., 1998; Doulias et al., 2013; Molina y Vedia et al., 1992; Xu et al., 1998). Further propagation of signals by transfer of NO groups between protein thiols through transnitrosation has been described across cellular compartments as well as systemically in the blood by s-nitrosohaemoglobin (Jia et al., 1996; Kornberg et al., 2010). However, S-nitrosothiols are exceptionally labile and rapidly react with other thiols to form disulfide bonds, which are suggested to be the predominant effectors (Wolhuter et al., 2018). Additionally, NO rapidly reacts with superoxide to produce peroxynitrite ($ONOO^-$) (Gryglewski et al., 1986):

$$NO + O_2^{\cdot -} \rightarrow ONOO^-$$

Peroxynitrite is one of the most highly reactive species in biology, oxidising and nitrating proteins, DNA, and lipids. Tyrosine nitration is frequently used as a marker of nitrosative damage in a range of diseases including diabetes, Alzheimer's disease, and atherosclerosis

(Buttery et al., 1996; Mercuri et al., 2001; Smith et al., 1997), and irreversibly disrupts tyrosine kinase activity (Kong et al., 1996).

1.1.3.3 Therapeutically targeting NO-redox imbalance in vascular disease

To regulate levels of ROS, RNS, and redox signalling, cells have several enzymatic and molecular antioxidant systems which donate electrons to oxidised molecules. Glutathione – a small tripeptide formed of glutamate, cysteine, and glycine – is the most abundant cellular antioxidant molecule, present at 1-10 mM concentrations in cytosol, mitochondria, and nuclei (Forman et al., 2009; Ribas et al., 2014). Other molecular antioxidants include vitamin C, vitamin E and thioredoxin. Enzymes such as SOD and catalase react directly with ROS, transferring electrons through metallic catalytic centres. Whereas glutathione reductase, glutathione peroxidase, thioredoxin reductase and peroxiredoxin enzymes donate electrons through redox sensitive thiols. In pathologies characterised by elevated ROS generation and evident oxidative damage – such as endothelial dysfunction – these intracellular antioxidant defences prove insufficient. In fact, lower levels of antioxidants have been observed in brains with Alzheimer's disease and plasma of patients with cardiovascular disease (Aksenov and Markesbery, 2001; Shimizu et al., 2004), and glutathione peroxidase-1 deficiency was shown to cause endothelial dysfunction in mice (Forgione et al., 2002). Unsurprisingly, attempts have been made to augment antioxidant levels to both prevent and treat diseases and, although some reports showed promising improvements in endothelial function following administration of vitamins C and E (Engler et al., 2003; Plantinga et al., 2007), many studies and meta-analyses reported the contrary and suggested no benefit on cardiovascular mortalities (Kinlay et al., 2004; Vivekananthan et al., 2003; Ye et al., 2013). The inability of these antioxidants to reach specific sites of oxidant damage are a proposed reason and in support of this antioxidants targeted to mitochondrial compartments – which are a major sites of ROS production and oxidation – have shown encouraging improvements

in hypertension and endothelial dysfunction in mice and more recently humans (Dikalova et al., 2010; Gioscia-Ryan et al., 2014a; Rossman et al., 2018). Overall, these studies highlight the benefit of using more targeted therapeutic approaches, which will be discussed further in **Section 1.2**.

In vascular pathologies, restoring depleted NO to sufficient levels is also a major therapeutic aim. Historically, administration of organic nitrate in the form of nitroglycerin proved beneficial at improving blood flow in angina patients; however, nitrate tolerance impeded long term effects (Caramori et al., 1998; Gori et al., 2001). More recently, dietary inorganic nitrate or nitrite supplementation were shown to improve blood pressure (Larsen et al., 2006; Webb et al., 2008); however, mixed outcomes have been reported regarding the improvement of endothelial function and the mechanisms involved, and long-term outcomes require further investigation (Bahra et al., 2012; Heiss et al., 2012). The reaction of NO with ROS to form peroxynitrite leads to decreased NO bioavailability, meaning that antioxidants are dually beneficial at restoring NO levels as well as ablating ROS. The production of NO is also diminished by ROS as tetrahydrobiopterin (BH_4) – an essential cofactor required for the production of NO by NOS enzymes – is susceptible to oxidation and is deficient is dysfunctional endothelium (Landmesser et al., 2003). Furthermore, without BH_4 eNOS instead generates superoxide, exacerbating elevated ROS levels (Crabtree et al., 2008; Vásquez-Vivar et al., 2002). BH_4 deficiency therefore detrimentally affects both NO and ROS levels and the role of BH_4 in NO and ROS generation as well as its therapeutic potential will be discussed further in **Sections 1.3** and **1.4**.

1.2 NO and ROS signalling in mitochondria and metabolism

1.2.1 Mitochondria and metabolism

Mitochondria have an integral role in oxidative metabolism as the site of aerobic respiration, the tricarboxylic acid (TCA) cycle, and β-oxidation of fatty acids; however, mitochondria also have important signalling roles in calcium storage and ROS generation. Oxidative phosphorylation in the inner-mitochondrial membrane is the major source of adenosine triphosphate (ATP) generation in most cells and requires oxygen and electrons donated from reduced nicotinamide adenine dinucleotide (NADH) and flavin adenine dinucleotide ($FADH_2$) carriers. Oxidation of glucose in the cytosol through the glycolysis pathway generates 2 molecules of ATP and NADH overall per molecule of glucose (Figure 1.2). Glycolysis is a relatively inefficient way of producing ATP, but can be rapidly up-regulated to generate ATP when oxygen is scarce or oxidative phosphorylation is inhibited (Everts et al., 2012; Robin et al., 1984). The glycolytic product, pyruvate, is transported into mitochondria via pyruvate carrier proteins (MPC1 and 2) where it is converted into acetyl CoA by the pyruvate dehydrogenase complex. Acetyl CoA – which is also produced through β-oxidation of fatty acids within mitochondria – enters the TCA cycle, which generates the main supply of NADH and $FADH_2$ for oxidative phosphorylation. During each cycle, the TCA cycle generates three molecules of NADH, one $FADH_2$, one guanosine triphosphate (GTP), and two molecules of carbon dioxide (CO_2) (Figure 1.3).

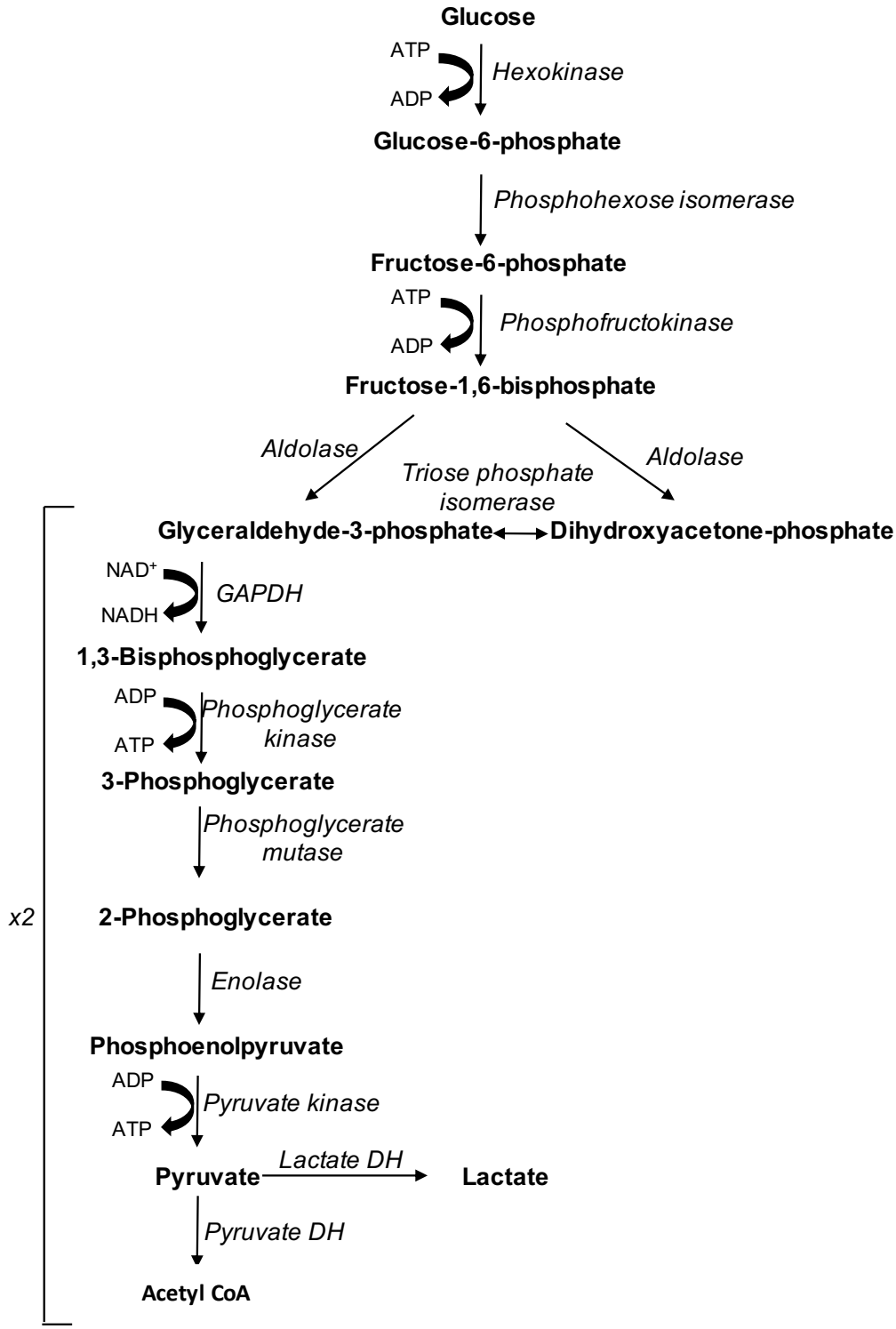


Figure 1.2 The glycolysis pathway

Metabolism of glucose through the glycolysis pathway requires multiple steps and generates 2 molecules of ATP per glucose molecule. The conversion of glyceraldehyde-3-phosphate to acetyl CoA occurs twice due to conversion of dihydroxyacetone phosphate into glyceraldehyde-3-phosphate by triose phosphate isomerase. (DH – dehydrogenase)

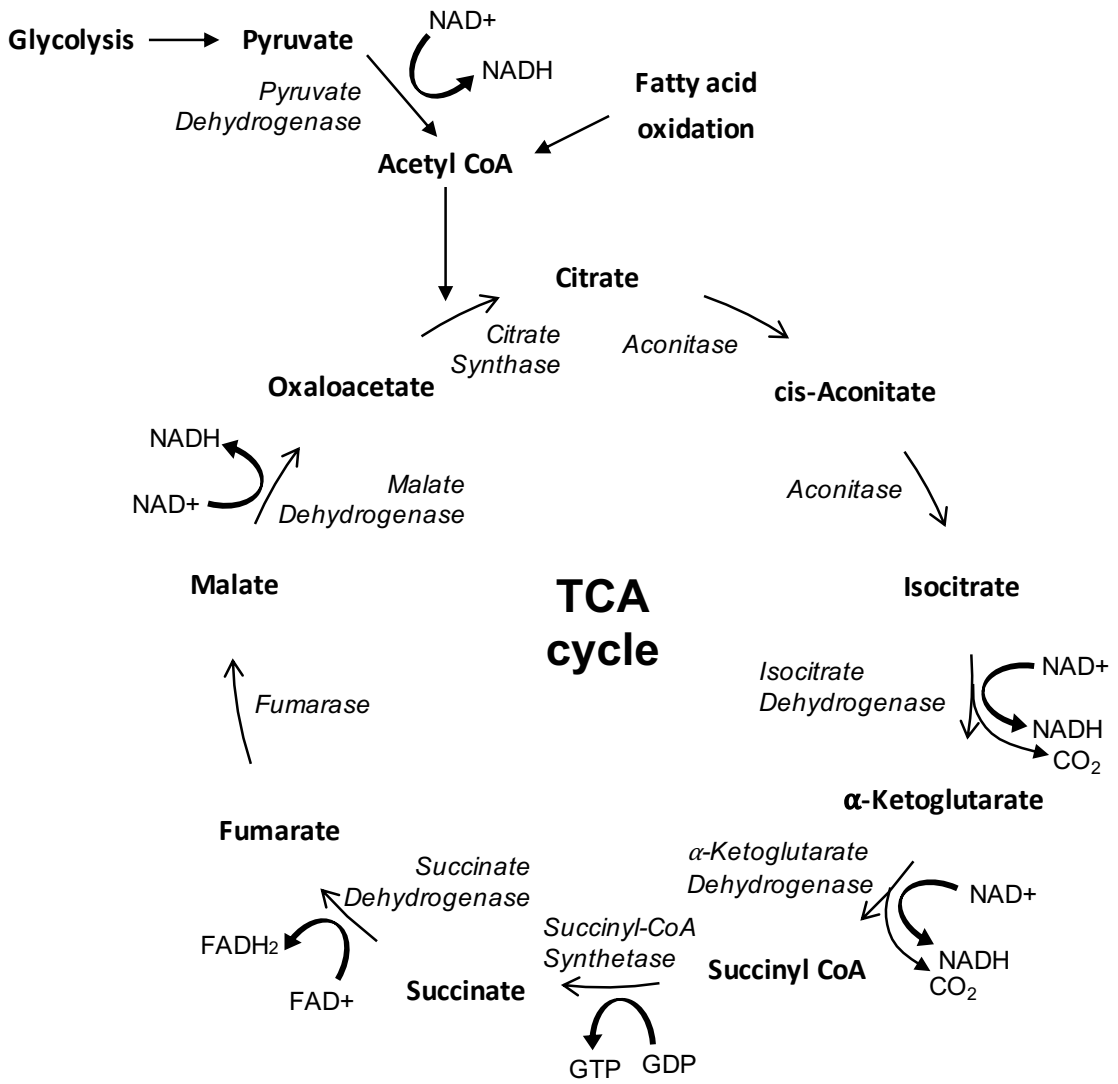


Figure 1.3 The tricarboxylic acid cycle

The TCA cycle involves 8 enzymes which generate electron donors (NADH and $FADH_2$), GTP and CO_2. Metabolic pathways – including glycolysis and fatty acid oxidation – feed acetyl CoA into the cycle to regenerate citrate.

1.2.1.1 Oxidative phosphorylation

Oxidative phosphorylation generates ATP using several enzymes and electron carrier molecules situated in the inner mitochondrial membrane. Electrons are transferred between four major protein complexes that make up the electron transport chain (ETC) and the energy released is used to pump protons (H^+) from the mitochondrial matrix into the intermembrane space (Figure 1.4). This creates a pH/H^+ gradient and proton-motive force, which is used by ATP synthase to generate ATP. ATP synthase allows H^+ to enter the matrix along their concentration gradient, and the favourable energy released drives catalytic production of ATP from adenosine diphosphate (ADP) and inorganic phosphate.

There are two main points of entry for electrons into the ETC. The first is NADH dehydrogenase (Complex I), which is a complex protein of almost 1000 kilodaltons (kDa) and formed of 44 subunits. A flavin mononucleotide (FMN) molecule in Complex I accepts 2 electrons from NADH and passes them along a series of [Fe-S] centres to coenzyme Q (CoQ). The second entry point is succinate dehydrogenase (SDH or Complex II), which is unusual in being part of both the ETC and TCA cycle, and is the only ETC Complex that does not pump H^+. SDH catalyses conversion of succinate into fumarate using an FAD cofactor and leads to reduction of CoQ. The cytochrome b-c_1 complex (Complex III) accepts electrons from reduced CoQ and passes them to the haem containing molecular electron carrier cytochrome C. Cytochrome C transfers electrons to the cytochrome C oxidase complex (Complex IV) which passes them to oxygen – the final electron acceptor – leading to formation of water.

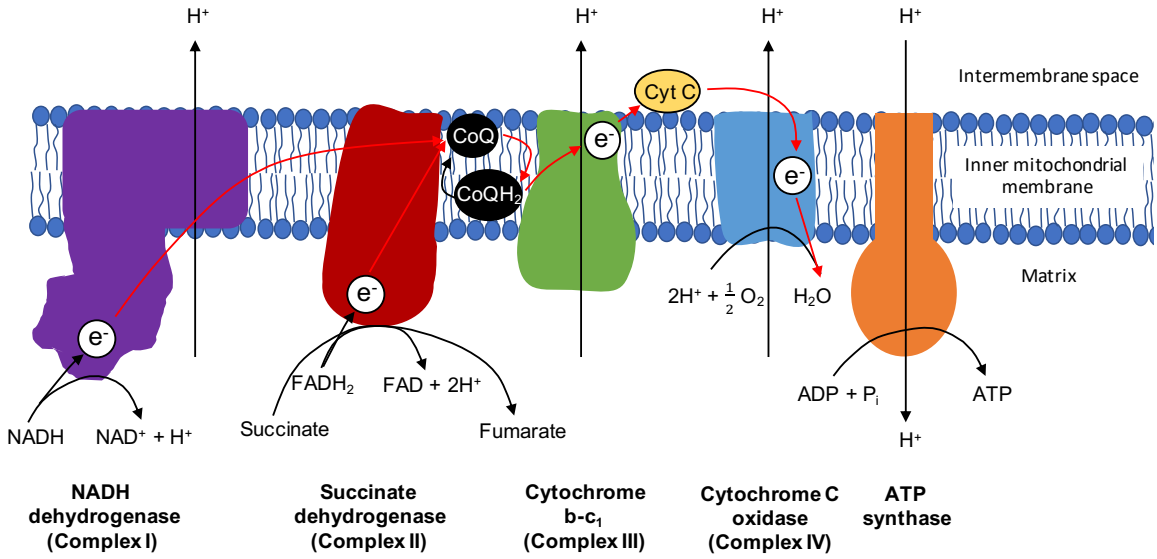


Figure 1.4 Oxidative phosphorylation

In the inner mitochondrial membrane electrons (e^-) are donated to Complex I by NADH and Complex II by $FADH_2$. These electrons are passed to Coenzyme Q (CoQ) which becomes reduced ($CoQH_2$). $CoQH_2$ donates electrons to Complex III which passes them to Complex IV via cytochrome C. Complex IV donates electrons to O_2 – which acts as the final electron acceptor – and water is produced. During electron transfer protons (H^+) are transported across Complexes I, III and IV into the intermembrane space creating a proton gradient. H^+ re-enter the matrix along their concentration gradient through ATP synthase, allowing generation of ATP due to favourable energy release. Red arrows depict transfer of electrons.

1.2.2 Mitochondrial ROS generation

Mitochondria produce superoxide from several sites including the ETC Complexes I & III and α-ketoglutarate dehydrogenase (Kussmaul and Hirst, 2006; Starkov et al., 2004; Turrens et al., 1985). Most of the superoxide is rapidly converted into H_2O_2 by mitochondrial specific manganese SOD (mnSOD) (Weisiger and Fridovich, 1973), but also reacts with NO to form peroxynitrite (Packer et al., 1996). Mitochondrial H_2O_2 transmits redox signals within the mitochondria and to the cytosol, and contributes to oxidative damage associated with aging and many diseases.

Complex I is considered a major source of mitochondrial superoxide and NADH oxidation generates superoxide through forward electron transport from reduced FMN ($FMNH_2$) when

the NADH:NAD^+ ratio is high (Kussmaul and Hirst, 2006). Succinate oxidation by SDH drives superoxide production through reverse electron transport (RET) at Complex I when the CoQ pool is highly reduced and the proton-motive force is large (Robb et al., 2018). The mechanisms of mitochondrial ROS generation were primarily defined in isolated mitochondria, however the relevance in physiological processes has now been demonstrated. For example, Complex I derived ROS has a proven redox signalling role in oxygen sensing and inflammatory macrophages, but is pathologically damaging during ischaemia-reperfusion injury (Chouchani et al., 2013; Fernández-Agüera et al., 2015; Mills et al., 2016).

1.2.2.1 Therapeutically targeting mitochondrial ROS

As discussed in **section 1.1.3.1**, ROS have the potential to be damaging and mitochondrial derived ROS have been implicated in endothelial dysfunction, diabetes, neurodegeneration and aging due oxidative damage of DNA, proteins and lipids (Kujoth et al., 2005; Li et al., 2004; Nishikawa et al., 2000). This has led researchers to design drugs to specifically alleviate elevated ROS levels in mitochondria. Taking advantage of the relatively negatively charged mitochondrial matrix, known antioxidant molecules have been conjugated with lipophilic triphenylphosphonium cations (TPP^+) and accumulate around 1000 fold within the matrix (Kelso et al., 2001; Smith et al., 1999). In rodents, mitochondria-targeted CoQ (MitoQ) has proven effective at protecting neurons against amyloid-β toxicity in models of Alzheimer's disease (Manczak et al., 2010) and at improving endothelial dysfunction (Gioscia-Ryan et al., 2014a; Graham et al., 2009a). Clinical trials in humans are also underway and very recently chronic MitoQ supplementation was deemed to improve endothelial dysfunction in aging adults (Rossman et al., 2018).

1.2.3 Regulation of mitochondrial function and metabolism by NO

NO is recognised as a key modulator of mitochondrial aerobic respiration and it also influences mitochondrial morphology (Cho et al., 2009; Cleeter et al., 1994; Rizza et al., 2018). These aspects, along with the concept of an emerging role for NO signalling in the regulation of metabolic pathways, will be discussed in further detail.

1.2.3.1 Mitochondrial respiration

NO inhibits mitochondrial respiration by targeting specific parts of the ETC. NO reversibly represses Complex IV (cytochrome C oxidase) activity by competing with oxygen (Brown and Cooper, 1994; Cleeter et al., 1994; Clementi et al., 1999) and inhibits the activity of Complex I through nitrosation (Burwell et al., 2006; Clementi et al., 1998). At physiological levels of NO, these mechanisms modulate respiratory function in endothelial cells (Clementi et al., 1999) and dramatically inhibit oxidative phosphorylation as part of the inflammatory phenotype of macrophages and dendritic cells (Everts et al., 2012; Van den Bossche et al., 2016). Furthermore, pharmacologically inducing nitrosation mediated inhibition of Complex I proved cardioprotective during ischaemia-reperfusion injury, due to inhibition of Complex I driven ROS production (Chouchani et al., 2013).

1.2.3.2 Mitochondrial morphology

Mitochondria are dynamic organelles which form networks undergoing constant fission and fusion, allowing beneficial sharing of components and also efficient isolation of old or damaged sections for degradation (Frank et al., 2012; Nakada et al., 2001; Twig et al., 2008). Mitochondrial fusion is controlled by mitofusin 1, mitofusin 2 and optic atrophy protein 1 (OPA1), whereas fission requires Fis1 and the GTPase dynamin related protein 1 (DRP1) (Smirnova et al., 2001; Song et al., 2009). NO activates DRP1 and mitochondrial fission through nitrosation and by stimulating phosphorylation of serine 616 (Bossy et al., 2010;

Cho et al., 2009; Rizza et al., 2018). Regulation of DRP1 mediated fission is crucial, as excessive fission is evident in endothelial dysfunction and neurodegenerative diseases and has been linked with causing mitochondrial ROS production (Cho et al., 2009; Shenouda et al., 2011).

1.2.3.3 Metabolic pathways

NO has been implicated in the regulation of several major metabolic pathways. In astrocytes, NO was shown to up-regulate glycolysis, increasing the activity of the rate limiting enzyme phosphofructokinase-1 (PFK-1) by increasing levels of the powerful allosteric activator fructose-2,6-bisphosphate (Almeida et al., 2004; Van Schaftingen et al., 1982). Intriguingly, in models of ovarian cancer, low levels of NO promoted glycolysis by inducing translocation of pyruvate kinase M2 to the nucleus where it induced transcription of glycolytic genes, whereas high levels were found to be inhibitory (Li et al., 2017). Additionally, it is well characterised that glyceraldehyde-3-phosphate dehydrogenase (GAPDH) is inhibited through nitrosation, which may be involved in glycolytic modulation and was shown to induce apoptosis (Hara et al., 2005; Mohr et al., 1996).

Nitrosation of cysteine thiols occurs in many metabolic enzymes; however, the consequences for protein function and flux through metabolic pathways are incompletely defined. Nitrosation dependent changes have been confirmed to modulate the activity of proteins involved in fatty acid/glutamate metabolism and the TCA cycle (Choi et al., 2016; Doulias et al., 2013; Raju et al., 2015). In particular, nitrosation of the TCA cycle protein isocitrate dehydrogenase (IDH) has been reported multiple times and inhibits its activity (Raju et al., 2015; Yang et al., 2002). NO has also been reported to inhibit proteins containing [Fe-S] centres in their catalytic sites (Duan et al., 2009; Gardner et al., 1997), such as the TCA cycle protein aconitase, although this possibly occurs indirectly through

peroxynitrite (Castro et al., 1994; Tórtora et al., 2007). Overall, there are many indications that NO modulates metabolic pathways but the specifics are still being elucidated.

1.2.4 Endothelial mitochondria and metabolism

The mitochondrial content of endothelial cells is relatively low (2-11% volume, depending upon location in rat tissues (Blouin et al., 1977; Oldendorf et al., 1977)) compared with many other cells types such as cardiomyocytes (32% volume in rats, 25% volume in humans (Barth et al., 1992)) and hepatocytes (28% volume in rats, (Blouin et al., 1977)). This is believed to reflect the dominance of glycolytic ATP generation in this cell type rather than mitochondrial oxidative phosphorylation (Culic et al., 1997; De Bock et al., 2013; Quintero et al., 2006; Spahr et al.) and growing evidence indicates that mitochondria perform important signalling roles in endothelial cells (Al-Mehdi et al., 2012; Quintero et al., 2006). In particular, ROS generated from mitochondria regulates the endothelial response to hypoxia and flow mediated dilation (Al-Mehdi et al., 2012; Liu et al., 2003) and mitochondrial calcium stores modulate mechano-transduction as well as calcium sensitive enzymes such as eNOS (Charoensin et al., 2017; Scheitlin et al., 2016). However, inappropriate signalling, including transduction through elevated mitochondrial ROS, leads to endothelial dysfunction and vascular diseases (Dikalov et al., 2014; Nishikawa et al., 2000). It is therefore vital to understand the mechanisms regulating mitochondrial function and signalling in endothelial cells.

1.2.4.1 Endothelial mitochondrial ROS in vascular disease

It is becoming increasingly evident that uncontrolled mitochondrial ROS generation is causal in endothelial dysfunction and vascular disease (Dikalov et al., 2014; Dikalova et al., 2010; Graham et al., 2009a). In mouse models of angiotensin-II mediated hypertension, NOX2 was shown to induce mitochondrial superoxide production in endothelial cells (Dikalov et al., 2014) and treatment with the mitochondria-targeted superoxide scavenger

mitoTEMPO attenuated hypertension and improved endothelial function (Dikalova et al., 2010). Additionally, ROS are generated by mitochondria in hyperglycaemic endothelial cells and lead to activation of pathways involved in pathogenesis of diabetes (Nishikawa et al., 2000). Mitochondrial ROS are also implicated in atherogenesis, which is decreased together with improved endothelial function in ApoE mice overexpressing mitochondrial thioredoxin-2 (Zhang et al., 2007a). Pharmacologically diminishing endothelial derived mitochondrial ROS is therefore a promising avenue for treating and preventing vascular disease and after showing improvements in rodents with dysfunction endothelium (Dikalova et al., 2010; Gioscia-Ryan et al., 2014a; Graham et al., 2009a), mitochondria-targeted antioxidants are being trialled in humans with recent success in improving endothelial function in aging adults (Rossman et al., 2018).

1.2.5 Macrophage metabolic remodelling in inflammation

Inflammation is a vital part of the innate immune response to infections; however, it is also associated with vascular disease and can cause potentially fatal sepsis. Inflammatory macrophages play a central role in removing pathogens and producing inflammatory cytokines to recruit and activate other leukocytes. To become inflammatory, macrophages are activated through binding of cytokines or pathogens to a variety of cell surface receptors. Recent findings demonstrate that the switch to an inflammatory phenotype involves dramatic metabolic remodelling to support macrophage function (Lampropoulou et al., 2016; Mills et al., 2016; Tannahill et al., 2013), and is also observed in inflammatory dendritic cells and T cells (Chang et al., 2013; Everts et al., 2012; Krawczyk et al., 2010; van der Windt et al., 2012).

In response to inflammatory stimuli, the induction of iNOS derived NO inhibits the ETC, switching off mitochondrial oxidative phosphorylation (Van den Bossche et al., 2016) and the rate of glycolysis is increased to become the primary source of ATP (Palsson-McDermott

et al., 2015). Elevated glycolysis is required for inflammatory cell survival and production of cytokines (Krawczyk et al., 2010; Tannahill et al., 2013) and it is orchestrated by accumulated hypoxia-inducible factor 1-α (HIF1α), which transcriptionally up-regulates key proteins involved in glucose metabolism (Liu et al., 2016; Wang et al., 2017). Inflammatory macrophages also up-regulate NADPH synthesis through the pentose phosphate pathway (PPP) (Haschemi et al., 2012), reduce oxidation of fatty acids and accumulate specific TCA cycle metabolites (Arts et al., 2016; Infantino et al., 2011; Mills et al., 2018; Tannahill et al., 2013). On the other hand macrophages polarised to an anti-inflammatory phenotype maintain fatty acid oxidation and oxidative phosphorylation (Vats et al., 2006), supress the PPP (Haschemi et al., 2012), but have been shown to similarly up-regulate glycolysis (Huang et al., 2016). Differences in arginine metabolism were identified as early distinguishing markers of pro- and anti-inflammatory macrophages, such that arginine is metabolised to NO and citrulline by iNOS in inflammatory cells but converted into ornithine by arginase in anti-inflammatory cells (Corraliza et al., 1995). This range of metabolic characteristics can now be used to interpret macrophage activation states and in the future may be manipulated to influence polarisation.

Accumulation of TCA cycle metabolites citrate, succinate and fumarate, and also itaconate are fundamental for metabolic reprogramming of inflammatory macrophages (Arts et al., 2016; Infantino et al., 2011; Mills et al., 2018; Tannahill et al., 2013). Carbon flux analyses have identified two ‘breaks’ in the cycle – at IDH and SDH (Jha et al., 2015) – leading to elevations in citrate and succinate respectively. Succinate has a pivotal pro-inflammatory role, with accumulation directing HIF1α-mediated up-regulation of glycolysis and interleukin-1β (IL-1β) production, as well as driving ROS generation through RET (Mills et al., 2016; Tannahill et al., 2013). Citrate is repurposed to produce lipids and the metabolite itaconate, and elevations in succinate have been attributed to inhibition of SDH by itaconate

(Cordes et al., 2016; Lampropoulou et al., 2016). Itaconate is one of the most highly induced metabolites in activated macrophages (Lampropoulou et al., 2016; Mills et al., 2018), and is produced from cis-aconitate by cis-aconitate decarboxylase (Michelucci et al., 2013). Interestingly, whilst demonstrating bactericidal properties, itaconate has been shown to be a potent anti-inflammatory mediator, limiting inflammation through kelch-like ECH-associated protein 1 (KEAP1) - nuclear factor erythroid 2-related factor 2 (NRF2) signalling (Mills et al., 2018). The mechanisms modulating these TCA cycle changes are still being elucidated.

1.3 Nitric oxide synthase enzymes

1.3.1 NOS isoforms

There are 3 human NOS isoforms encoded by separate genes with 50-60% homology, and located on different chromosomes; these are: eNOS (NOS3 (Chromosome 7)), iNOS (NOS2 (Chromosome 17)) and neuronal NOS (nNOS, NOS1 (Chromosome 12)) (Charles et al., 1993; Marsden et al., 1992; Nakane et al., 1993). They share bidomain structures consisting of N-terminal oxygenase and C-terminal reductase domains linked by a calmodulin binding site (Chen et al., 1996; Ghosh and Stuehr, 1995; Sheta et al., 1994). The NOS enzymes function as homodimers to catalyse production of NO from L-arginine, in a reaction which requires NADPH, BH_4, FAD, FMN and haem cofactors (Baek et al., 1993; Stuehr and Ikeda-Saito, 1992). The availability of L-arginine, NADPH and BH_4 determine activity of all isoforms, however they are differentially regulated at the levels of gene expression, PTM, and calcium sensitivity. These differences in modulation, together with tissue specificity and subcellular localisation, are key to understanding the various functions of the NOS isoforms – which will be discussed below in the cases of eNOS and iNOS.

1.3.2 NOS catalysis

NOS enzymes catalyse the production of NO from L-arginine and oxygen, generating L-citrulline as a by-product (Figure 1.5A). NOS enzymes function as homodimers and electrons flow from the reductase domain of one monomer to the oxygenase catalytic site of the other. In the reductase domain, bound NADPH molecules donate electrons that are transported across FAD and FMN flavins, before being transferred to haem in the oxygenase domain upon calcium induced calmodulin binding (Abu-Soud and Stuehr, 1993). In the oxygenase domain, L-arginine is first converted into N-hydroxy-L-arginine before L-citrulline and NO, requiring electron donations to the ferrous-dioxygen complex in haem from BH_4 as well as the flavins in the reductase domain (Abu-Soud et al., 1997; Berka et al., 2004). BH_4 forms a protonated trihydrobiopterin cation radical during the reaction ($BH_3{\cdot}H^+$) but is ultimately regenerated as BH_4 (Hurshman et al., 2003; Schmidt et al., 2001; Wei et al., 2003).

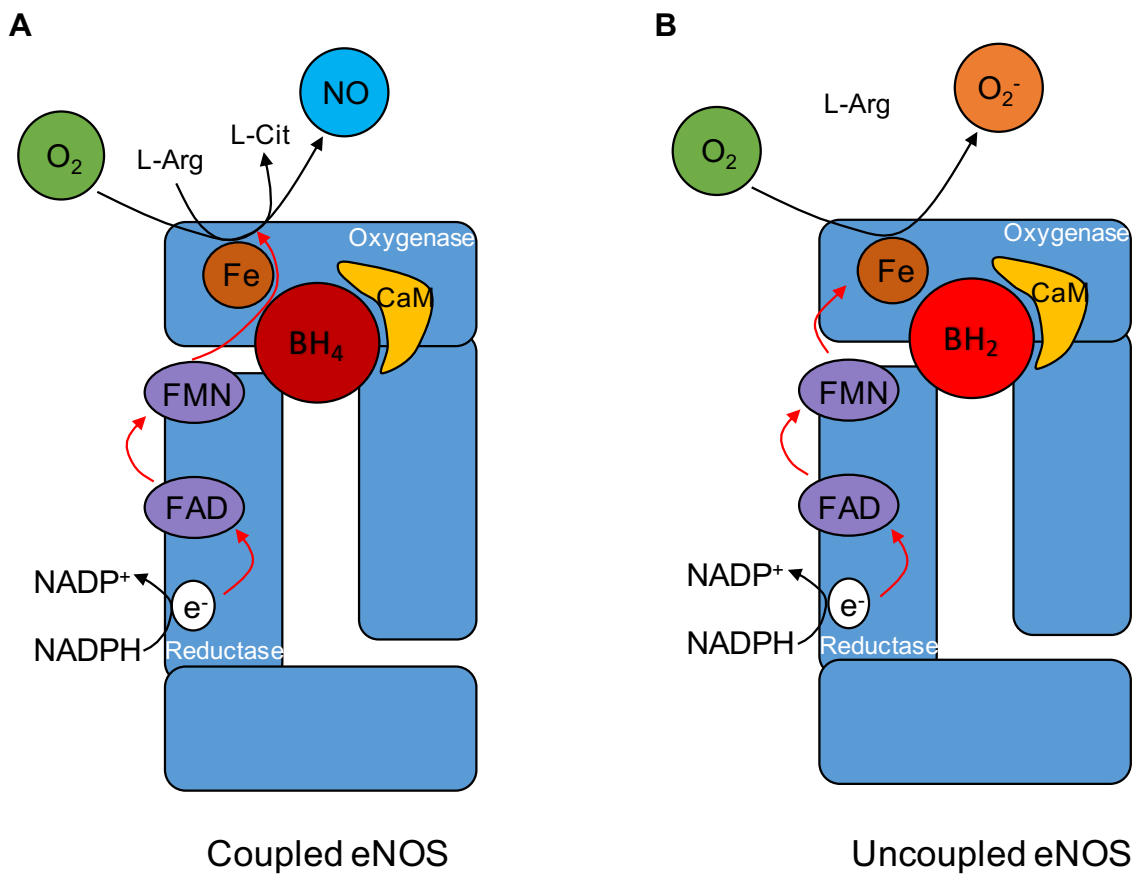


Figure 1.5 eNOS catalysis and uncoupling

(A) Coupled eNOS generates NO and L-citrulline (L-cit) from L-arginine (L-Arg) using electrons (e^-) donated from NADPH in the reductase domain of one monomer and transported to the oxygenase domain of the other monomer. This occurs via FAD, FMN and haem iron, and requires BH_4 is as a cofactor. (B) In the absence of BH_4 (or binding of BH_2), electrons transferred from the flavins become 'uncoupled' from L-arginine oxidation and superoxide (O_2^-) is produced following dissociation of the ferrous-dioxygen complex. The red arrows depict the flow of electrons. Based on a figure from (Schmidt and Alp, 2007).

1.3.3 Endothelial NOS in vascular disease

eNOS is constitutively expressed in endothelial cells and cardiac myocytes (Balligand et al., 1995; Janssens et al., 1992) and is an important regulator of vascular homeostasis (Huang et al., 1995), with decreased activity underlying the reduced NO bioavailability causing endothelial dysfunction and vascular pathologies. In addition to substrate and cofactor availability, the main determinants of eNOS function are calcium levels, PTMs, protein-

protein interactions and subcellular localisation. eNOS is primarily localised to plasma membrane caveolae and Golgi apparatus by S-palmitoylation and N-myristoylation (García-Cardeña et al., 1996; Liu et al., 1997); however translocation to the cytosol or perinuclear region have been described in response to certain stimuli (Goetz et al., 1999; Prabhakar et al., 1998; Sánchez et al., 2006). Membrane localised eNOS is ideally placed for efficient diffusion of NO into neighbouring smooth muscle cells to regulate vasomotor tone, and the inner vessel to modulate platelet and leukocyte adhesion and maintain vascular health. In its resting state, membrane localised eNOS binds caveolin-1(Ju et al., 1997); activation occurs when this is displaced by calmodulin, following elevated intracellular calcium in response to fluid shear stress and receptor agonists (Michel et al., 1997; Shen et al., 1992). These extracellular stimuli further modulate eNOS through phosphorylation, where by serine 1177, ser 633, and tyrosine 81 are activating (Chen et al., 1999; Dimmeler et al., 1999; Fleming et al., 2001; Michel et al., 1997; Shen et al., 1992), and tyrosine 567 and threonine 495 are inhibitory (Dimmeler et al., 1999; Ju et al., 1997). Threonine 495 is located in the calmodulin binding domain, therefore preventing binding when phosphorylated and exemplifying the interplay between modulatory mechanisms to refine activity (Fleming et al., 2001).

1.3.3.1 Superoxide generation by uncoupled eNOS

The vital role for endothelial derived NO in vascular function was clear before the NOS enzymes were revealed and characterised (Ignarro et al., 1987; Janssens et al., 1992), but the requirement of eNOS was soon confirmed in knockout (KO) mice, which displayed hypertension and defective reparative angiogenesis following ischaemic injury (Huang et al., 1995; Murohara et al., 1998). Augmentation of NOS derived NO in dysfunctional endothelium became a promising therapeutic aim with nNOS gene transfer improving vascular function in atherosclerotic rabbits (Channon et al., 1998). However, ApoE KO transgenic mice overexpressing eNOS presented accelerated atherosclerotic plaque

formation, lower NO production relative to eNOS expression levels and elevated vascular superoxide, which were normalised by BH_4 supplementation (Ozaki et al., 2002). The fact that eNOS could produce superoxide instead of NO (termed 'uncoupling') had previously been reported (Pritchard et al., 1995), as well as the fact that BH_4 deficiency was the causative factor (Vásquez-Vivar et al., 1998). The study by Ozaki et al. (2002) highlighted the role of BH_4 deficiency induced eNOS uncoupling in vascular pathogenesis, and this was subsequently confirmed in both atherogenesis and hypertension (Alp et al., 2004; Landmesser et al., 2003; Takaya et al., 2007).

As discussed, BH_4 participates in NO generation in the oxygenase domain of eNOS by donating electrons to the ferrous-dioxygen complex in addition to electrons transferred from flavins in the reductase domain (Berka et al., 2004). When BH_4 is unavailable electrons transferred from the flavins become 'uncoupled' from L-arginine oxidation and superoxide is produced following dissociation of the ferrous-dioxygen complex (Stroes et al., 1998; Vásquez-Vivar et al., 1998) (Figure 1.5B). Furthermore, S-glutathionylation of redox sensitive cysteine residues in eNOS leads to uncoupling by a distinct mechanism, but can be stimulated by BH_4 deficiency induced reductions in the intracellular reduced glutathione:oxidised glutathione ratio (Chen et al., 2010; Crabtree et al., 2013).

1.3.4 Inducible NOS in macrophages

As the name suggests, synthesis of iNOS is induced in response to inflammatory stimuli rather than being constitutively expressed (Marks-Konczalik et al., 1998), although it is reportedly present in unstimulated lung epithelial cells (Dweik et al., 1998). iNOS was first described in macrophages stimulated with inflammatory cytokines (Kilbourn et al., 1990a, 1992), but has been shown to be inducible in most cell types, including endothelial cells, smooth muscle cells, and cardiomyocytes (Balligand et al., 1994; Gross et al., 1991; Nakayama et al., 1994). Calmodulin binds to iNOS with high affinity and even at low basal

levels of calcium, so it is considered calcium insensitive and is usually active once present (Cho et al., 1992; Spratt et al., 2007). In macrophages, NO produced by iNOS together with superoxide and their reactive product, peroxynitrite, help to damage and eliminate pathogens during infection (MacMicking et al., 1995; Vazquez-Torres et al., 2000; Wei et al., 1995). However, iNOS derived NO has a role in the potentially pathogenic hypotension observed in systemic bacterial infections that cause septic shock (Kilbourn et al., 1990a, 1990b), as well as cancers and inflammatory bowel disease (Singer et al., 1996; Wilson et al., 1998). Furthermore, iNOS has been implicated in atherogenesis due to detection of iNOS and nitrotyrosine peroxynitrite oxidation products in human atherosclerotic plaques, and the observed reduction in atherosclerosis in combined ApoE KO and iNOS KO mice (Buttery et al., 1996; Detmers et al., 2000).

1.3.4.1 iNOS in human vs murine macrophages

In cell culture systems, murine macrophages readily induce NO production from iNOS in response to LPS and IFNγ (Stuehr et al., 1989); however, the same stimuli appear to be ineffective at promoting NO generation by human mononuclear phagocytes (Schneemann et al., 1993). This has led to much debate and controversy around whether or not human macrophages generate NO (Bogdan, 2002; Fang and Vazquez-Torres, 2002; Schneemann and Schoedon, 2002), despite copious amounts of literature providing evidence of iNOS encoding mRNA, protein, and activity in human macrophages and monocytes from patients with a range of infections including *Mycobacterium tuberculosis*, IFNα treated hepatitis C and *Leishmania major* (Nicholson et al., 1996; Sharara et al., 1997; Vouldoukis et al., 1995). It is proposed that a different – and perhaps more complex – set of signals are required to induce human iNOS compared with the murine enzyme (Sharara et al., 1997; Villalta et al., 1998), with an incomplete understanding leading to an inability to recreate *in vivo* conditions and accounting for discrepancies in culture. One clear difference between the human versus

murine gene encoding iNOS (*NOS2*), is that the murine promotor contains one nuclear factor kappa-B (NF-κB) binding sequence required for transcriptional activation, whereas the human *NOS2* gene contains several, indicating more complex transcriptional regulation (Marks-Konczalik et al., 1998; Taylor et al., 1998; Xie et al., 1994). The importance of the human *NOS2* promotor region was further highlighted by polymorphisms that increase NO generation and protection against Malaria (Kun et al., 2001). Furthermore, there is evidence of DNA methylation in the human *NOS2* gene but not the mouse gene, indicative of epigenetic regulation (Gross et al., 2014). Overall it can be concluded that human and murine macrophages both generate NO from iNOS enzymes and that it is appropriate to study this process in the context of human pathologies. However, as with all model systems, the different cellular processes involved in mice compared with humans – especially regarding iNOS induction – must be considered in translation of findings between organisms.

1.3.4.2 Superoxide generation by iNOS

The activity of iNOS is limited by substrate and BH_4 availability similar to the other NOS isoforms (McNeill et al., 2015; Schoedon et al., 1993). It is certain that iNOS is unable to generate NO in the absence of BH_4 (McNeill et al., 2015), however it is less clear whether iNOS displays uncoupling analogous to eNOS and generates superoxide in this circumstance. Early reports suggested that iNOS can produce superoxide from the reductase domain in the absence of L-arginine (Xia and Zweier, 1997; Xia et al., 1998). Other studies reporting iNOS derived superoxide are sparse, but it has been implicated in myocardial hypertrophy and contractile dysfunction in models of heart failure (Heusch et al., 2010; Zhang et al., 2007b). Only one study associates BH_4 levels with superoxide generation from iNOS, reporting that iNOS derived superoxide was decreased by BH_4 supplementation and led to decreased infarct sizes after ischaemia/reperfusion injury in diabetic rat hearts (Okazaki et al., 2011). More recently, elevated ROS production was observed in BH_4

deficient macrophages however it did not appear to be generated by iNOS and was insensitive to specific inhibitors (McNeill et al., 2015). BH_4 deficiency induced iNOS uncoupling therefore remains inconclusive.

1.3.5 Mitochondrial NOS

It is clear that NO signalling modulates respiratory function (Cleeter et al., 1994) and this has led to investigations into the co-localisation of NOS enzymes and mitochondria. There have been reports separately demonstrating the presence of eNOS (Bates et al., 1995, 1996), iNOS (Valdez et al., 2004) and nNOS (Elfering et al., 2002) in mitochondria by either immunocytochemistry, Western blotting or proteomics, and evidence of mitochondrial nNOS activity (Kanai et al., 2001). However, other studies indicated that mitochondrial NOS is actually a distinct isoform (Lacza et al., 2003; Zemojtel et al., 2006), or even refute the possibility of NOS within mitochondria (Gao et al., 2004; Tay et al., 2004). An association between eNOS and the outer mitochondrial membrane was shown (Gao et al., 2004; Reiner et al., 2001) and the debate continues over whether or not mitochondria contain a NOS isoform.

1.4 Tetrahydrobiopterin

1.4.1 An essential enzyme cofactor

5,6,7,8-tetrahydrobiopterin (BH_4) is a redox active molecule formed of a heterocyclic pteridine ring structure and has roles as an antioxidant and a required cofactor for 3 groups of enzymes. It was first described as an enzymatic cofactor for the hydroxylation of phenylalanine, tyrosine and tryptophan by the amino acid hydroxylase enzymes (AAHs), which are the rate limiting enzymes in the production of the monoamine neurotransmitters dopamine, adrenaline, noradrenaline, and serotonin (Kaufman, 1959; Nagatsu et al., 1964;

Tong and Kaufman, 1975). It was next discovered to be an essential cofactor for the production of NO by the NOS enzymes (Kwon et al., 1989; Tayeh and Marletta, 1989); and most recently BH_4 was uncovered as a cofactor for alkylglycerol mono-oxygenase (AGMO) which is involved in ether lipid metabolism (Watschinger et al., 2010). The diverse functions of these enzymes contribute to many vital biological processes including signalling in the central and peripheral nervous systems, the immune response and vascular function. BH_4 deficiency has therefore been linked to several neurological and cardiovascular pathologies (Ichinose et al., 1994; Landmesser et al., 2003).

1.4.2 Synthesis of tetrahydrobiopterin

De novo synthesis of BH_4 from GTP requires sequential catalysis by 3 enzymes: GTP cyclohydrolase (GTPCH), 6-pyruvoyl tertrahydropterin synthase (PTPS) and sepiapterin reductase (SR) (Figure 1.6). In the first and rate-limiting step in the pathway, GTPCH catalyses production of 7,8-dihydroneopterin triphosphate (DNTP) from GTP. GTPCH is encoded by the *GCH1* gene located on chromosome 14 in humans and mice, and is transcriptionally induced in response to pro-inflammatory stimuli in many cell types including macrophages (Hattori et al., 1995; Werner et al., 1989). The expression of *GCH1* is also increased in response to hydrogen peroxide in endothelial cells (Shimizu et al., 2003). At the post-translational level GTPCH is modulated by phosphorylation and interactions with GTPCH feedback regulatory protein (GFRP). Phosphorylation increases the activity of GTPCH to increase BH_4 synthesis in response to laminar shear stress in human endothelial cells (Widder et al., 2007), and interactions with GFRP are inhibitory (Harada et al., 1993; Milstien et al., 1996). Following the activity of GTPCH, PTPS converts DNTP into 6-pyruvoyl tetrahydropterin, which is reduced to BH_4 by SR in the final reaction.

1.4.3 BH_4 oxidation, recycling, and the salvage pathway

During NOS catalysis, BH_4 temporarily donates an electron and becomes protonated ($BH_3 \cdot H^+$) before being reduced back to BH_4 by NOS flavins (Hurshman et al., 2003; Schmidt et al., 2001). Conversely, BH_4 is oxidised to tetrahydrobiopterin-4a-carbinolamine during AAH reactions and must be regenerated by other enzymes. Tetrahydrobiopterin-4a-carbinolamine is converted into quinoid dihydrobiopterin (qBH_2) by pterin-4a-carbinolamine dehydrogenase (PCD), which is reduced to BH_4 by dihydropteridine reductase (DHPR) (Figure 1.6). In addition, BH_4 is susceptible to oxidation to 7,8-dihydrobiopterin (BH_2) and is regenerated by dihydrofolate reductase (DHFR). This step also forms an important part of the 'salvage pathway' – responsible for converting sepiapterin into BH_4 – following intermediate production of BH_2 from sepiapterin in a reaction catalysed by SR (Nichol et al., 1983) (Figure 1.6). Sepiapterin supplementation is therefore an approach frequently used to pharmacologically augment BH_4 levels.

BH_2 is unable to act an enzyme cofactor, however notably competes with BH_4 for binding to the NOS enzymes (Crabtree et al., 2008). The mechanisms through which BH_4 is oxidised to BH_2 have therefore been investigated. BH_4 reacts directly with superoxide with a rate constant of 3.9×10^5 M^{-1} s^{-1} (Vásquez-Vivar et al., 2001), however reactions of NO with superoxide to produce peroxynitrite have a much higher rate constant of 6.7×10^9 M^{-1} s^{-1} (Huie and Padmaja, 1993). It is considered that reactions of BH_4 with peroxynitrite therefore have a significant influence on generation of BH_2, and the rate constant of this reaction is 6×10^3 M^{-1} s^{-1} which is higher than reactions of peroxynitrite with ascorbate (236 M^{-1} s^{-1}), cysteine thiols (10^3 M^{-1} s^{-1}) or glutathione (5.8×10^2 M^{-1} s^{-1}) (Kuzkaya et al., 2003).

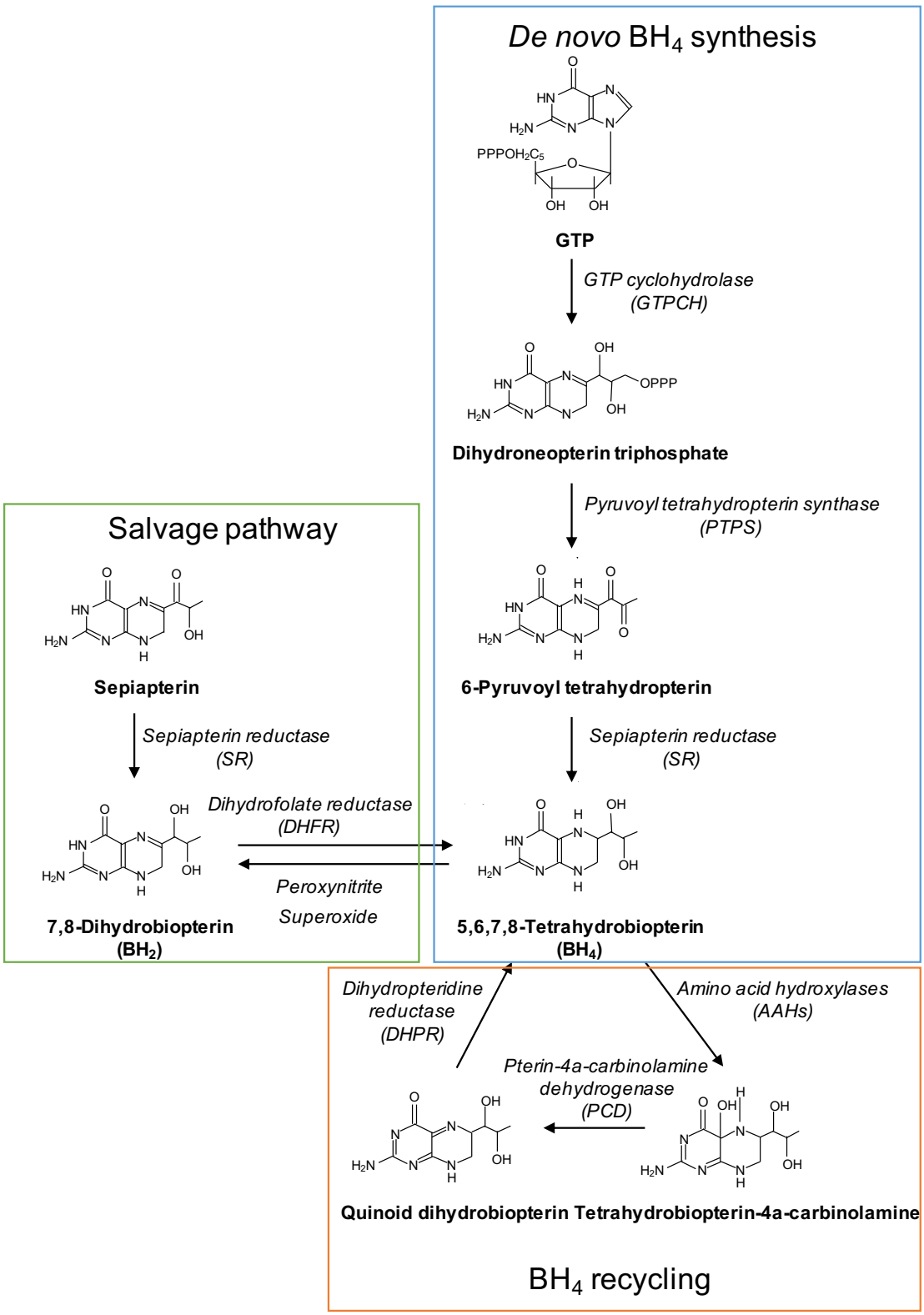


Figure 1.6 BH_4 synthesis

In cells BH_4 is synthesised *de novo* from GTP in three steps. BH_4 is also generated from sepiapterin via the salvage pathway and recycled from tetrahydrobiopterin-4a-carbinolamine (following AAH catalysis). Based on a figure from (Schmidt and Alp, 2007).

1.4.4 BH_4 in the mitochondria

There have been several reports recording the presence of BH_4 within mitochondria (Du et al., 2012; Rembold and Buff, 1972a; Shimizu et al., 2013). The first of these, in 1972, suggested an intriguing role for BH_4 in transfer of electrons to cytochrome C and influencing 'intramitochondrial redox potential' (Rembold and Buff, 1972a). However, these claims were not followed further and mentions of mitochondrial BH_4 remained elusive in the literature for many years.

In the 21st century, there have been reported links between BH_4 and mitochondrial function, but its proposed roles have varied. In both dopaminergic neurons and cardiomyocytes, elevated BH_4 levels were shown to inhibit mitochondrial respiration, however in both cases very high levels were supplemented or induced (Choi et al., 2006; Sethumadhavan et al., 2016). In fact BH_4 levels were elevated several hundred fold in cardiomyocytes and led to drastic redox changes which were the likely cause (Sethumadhavan et al., 2016). Interestingly, cardiac BH_4 deficiency was shown to induce mitochondrial swelling and accumulation of mitochondrial ROS – as well as NOS uncoupling and contractility defects – thus linking BH_4 with mitochondrial redox signalling (Ceylan-Isik et al., 2009). Furthermore, BH_4 was detected in rat cardiac mitochondria, and in response to cardiac pressure overload BH_4 levels were decreased whereas oxidised biopterins were elevated (Shimizu et al., 2013). This was suggested to lead to NOS uncoupling and cardiac dysfunction. How BH_4 enters mitochondria is unverified, however a study investigating the binding partners of GTPCH, proposed GTPCH localisation within mitochondria due to co-immunoprecipitation with the mitochondrial protein very long-chain acyl CoA dehydrogenase (VLCAD) (Du et al., 2012). This led this group to hypothesis that BH_4 is synthesised within mitochondria, and both BH_4 and GTPCH were measured in mitochondrial fractions from rat liver in this study (Du et al., 2012).

1.4.5 BH_4 deficiency in disease

BH_4 deficiency results from either decreased synthesis or oxidation to BH_2 and is observed in many cardiovascular and neurological diseases. In vascular pathogenesis endothelial dysfunction is caused by low levels of NO and high levels of superoxide produced by uncoupled eNOS when BH_4 levels are insufficient for catalysis (Landmesser et al., 2003; Vásquez-Vivar et al., 1998). The importance of endothelial BH_4 was confirmed using a specific knockout of *Gch1* in endothelial cells which proved that abolishing BH_4 synthesis in this cell type led to elevated blood pressure in mice (Chuaiphichai et al., 2014). Furthermore, increased BH_4 production through endothelial *Gch1* overexpression reduced endothelial dysfunction and atherosclerosis in ApoE mice (Alp et al., 2004). Oxidation of BH_4 to BH_2 by peroxynitrite is the predominant mechanism reducing BH_4 bioavailability in dysfunctional endothelium (Landmesser et al., 2003; Milstien and Katusic, 1999). The BH_4:BH_2 ratio is a key determinant of eNOS function as BH_2 competes for the BH_4 binding site but does not support catalysis (Crabtree et al., 2008, 2009a; Vásquez-Vivar et al., 2002) and results in a feed forward exacerbation of eNOS uncoupling, BH_4 oxidation and an overall increasingly oxidative environment.

Dopamine deficiency resulting from decreased BH_4 levels due to mutations in the GTPCH gene, *GCH1*, lead to motor disorders such as Dopamine-responsive dystonia (Ichinose et al., 1994), and single nucleotide polymorphisms have been linked with Parkinson's disease (Mencacci et al., 2014; Nalls et al., 2014). Mutations leading to disrupted synthesis of the enzymes required for both biosynthesis and recycling of BH_4 have been attributed to BH_4 deficient hyperphenylalaninaemia, which displays metabolic and neurological abnormalities (Citron et al., 1993; Dianzani et al., 1998; Thöny et al., 1994).

1.4.6 Therapeutically augmenting BH_4 levels

BH_4 supplementation has been successful at treating patients with hyperphenylalaninaemia caused by BH_4 deficiencies (Levy et al., 2007). Increasing BH_4 levels through transgenic overexpression of endothelial GTPCH has been effective at normalising endothelial function and ROS production in mouse models of diabetes and atherosclerosis (Alp et al., 2003, 2004). Therefore, as a promising therapeutic target for patients with endothelial dysfunction, clinical trials of BH_4 supplementation have been carried out with varying degrees of success. Acute infusion of high levels of BH_4 improved endothelium dependent relaxation and vasodilation in chronic smokers, aging vessels and patients with hypercholesterolaemia, hypertension or coronary artery disease (Heitzer et al., 2000; Higashi et al., 2002, 2006; Maier et al., 2000; Stroes et al., 1997). However, a study of chronic oral BH_4 administration to coronary artery disease patients had no beneficial effects on endothelial function and superoxide production (Cunnington et al., 2012). Although this study elevated plasma and vascular BH_4 levels it also raised BH_2 levels, highlighting that a major limitation of BH_4 supplementation is the unavoidable systemic and vascular oxidation of BH_4 to BH_2 (Cunnington et al., 2012). It is also of note that a discordance between plasma and vascular BH_4 levels has been reported, with decreased vascular but increased plasma levels in patients with coronary artery disease (Antoniades et al., 2007). This correlates with plasma inflammatory markers and is probably related to increased pathological inflammation which induces *GCH1* expression in many cell types (Antoniades et al., 2007), but it also suggests that elevating plasma BH_4 is ineffective at replenishing endothelial BH_4 content. This may have implications for pharmacological supplementation methods and even if BH_4 enters dysfunctional endothelial cells, the already high ROS levels leading to its oxidation also need to be overcome. Moving forward, a combination of more stable BH_4 preparations and targeted antioxidants to prevent oxidation at the relevant cellular locations could be more effective at treating endothelial dysfunction and vascular disease.

1.4.7 Evidence of non-cofactor roles for BH_4

BH_4 is oxidised by reactive species – particularly peroxynitrite (Laursen et al., 2001) – and has been shown to have antioxidant effects as well as being a cofactor for several enzymes. It scavenges superoxide in solutions and was suggested to protect dopaminergic neurons from oxidative damage by this mechanism (Nakamura et al., 2001). Interestingly, there have been other reports indicating that non-cofactor roles of BH_4 may have significance in cellular function. It is well known that eNOS produces superoxide rather than NO under conditions of BH_4 deficiency (Vásquez-Vivar et al., 1998); however, it has previously been shown that eNOS only accounts for a small proportion of the elevated superoxide generated following BH_4 depletion in fibroblasts stably co-transfected with eNOS and tetracycline repressible *GCH1* plasmids (Crabtree et al., 2009a). This study also showed that depletion of BH_4 in fibroblasts stably transfected with *GCH1* alone led to elevated superoxide, therefore presenting strong evidence of a NOS-independent ROS source that was regulated by BH_4 levels. Furthermore, BH_4 deficient macrophages were shown to have elevated ROS levels that were insensitive to iNOS inhibitors – therefore, also indicating an alternative BH_4 sensitive ROS source that remains unidentified (McNeill et al., 2015).

In addition to the NOS enzymes, other potential sites of ROS generation include mitochondria, NADPH oxidases, and xanthine oxidase. The presence of BH_4 inside mitochondria has previously been described (Du et al., 2012; Rembold and Buff, 1972a; Shimizu et al., 2013), and it was shown to act as a mitochondrial superoxide scavenger in fibroblasts and to decrease respiratory function at high levels in cardiomyocytes (Nakamura et al., 2001; Sethumadhavan et al., 2016), in both cases acting via NO-independent mechanisms. It is thus logical to hypothesise that BH_4 has a role in regulating mitochondrial redox signalling and function in endothelial cells and macrophages, and that this can occur independent from – as well as through – its NOS cofactor function.

1.5 Hypotheses and aims

1.5.1 Hypothesis

The work in this thesis tested the hypothesis that BH_4 levels regulate novel pathways including mitochondrial redox signalling and function in endothelial cells and inflammatory macrophages. These roles of BH_4 were hypothesised to occur independent from – as well as through – its NOS cofactor function.

It is of note that the specific hypotheses outlined in each chapter evolved during the study. The initial inhibitor screen identifying mitochondria as the major source of elevated superoxide produced by BH_4 deficient endothelial cells led to further hypotheses that BH_4 levels modulated mitochondrial function and metabolism.

1.5.2 Aims

This study used BH_4 deficient endothelial cells and inflammatory bone marrow derived macrophages to identify novel pathways modulated by BH_4. In particular, the role of BH_4 in mitochondrial redox signalling and function was investigated. Fibroblasts and macrophages devoid of NOS were used to examine the NOS-independent effects of BH_4. The specific aims were:

- To identify novel pathways modulated by BH_4.
- To investigate the effects of BH_4 deficiency on mitochondrial ROS production from endothelial cells and macrophages, and whether changes occurred independent from NOS function.
- To investigate the effects of BH_4 deficiency on mitochondrial function and metabolism, and whether changes occurred due to loss of NO signalling.

Chapter 2:
Materials and Methods

Chapter 2: Materials and methods

This chapter outlines the general methods used in this thesis. Individual results chapters will provide descriptions of techniques optimised or used exclusively in those chapters.

2.1 Cell culture

2.1.1 Culture conditions

All cell lines and primary cells were cultured using aseptic technique in humidified incubators at 37 °C with 5% CO_2.

2.1.2 Cell lines

2.1.2.1 sEnd.1 cells

sEnd.1 cells were a kind gift from Professor John Garthwaite at University College London (passage 4 stocks from UCL). They are an adherent murine endothelial cell line which were previously developed from subcutaneous endothelial cells transformed with polyoma virus middle T-antigen oncogene (Williams et al., 1988). sEnd.1 cells were cultured in Dulbecco's modified Eagle's medium (DMEM, Sigma) containing glucose (25 mM) and supplemented with L-glutamine (2 mM), penicillin (100 units/ml), streptomycin (0.1 mg/ml) and 10% fetal bovine serum (FBS) termed ‘Complete media’.

2.1.2.2 TET and GCH cells

TET and GCH cell lines were previously established and used by the Channon laboratory as a model system of regulatable GTPCH synthesis and therefore BH_4 production (Crabtree et al., 2009a). Murine NIH 3T3 fibroblast cells were previously stably transfected with a *tet*-off transactivator construct (TET cells) and a plasmid encoding hemagglutinin tagged human *GCH1* under the control of a tetracycline-response element (TRE) (GCH cells). In the presence of a tetracycline antibiotic, binding of the transactivator to the TRE is blocked,

and transcription of *GCH1* is prevented. TET cells were used as a control to assess the effects of the tetracycline antibiotic doxycycline. The *tet*-off transactivator construct also encoded a hygromycin resistance gene and the *GCH1* construct contained a neomycin resistance gene. To maintain selection TET cells were therefore cultured in Complete media with the addition of hygromycin (200 μg/ml; Sigma), and GCH cells were cultured in this media with the addition of geneticin (200 μg/ml; Sigma). Where appropriate, doxycycline (1 μg/ml) was added to TET and GCH cell culture media for at least 72 hours to abolish transcription of *GCH1* mRNA and deplete BH_4 levels.

2.1.2.3 Maintenance of cell lines

Cells were cultured in the specified media in sterile tissue culture treated T175 flasks. At around 90% confluency medium was removed, cells were washed in warm calcium chloride and magnesium chloride free phosphate buffered saline (PBS) and 5 ml trypsin was added to cover cells. Cells were incubated in trypsin for 5 minutes at 37 °C to detach and 10 ml of Complete media was added to create a cell suspension and neutralise trypsin. Cells were pelleted at 500 x g for 5 minutes and resuspended in media. One fifth of the resuspended cells were re-seeded into T175 flasks containing growth media to continue culture. Alternatively, cells were counted using the Cellometer Auto 2000 (Nexcelom Bioscience) and seeded at the required density for assays or transfections in flasks or 6 well plates.

2.1.3 Primary cells

2.1.3.1 Bone marrow derived macrophages

Culture of bone marrow derived macrophages was optimised and outlined in Chapter 4.

2.2 Animals

All animal maintenance and harvesting was carried out by the colony managers Mr Ashley Hale (a research assistant within the group), Dr Surawee Chuaiphichai and Dr Eileen McNeill (postdoctoral researchers within the group) and staff in the Functional Genomics Facility (Wellcome Centre for Human Genetics) in accordance with the UK Home Office Animals (Scientific Procedures) Act 1986 under Project Licence 30/3080. Mice were culled by a Schedule 1 method of humane killing, by cervical dislocation.

2.2.1 Housing and diet

Mice were housed in individually ventilated cages in a Specific Pathogen Free (SPF) environment in the Functional Genetics Facility at the Wellcome Centre for Human Genetics, University of Oxford, UK. Temperatures were maintained at 20 - 22 °C with 12-hour light/dark cycles. Mice were given access to standard chow (19.67% protein, 4.13% oil and 3.22% fibre; B & K Universal Ltd, Aldbrough, UK) and sterile water *ad libitum*.

2.2.2 Generation of $Gch^{fl/fl}$Tie2cre mice

Global *Gch1* deficiency is embryonically lethal (Douglas et al., 2014), so mice containing a *Gch1* conditional KO (floxed) allele were generated by our laboratory using the Cre/loxP strategy as described previously (Chuaiphichai et al., 2014; McNeill et al., 2015). In brief, constructs were created with loxP sites flanking the exons encoding the active site of *Gch1* (exons 2 and 3). Homologous recombination in embryonic stem cells generated $Gch1^{fl/fl}$ mice (termed $Gch^{fl/fl}$ mice hereafter) which were back crossed onto a C57BL6/J background. To produce mice with specific *Gch1* KO in endothelial and myeloid cells, $Gch^{fl/fl}$ mice were bred with Tie2cre transgenic mice in which Cre recombinase is driven to splice loxP sites specifically in these cell types. As the Tie2cre transgene is active in the female germline, only male Tie2cre and female $Gch^{fl/fl}$ animals were used in breeding pairs to produce

Gch1$^{fl/fl}$Tie2cre mice (termed Gch$^{fl/fl}$Tie2cre mice hereafter). Experiments were performed using bone marrow isolated from 10-16 weeks old adult male and female Gch$^{fl/fl}$Tie2cre mice and their Gch$^{fl/fl}$ littermates. Mice were genotyped according to the published protocol outlined in **Section 2.3.3** (Chuaiphichai et al., 2014; McNeill et al., 2015).

2.2.3 iNOS KO mice

Nos2$^{-/-}$ (iNOS KO) mice were purchased from The Jackson Laboratory (*Nos2*^{tm1Lau}, Cat#002609). Homozygous mutants with a neomycin cassette replacing exons 12 and 13 of the *Nos2* gene were created by Dr Victor Laubach (University of Virginia) and targeted KOs were made on a C57BL6/J background.

2.3 DNA techniques

2.3.1 DNA extraction from cell pellets

DNA was extracted from cell pellets using the DNeasy Blood and Tissue kit (Qiagen) following the manufacturer's protocol.

2.3.2 DNA extraction from ear notches

Ear notches were incubated in alkaline lysis buffer (Sodium hydroxide (25 mM) and EDTA (0.2 mM)) at 95 °C for 30 minutes to extract DNA. Samples were cooled to 4 °C briefly, then an equal volume of neutralisation buffer (Tris-HCl (40 mM)) was added and DNA was used for PCR reactions.

2.3.3 Genotyping PCR

Mice were genotyped using polymerase chain reaction (PCR) and DNA extracted from ear notches or bone marrow pellets. Genotyping was carried out by Mr Ashley Hale and representative gels are shown in Figure 2.1.

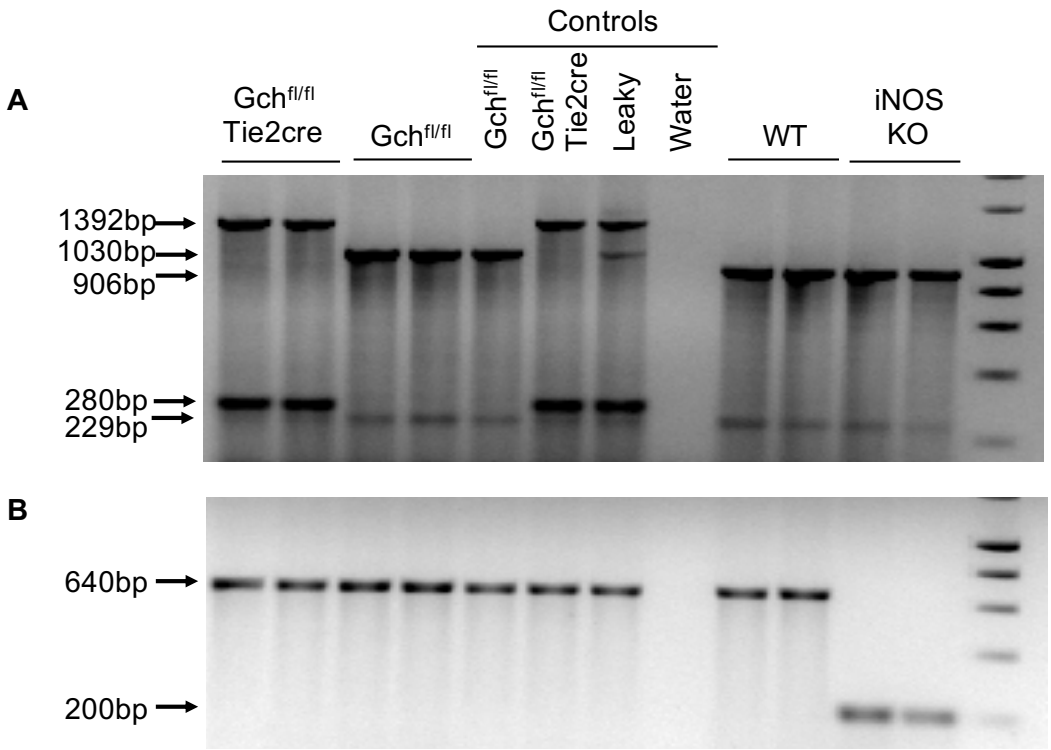


Figure 2.1 Genotyping Gch$^{fl/fl}$Tie2cre and iNOS KO mice

Representative genotyping gels. (A) PCR products from *Gch1* and Tie2cre reactions were separated by electrophoresis. Wild type (WT) *Gch1* products (906 bp) were observed in WT and iNOS KO samples, floxed *Gch1* products (1030 bp) were observed in Gch$^{fl/fl}$ samples and excised *Gch1* products (1392 bp) were observed in Gch$^{fl/fl}$Tie2cre samples. The Tie2cre reaction products were 280 bp in Gch$^{fl/fl}$Tie2cre samples but 229 bp in Tie2cre negative samples (Gch$^{fl/fl}$, WT and iNOS KO). (B) PCR products from iNOS reactions were 640 bp in samples containing wild type *Nos2* (WT, Gch$^{fl/fl}$ and Gch$^{fl/fl}$Tie2cre) but 200 bp in mutant *Nos2* samples from iNOS KO mice. All samples were compared to a molecular weight marker (final lane) and samples containing water instead of DNA were included to exclude contamination. Known Gch$^{fl/fl}$, Gch$^{fl/fl}$Tie2cre and incompletely excised *Gch1* ('Leaky') samples were included as positive controls for *Gch1* and Tie2cre reactions.

2.3.3.1 Gch$^{fl/fl}$Tie2cre mice

The primers used for the *Gch1* excision PCR were:

Gx5128 (Forward): 5'- GTCCTTGGTCTCAGTAAACTTGCCAGG -3'

Gch New (Reverse): 5'- GCCCAGCCAAGGATAGATGCA -3'

Pri5 (Forward): 5'- GCTCATCCCCCACACTTGTCT -3'

Primer stocks were made up at 100 µM. The PCR reaction mix (25 µl) consisted of 2 µl crude DNA stock, 9.5 µl water, 12.5 µl (2x) Biomix Red (Bioline), 0.25 µl Gx5128 primer, 0.5 µl Gch new primer and 0.25 µl Pri5 primer. The PCR reaction was run on a Thermocycler following the protocol outlined in Table 2.1. The expected PCR product sizes were: Floxed *Gch1* 1030 base pairs (bp), Excised *Gch1* 1392 bp, Wild type *Gch1* 906 bp (Figure 2.1A).

	Temperature (°C)	Time (mins or secs)
	94	10 mins
35 cycles	94	30 secs
	63.5	30 secs
	68	1 min
	68	5 mins
	10	5 mins

Table 2.1 Thermocycler settings for *Gch1* genotyping PCR

The primers used for the Tie2cre PCR were:

S1XA (Forward): 5' - GCATAACCAGTGAAACAGCATTGCTG - 3'

S1XB (Reverse): 5' - GGACATGTTCAGGGATCGCCAGGCG - 3'

EMcN_HPRTF (Forward): 5'- CATCGCATAAACTGGGTGTG - 3'

EMcN_HPRTR (Reverse): 5'- TGAATCCCAAGCCATCTAGG - 3'

Primer stocks were made up at 100 µM. The PCR reaction mix (25 µl) consisted of 9 µl water, 12.5 µl (2x) Biomix Red (Bioline), 0.5 µl $MgCl_2$ (50 mM stock), 0.25 µl each primer and 2 µl crude DNA. The PCR reaction was run on a Thermocycler following the protocol outlined in Table 2.2. The expected PCR product sizes were: Tie2cre 280 bp, Wild type 229 bp (Figure 2.1A).

	Temperature (°C)	Time (mins or secs)
	94	7 mins
30 cycles	95	30 secs
	55	30 secs
	72	1 min
	72	10 mins
	10	5 mins

Table 2.2 Thermocycler settings for Tie2cre genotyping PCR

2.3.3.2 iNOS KO mice

The primers used to genotype WT and iNOS KO mice were:

17864 (WT Forward): 5' - TCCGATTTAGAGTCTTGGTGA - 3'

17864 (Reverse): 5' - TCACCACCAGCAGTAGTTGC - 3'

oIMR6218 (KO Forward): 5' - CCTTCTATCGCCTTCTTGACG - 3'

Primer stocks were made up at 10 µM. The PCR reaction mix (25 µl) consisted of 2 µl crude DNA, 6.5 µl water, 12.5 µl (2x) Biomix Red (Bioline), 1 µl WT forward primer, 1 µl KO forward primer and 2 µl Reverse primer. The PCR reaction was run on a Thermocycler

following the protocol outlined in Table 2.3. The expected PCR product sizes were: WT *Nos2* 640 bp, Mutant *Nos2* 200 bp (Figure 2.1B).

	Temperature (°C)	Time (mins or secs)
	95	4 mins
30 cycles	95	40 secs
	57	30 secs
	72	30 secs
	72	10 mins
	10	5 mins

Table 2.3 Thermocycler settings for iNOS KO genotyping PCR

2.3.4 Gel electrophoresis

PCR products were run on 2% agarose gels made in TAE buffer (Tris acetate (2 M) and Na_2EDTA (100 mM)) with addition of ethidium bromide (0.004%). Gels were run at 120 V for 60 minutes in TAE running buffer and DNA was visualised using UV illumination. An outer lane running the Bioline hyperladder I (Bioline) was used to determine the size of PCR products.

2.4 RNA techniques

All RNA techniques were carried out using filter tips, molecular biology grade DNase and RNase free water on a bench cleaned with RNase*Zap* RNase Decontamination Solution (Thermo Fisher Scientific) and DNA*Zap* PCR DNA Degradation Solutions (Thermo Fisher Scientific) to avoid contamination with nucleic acid or RNase.

2.4.1 RNA extraction and quantification

Cells grown in 6 well plates were harvested directly into 1 ml TRIzol Reagent (Thermo Fisher Scientific) by scraping and transferred into Eppendorf tubes which were stored at -80 °C. To extract RNA TRIzol samples were defrosted and incubated at room temperature for 5-10 minutes before adding 200 µl chloroform and vortexing. Samples were incubated for 2 minutes at room temperature before centrifugation at 12,000 x g for 15 minutes at 4 °C. The transparent upper phase was transferred to a fresh tube and an equal volume (around 450 µl) of 70% ethanol was added and vortexed. RNA was extracted using an RNeasy Mini Kit (Qiagen) using the manufacturer's protocol after transfer to RNeasy Mini spin columns. At the end RNA was eluted from the column in RNase-free water and kept on ice. RNA levels were quantified by measuring the absorbance at 260 nm using a NanoDrop and RNA purity was assured by a 260 nm to 280 nm absorbance ratio of around 2.

2.4.2 Generation of cDNA by RT-PCR

Using reverse transcriptase PCR (RT-PCR) RNA was converted into complementary DNA (cDNA) using a QuantiTect Reverse Transcription Kit (Qiagen). To eliminate contamination from genomic DNA, RNA samples were first incubated with gDNA Wipeout Buffer (1000 ng template RNA and 2 µl gDNA Wipeout Buffer made up to 14 µl with RNase-free water) for 2 minutes at 42 °C in the thermocycler. Mastermix containing reverse transcriptase and primers (1 µl Quantiscript Reverse Transcriptase, 1 µl RT Primer Mix and 4 µl Quantiscript RT Buffer) were added to samples. The protocol on the thermocycler was continued at 42 °C for 30 minutes to generate cDNA and 95 °C for 3 minutes to inactivate the reverse transcriptase. Negative control samples replacing Quantiscript Reverse Transcriptase with RNase-free water (-RT) were included to reveal possible genomic DNA contamination. At this stage the resulting cDNA was at 50 ng/µl and stored at -20 °C until quantitative real time RT-PCR (qRT-PCR) was performed.

2.4.3 qRT-PCR primers

To perform qRT-PCR, TaqMan gene expression assays (Applied Biosystems) were used (Table 2.4), and contained primers and probes designed to span exon-exon junctions complementary to the target cDNA sequence. Probes annealed to a sequence of target DNA between the forward and reverse primers, and were labelled with a 5' 6-carboxyfluorescien (FAM) reporter fluorophore. The fluorophore remained quenched by close proximity of a 3' quencher until primer extension led to cleavage by the 5' exonuclease activity of Taq polymerase. No longer quenched, fluorescence from the fluorophore was detectable and proportional to the amount of cDNA present.

Assay	Assay ID
TaqMan murine *Il1b* assay	Mm00434228_m1
TaqMan murine *Ndufv2* assay	Mm01239727_m1
TaqMan murine *Slc2a1* assay	Mm00441480_m1
TaqMan murine *Irg1* assay	Mm01224532_m1
TaqMan murine *Idh1* assay	Mm00516030_m1
TaqMan murine *Idh2* assay	Mm00612429_m1
TaqMan murine *Gapdh* assay	Mm99999915_g1

Table 2.4 Details of TaqMan assays used in qRT-PCR reactions

2.4.4 Quantitative real-time RT-PCR

cDNA was diluted from 50 ng/µl to 2.2 ng/µl in RNase-free water. 11.25 µl of cDNA (25 ng) was pipetted into each well of a 96 well Bio-Rad PCR plate in duplicate, as well as –RT and water samples as negative controls for each gene expression assay to indicate contamination of the RT-PCR reaction and qRT-PCR reaction respectively. Mastermixes for each gene expression assay were made up of 12.5 µl 2x TaqMan Universal Master Mix and 1.25 µl 20x Taqman gene expression assay (Totalling 13.75 µl) and were added to each

well. For each sample a *Gapdh* gene expression assay was included as a house keeping gene to control for sample variability. Once prepared, plates were covered with an adhesive strip, centrifuged briefly and cDNA was amplified on an iCycler IQ real-time detection system (BioRad Laboratories Ltd) using the protocol outlined in Table 2.5.

	Temperature (°C)	Time (minutes)	Step
	50	2:00	Taq polymerase activation
	95	0:20	Denaturation
40 cycles	95	0:03	Annealing
	60	0:30	Extension

Table 2.5 Thermocycler settings for qRT-PCR

During the qRT-PCR reaction there was an exponential increase in product (and therefore fluorescence) until reaction components became limiting and a plateau was reached. The software determined a threshold cycle (Ct) value in the linear phase of amplification and above an arbitrary threshold set above background fluorescence. To determine relative gene expression all samples Ct values were normalised to parallel *Gapdh* Ct values and the following calculation was carried out: $2^{-\Delta Ct(\text{Gene of interest (GOI)} - \textit{Gapdh})}$

2.5 Protein detection

2.5.1 Preparation of protein lysates

Sample pellets were resuspended in lysis buffer – consisting of 10 ml CelLytic M buffer (Sigma), 1x Complete Mini EDTA-free Protease Inhibitor Cocktail tablet (Sigma) and (if required) 1x PhosSTOP Phosphatase Inhibitor Cocktail tablet (Sigma) unless an alternative lysis buffer was specified. After one freeze thaw cycle on dry ice, samples were centrifuged at 17,000 x g and 4 °C for 10 minutes. Supernatant lysates were transferred to fresh tubes and protein levels quantified using a BCA protein assay as described in **Section 2.5.2**.

2.5.2 Measuring protein content

The total protein content in each lysate was quantified using the Pierce bicinchoninic acid (BCA) Protein Assay kit (Thermo Fisher Scientific). A blank sample and BSA standards serially diluted from 4 to 0.0625 mg/ml were made up in sample buffer. 12 µl of each sample or standard was incubated with 12 µl iodoacetamide (20 mg/ml in 0.4% sodium hydroxide) in a water bath at 37 °C for 15 minutes to prevent reaction of BCA reagents with thiols, thus improving the accuracy of the assay (Hill and Straka, 1988). BCA reagents were made up according to the manufacturer's instructions (1:50 Solution A: Solution B) and 480 µl was added to each sample and standard which were incubated in a water bath at 37 °C for 30 minutes. Samples and standards were transferred in duplicate (200 µl) to clear 96 well microtiter plates and read at 590 nm. The concentration of protein within each sample was calculated using the BSA standard curve with blank correction and the mean of duplicate wells.

2.5.3 Western blotting

To prepare samples, lysates of known protein concentrations (**Section 2.5.1**) were normalised by diluting in water before adding x10 NuPAGE Sample Reducing agent (Thermo Fisher Scientific) and x4 NuPAGE LDS Sample Buffer (Thermo Fisher Scientific) to the final concentration (usually 5 µg/ml unless specified) required for analysis. Samples were incubated at 90 °C for 5 minutes to denature proteins before loading onto a gel. At this stage samples were generally stored at -20 °C, but -80 °C for detection of phosphorylated proteins.

Sodium dodecyl sulfate-poly acrylamide gel electrophoresis (SDS-PAGE) was used to separate proteins based on denatured molecular weights. Samples were heated at 90 °C for 5 minutes and loaded onto NuPAGE Novex 4-12% gradient Bis-Tris 1 mm pre-cast

polyacrylamide gels (Thermo Fisher Scientific) with 50ml 20x NuPAGE MOPS SDS Running Buffer per litre (Thermo Fisher Scientific) at a constant voltage of 200 V until sample dye reached the bottom (around 60 minutes). 6 µl of Amersham ECL Full Range Recombinant Molecular Weight Rainbow Marker (GE Healthcare Life Sciences) was included in an outer lane to estimate the mass of target proteins. Proteins were transferred from gels to PVDF membrane using a wet transfer in buffer consisting of Tris-base (3.03 g/l), glycine (15 g/l) and methanol (20%) for 90 minutes with a constant current of 300 mA.

Membranes were blocked in 5% milk in PBST (0.1% Tween in PBS) for a minimum of 1 hour at room temperature or overnight at 4 °C on a rocker. Primary antibodies (Table 2.6) against proteins of interest were incubated with membranes overnight at 4 °C on a rocker. The following day membranes were washed three times briefly in PBST followed by three 5 minute washes on a rocker. Secondary antibodies conjugated to horseradish peroxidase (HRP) (Table 2.6) were incubated with membranes for 1 hour at room temperature on a rocker. Membranes were again washed three times briefly in PBST followed by three 5 minute washes on a rocker before development using enhanced chemiluminescent (ECL) reagents, film and XOgraph developer.

Antibody	Dilution	Specificity	Species	Product information
Anti-iNOS	1:1000	Mouse	Mouse	Abcam (ab49999)
Anti-eNOS	1:1000	Mouse	Mouse	BD transduction (610269)
Anti-GTPCH	1:5000	Mouse	Rabbit	Prof S. Gross, Cornell University
Anti-β-tubulin	1:20,000	Mouse	Rabbit	Abcam (ab6046)
Anti-GAPDH	1:20,000	Mouse	Mouse	Millipore (MAB374)
Anti-NDUFV2	1:1000	Mouse	Rabbit	Abcam (ab183715)
Anti-HIF1α	1:500	Mouse	Rabbit	Novus (NB100-449)
Anti-hexokinase 2	1:1000	Mouse	Rabbit	Cell signalling (2867S)
Anti-IDH1	1:1000	Mouse	Rabbit	Cell signalling (8137S)
Anti-cytochrome C	1:1000	Mouse	Rabbit	Cell signalling (4280)
Anti-VDAC	1:1000	Mouse	Rabbit	Cell signalling (4661)
Anti-SDH (subunit A)	1:1000	Mouse	Rabbit	Cell signalling (11998)
Anti-mitofusin 2	1:1000	Mouse	Rabbit	Cell signalling (9482)
Anti-OPA1	1:1000	Mouse	Rabbit	Cell signalling (80741)
Anti-DRP1	1:1000	Mouse	Rabbit	Cell signalling (8570)
Anti-p(637)DRP1	1:1000	Mouse	Rabbit	Cell signalling (4867)
Anti-p(616)DRP1	1:1000	Mouse	Rabbit	Cell signalling (3455)
Anti-mouse-IgG-HRP	1:5000	Mouse	Rabbit	Promega (W402B)
Anti-rabbit-IgG-HRP	1:5000	Rabbit	Goat	Promega (W4011)

Table 2.6 Antibodies used for Western blot analysis of proteins

2.6 Biopterin quantification by HPLC

Biopterins were quantified using HPLC and an electrochemical detector for BH_4, and a fluorescent detector to measure BH_2 and biopterin. Samples for analysis were collected and rapidly stored at -80 °C to minimise biopterin oxidation, and prepared for HPLC analysis on ice. To analyse sample pellets (cells and mitochondria), samples were lysed in ice cold Resuspension buffer (phosphate-buffered saline (50 mM), pH 7.4, containing dithioerythritol (1 mM) and EDTA (100 μM)) and centrifuged at 17,000 x g for 15 minutes at 4 °C. Supernatants were transferred to fresh tubes. For liquid samples (such as media or FBS), samples were diluted in Resuspension buffer to the desired dilution. Subsequently, for all sample types Precipitation buffer (x10 solution made up of phosphoric acid (1 M), trichloroacetic acid (2 M) and dithioerythritol (1 mM) in PBS (50 mM), pH 7.4) was added, samples were vortexed to mix and centrifuged at 17,000 x g for 15 minutes at 4 °C. Supernatants were injected onto an isocratic HPLC system and quantified using sequential electrochemical (Coulochem III, ESA Inc.) and fluorescence (Jasco) detection. HPLC separation was performed using a 250 mm, ACE C-18 column (Hichrom) and mobile phase comprising of sodium acetate (50 mM), citric acid (5 mM), EDTA (48 μM), and dithioerythritol (160 μM) (pH 5.2) at a flow rate of 1.3 ml/min. Background currents of +500 μA and -50 μA were used for the detection of BH_4 on electrochemical cells E1 and E2, respectively. BH_2 and biopterin were measured using a Jasco FP2020 fluorescence detector. Quantification of BH_4, BH_2, and biopterin was done by comparison with authentic external standards and analysis of peak areas. All data were normalised to sample protein content using the BCA assay.

2.7 Quantification of superoxide by HPLC

Dihydroethidium (DHE) is oxidised by superoxide to form 2-hydroxyethidium which can be quantified using HPLC with a fluorescent detector (Zhao et al., 2005; Zielonka et al., 2008). DHE is also oxidised to ethidium which is detectable as a separate peak using HPLC, but this reaction is less well characterised and proposed to involve various processes including reactive molecules, oxidases and cytochromes (Zhao et al., 2005; Zielonka and Kalyanaraman, 2010). DHE (at a concentration dependent upon the cell type – to be specified in chapter specific methods) was added to live cells grown in 6 well plates in a dark tissue culture hood and incubated for 20 minutes at 37 °C in the tissue culture incubator. The reaction was stopped by washing and harvesting cells into ice cold PBS, followed by centrifugation at 400 x g for 5 minutes at 4 °C to produce pellets which were stored at -80 °C. In preparation for HPLC analysis, pellets were resuspended in 100 µl of ice cold methanol by pipetting. 100 µl of ice cold hydrochloric acid (100 mM) was added and samples vortexed, before centrifugation at 17,000 x g for 5 minutes at 4 °C. Supernatants were transferred to darkened HPLC vials protected from light and loaded into the autosampler for injection onto the HPLC or stored at -80 °C until analysis. An ODS3 reverse phase column (250 mm, 4.5 mm; Hichrom) was used to separate DHE, 2-hydroxyethidium, and ethidium over a 23 minute linear gradient from 30-50% acetonitrile applied from Mobile phase A (0.1% trifluoroacetic acid in water) to Mobile phase B (0.085% trifluoroacetic acid in acetonitrile). Peak areas were quantified and plotted as arbitrary units and considered comparable between cells of equal seeding density. Samples being compared were run during a single continuous analysis to avoid day to day HPLC variations.

2.8 Measurement of NO_x accumulation using the NO analyser

The levels of nitrite/nitrate (NO_x) produced by cells were determined using the CLD88 NO analyser (Ecophysics). Briefly, media was collected from cells following overnight incubation and stored at -80 ºC for analysis. Samples were then thawed on ice, and NO liberation from 100 µl sample media (following chemical reduction by vanadium(III) chloride (VCl_3) dissolved in HCl in the reaction chamber at 95 ºC) was measured via a chemiluminescent reaction with ozone. Quantification of NO_x accumulation was obtained by comparison with external sodium nitrate standards and normalised to protein concentration, determined by the BCA protein assay (**Section 2.5.2**).

2.9 Measurement of nitrite accumulation using the NO analyser

The levels of nitrite were determined similarly to detection of NO_x by the CLD88 NO analyser (**Section 2.8**), except potassium iodide (1 ml at 50 mg/ml) was added to acetic acid (5 ml) in the reaction chamber and maintained at room temperature throughout. The standard curve was created using sodium nitrite standards and a sodium nitrate standard curve was used to ensure nitrate was not detected.

2.10 Measurement of nitrite accumulation using the Griess assay

Culture media was centrifuged at 500 x g for 10 minutes at 4 °C to pellet cell debris, and 100 µl of supernatant was carefully transferred in duplicate into clear 96 well microtiter plates. 100 µl of Griess assay reagent was added (made up of a 1:1 mixture of Griess solution 1 (0.1% w/v N-(1-Naphthyl)ethylenediamine dihydrochloride (Sigma) in water stored at 4 °C wrapped in foil) and Griess solution 2 (1% w/v sulphanilamide (Sigma) in 5% orthophosphoric acid stored at 4 °C wrapped in foil)) and the plate was incubated at room temperature for 15 minutes before reading at 550 nm absorbance. Nitrite accumulation was determined against a standard curve prepared from a 500 mM sodium nitrite stock, serially

diluted from 100 to 3.15 μM in sample media and a blank media sample for background correction.

2.11 NOS activity assay

Conversion of arginine into citrulline was carried out by Dr Mark Crabtree and measured using radiolabelled substrates and HPLC as previously described to determine NOS activity (de Bono et al., 2007). Cells grown in 12-well plates were washed with Krebs Hepes buffer (KHB, consisting of NaCl (99 mM), KCl (4.7 mM), $MgSO_4$ (1.2 mM), KH_2PO_4 (1 mM), $CaCl_2$ (1.9 mM), $NaHCO_3$ (25 mM), glucose (11.1 mM), and Na-Hepes (20 mM)). KHB containing the arginase inhibitor nor-NOHA (5 mM) was added to the cells, and they were incubated for 15 min at 37 °C in the presence or absence of 1 mM of the competitive NOS inhibitor L-NAME (Sigma). 1 μl of ubiquitously labelled ^{14}C-arginine (1.85 MBq/ml, Hartmann Analytic) and calcium ionophore A23187 (1 μM; Sigma) was added to each well and incubated for 45 minutes (sEnd.1)/ 30 minutes (macrophages) at 37 °C. Supernatants were transferred to Eppendorf tubes and cells were lysed in 150 μl water by freeze thawing on dry ice. Lysates were transferred to the tubes containing the supernatants and trichloroacetic acid (10%) was added to precipitate protein. Samples were centrifuged at 17,000 x g for 5 minutes and supernatants were stored at -80 °C until HPLC analysis. The percentage conversion of radiolabelled arginine to citrulline was determined by resolving these molecules using HPLC fractionation (250 × 4.6 mm Supelcosil LC-SCX five cation exchange column (Sigma)) coupled with a scintillation detector (β-RAM Model 3 (Lablogic)). Mobile phases were run at 1 ml/minute with Buffer A (distilled water) for 5 minutes followed by a linear gradient from 100% Buffer A to 100% Buffer B (sodium citrate (200 mM), pH 3) over 10 minutes. Scintillant fluid (Lablogic) was mixed at a ratio of 0.5:1 after elution from the column, before passage through the detector. Standards of ^{14}C-labelled L-arginine, L-citrulline, and L-ornithine (Hartmann Analytic) were used to determine

elution times. Peak areas were determined manually and the L-NAME inhibitable percentage conversion of arginine to citrulline was determined.

2.12 Seahorse XF^{e}96 extracellular flux assays

Extracellular flux assays were carried out using a Seahorse XF^{e}96 Bioanalyzer (Agilent Technologies). Oxygen consumption rate (OCR) and extracellular acidification rate (ECAR) of the media surrounding a monolayer of live cells seeded into Seahorse XF^{e}96 microplates were measured using Seahorse XF^{e}96 FluxPacks. FluxPacks comprised 96 sensors which were lowered to 200 μm above the cells creating a transient microchamber, and fluorophores sensitive to oxygen and pH changes allowed measurements of OCR and ECAR respectively. Injection of compounds that modulate metabolism allowed metabolic parameters to be calculated. For these assays all reagents were bought from Agilent Technologies unless specified.

2.12.1 Preparation for Seahorse extracellular flux assays

The day prior to carrying out Seahorse extracellular flux assays, cells were seeded into Seahorse XF^{e}96 microplates in cell specific growth media. Seeding densities were optimised for each cell type (outlined in chapter specific methods) to achieve a monolayer of cells on the day of the assay, with basal OCR readings of around 100-200 pmol O_2/min/well to allow response to compound injections without limited oxygen levels. Also carried out the day before the assay, Seahorse XF^{e}96 FluxPacks were hydrated in 200 μl of Seahorse XF Calibrant per well, wrapped in Parafilm and incubated in a 37 °C incubator at atmospheric CO_2 levels overnight.

2.12.2 Seahorse MitoStress Test to analyse mitochondrial respiration

Seahorse MitoStress test assays contained compounds for analysis of intracellular mitochondrial function. The manufacturer's standard protocol was used after optimisation

of carbonyl cyanide-p-trifluoromethoxyphenylhydrazone (FCCP) concentrations for each cell type. On the day of the experiment Seahorse MitoStress test assay medium (pH 7.4) was made, consisting of Seahorse XF Base Medium (modified bicarbonate free DMEM with Phenol Red, pH 7.4), supplemented with glucose (10 mM, Sigma), L-glutamine (2 mM, Sigma), and sodium pyruvate (2 mM, Sigma). Culture media on cells seeded in Seahorse XF^e96 microplates was replaced with 175 µl of Seahorse MitoStress test assay media following a wash step to remove previous media. The cell plate was placed inside a bag in a 37 °C incubator at atmospheric CO_2 levels for 45 minutes to 1 hour before beginning the assay. In the meantime, oligomycin, FCCP and a combined vial of rotenone and antimycin A were reconstituted and diluted to working concentrations (cell type specific to be outlined in chapter specific methods) in MitoStress test assay media according to the manufacturer's instructions. Drugs were then loaded into injection ports of a rehydrated Seahorse XF^e96 FluxPack as follows: Port A Oligomycin, Port B FCCP and Port C Rotenone and Antimycin A. The FluxPack was loaded into the Seahorse Bioanalyzer to calibrate and once finished the cell plate was loaded, equilibrated and the MitoStress Test commenced using the settings outlined in Table 2.7.

Settings (minutes:seconds)	Basal (3 cycles)	Oligomycin (3 cycles)	FCCP (3cycles)	Rot/antimycinA (3 cycles)
Mix	3:00	3:00	3:00	3:00
Wait	0:00	0:00	0:00	0:00
Measure	3:00	3:00	3:00	3:00
Total duration	18:00	18:00	18:00	18:00

Table 2.7 Settings used to carryout Seahorse XF^e96 MitoStress Test

At the end of the assay the media was removed from the cell plate and it was retained for normalisation. Normalisation procedures varied with cell type and are outlined in chapter specific methods.

2.12.2.3 Seahorse MitoStress Test calculations

OCR readings were used to determine mitochondrial respiratory function (Figure 2.2). Baseline OCR measurements were made up of oxygen consumed by the ETC during oxidative phosphorylation as well as consumption by other oxidase enzymes. In the first injection, oligomycin inhibited ATP synthase and was used to calculate ATP-linked OCR. FCCP dissipated the proton gradient across the mitochondrial inner membrane by transporting H^+ through the membrane, thus uncoupling ATP synthesis from the ETC which then transferred electrons uninhibited and allowed mitochondrial OCR to reach its maximum. Finally, rotenone inhibited Complex I and antimycin A inhibited Complex III of the ETC, shutting down mitochondrial oxygen consumption and allowing the proportion of baseline OCR attributed to mitochondrial respiration to be calculated. A full list of the calculations are outlined in Table 2.8. For calculations the third reading in each case was used as the most stable point, with the exception of the highest reading following addition of FCCP.

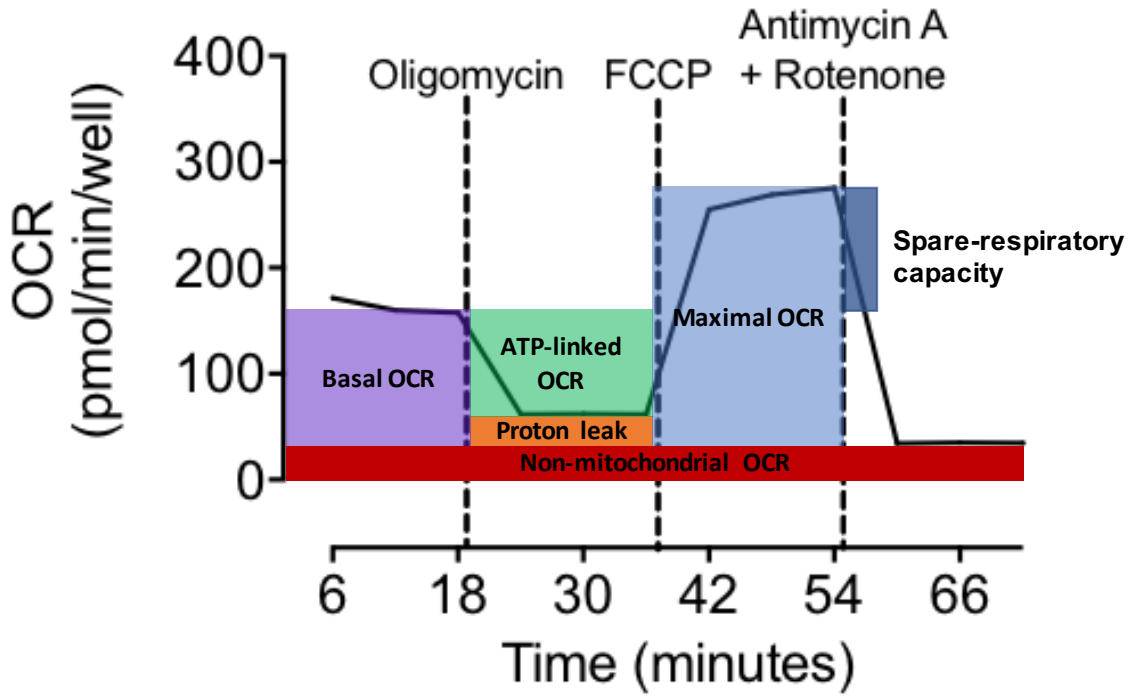


Figure 2.2 Representative MitoStress test trace and calculated parameters

Representative oxygen consumption rate (OCR) trace measured by a Seahorse XF^{e}96 Bioanalyzer during a MitoStress test assay to determine mitochondrial respiratory function. Baseline readings and readings taken following sequential injection of oligomycin, FCCP and combined rotenone/antimycin A allow determination of basal, ATP-linked, maximal, spare-respiratory capacity, proton leak and non-mitochondrial OCR.

Respiratory function parameter	Calculation
Basal OCR	Baseline - Rotenone/antimycin A
ATP-linked OCR	Baseline - Oligomycin
Maximal OCR	FCCP - Rotenone/antimycin A
Spare respiratory capacity OCR	FCCP - Baseline
Proton leak OCR	Oligomycin - Rotenone/antimycin A
Non-mitochondrial OCR	Rotenone/antimycin A

Table 2.8 Calculations to determine respiratory function

2.12.3 Glycolytic activity using ECAR

During all extracellular flux assays ECAR is determined simultaneous to OCR. During MitoStress tests ECAR reading were obtained, and ECAR has been described as an indicator of glycolytic activity as it is largely due to proton extrusion following lactate production, which is a glycolytic end-point. 2-deoxyglucose (50 mM; Sigma) inhibits hexokinase oxidation of glucose and was included in the final injection port (Port D) to investigate glucose metabolism. ECAR inhibited by 2-deoxyglucose was considered basal glycolysis. However this is an imperfect indicator of glycolysis and should not be taken as a definitive indicator of glycolysis. There are other sources of media acidification including CO_2 from the TCA cycle (Mookerjee et al., 2015), and a subsequent assay was used to assess this in later experiments as described in Chapter 5.

2.13 Mitochondrial isolation

Certain experiments required mitochondrial fractions, so an isolation method was selected by comparing fractionation using the Qproteome Mitochondria Isolation Kit (Qiagen) and a published protocol (Frezza et al., 2007), with Western blot analysis to assess purity of mitochondrial fractions.

2.13.1 Qproteome kit isolation

Cells grown to confluency in T175 flasks (or equivalent area) were harvested by trypsinisation and pelleted at 400 x g and 4 °C for 5 minutes. Mitochondria were then directly isolated using the Qproteome Mitochondria Isolation Kit (Qiagen), as per the manufacturer's instructions. In brief, cells were washed in a PBS resuspension, pelleted and resuspended in 1 ml of Lysis Buffer. Cells were incubated on an end over rotator for 10 minutes at 4 °C, and spun at 10,000 x g for 10 minutes at 4 °C with the resulting supernatant discarded as Fraction 1 'Cytosolic fraction'. The pellet was resuspended in 1.5 ml of

Disruption Buffer, homogenised by passing 10 times through a 25 gauge needle, and spun again at 10,000 x g for 10 minutes at 4 °C. The supernatant was transferred to a fresh tube and the pellet discarded as Fraction 2 'nuclei, cell debris and unbroken cells'. The supernatant was centrifuged at 6000 x g for 10 minutes at 4 °C with the resulting pellet forming the 'Mitochondrial Fraction'. The supernatant was discarded as Fraction 3 'microsomes and plasma membrane'. All steps were carried out on ice or 4 °C and mitochondrial pellets were stored at -80 °C for analysis.

2.13.2 Frezza et al. isolation

Cells grown to confluency in T175 flasks (or equivalent area) were harvested by trypsinisation and pelleted at 400 x g and 4 °C for 5 minutes. Mitochondria were then directly isolated using the Frezza et al. published protocol for isolation of mitochondria from fibroblasts (Frezza et al., 2007). In brief, a cell pellet was resuspended in 3 ml of ice-cold Isolation Buffer (Tris-MOPS (10 mM), EGTA/Tris (10 mM), sucrose (200 mM); pH 7.4), homogenised with 30 strokes in a cold Teflon pestle, and centrifuged at 600 x g for 10 minutes at 4 °C. The pellet was discarded as 'Fraction 1', while the supernatant was collected and centrifuged at 7000 x g for 10 minutes at 4 °C. The resulting supernatant was discarded as 'Fraction 2', and the pellet was resuspended in 200 µl Isolation Buffer. The sample was centrifuged again at 7000 x g for 10 minutes at 4 °C, and the supernatant was discarded as 'Fraction 3', while the pellet was stored for further analysis as the 'Mitochondrial fraction'.

2.13.3 Comparison of methods

The isolation methods described in **Sections 2.13.2 and 2.13.3** were compared for purity using Western blot analysis of fractions (Figure 2.2A and B). This revealed an enrichment of mitochondrial markers in 'Mitochondrial fractions' collected using both protocols. However, comparatively more cytosolic (GAPDH), endoplasmic reticulum (KDEL) and membrane proteins (Tie2 and CD102) in 'Mitochondrial fractions' collected using the

Frezza et al. protocol led to the decision to use the purer Qproteome mitochondria in future experiments. Interestingly, GTPCH was detected in mitochondrial fractions collected using both protocols (Figure 2.2C), suggesting its presence or association with mitochondria as previously suggested (Du et al., 2012).

2.13.4 Yield of isolated mitochondria

The mitochondrial content of endothelial cells in known to be relatively low and was shown to be 2-11% depending upon location in rats (Blouin et al., 1977; Oldendorf et al., 1977). When the Qproteome isolation kit was used to isolate mitochondria from sEnd.1 cells the yield was around 6.25% of the starting material – around 0.0625 mg of mitochondria was isolated per 1 mg of starting cells (by protein quantification). Based on the above estimates in rats, it is plausible that this 6.25% yield represents the mitochondrial content of sEnd.1 cells. However, mitochondrial isolation methods have been shown not to efficiently isolate 100% of cellular mitochondria (Fernández-Vizarra et al., 2010), and carrying out citrate synthase assays on cells before isolation and the resulting mitochondrial isolates would allow estimation of the proportion actually isolated.

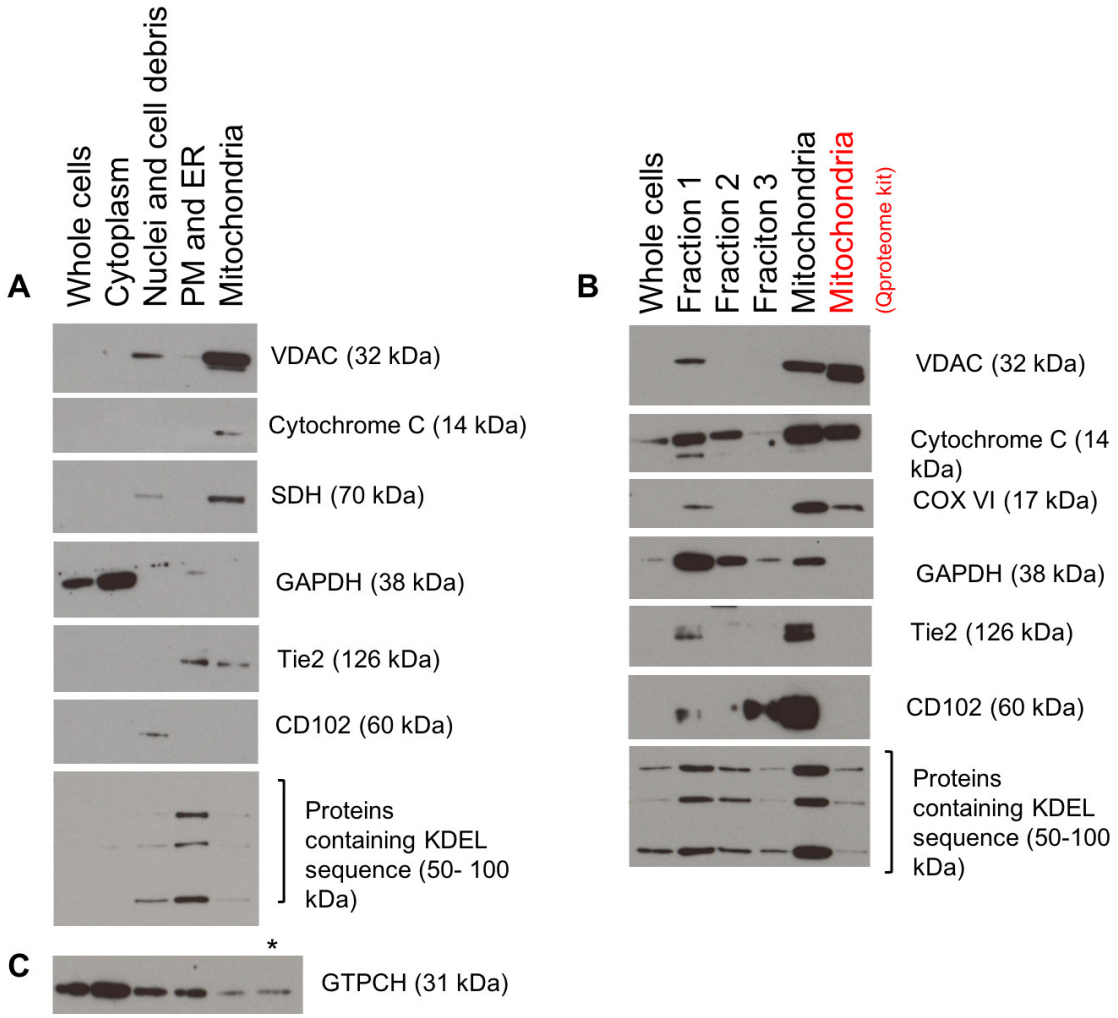


Figure 2.2 Comparison of mitochondria isolation protocols

Mitochondrial fractions were collected using (A) the Qproteome isolation kit and (B) the Frezza et al. protocol. Western blot analysis of 5 µg of fractions collected at all stages are shown, and (B) included a mitochondrial fraction from the Qproteome kit for comparison of purity with the Frezza et al. protocol. Mitochondrial markers included VDAC (outer mitochondrial membrane), cytochrome C (intermembrane space), SDH and COX IV (inner mitochondrial membrane). GADPH (cytosolic), KDEL containing proteins (endoplasmic reticulum), Tie2 and CD102 (plasma membrane) were used as markers of contamination from other cellular components. (C) Western blot analysis of GTPCH in all fractions from the Qproteome isolation protocol (as labelled in A) with inclusion of a mitochondrial fraction from the Frezza et al. protocol in the final lane labelled *.

2.14 Statistical Analysis

All statistical analyses were carried out using Microsoft Excel (Microsoft) and GraphPad Prism 7 (GraphPad Inc.) software. Data were expressed as mean ± standard error of the mean (SEM), apart from optimisation data involving low sample sizes where data were presented as ± range. A Student's t-test was used to compare two groups affected by one single variable. Two-way ANOVA was used to compare multiple data groups affected by two independent variables, with Tukey's post-test to compare groups with each other. Differences were considered statistically significant at *P* values of * $P<0.05$, ** $P<0.01$, *** $P<0.001$.

2.15 Acknowledgement of collaborations

The majority of experiments and their analysis were carried out by myself, and care has been taken to acknowledge all assistance from others in generating and analysing data where appropriate throughout this thesis. However, for clarity a table transparently outlining these collaborations is included (Table 2.9).

Collaborator	Experimental details
Mr Ashley Hale	All animal maintenance, harvesting, genotyping
Dr Surawee Chuaiphichai	$Gch^{fl/fl}$Tie2cre animal maintenance and harvesting
Dr Eileen McNeil	iNOS KO animal maintenance and harvesting
Dr Mark Crabtree	Radioactive NOS activity assay
Dr Errin Johnson	Preparing and acquiring electron microscopy images
Prof James McCullagh	Preparation and analysis of metabolites by mass spectrometry
Metabolon Inc.	Preparation and analysis of metabolites by mass spectrometry
Mr Simon Davis	Proteomic analysis of peptides by mass spectrometry
Dr Roman Fischer	Analysis proteomic data – from raw mass spectrometric chromatograms to determining scaled abundances
Dr Anuj Goel	Statistical analysis of proteomic data
Dr Jyoti Patel	FACS experiment and analysis
Dr Thomas Nicol	Complex I activity assay
Dr Marina Diotallevi	IDH and aconitase activity assays

Table 2.9 Details and acknowledgment of collaborators

All collaborators were part of the University of Oxford apart from the external company Metabolon Inc.

Chapter 3:
Investigating the effects of BH_4 deficiency on mitochondrial function and redox signalling in endothelial cells

Chapter 3: Investigating the effects of BH_4 deficiency on mitochondrial function and redox signalling in endothelial cells

3.1 Introduction

NO regulates vasodilation, has anti-atherogenic properties and is important for the maintenance of vascular health. *De novo* synthesis of NO by eNOS within endothelial cells requires BH_4 as a cofactor, and loss of BH_4 leads to decreased NO bioavailability and endothelial dysfunction. Endothelial dysfunction is involved in the pathogenesis of vascular diseases such as atherosclerosis, and is also characterised by elevated ROS levels. BH_4 levels are a critical determinant of endothelial NO-redox balance through eNOS, as it is not only required for NO synthesis, but in the absence of BH_4 eNOS becomes uncoupled and generates superoxide instead (Vásquez-Vivar et al., 1998). Loss of BH_4 occurs due to decreased synthesis by GTPCH or oxidation to BH_2 (Landmesser et al., 2003), and mice with targeted knockout of *Gch1* in endothelial cells have elevated blood pressure (Chuaiphichai et al., 2014). Encouragingly, specific transgenic augmentation of endothelial *Gch1* was sufficient to normalise endothelial function, eNOS coupling, and ROS production in mouse models of diabetes and atherosclerosis (Alp et al., 2003, 2004). However, attempts to restore BH_4 levels through supplementation have been limited by systemic oxidation and inefficient endothelial uptake (Cunnington et al., 2012). This highlights the need for alternative approaches to therapeutically target BH_4 deficiency in vascular disease, and exploring the wider roles of BH_4 has the potential to provide novel targets.

There are several lines of evidence that BH_4 has roles outside of its enzyme cofactor functions. In one such example, our laboratory has demonstrated that uncoupled eNOS only represents a fraction of the elevated superoxide generated following BH_4 depletion in fibroblasts stably co-transfected to produce eNOS and tetracycline repressible GTPCH (Crabtree et al., 2009a). Furthermore, this study showed that depletion of BH_4 in fibroblasts

stably transfected with *GCH* alone led to elevated superoxide, therefore presenting strong evidence of a NOS-independent ROS source that was regulated by BH_4 levels. Mitochondria and NOX enzymes are also sites of superoxide production in dysfunctional endothelial cells (Dikalov et al., 2014) but are so far not linked with BH_4 deficiency. However, BH_4 was shown to act as a mitochondrial superoxide scavenger in fibroblasts and to decrease respiratory function at high levels in cardiomyocytes (Nakamura et al., 2001; Sethumadhavan et al., 2016), acting via NO-independent mechanisms. Furthermore, there are several reports indicating the presence of BH_4 inside mitochondria (Du et al., 2012; Rembold and Buff, 1972a; Shimizu et al., 2013). This chapter aimed to identify the NOS-independent source of superoxide induced by BH_4 depletion of endothelial cells and hypothesised it to be mitochondrial in origin. The role of BH_4 in modulating mitochondrial structure, function and metabolism were also explored.

3.2 Aims and hypotheses

3.2.1 Hypotheses

In previous work from our laboratory, increased superoxide generation from a NOS-independent source was described in fibroblasts following BH_4 depletion. In this chapter it was hypothesised that the role of BH_4 in endothelial cells is wider than its essential eNOS cofactor function and that BH_4 contributes to regulating mitochondrial function and redox state.

3.2.1 Aims

This study used RNA interference (RNAi) targeting *Gch1* to deplete BH_4 in endothelial cells and investigated the effects of BH_4 deficiency on mitochondrial redox signalling and metabolism. The specific aims were:

- To investigate whether mitochondria were the major source of increased superoxide production in BH_4 depleted endothelial cells, and whether BH_4 regulated this independent of its NOS cofactor role.
- To measure biopterin content of mitochondria from BH_4 depleted cells.
- To determine whether BH_4 deficiency led to changes in mitochondrial structure and function; including morphology, aerobic respiration and TCA cycle metabolism.

3.3 Methods

General methods were outlined in Chapter 2. Methods specific to this chapter are outlined below.

3.3.1 Gch1 targeted RNA interference

Gch1 was knocked down in sEnd.1 cells using *Gch1*-specific, ON-TARGETplus SMARTpool siRNA purchased from Dharmacon GE Life Sciences. The *Gch1* siRNA pool (subsequently referred to as Gch siRNA) contained four specific duplexes with the following sequences:

Duplex 1, GGUAGAAUGCUAAGUACGU

Duplex 2, CGAGAAGUGUGGCUACGUA

Duplex 3, GAGAAGGGAGAAUCGCUUU

Duplex 4, AGUAGUGAUUGAAGCGACA

A Non-specific (NS), ON-TARGETplus Non-targeting Control Pool of siRNA was used as a negative control (Dharmacon). Before use, 50 nmol siRNA was resuspended in 500 µl PBS and put on a shaker for 30 minutes. This 100 µM stock was aliquoted to minimise freeze thawing, and stored at -20 °C.

24 hours prior to transfection, sEnd.1 cells were seeded to reach 40% confluency the following day. (Seeding densities used were 50,000 cells/well of a 6 well plate, 500,000 cells/T75 flask, 1,000,000 cells/T175 flask). Cells were transfected with siRNA and DharmaFect1 transfection reagent (Dharmacon). To prepare the transfection mixture, solutions A and B were made (Table 3.1) and incubated at room temperature for 5 minutes before adding A to B and incubating for a further 20 minutes. The transfection mixture was

added dropwise to the cells and plates were rocked briefly to mix. Cells were incubated for 72 hours before harvesting.

Solution	Stock	1 x well of 6 well plate	1 x T75 flask	1 x T175 flask
A	100μM siRNA (μl)	2.2	16.5	38.5
	PBS (μl)	215	808.5	1886.5
	DMEM (only) (μl)	0	825	1925
B	2μM Dharmafect 1 (μl)	2	16.5	38.5
	DMEM (only) (μl)	215	1633.5	3811.5

Table 3.1 Composition of Solutions A and B for transfection of sEnd.1 cells with siRNA

3.3.2 Superoxide measurements using DHE

Measurement of 2-hydroxyethidium formation by HPLC was used to quantify superoxide production as described in **Section 2.7**. Cells grown in 6 well plates to 70–80% confluency were incubated in the presence or absence of L-NAME (200 μM), rotenone (20 μM), apocynin (100 μM), oxypurinol (100 μM), and sepiapterin (10 μM) for 30 minutes at 37 °C. DHE (25 μM) was added and cells were incubated for a further 20 minutes at 37 °C. Media was removed and cells were washed and then harvested into ice cold PBS by scraping and pelleted by centrifuging at 500 x g for 5 minutes. Cell pellets were stored at -80 °C until prepared for HPLC analysis using the protocol outlined in **Section 2.7**.

Rotenone inhibits Complex I in the ETC and inhibition of respiration can lead to cell death and detachment which may invalidate assay results if cells are washed away before analysis. GCH cells were therefore treated with increasing concentrations of rotenone to determine the optimal amount for inhibition of superoxide generation without causing cells to detach. A 20 μM rotenone treatment was deemed appropriate (Figure 3.1A) and a protein assay

carried out on attached cells from wells that were harvested in parallel to those used for HPLC analysis confirmed little change in amounts of protein and thus cell number (Figure 3.1B). Together with prior confirmation of cell adherence using microscopy (not shown) this suggested that 20 μM rotenone treatment was not causing cells to detach at this time point. Further experiments measuring respiratory function and Complex I activity in response to these concentrations of rotenone would be useful to determine whether they are inhibited in parallel to superoxide generation. Interestingly, Complex I derived superoxide does not necessarily require damage or inhibition of the respiratory chain (Pryde and Hirst, 2011).

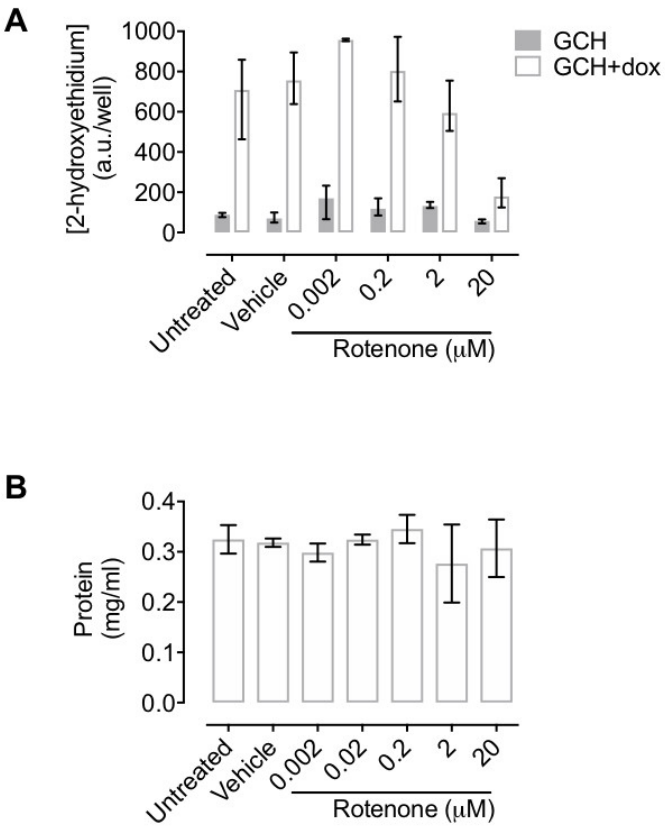


Figure 3.1 Dose response of superoxide inhibition by rotenone

GCH cells were treated with increasing levels of rotenone and incubated with DHE. (A) 2-hydroxyethidium was measured by HPLC (n=3) and (B) protein levels were measured from parallel wells as a control for cell loss following rotenone treatment (n=2). Data are presented as means ± range.

3.3.3 Imaging ROS production

Cells grown on confocal dishes were washed once in Krebs-HEPES buffer, incubated with MitoTracker Green (100 nM;Thermo Fisher Scientific), before exposure to MitoSOX Red (5 μM; Thermo Fisher Scientific) for 20 minutes at 37 °C. Hoechst nuclear stain (20 μM) was added 5 minutes before imaging with a Zeiss 510 Metahead confocal microscope. The following settings were used:

MitoSOX Red – 488 nm excitation and 595 nm emission

MitoTracker Green – 488 nm excitation and 510 nm emission

Hoechst – 405 nm excitation and 460 nm emission

3.3.4 Transmission electron microscopy and mitochondrial measurements

Cells were grown and transfected on plastic coverslips. 72 hours post-transfection, cells were washed in PBS, and fixed in warm glutaraldehyde (2.5%), PFA (2%), and PIPES buffer (0.1 M, pH7.2) for 30 minutes at room temperature. At this stage samples were transported to the lab of Dr Errin Johnson in the Electron Microscopy Facility, Dunn School of Pathology, University of Oxford. The following steps were carried out by Dr Errin Johnson: Secondary fixation was carried out for 1 hour at 4 °C in osmium tetroxide (1%) in PIPES buffer (0.1 M, pH 7.2), followed by tertiary fixation in uranyl acetate (0.5%) over night at 4 °C. Samples were embedded in resin after ethanol dehydration and gradual infiltration with Agar100 epoxy resin. After heat polymerisation, samples were sectioned (90 nm) using the Leica UC7 ultramicrotome with a diamond knife and post stained with Reynolds' lead citrate. 5–7 cells per sample were imaged using a FEI Tecnai 12 Transmission Electron Microscope (TEM) at 120 kV, using a Gatan US1000 digital CCD camera.

Images were analysed (by myself) in the following way: images were 'blinded' by Dr Andrew Shaw, then mitochondria were counted and the length (by placing a tip-to-tip line

across the longest axis of each mitochondrion), and area (by drawing around and selecting each individual mitochondrion) quantified using scale bars and ImagePro Plus 6 (Media Cybernetics) (Figure 3.2) similar to descriptions in previous publications (Khoo et al., 2014; Wang et al., 2013).

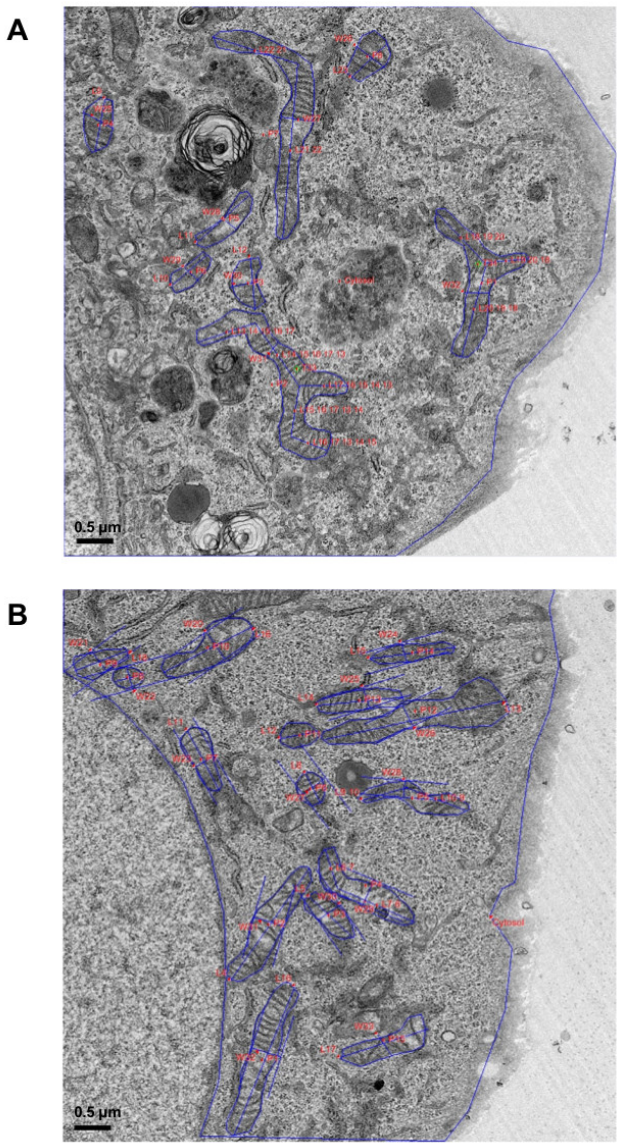


Figure 3.2 Analysis of mitochondria in electron micrographs

(A and B) Examples of mitochondrial analysis using electron micrographs. Image ProPlus 6 software was used to draw around mitochondria to determine their area in the plane of view, and lines were draw through the centre of mitochondria to measure their length relative to the scale bar.

3.3.5 Mitochondrial DNA content

Mitochondrial DNA (mtDNA) relative to nuclear DNA (nDNA) was assessed using real-time PCR and a Bio-Rad CFX96 detection system and iTaq Universal SYBR Green Supermix (Bio-Rad). DNA was extracted from cell pellets using the DNeasy Blood and Tissue kit (Qiagen) following the manufacturer's protocol. In each real time PCR reaction mixture 2 ng of DNA, 50 µM of each primer (detailed below) and 5 µl 2x iTaq Universal SYBR green mix was made up to a final volume of 10 µl in water.

Primers specific to nDNA genes:

Actin (*Actb*)

Forward - CTGCCTGACGGCCAGG

Reverse - GAAAAGAGCCTCAGGGCA

Succinate dehydrogenase complex subunit A (*Sdha*)

Forward - TACTACAGCCCCAAGTCT

Rev - TGGACCCATCTTCTATGC

Primers for mtDNA genes:

Cytochrome B (*mtCytb*)

Forward - CCACTTCATCTTACCATTTATTATCGC,

Reverse - TTTTATCTGCATCTGAGTTTAATCCTGT

Subunit II of mitochondrial cytochrome C oxidase (*mtCO2*)

Forward - CTACAAGACGCCACAT

Reverse - GAGAGGGGAGAGCAAT

Reactions were carried out in 96-well Hard-Shell PCR plates (Bio-Rad Green shell/white well, thin wall, cat HSP9645) using the settings outlined in Table 3.2.

	Temperature (°C)	Time (minutes)
	95	3:00
40 cycles	95	0:10
	60	0:30
	95	0:10
Melt curve	65	0:05
	95	0:50

Table 3.2 Thermocycler settings for real-time PCR quantifying nDNA and mtDNA

The ratio of mtDNA:nDNA was calculated using Ct values determined by the software to be in the early linear range of amplification and above an arbitrary background threshold.

3.3.6 Seahorse XF^{e}96 analysis

Oxygen consumption rate (OCR) and extracellular acidification rate (ECAR) were measured using the Seahorse XF^{e}96 Bioanalyser (Agilent Technologies) following the protocol outlined in **Section 2.12**.The day prior to the assay (and 72 hours post siRNA transfection), sEnd.1 cells were plated in quintuplicate at a density of 20,000 cells per well into XF^{e}96 microplates in Complete medium. 20,000 cells was deemed suitable as this was in the linear range of a cell density optimisation experiment and gave raw OCR readings around 140 pmol/min/well, and allows for elevations during maximal (FCCP stimulated) respiration that will not be limited by oxygen levels (Figure 3.3). Basal OCR measurements were taken followed by injection of the following compounds from the XF Cell Mito Stress Test Kit: oligomycin (1 µM, injection port A), FCCP (1 µM, injection port B), and combined antimycin A (0.5 µM), and rotenone (0.5 µM) (injection port C). An additional injection of

2-deoxyglucose (50 mM; Sigma) in Port D was included to investigate glucose oxidation dependent changes in ECAR. All data were normalised to protein concentration, measured via a BCA assay, and calculations were made as detailed in **Section 2.12**.

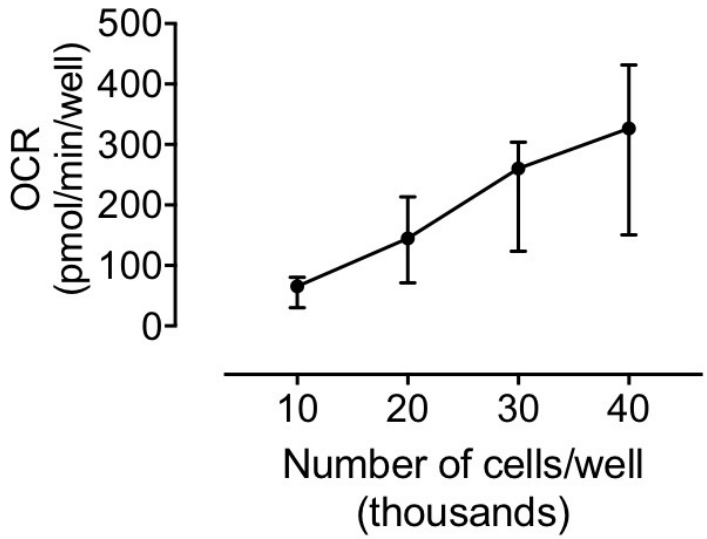


Figure 3.3 Optimisation of cell density for analysis of OCR in sEnd.1 cells

sEnd.1 cells were seeded at varying densities and OCR was measured using a Seahorse Bioanalyzer. Data are presented as means ± range (n=1, using 20 replicate wells).

3.3.7 Metabolomics

Metabolomic analysis was carried out by Prof James McCullagh in the Department of Chemistry at the University of Oxford. Metabolite extraction: sEnd.1 endothelial cells transfected with *Gch1*-specific siRNA were compared to cells transfected with NS control siRNA. Briefly, 200 µL of 80% ice-cold, aqueous methanol was added to the cell pellet containing approximately 1 million (pre-counted) frozen cells. The cell pellet was disrupted through aspiration to obtain a cell suspension in 80% methanol. The cell suspension was then clarified by centrifugation at 14,800 x g for 20 minutes at 4 °C. The supernatant was removed and placed in an autosampler vial and kept at −80 °C. On the day of analysis, the extract was allowed to warm to 4 °C in the chilled autosampler and then injected directly onto the system.

Metabolite analyses were performed using a Thermo Scientific ICS-5000+ ion chromatography system coupled directly to a Q-Exactive HF Hybrid Quadrupole-Orbitrap mass spectrometer with a HESI II electrospray ionisation source (Thermo Fisher Scientific). The ICS-5000+ HPLC system incorporated an electrolytic anion generator (KOH) programmed to produce an OH- gradient over 37 min. An inline electrolytic suppressor removed the OH- ions and cations from the post-column eluent prior to MS analysis (Thermo Scientific Dionex AERS 500). A 10 μL partial loop injection was used for all analyses and the separation was performed using a Thermo Scientific Dionex IonPac AS11-HC 2×250 mm, 4 μm particle size column with a Dionex Ionpac AG11-HC 4 μm 2×50 guard column inline. The IC flow rate was 0.250 ml/min. The total run time was 37 min and the hydroxide ion gradient comprised as follows: 0 mins, 0 mM; 1 min, 0 mM; 15 mins, 60 mM; 25 mins, 100 mM; 30 mins, 100 mM; 30.1 mins, 0 mM; 37 mins, 0 mM. Analysis was performed in negative ion mode using ascan range from 80 to 900 and resolution set to 70,000. The tune file source parameters were set as follows: sheath gas flow 60; aux gas flow 20; spray voltage 3.6; capillary temperature 320; S-lens RF value 70; heater temperature 450. AGC target was set to 1E6 and the Max IT value was 250 ms. The column temperature was kept at 30 °C throughout the experiment. Full scan data were acquired in continuum mode. Peaks retention times were identified from the injection of authentic standards and peaks from unknown samples were identified using a combination of accurate mass analysis (<2 ppm) and retention time using Thermo Scientific Quanbrowser software (Thermo Fisher Scientific).

3.4 Results

3.4.1 Characterisation of Gch1 knock down induced BH_4 deficiency in sEnd.1 cells

The *in vitro* model of BH_4 deficiency was characterised by assessing the effects of *Gch1* knockdown in sEnd.1 cells on GTPCH protein levels, BH_4 production, and eNOS activity. RNA interference (RNAi) using a pool of small interfering RNA (siRNA) duplexes targeted to sections of *Gch1* mRNA (referred to as Gch siRNA), were transfected onto sEnd.1 cells 72 hours before they were harvested and prepared for analysis. Western blotting was used to confirm diminished levels of GTPCH in Gch siRNA treated cells compared with consistently higher levels in untreated, transfection reagent only, non-targeted (non-specific, NS) siRNA and *Gapdh* siRNA treated cells (Figure 3.4A). This confirmed specific knock down of GTPCH by Gch siRNA but not NS siRNA, however to control for potential effects of treating sEnd.1 cells with foreign RNA and transfection reagent, NS siRNA treated cells were used as the control group in all subsequent experiments.

Dramatically decreased GTPCH protein (Figure 3.4A) lead to a significant reduction in BH_4 synthesis and overall biopterin levels (Figure 3.4B), measured using HPLC. 6.37% ± 1.467 SEM of the biopterins were oxidised to BH_2 and biopterin in NS siRNA cells and 10.87% ± 1.933 SEM in Gch siRNA cells but this was not significantly different (Figure 3.4C), and led to ratios of BH_4:BH_2+B averaging 19 ± 5.457 SEM and 9.445 ± 1.947 SEM respectively (Figure 3.4D). As BH_4 is an essential cofactor for the production of NO from L-arginine by eNOS, it was unsurprising to find substantially decreased conversion into citrulline and therefore decreased eNOS activity in BH_4 deficient cells (Figure 3.4E). Lower levels of oxidised NO products (nitrite and nitrate (NO_x)) secreted in the media also indicated less NO production (Figure 3.4F), and unchanged amounts of eNOS protein detected by Western blotting (Figure 3.4A) proved this was a BH_4 driven change in eNOS activity rather than

abundance. Gch knock down in sEnd.1 cells was therefore deemed a suitable model for investigating the effects of BH_4 depletion on mitochondrial function and redox signalling.

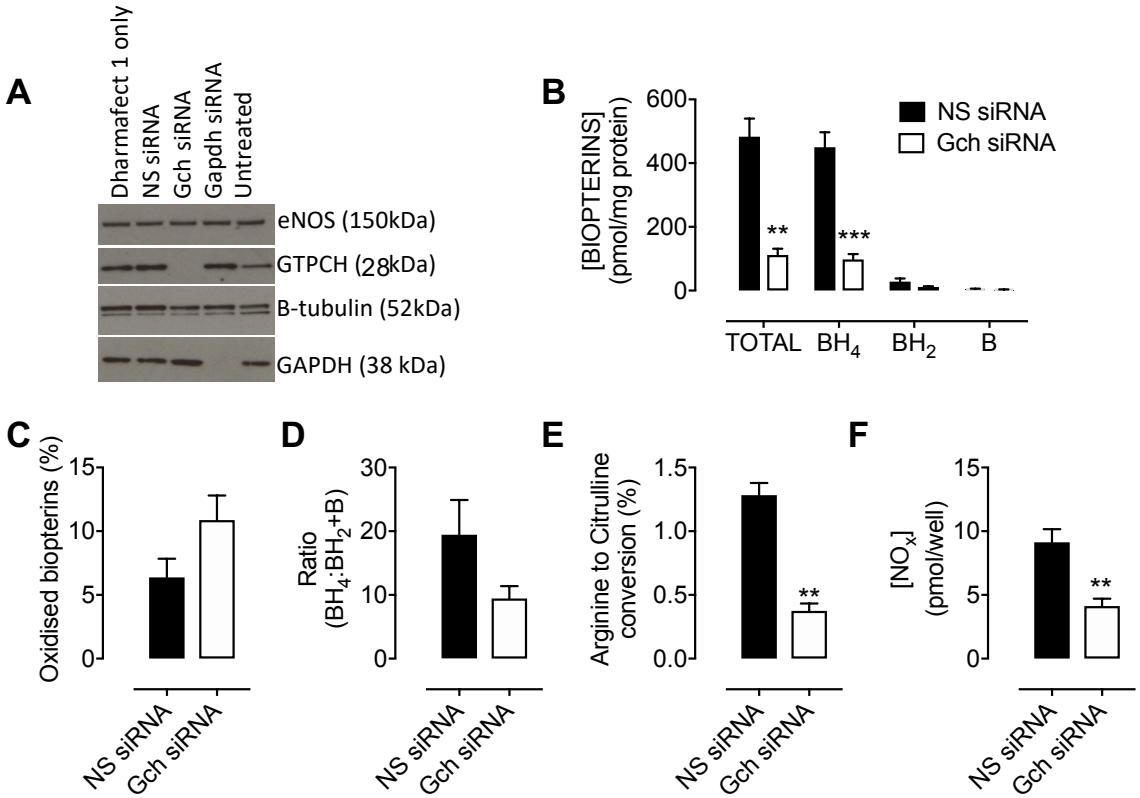


Figure 3.4 *Gch1* siRNA diminished GTPCH, biopterins and NOS activity in sEnd.1 cells

Murine sEnd.1 cells were transfected with non-targeting (NS) or *Gch1* targeted (Gch) siRNA for 72 hours. (A) Diminished GTPCH protein in Gch siRNA cells was confirmed by Western blotting in comparison with NS siRNA, *Gapdh* siRNA, Dharmafect 1 treated and untreated cells. eNOS protein levels were unchanged and β-tubulin was used as a loading control. (B) Biopterin levels were dramatically decreased in Gch siRNA cells, as measured by HPLC. (C) The proportion of oxidised biopterins (BH_2 + Biopterin) and (D) ratio of BH_4 to oxidised biopterins were calculated. (E) NOS activity was decreased as measured by the L-NAME inhibitable conversion of radio labelled arginine into citrulline, (F) and NO_x (nitrite + nitrate) in the culture medium was likewise lower. All data are n=4 of triplicate samples presented as means ± SEM. Statistical analyses were carried out using unpaired Student's t-tests (* P<0.05, ** P<0.01, *** P<0.001).

3.4.2 Characterisation of doxycycline induced BH_4 deficiency in 3T3 fibroblasts stably transfected with tet-off GCH1

Previously, our group generated murine 3T3 fibroblasts expressing human *GCH* regulated by a tetracycline response element in the promotor region and stable co-transfection with *tet*-off trans-activator plasmids (termed GCH cells) (Crabtree et al., 2009a). This allowed for a system in which *GCH* expression could be turned off in response to doxycycline and BH_4 depleted after 72 hours, in a cell type proven devoid of NOS (Crabtree et al., 2009a). GCH cells were therefore used to look at the NOS independent effects of BH_4 depletion and to complement findings in sEnd.1 cells transfected with Gch siRNA. Successful knockdown of *GCH* after doxycycline treatment was confirmed by decreased GTPCH protein detection by Western blotting, which also demonstrated the absence of eNOS (Figure 3.5A). Similar to Gch siRNA sEnd.1 cells, BH_4 and total biopterin levels were also decreased (Figure 3.5B) and the ratio of BH_4 to oxidised biopterins was not significantly changed (Figure 3.5C). Cells only transfected with *tet*-transactivator constructs (TET cells) contained no GTPCH (Figure 3.5A), and were used to control for the effects of doxycycline and transactivator expression independent of GTPCH levels in subsequent experiments. This was particularly important as tetracycline antibiotics have been reported to affect nuclear gene expression and mitochondrial function (Chatzispyrou et al., 2015; Moullan et al., 2015) which could confound effects of knocking down *GCH*.

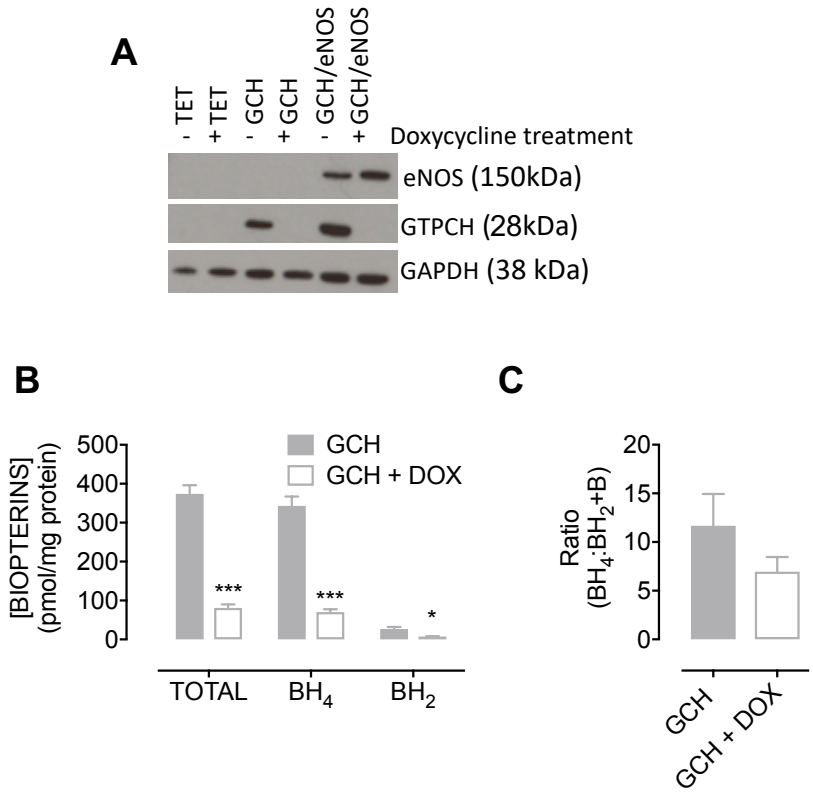


Figure 3.5 Doxycycline decreased GTPCH and biopterins in 3T3 fibroblasts stably transfected with *tet*-off GCH1 plasmids

Murine 3T3 fibroblast cells stably transfected with a *tet*-off transactivator construct (TET), and co-transfected with plasmids encoding human *GCH1* under control of a tetracycline response element (GCH) and eNOS (GCH/eNOS) were treated with doxycycline for 72 hours. (A) Diminished GTPCH protein levels in doxycycline treated GCH cells were confirmed by Western blotting and compared with untreated GCH and TET cells with GAPDH as a loading control. Importantly GCH cells contained no detectable eNOS, and GCH/eNOS cells were used as a positive control for eNOS. (B) Biopterins were dramatically decreased in GCH cells following doxycycline treatment, (C) and the ratio of BH_4 to oxidised biopterins was unchanged. NOTE: TET cells contained undetectable levels of biopterins (not shown). All data are n=3 of triplicate samples presented as means ± SEM. Statistical analyses were carried out using unpaired Student's t-tests (* $P<0.05$, *** $P<0.001$).

3.4.3 Elevated mitochondrial superoxide generation in BH_4-deficient cells

In accordance with previous reports from our laboratory (Crabtree et al., 2009b, 2009a), BH_4-depleted sEnd.1 cells generated much greater amounts of superoxide, quantified using HPLC to measure the oxidation of DHE into 2-hydroxyethidium (Figure 3.6A). A small proportion was L-NAME inhibitable and therefore produced by eNOS (Figure 3.6A). Therefore, the main aim of this experiment was to define the other major sites of superoxide generation in these cells by systematically inhibiting each potential source. These results showed that inhibitors of NADPH oxidase and xanthine oxidase, apocynin and oxypurinol respectively, had no effects on superoxide, whereas the mitochondrial Complex I inhibitor, rotenone, completely abolished superoxide levels in Gch siRNA cells to the levels of NS siRNA cells (Figure 3.6A). Rotenone also inhibited elevated superoxide generation from BH_4 deficient GCH cells, demonstrating that BH_4 depletion led to increased mitochondrial superoxide independent of the presence or function of NOS enzymes (Figure 3.6B). Importantly, doxycycline had minimal effect on superoxide in control TET cells, which were also unaffected by rotenone treatment, suggesting that Complex I is not a superoxide source in fibroblasts until they have been introduced to and depleted of BH_4 (Figure 3.6B). Interestingly, expressing *GCH* in TET cells decreased basal superoxide levels in untreated fibroblasts, which indicated a profound effect of BH_4 on intracellular superoxide (Figure 3.6B). Furthermore, restoring BH_4 levels by supplementing deficient cells with sepiapterin attenuated superoxide production from Gch siRNA sEnd.1 and *tet*-off GCH cell systems (Figure 3.6C-F).

In addition, BH_4 depleted cells were also imaged following incubation with a mitochondrially targeted superoxide probe (MitoSOX red) designed to emit red fluorescence upon oxidation by superoxide and other ROS. This probe is a modified version of DHE conjugated to TPP^+ which targets it to mitochondria (Mito-DHE), and – similar to DHE –

forms the detectable fluorescent superoxide specific product 2-hydroxy-Mito-ethidium (Robinson et al., 2006). In this study, analysis showed increased red fluorescence in Gch siRNA cells, in characteristic mitochondrial networks, which were confirmed to co-localise with a fluorescent mitochondrial label (MitoTracker green) (Figure 3.7A). Mito-DHE is also oxidised to Mito-ethidium by a range of molecules and will also be detected by this method due to their overlapping wavelengths, therefore it cannot be concluded that this fluorescence indicated increased mitochondrial ROS (Robinson et al., 2006; Zielonka and Kalyanaraman, 2010). However, in combination with the other data this seems probable. Moreover, elevated superoxide levels were attenuated after treatment with a mitochondrial ROS scavenger (mitoTEMPO) as detected using DHE and HPLC (Figure 3.7B). These results together provide substantial evidence that mitochondria are a major source of superoxide generation from BH_4 depleted cells, and this is independent from eNOS function.

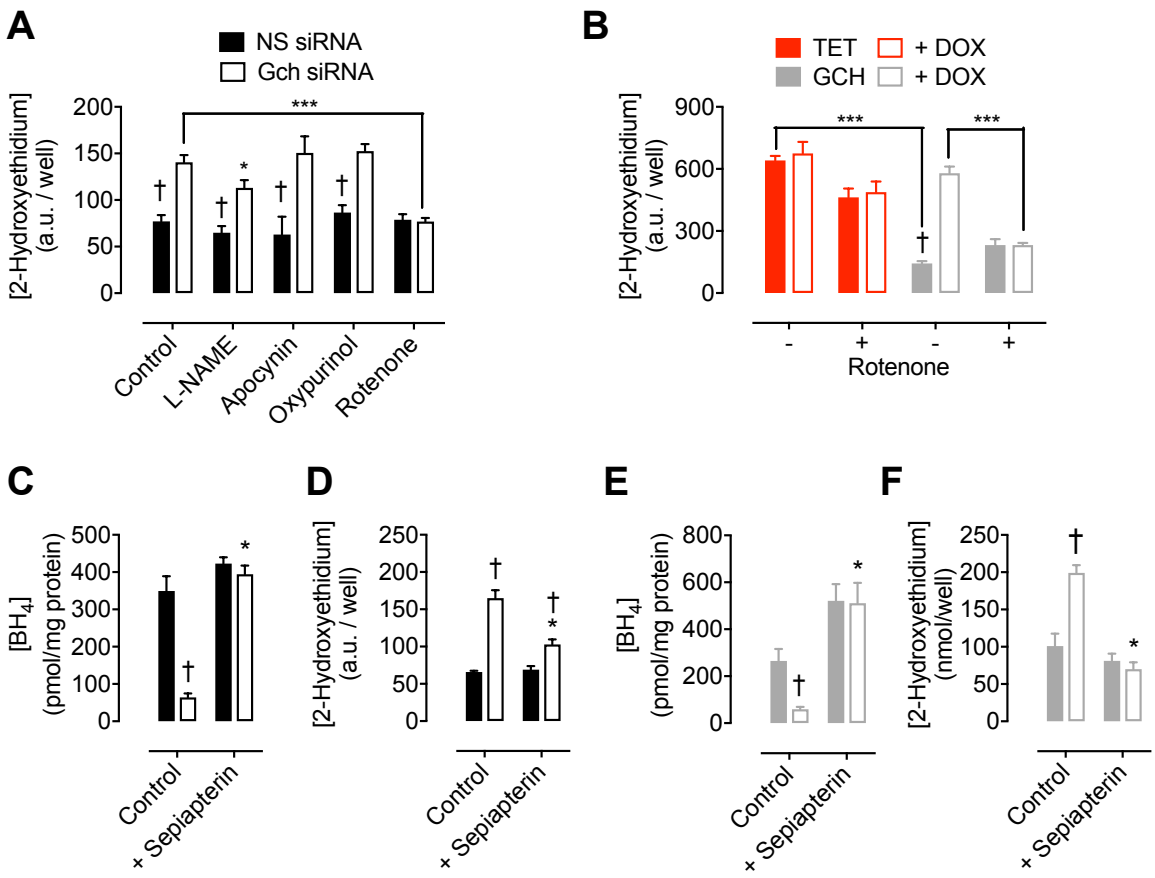


Figure 3.6 BH_4 depletion leads to increased mitochondrial superoxide generation

Oxidation of DHE into 2-hydroxyethidium was measured by HPLC and used to determine superoxide production in BH_4 depleted sEnd.1 cells transfected with *Gch1* siRNA and GCH fibroblasts treated with doxycycline (GCH cells). (A) The sources of superoxide were identified in sEnd.1 cells using targeted inhibitors of NOS (L-NAME), NADPH oxidase (apocynin), xanthine oxidase (oxypurinol) and mitochondrial Complex I (rotenone). (B) GCH cells were treated with rotenone to deduce whether Complex I was a superoxide source in cells devoid of NOS. TET cells were used as a control for the effects of doxycycline. (C-F) BH_4 levels were restored in deficient sEnd.1 and GCH cells by sepiapterin supplementation, and led to decreased DHE oxidation. All data are n=3-4 of triplicate samples presented as means ± SEM. Statistical analyses were carried out using 2-way ANOVA with Tukey's post-test (* $P<0.05$ and *** $P<0.001$ for comparisons between pharmacological treatments, † $P<0.05$ for comparison between siRNA or dox treatment).

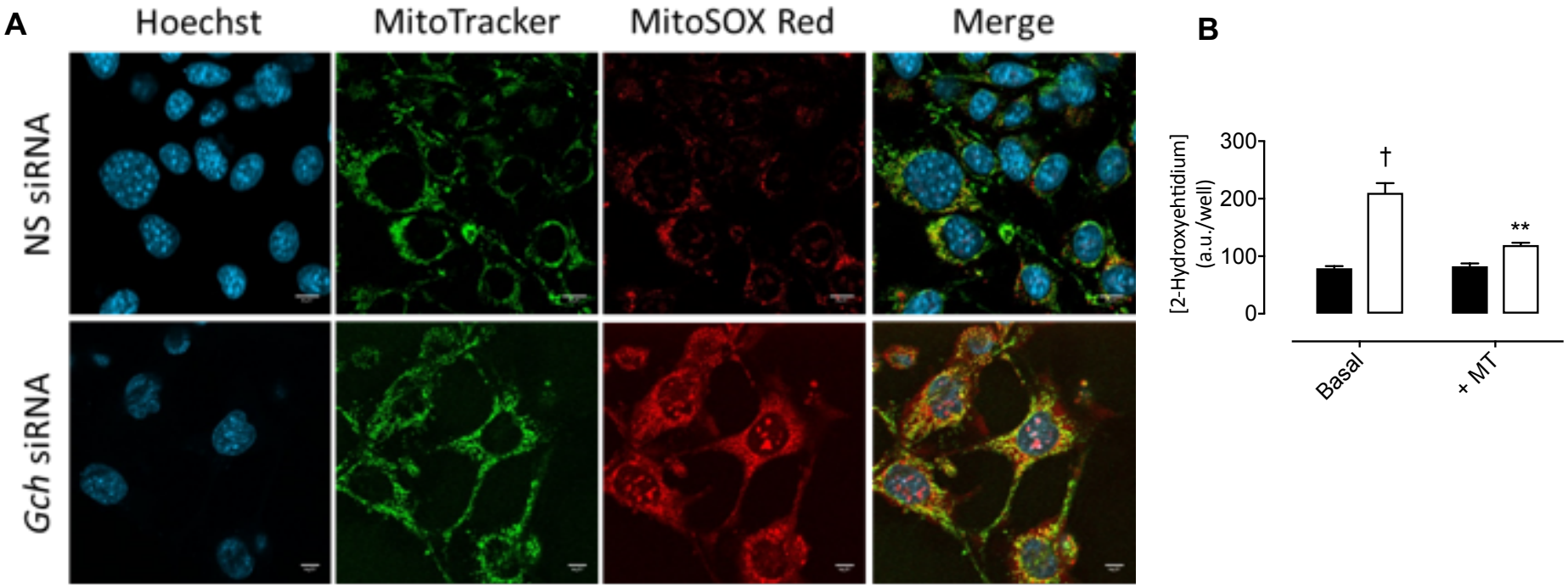


Figure 3.7 Mitochondrial localisation of elevated ROS in BH_4 deficient endothelial cells

(A) sEnd.1 Gch siRNA cells were incubated with HOECST nuclear stain, mitochondrially targeted DHE (MitoSOX) and mitochondrial marker mitoTracker green. (B) Gch siRNA cells were incubated with mitochondrial ROS scavenger MitoTEMPO and DHE oxidation was measured. All data are n=3-4 of triplicate samples presented as means ± SEM. Statistical analyses were carried out using 2-way ANOVA with Tukey's post-test (* $P<0.05$ and ** $P<0.01$ for comparisons between pharmacological treatments, † $P<0.05$ for comparison between siRNA or dox treatment).

3.4.4 Mitochondrial biopterins are depleted in BH_4-deficient cells

After finding that BH_4 modulated mitochondrial superoxide generation, biopterins were quantified within mitochondria followed by evaluation of changes in mitochondrial biopterin content upon *Gch1* knockdown. Mitochondrial fractions were prepared (as described in **Section 2.13**) and successful enrichment was confirmed by Western blotting for mitochondrial markers (SDH, VDAC, and cytochrome C) which showed prominent bands compared with equal protein loading of whole cell lysates (Figure 3.8A). The purity of preparations were indicated by the absence of cytosolic GAPDH protein in mitochondrial fractions (Figure 3.8A), and a more thorough evaluation using a variety of antibodies against proteins found in non-mitochondrial fractions (eg. endoplasmic reticulum and plasma membrane) was carried out during method development (**Section 2.13**). Biopterins were quantified in whole cell and mitochondrial fractions using HPLC, and showed that mitochondria contained substantial amounts of biopterin species, but a lower concentration of total biopterins and BH_4 than the whole cell when normalised to protein content (Figure 3.8B). Surprisingly, the mitochondrial BH_4:BH_2+B ratio was dramatically lower (Figure 3.8C) due to biopterins that were significantly more oxidised in mitochondria (42% ± 2.403 SEM) than whole cell preparations (6.37% ± 1.467 SEM) (Figure 3.8D). Samples destined for BH_4 analysis are usually rapidly frozen to avoid oxidation, so it was important to determine whether mitochondrial biopterins were oxidised artefactually during the fractionation procedure which took around 2 hours on ice. A control experiment was carried out, incubating an aliquot of whole cells throughout the isolation to measure time dependent BH_4 oxidation, and supplementing all isolation solutions with the reducing agent DTE to protect BH_4 during fractionation, as used during measurement by HPLC. This revealed that although DTE was protective and the time taken did contribute to biopterin oxidation, both were relatively small effects, and artefactual oxidation was therefore unlikely to account for the large changes observed in this data (Figure 3.9A-F).

Next, mitochondria were isolated from Gch siRNA cells and biopterin measurements revealed that levels of BH_4 and BH_2 were lower (Figure 3.10A), and the percentage decrease of total biopterins in whole cells and mitochondria was similar (Figure 3.10B-C). This suggests that disrupting cellular BH_4 synthesis depletes BH_4 within mitochondria. The BH_4:BH_2+B and proportion of oxidised biopterins in Gch siRNA mitochondria remained unchanged (Figure 3.10D-E).

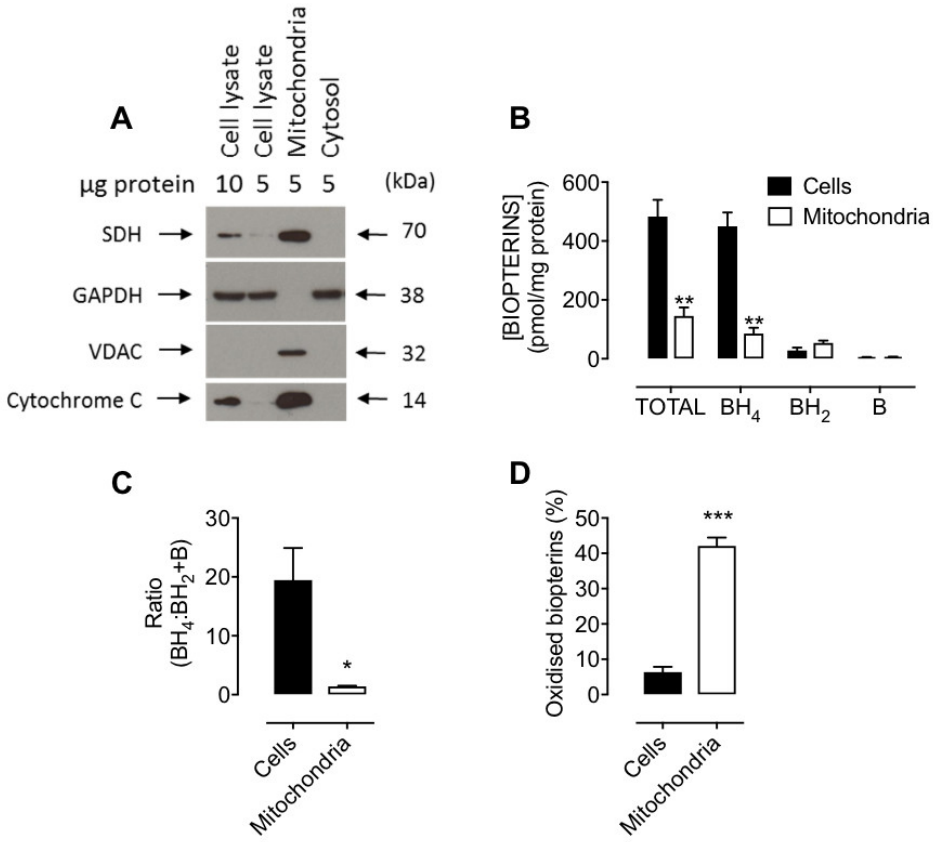


Figure 3.8 Mitochondria contained BH_4 and a greater proportion was oxidised in this fraction than in whole cell preparations

(A) Mitochondrial preparations were isolated from sEnd.1 cells and the purity and enrichment was confirmed by Western blotting for succinate dehydrogenase (SDH), voltage gated anion channel (VDAC), cytochrome C and GAPDH. (B) Biopterins were measured in whole cell and mitochondrial preparations by HPLC. (C) The ratio of BH_4:BH_2+B was decreased in mitochondria, (D) due to mitochondria containing a greater proportion of oxidised biopterins (BH_2+B). All data are n=3-4 of triplicate samples presented as means ± SEM. Statistical analyses were carried out using unpaired Student's *t*-tests (* $P<0.05$, ** $P<0.01$, *** $P<0.001$).

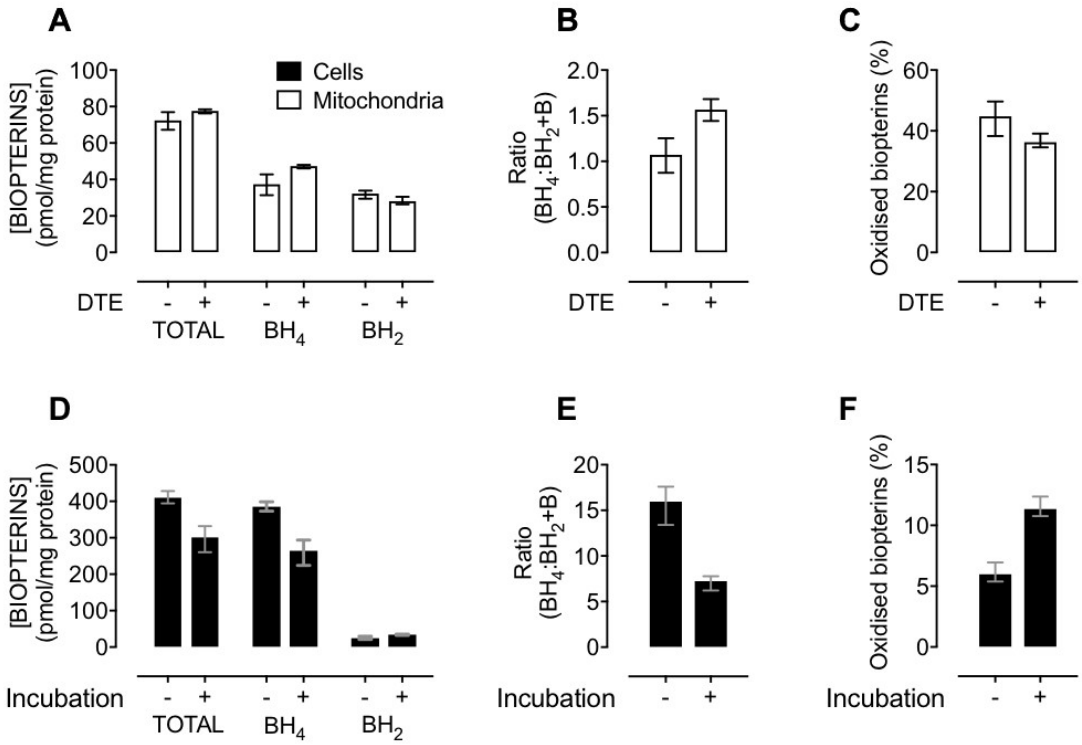


Figure 3.9 Artefactual oxidation of biopterins during mitochondrial isolation

To determine the extent of artefactual oxidation of biopterins during mitochondrial isolation, (A-C) the antioxidant DTE was added to all buffers used in preparation of mitochondrial fractions and (D-F) an aliquot of whole cells were incubated on ice throughout the process. (A and D) Biopterins were then measured by HPLC. (B and E) The ratio of BH_4:BH_2+B and (C and F) proportion of oxidised biopterins were calculated. Data are presented as means ± range of n=1 experiment in triplicate.

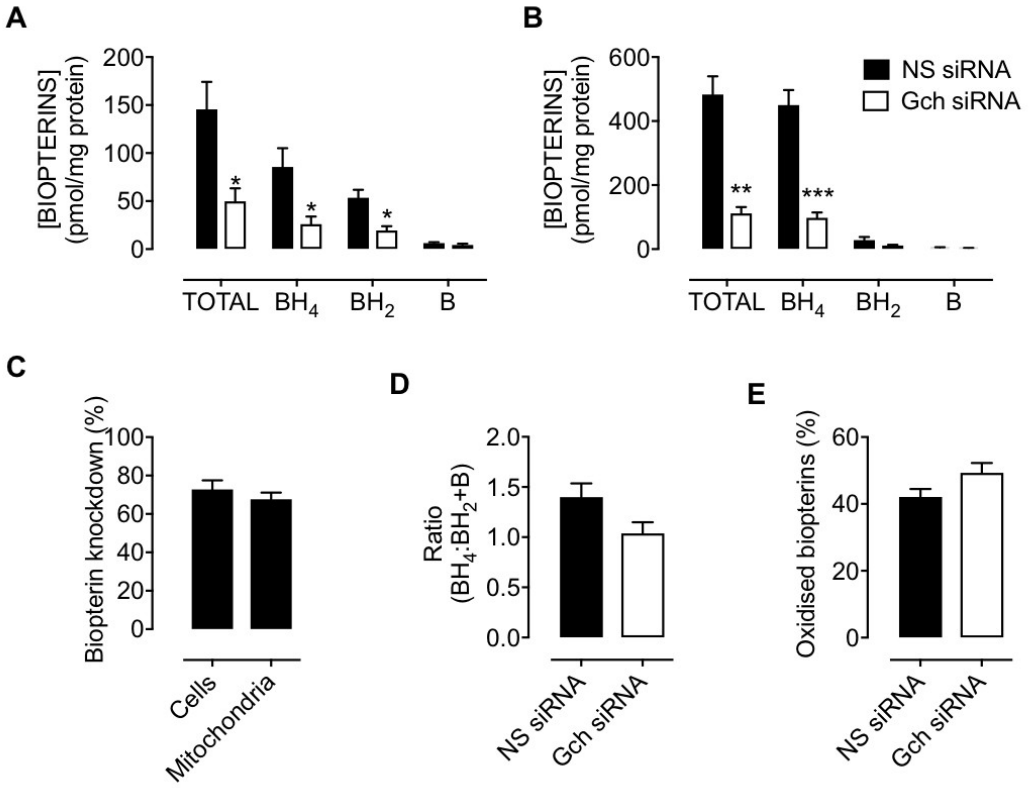


Figure 3.10 Mitochondrial biopterins were decreased in *Gch1* knockdown sEnd.1 cells

Mitochondria were isolated from cells following transfection with NS or *Gch1* siRNA and biopterins were measured in (A) mitochondrial fractions and (B) aliquots of starting cells using HPLC. (C) The percentage decrease of total biopterins in cells and mitochondria following treatment with *Gch1* siRNA was calculated. (D) The ratio of BH_4:BH_2+B and (E) the proportion of oxidised biopterins in mitochondrial fractions were calculated. All data are n=3 of triplicate samples presented as means ± SEM. Statistical analyses were carried out using unpaired Student's *t*-tests (* $P<0.05$).

3.4.5 Decreased phosphorylation of DRP1 at serine 616 leads to enlarged mitochondria in BH_4-deficient cells

To investigate the effects of BH_4 levels on mitochondrial morphology, cells were prepared for imaging by electron microscopy. Electron micrographs were of sufficient detail to distinguish individual mitochondria, but lacked consistent definition of inner membrane cristae structures (Figure 3.11A and B). Image analysis software was used to quantify the average number, length and area of mitochondria in the plane of view imaged for each cell. This revealed that the average mitochondrial length increased by 16% (Figure 3.11C), with indications of increased area (Figure 3.11D), but no differences were found in absolute mitochondrial numbers (Figure 3.11E) in Gch compared with NS siRNA cells. Western blots supported evidence of increased mitochondrial size, and showed increased amounts of inner and outer mitochondrial membrane markers, COXIV and TOM20, in BH_4-deficient cells (Figure 3.11F). To determine whether these changes were modulated by proteins regulating mitochondrial fission or fusion Western blots were carried out for key candidates (Figure 3.12A). These showed decreased phosphorylation of the master regulator of mitochondrial fission, DRP1, at the activating site serine 616 (Figure 3.12B), concomitant with no changes in inhibitory phosphorylation at serine 637 (Figure 3.12C) or total DRP1 (Figure 3.12D). There were also no changes detected in fusion regulators mitofusin-2 or OPA-1 (Figure 3.12A). The ratio of mitochondrial DNA (mtDNA) to nuclear DNA (nDNA) was unchanged indicating no increased mitochondrial biogenesis (Figure 3.12E and F).

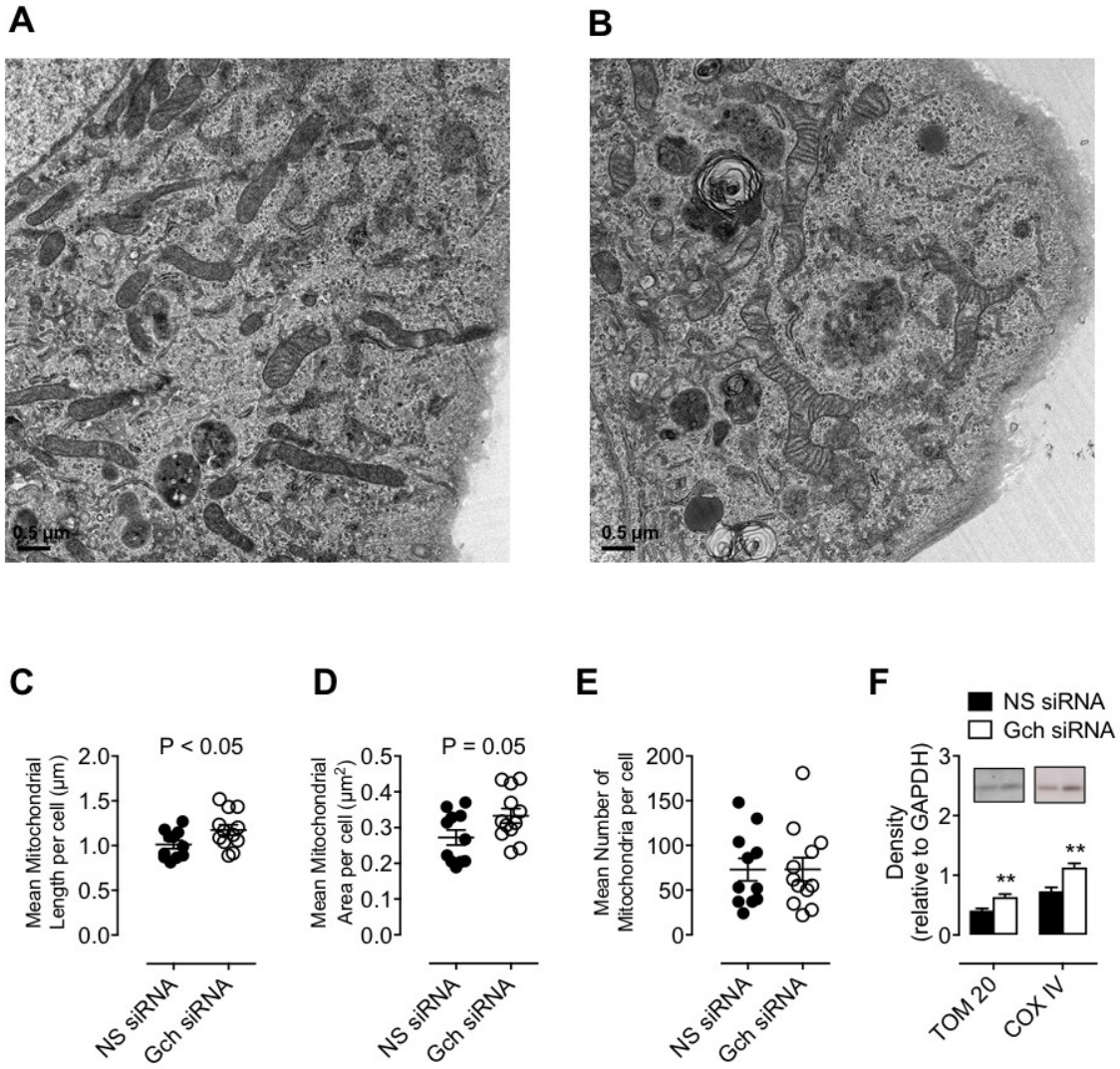


Figure 3.11 Mitochondria were larger in BH_4-deficient cells

(A-B) Electron microscopy images were taken of (A) NS and (B) Gch siRNA sEnd.1 cells, and representative images are shown for a section of one cell from each group. (C) The mean length, (D) area and (E) number of mitochondria were determined, with dots representing the mean from one cell. (C-E) The graphs show the mean of the points ± SEM for n=11-12 cells. (F) Western blot analysis of TOM20 and COX IV in cell lysates (n=4-6). Data are presented as means ± SEM. Statistical analyses were carried out using unpaired Student's t-tests (* P<0.05, ** P<0.01). Electron microscopy images were taken by Dr Errin Johnson and TOM20 and COX IV Western blots were carried out by Dr Brent Ryan.

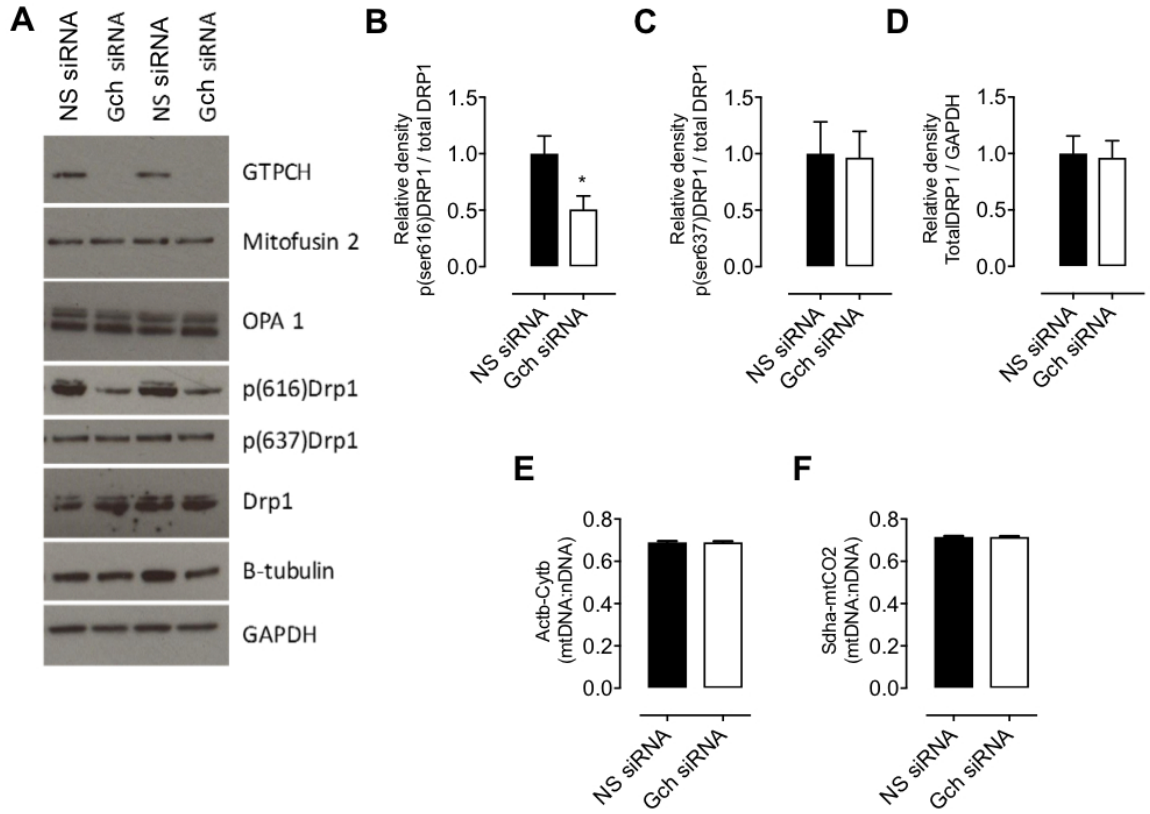


Figure 3.12 Phosphorylation of DRP1 at serine 616 was decreased in BH_4-deficient cells

(A) Representative Western blots for GTPCH, mitofusin-2, OPA-1, phosphorylated DRP1 at serine 616 and 637 and total DRP1 with β-tubulin and GAPDH used as loading controls. (B-C) The levels of phosphorylated DRP1 at (B) ser616 and (C) 637 were determined relative to total DRP1. (D) Total DRP1 levels were determined relative to GAPDH. (E-F) The amount of mitochondria DNA (mtDNA) relative to nuclear DNA (nDNA) was calculated using the ratio of mitochondrially encode genes (*Cytb* and *mtCO2*) to nuclear genes (*Actb* and *Sdha*). Data are presented as means ± SEM. Statistical analyses were carried out using unpaired Student's t-tests (* $P<0.05$). (n=4-6 for Western blots, n=4 for DNA measurements.)

3.4.6 Mitochondrial respiratory function remains unaffected by BH_4 depletion

The impact of BH_4 depletion and changes in mitochondrial redox signalling and morphology on aerobic mitochondrial respiration were assessed. A Seahorse Bioanalyzer Mito Stress Test was used to determine respiratory function by measuring oxygen consumption rate (OCR) under basal conditions and following sequential injections of oligomycin, FCCP and rotenone + antimycin A, which inhibit or accelerate the electron transport chain. The resulting OCR traces overlapped (Figure 3.13A), and respiratory parameters calculated revealed no changes in respiratory function upon BH_4 depletion (Figure 3.13B).

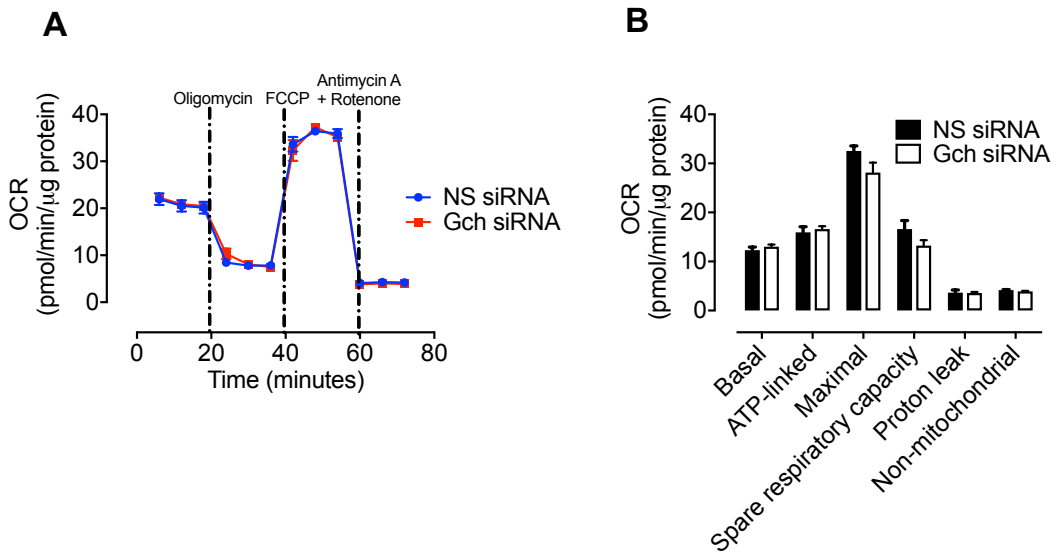


Figure 3.13 Mitochondria respiratory function was unaffected by BH_4 deficiency

sEnd.1 cells were transfected with NS and Gch siRNA for 48 hours before re-plating into XF^e96 Seahorse plates overnight. (A) Oxygen consumption rate (OCR) was measured using a Seahorse bioanalyzer at baseline and following injections of oligomycin, FCCP, rotenone and antimycin A. The resulting trace is shown following normalisation to protein. (B) Measurements were used to determine basal, ATP-linked, maximal, spare respiratory capacity, proton leak and non-mitochondrial OCR. All data are n=6 of quintuplet wells presented as means ± SEM. Statistical analyses were carried out using unpaired Student's *t*-tests (* $P<0.05$).

3.4.7 BH_4 depletion increases the OCR:ECAR ratio

Concomitant with OCR readings, the Seahorse Bioanalyzer measured extracellular acidification rate (ECAR) which is a pH dependent indicator of glycolytic lactate production (Figure 3.14A). Baseline measurements of OCR and ECAR were not significantly changed between NS or Gch siRNA cells (Figure 3.14B and C) and whereas OCR readings were almost identical (Figure 3.14C), ECAR measurements were slightly but not significantly decreased (Figure 3.14B). This led to a significantly increased OCR:ECAR ratio in BH_4 depleted cells (Figure 3.14D). The change in OCR:ECAR may indicate that glycolytic rate was decreased relative to unchanged mitochondrial respiration. A final injection of glycolytic inhibitor 2-deoxyglucose was used to determine the change in ECAR due to glycolysis and showed decreased 2-deoxyglucose inhibitable ECAR in Gch siRNA cells (Figure 3.14E), and although this may further indicate changes in glycolysis the ECAR trace has not plateaued following this injection making it unreliable to draw conclusions. These results suggest that glycolysis was slightly less active in BH_4-deficient sEnd.1 cells but we are not able to conclude this.

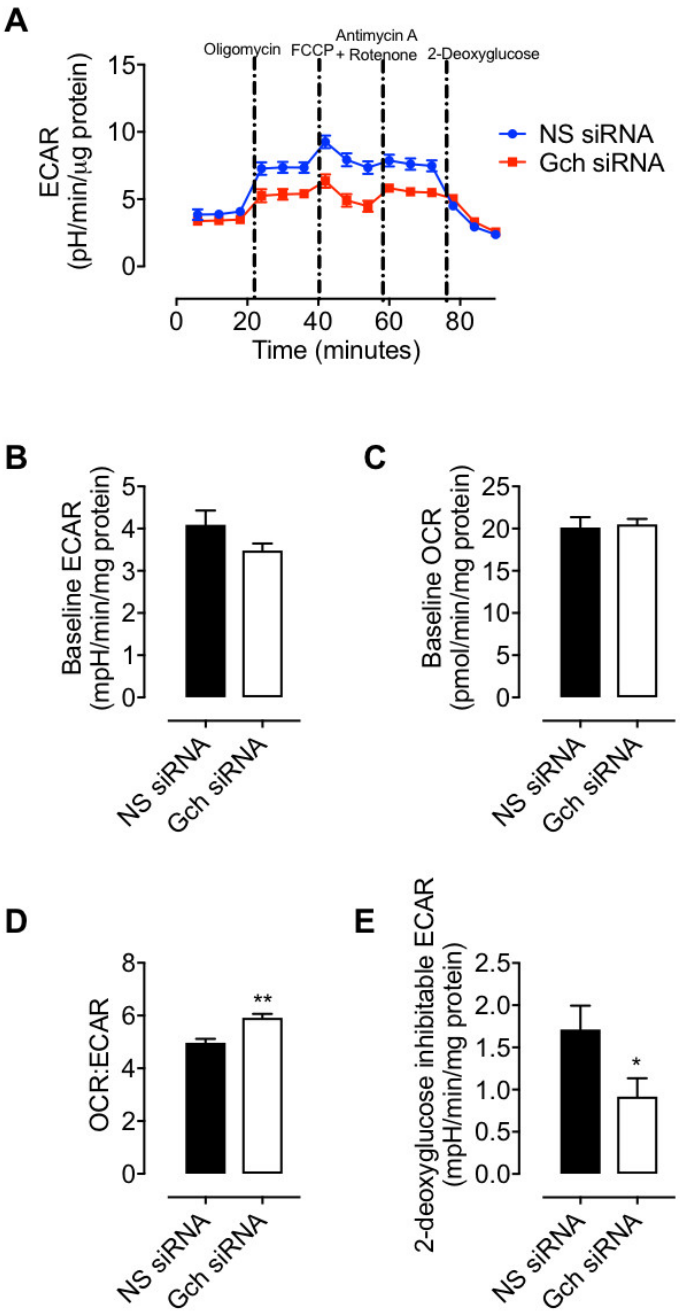


Figure 3.14 OCR:ECAR increased in BH_4 deficient cells

The extracellular acidification rate (ECAR) was measured simultaneous to OCR during mitochondrial respiratory function tests on the Seahorse bioanalyzer. (A) ECAR trace is shown throughout the respiratory test with baseline measurements followed by injections of oligomycin, FCCP, rotenone, antimycin A and 2-deoxyglucose. (B) Baseline ECAR and (C) OCR measurements. (D) The OCR:ECAR ratio was calculated from baseline OCR and ECAR readings. (E) An estimate of basal glycolysis was calculated by subtracting the 2-deoxyglucose inhibitable proportion from baseline values. All data are n=6 of quintuplet wells presented as means ± SEM. Statistical analyses were carried out using unpaired Student's *t*-tests (* $P<0.05$).

3.4.8 BH_4 deficiency leads to changes in glycolytic and TCA cycle metabolites

Mass spectrometry was used to measure the abundance of metabolites integral to glycolysis and the TCA cycle to further investigate the impact of BH_4 depletion on cellular bioenergetics. This method successfully detected and quantified 8 glycolytic and 6 TCA cycle intermediates (Figure 3.15). Analysis highlighted elevated fructose-1,6-bisphosphate in the glycolysis pathway (Figure 3.16), and increased succinate but decreased isocitrate accumulations in the TCA cycle in Gch siRNA cells (Figure 3.17), showing that BH_4 levels affected these pathways.

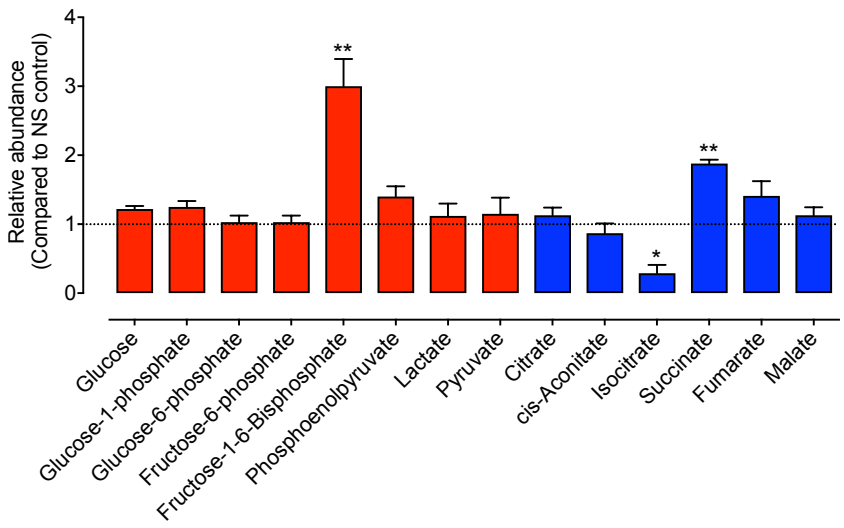


Figure 3.15 Metabolomics revealed BH_4-dependent changes in glycolysis and TCA cycle metabolites

Cellular glycolytic (red) and TCA cycle (blue) metabolites were measured by mass spectrometry. The relative abundance of metabolites in Gch siRNA cells was calculated relative to NS siRNA control cells (n=4). Data are presented as means ± SEM. Statistical analyses were carried out using unpaired Student's t-tests (* $P<0.05$, ** $P<0.01$).

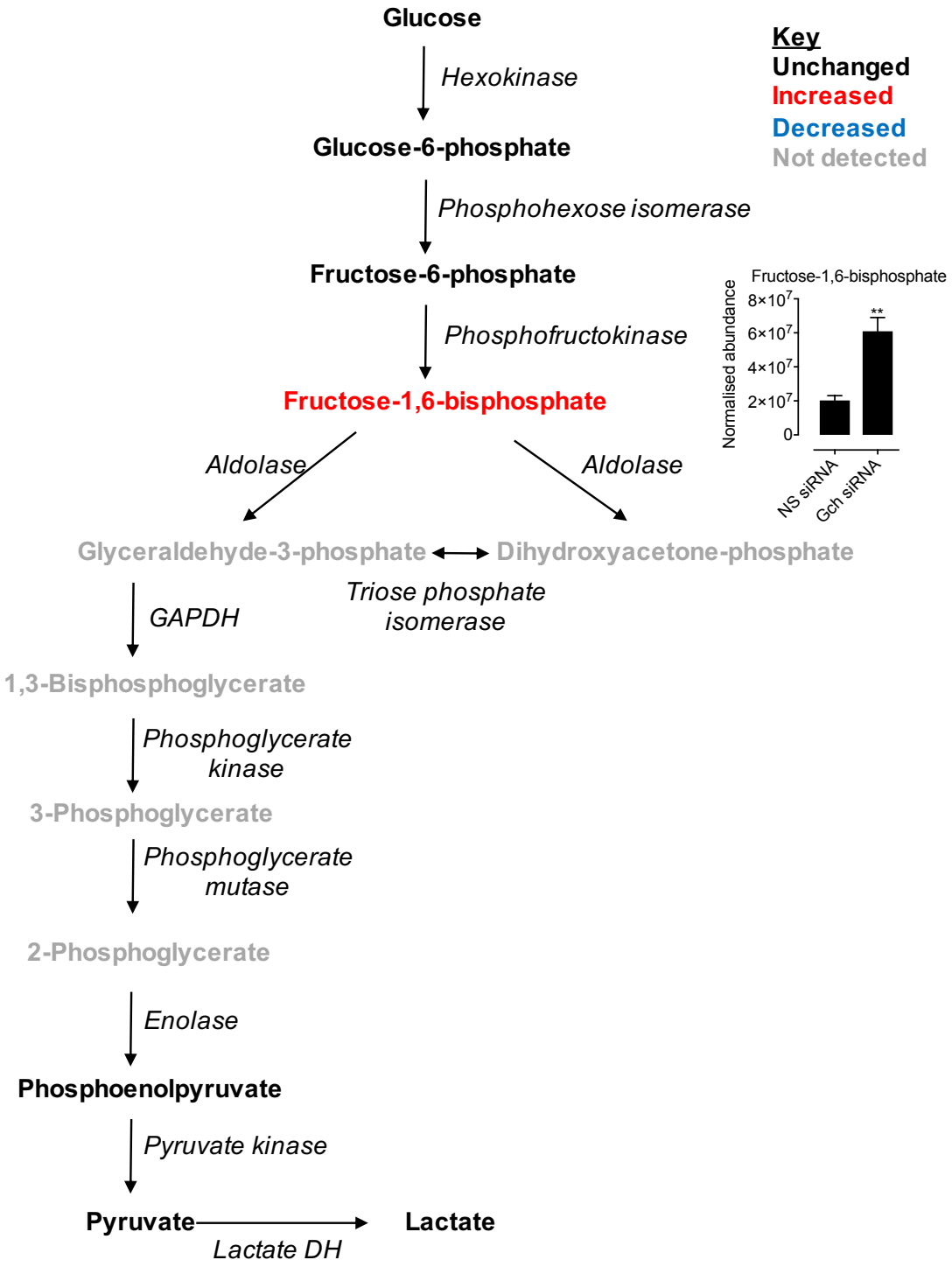


Figure 3.16 Glycolytic intermediate fructose-1,6-bisphosphate was elevated in BH_4-deficient cells

The glycolysis pathway showing changes in metabolite levels, with a graphical insert of the significantly altered metabolite fructose-1,6-bisphosphate (n=4). Data are presented as means ± SEM. Statistical analyses were carried out using unpaired Student's t-tests (* P<0.05, ** P<0.01).

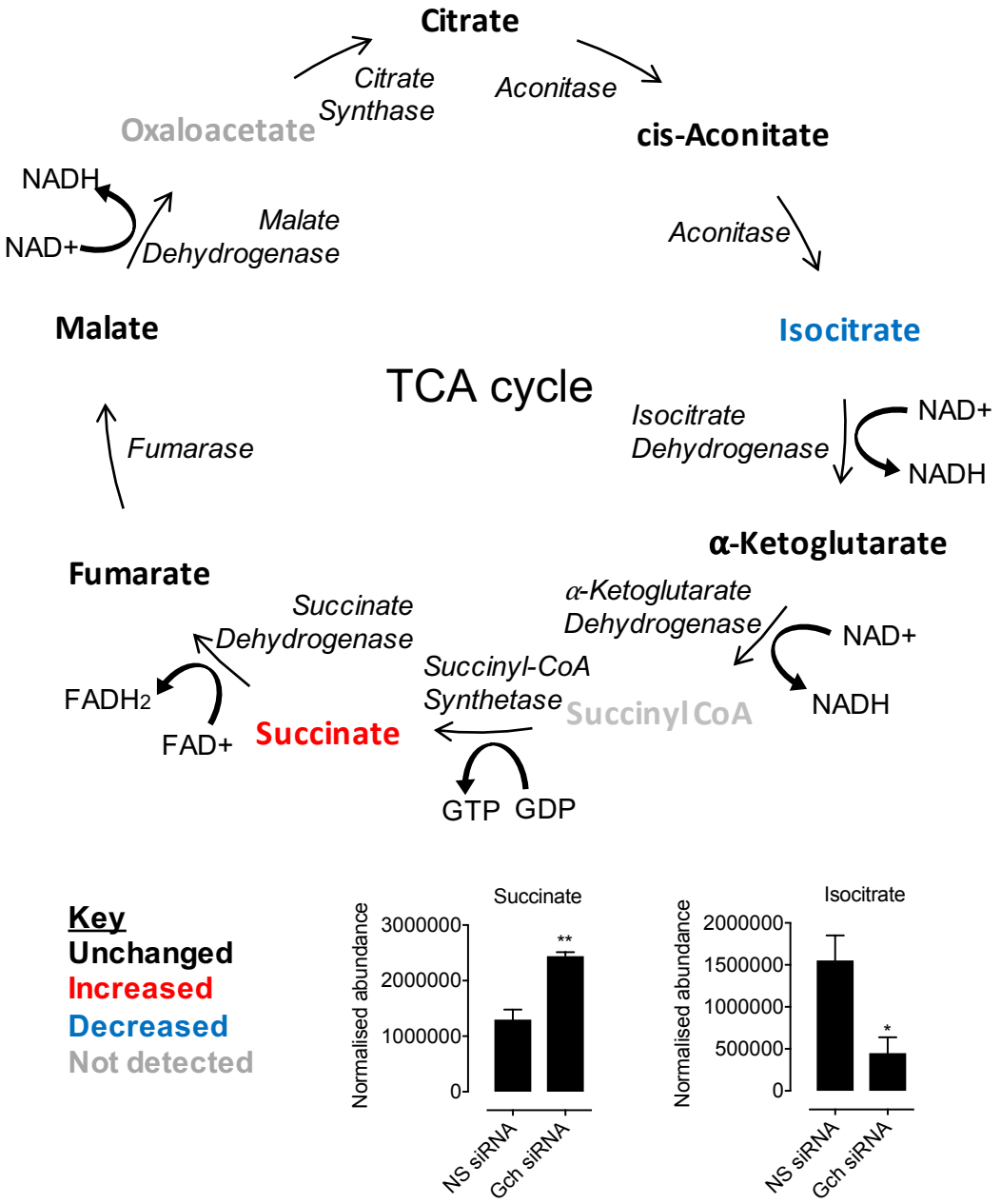


Figure 3.17 TCA cycle intermediate succinate was elevated and isocitrate was decreased in BH_4-deficient cells

The TCA cycle pathway showing changes in metabolite levels, with graphical inserts of the significantly altered metabolites succinate and isocitrate (n=4). Data are presented as means ± SEM. Statistical analyses were carried out using unpaired Student's t-tests (* P<0.05, ** P<0.01).

3.5 Discussion

3.5.1 Overview

The role of endothelial BH_4 as a cofactor for eNOS is well described, and diminished levels observed in vascular pathologies lead to eNOS uncoupling which alters the cellular balance of NO and ROS. In this chapter RNAi was used to knockdown *Gch1* and therefore disrupt BH_4 synthesis in sEnd.1 endothelial cells *in vitro*, to investigate the effects of BH_4 depletion on mitochondrial redox signalling and bioenergetics. This revealed that mitochondria were the predominant source of superoxide generated by BH_4-deficient endothelial cells, in a mechanism independent of its NOS cofactor function. Furthermore, although respiratory function was maintained, changes were observed in mitochondrial morphology and levels of TCA cycle metabolites. Overall these results suggest a novel role for BH_4 in modulating mitochondrial redox signalling and homeostasis.

3.5.2 BH_4 as a regulator of mitochondrial redox state

Elevated ROS is a marker of endothelial dysfunction, and BH_4 deficiency is known to be causal through eNOS uncoupling (Vásquez-Vivar et al., 1998). In this report this finding was reproduced, and went further, showing that in addition to eNOS, mitochondria were responsible for generating superoxide in cells depleted of BH_4. In fact, only a small proportion was inhibited by L-NAME and therefore derived from eNOS; whereas pharmacological inhibition of Complex I in the mitochondrial inner membrane by rotenone and targeted scavenging by MitoTEMPO dramatically decreased superoxide levels, revealing that mitochondria were the major source of superoxide in these cells. Furthermore, elevated superoxide produced by BH_4-deficient GCH cells (devoid of NOS) was also rotenone inhibitable, showing mitochondrial superoxide generation occurs independent of eNOS function. It is interesting to note that whilst rotenone abolishes superoxide to basal levels in GCH cells, the same is true for BH_4 depleted sEnd.1 cells in which eNOS would

presumably remain uncoupled. It is plausible that BH_4 depletion may cause mitochondrial superoxide production before eNOS uncoupling occurs, but it could also be a pre-requisite, or else cumulative inhibition by combined rotenone and L-NAME may indicate a lowered baseline in these cells. Further investigations into this would be interesting, as crosstalk between ROS sources in endothelial cells have previously been described, with the requirement of active NOX2 in angiotensin-II mediated mitochondrial superoxide production (Dikalov et al., 2014), and NOX derived ROS leading to BH_4 oxidation and eNOS uncoupling in hypertensive mice (Landmesser et al., 2003).

There are several possibilities regarding the precise mechanisms by which BH_4 depletion led to elevated mitochondrial ROS. A complex signal transduction pathway towards or within mitochondria was perhaps triggered in response to BH_4 depletion, or BH_4 may exert a more direct role in mitochondrial function. Although the answer remains unclear, the data presented in this chapter showed that not only was BH_4 present within mitochondria, its concentration was decreased following *Gch1* knockdown, therefore indicating the potential for a direct intra-organelle effect. Moreover, it was intriguing to find that BH_4 was more prone to oxidation within mitochondrial fractions, as a much greater proportion was oxidised to BH_2 and biopterin than in whole cells preparations (42% versus 6.37%). Although mitochondria generate notable amounts of superoxide from the ETC (Boveris and Chance, 1973), they also contain dedicated antioxidant systems, such as mnSOD, glutathione, glutaredoxin-2, glutathione peroxidase-4 and thioredoxin-2, to alleviate potential damage to organellar components (Chang et al., 2004; Griffith and Meister, 1985; Lundberg et al., 2001; Spyrou et al., 1997; Weisiger and Fridovich, 1973). It might be predicted that these copious antioxidant mechanisms would similarly protect BH_4 from reacting with oxidants, however as a redox sensitive molecule (Crabtree et al., 2009a; Kotsonis et al., 2000) it is also possible that BH_4 contributes to modulating the mitochondrial redox environment. The large proportion of oxidised biopterins would support this idea, and BH_4 was previously

shown to scavenge superoxide (including that of mitochondrial origin) in dopaminergic neurons and *in vitro* solutions (Nakamura et al., 2001). Furthermore, in 1972 Rembold and Buff implicated mitochondrial BH_4 in regulating 'intramitochondrial redox potential' and respiratory function (Rembold and Buff, 1972a, 1972b), but since then a role for BH_4 in mitochondria has only been alluded to by its presence there (Du et al., 2012; Nakamura et al., 2001; Shimizu et al., 2013). The data presented in this chapter suggests that it would be of interest to study the role of BH_4 in mitochondrial redox signalling and state in more detail.

3.5.3 How does BH_4 enter mitochondria?

In accordance with this study, several groups have previously reported the presence of mitochondrial BH_4 (Du et al., 2012; Rembold and Buff, 1972a; Shimizu et al., 2013), with one suggesting intramitochondrial synthesis due to localised GTPCH (Du et al., 2012). Similarly, GTPCH was detected in mitochondrial fractions by Western blotting, however as preparations of isolated mitochondria are impure and proteins associated with the outer membrane may also be present, more detailed analyses would be required to determine whether it is in fact even associated with this organelle. Another possibility is entrance via a BH_4 transporter, an area currently poorly understood although recently shown to occur via organic anion channels (OATs) (Ohashi et al., 2009, 2017). The fact that BH_4 restoration by sepiapterin supplementation rescued mitochondrial ROS generation suggests that BH_4 may be transported there, but this is uncertain as whole cell, but not mitochondrial biopterins were measured in this case.

3.5.4 BH_4 and NO signalling regulate mitochondrial fission

Mitochondria are dynamic organelles which form networks undergoing constant fission and fusion, allowing beneficial sharing of components and also efficient isolation of old or damaged sections for degradation (Frank et al., 2012; Nakada et al., 2001; Twig et al., 2008). Mitochondrial fusion is controlled by mitofusin 1, mitofusin 2 and OPA1 whereas fission

requires Fis1 and the GTPase DRP1 (Smirnova et al., 2001; Song et al., 2009). Mitochondrial fission has been linked with both causing mitochondrial ROS production and resulting from mild oxidative damage in endothelial cells (Giedt et al., 2012; Shenouda et al., 2011), and excessive fission is evident is endothelial dysfunction and neurodegenerative diseases (Cho et al., 2009; Shenouda et al., 2011). Despite elevated ROS, mitochondria were on average slightly larger in BH_4-deficient sEnd.1 cells, and although levels of fusion proteins and master fission regulator DRP1 were unchanged, phosphorylation of DRP1 at serine 616 was decreased. Phosphorylation of DRP1 at serine 616 activates the enzyme and is inhibitory at serine 637 (Chang and Blackstone, 2007; Kashatus et al., 2015), thus the observed loss of phosphorylation at serine 616 and unchanged serine 637 would have led to less active DRP1 and inhibited fission. This was probably due to loss of NO signalling in BH_4-deficient cells as NO has been shown to activate fission through DRP1 in neurons (Bossy et al., 2010; Cho et al., 2009; Rizza et al., 2018). It is suggested that DRP1 is activated by nitrosation (Cho et al., 2009; Rizza et al., 2018) and one report suggests that NO increases phosphorylation at serine 616 (Bossy et al., 2010) which would fit with the decrease in NO and DRP1 serine 616 phosphorylation in BH_4-deficient cells. As this model of BH_4 deficiency was relatively short term (72 hour siRNA knockdown) it would be interesting to observe the consequences of inhibited fusion in a longer term knockdown or primary cells from an endothelial *Gch1* knockout mouse. This would test whether morphological changes persist or become more evident, and whether inhibited fission ultimately has a detrimental effect on clearance of damaged mitochondria and potentially contributes to endothelial dysfunction.

3.5.5 BH_4 and mitochondrial respiratory function

In this study, it was hypothesises that BH_4 depletion would lead to changes in mitochondrial aerobic respiration, either through loss of NO signalling as NO is known to inhibit the ETC

(Chouchani et al., 2013; Clementi et al., 1998), or functions independent of NOS as BH_4 was previously shown to decrease respiration in cardiomyocytes (Sethumadhavan et al., 2016). It was therefore surprising to find that respiratory function was unaffected by BH_4 depletion in endothelial cells. Inhibition of NO production by eNOS was previously shown to elevate OCR in endothelial cells in real-time measurements taken immediately after eNOS inhibition (Clementi et al., 1999), but our data were collected following a longer period of NO deprivation allowing for potential adaptive changes. A possible NO-independent effect of BH_4 depletion was not pursued after finding unchanged OCR, but the changes previously observed in cardiomyocytes involved several hundred fold elevations of BH_4, far above physiological levels, and this limitation therefore led to a range of consequences that included profound redox changes, making it difficult to interpret the mechanisms affecting mitochondria in that study.

3.5.6 BH_4 modulates the TCA cycle and glycolysis

Glycolysis is the major source of ATP generation in endothelial cells (Culic et al., 1997; De Bock et al., 2013; Quintero et al., 2006; Spahr et al.) and it was therefore interesting to find that BH_4 depletion led to changes in this pathway. Whereas a increased OCR:ECAR ratio only hinted at decreased glycolysis and most measurable glycolytic metabolites were unchanged, a 3 fold accumulation of fructose-1,6-bisphosphate was very striking and its production by phosphofructokinase-1 (PFK-1) is an important rate limiting step. These snap shot metabolite measurements do not explore flux through the pathway and it is unclear whether increased fructose-1,6-bisphosphate abundance resulted from decreased metabolism by aldolase or increased production by PFK-1. NO has previously been shown to up-regulate glycolysis by increasing levels of fructose-2,6-bisphosphate (Almeida et al., 2004) which is a powerful allosteric activator of PFK-1 (Van Schaftingen et al., 1982). It would therefore be interesting to investigate whether loss of NO in BH_4-deficient endothelial

cells affects PFK-1 activity and overall glycolytic rate. In addition, it is possible that the activity of GAPDH is decreased downstream of aldolase and contributes to fructose-1,6-bisphosphate accumulation. This is plausible as superoxide levels were elevated in BH_4 deficient cells and an active site cysteine in GAPDH is sensitive to reversible oxidation that inhibits catalysis (Peralta et al., 2015). Also of note, fructose-1,6-bisphopspahte has been suggested to protect neurons from oxidative stress by preserving reduced glutathione (Vexler et al., 2003), so increased levels in ROS producing BH_4 depleted cells may be beneficial.

Two metabolites found in the TCA cycle were also significantly changed in BH_4-deficient cells, as succinate was increased and isocitrate was decreased. It is again uncertain whether altered activity of the enzymes synthesising or using these metabolites led to these changes, but it is plausible that decreased isocitrate resulted from increased IDH activity when NO levels were decreased, as the cytosolic $NADP^+$-dependent isoform is known to be inhibited by NO through nitrosation (Yang et al., 2002). Exploring whether this is the case could be an important part of understanding the redox environment of BH_4-deficient cells because increased activity of $NADP^+$ dependent isocitrate dehydrogenase was shown to modulate cellular redox state and limit damage (Lee et al., 2002). In addition, aconitase activity may be decreased in BH_4-deficient cells that generate more mitochondrial superoxide, as reaction of superoxide with catalytic [Fe-S] centres leads to inhibition and decreased isocitrate production (Flint et al., 1993).

The changes in TCA cycle metabolites may reflect dysfunction in the production of substrates (NADH and $FADH_2$) for oxidative phosphorylation, however as mitochondrial respiration is a minor contributor to ATP production in endothelial cells, even if this is the case it may have more pronounced implications for the redox environment in which NAD^+/NADH play a prominent part (Schafer and Buettner, 2001; Williamson et al., 1967).

Additionally, TCA cycle metabolites are gaining appreciation as signalling molecules, and this includes succinate which is involved in inflammation and tumorigenesis by inhibiting prolyl hydroxylase and leading to HIF1α mediated signalling (Mills et al., 2016; Selak et al., 2005). Accumulated succinate has also been shown to drive mitochondrial ROS formation through reverse electron transport via succinate dehydrogenase in inflammatory macrophages, reperfused ischaemic hearts and hypoxic endothelial cells (Chouchani et al., 2014; Koziel and Jarmuszkiewicz, 2017; Mills et al., 2016). It is unclear whether conditions would allow this to be a possible source of ROS generation in BH_4-deficient endothelial cells.

3.5.7 Mitochondria as a therapeutic target in BH_4-deficient endothelium

The most robust and profound finding in this study was the evidence indicating elevated mitochondrial superoxide generation in BH_4-deficient cells, which was also notable due to the fact that this occurred independent from the function of NOS. Previous attempts to restore BH_4 levels by supplementation were limited by systemic oxidation (Cunnington et al., 2012) and the use of vitamins C and E as antioxidant therapies to target elevated ROS in endothelial dysfunction and cardiovascular diseases have had mixed outcomes with many showing no benefit (Ashor et al., 2015; Engler et al., 2003; Kinlay et al., 2004; Plantinga et al., 2007; Vivekananthan et al., 2003; Ye et al., 2013). Mitochondria-targeted antioxidants (Kelso et al., 2001; Smith et al., 1999) have shown more success, improving endothelial dysfunction in hypertensive rodents as well as aging mice and humans (Dikalova et al., 2010; Gioscia-Ryan et al., 2014b; Graham et al., 2009b; Rossman et al., 2018). Treating patients presenting with BH_4-deficient endothelium using these mitochondria-targeted antioxidants is likely to be beneficial by improving their endothelial dysfunction.

3.5.8 Conclusions

The data presented in this chapter demonstrated that BH_4 depletion of endothelial cells led to changes in mitochondrial redox signalling, morphology and levels of the TCA cycle metabolites succinate and isocitrate. Importantly, and for the first time, this report revealed that mitochondria were the predominant source of superoxide generation in BH_4-deficient endothelial cells, in a mechanism independent of its NOS cofactor function. Overall this study has uncovered a novel role for BH_4 in modulating mitochondrial redox signalling and aspects of metabolism, and indicates that mitochondrial ROS generation is a viable therapeutic target in patients with BH_4 deficiency and endothelial dysfunction. The possibility that some of these BH_4-dependent changes are common to other BH_4-deficient cells types will be discussed in subsequent chapters, with a focus on inflammatory macrophages.

Chapter 4:
Optimising culture of bone marrow derived macrophages

Chapter 4: Optimising culture of bone marrow derived macrophages

4.1 Introduction

4.1.1 Macrophage heterogeneity and polarisation

Macrophages are a diverse population of cells that are derived from haematopoietic progenitors (Sheng et al., 2015), and adapt their functions in response to external stimuli. As part of the innate immune response, monocytes are recruited to sites of inflammation where growth factors such as macrophage colony stimulating factor (MCSF) stimulate their differentiation into macrophages. These macrophages infiltrate tissues to eliminate pathogens and secrete cytokines to recruit other leukocytes, but are also involved in tissue repair. In addition, distinct populations of tissue-resident macrophages carry out specialised homeostatic roles and are maintained by self-renewal throughout adult life (Hashimoto et al., 2013; Yona et al., 2013); these include Kupffer cells in the liver, microglia in the brain, alveolar macrophages in the lungs and peritoneal macrophages.

Macrophages display a variety of cell surface receptors that recognise numerous molecules including cytokines, components of pathogens and damaged tissues, which allow rapid responses to environmental changes. The ability to integrate multiple signals which elicit intracellular changes in transcription, protein expression and metabolism, form macrophages with differing activation/polarisation states. The initial concept that macrophage polarisation existed on a spectrum between ‘classically’ activated inflammatory or ‘alternatively’ activated anti-inflammatory states has been revised, and studies have revealed that the vast range and possible combinations of stimuli lead to a far more diverse multi-dimensional array of activation states (Xue et al., 2014). The diversity of polarisation states contributes to macrophage heterogeneity.

4.1.2 Studying macrophage function in vitro

To study macrophages *in vitro* they are typically either removed from their *in vivo* origin – such as the peritoneum – or cultured from bone marrow progenitor cells to form bone marrow derived macrophages (BMDMs). As discussed, macrophages are particularly sensitive to exogenous stimuli, and these conditions will differ compared to situations encountered *in vivo* and therefore potentially change their function. This is a major limitation of culturing primary cells and it is advisable to follow-up *in vitro* studies with direct analysis of cells isolated from animals. However, the ability to completely control conditions *in vitro* can be advantageous and allows researchers to fully characterise the response of macrophages to specific stimuli, and this forms the rationale for using BMDMs in this study. Unfortunately some of the reagents used in the literature can be detrimental and efforts are being made to rectify this (Murray et al., 2014). For example, MCSF causes differentiation of haematopoietic stem cells into macrophages and is involved in their proliferation and survival (Wiktor-Jedrzejczak et al., 1990). It has been used to generate *in vitro* BMDMs from bone marrow progenitor cells for decades (Stanley and Heard, 1977), but it is common to use whole conditioned media from L929 cells – which are known to secrete MCSF – as the source. L-cell conditioned media (LCM) is easy to self-produce but varies between batches and is not completely defined, so use of recombinant MCSF is increasingly preferred (Murray et al., 2014). Other variability arising from media composition includes the base medium used, FBS source and concentration, glucose content and antibiotics, and these are easily reported.

Our laboratory generated mice with *Gch1* knocked out specifically in endothelial and myeloid cells to study the physiological and cellular consequences of BH_4 deficiency in these cell types (Chuaiphichai et al., 2014; McNeill et al., 2015). As LPS and IFNγ induced inflammatory polarisation of BMDMs includes iNOS derived NO and BH_4 synthesis, the

response of *Gch1* KO BMDMs to these stimuli was studied. This revealed that in the absence of BH_4, NO was not produced despite iNOS induction, NRF2 signalling was disrupted and ROS levels were elevated from a NOS-independent unidentified origin (McNeill et al., 2015). The aims of this thesis were focused on uncovering novel pathways modulated by BH_4 – including NOS-independent roles and identifying this ROS source in macrophages – which led to investigations into the effects of BH_4 deficiency on mitochondrial function and metabolism. However, during previous experiments in our laboratory BMDMs were cultured in LCM and activation media contained reduced serum levels, which compromised cellular health and compromised assays. To proceed with the main thesis aims, steps were taken to maintain adherent BMDMs throughout culture, which led to the discovery that LCM and FBS contain substantial amounts of biopterins. In a model studying BH_4 deficiency this was problematic and in this chapter a new protocol was optimised to culture BMDMs in media containing minimal biopterins.

4.2 Aims and hypotheses

This chapter aimed to develop a new protocol to culture adherent BMDMs in media containing minimal biopterins and undefined constituents, that would be suitable to test the hypothesis that BH_4 has NOS-independent roles in macrophage mitochondrial function and metabolism.

4.3 Methods

General methods were specified in Chapter 2. Chapter specific methods and optimisation are outlined below.

4.3.1 Bone marrow extraction

Male and female mice were culled by Schedule 1 and legs were dissected by Mr Ashley Hale and Dr Surawee Chuaiphichai. Using aseptic technique, bone marrow was extracted from tibia and femur bones following removal of surrounding muscle. To do so, joints were cut using a scalpel and the exposed bone marrow was flushed out the ends of the bones using a 25 gauge needle and a 10 ml syringe filled with PBS. Clumps were gently disaggregated using a needle-less syringe and passed through a 70 µm cell strainer. The cell suspension was centrifuged at 250 x g for 5 minutes at room temperature to pellet cells. The supernatant was discarded and cells were resuspended in ultra-low endotoxin FBS containing 10% DMSO, divided into 4 cryovial aliquots per mouse and stored at -80 °C in Mr Frosty™ Freezing Containers overnight before transfer to liquid nitrogen storage.

4.3.2 Established protocol for growing bone marrow derived macrophages

Vials of bone marrow stored in liquid nitrogen were defrosted and resuspended in 5 ml of DMEM F12 media before centrifuging at 250 x g for 5 minutes to pellet cells. The supernatants were discarded and cells were resuspended in 1 ml of DMEM F12 growth media containing L-glutamine (2 mM), penicillin (100 units/ml), streptomycin (0.1 mg/ml), 10% FBS and 10% LCM as a source of MCSF growth factor (DMEM F12 LCM growth media). 20 µl of cell suspension was counted using the Cellometer Auto 2000 (Nexcelom Bioscience), and the value was used to seed cells at a density of 500,000 cells/well of a non-tissue culture treated 6 well plate in 2 ml DMEM F12 LCM growth media on Day 0 (Figure 4.1). Cells were cultured for 7 days and fed with addition of 1 ml DMEM F12 LCM growth

media on Day 5 of culture. On Day 7 cells were washed with warm PBS to remove unadhered cells and media was replaced with OptiMEM containing GlutaMAX, penicillin (100 units/ml), streptomycin (0.1 mg/ml) and 0.2% BSA. Cells were either left unstimulated or were stimulated with LPS (100 ng/ml) and IFNγ (10 ng/ml) overnight (16 hours).

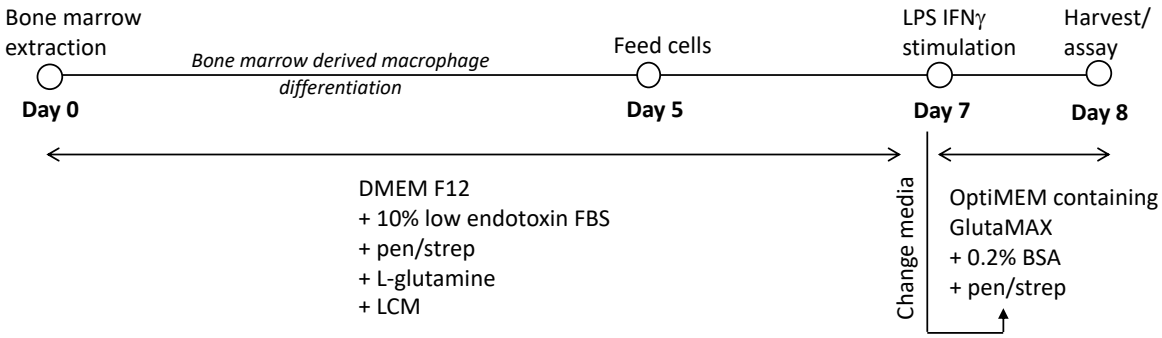


Figure 4.1 Established laboratory protocol for BMDM culture in L-cell conditioned media

4.3.3 Optimised protocol for growing bone marrow derived macrophages

Vials of bone marrow stored in liquid nitrogen were defrosted and resuspended in 5 ml of DMEM F12 media before centrifuging at 250 x g for 5 minutes to pellet cells. The supernatants were discarded and cells were resuspended in 1 ml of DMEM F12 growth media containing L-glutamine (2 mM), penicillin (100 units/ml), streptomycin (0.1 mg/ml), 5% FBS and recombinant MCSF (25 ng/ml) growth factor (DMEM F12 MCSF growth media). 20 µl of cell suspension was counted using the Cellometer Auto 2000 (Nexcelom Bioscience), and the value was used to seed cells at a density of 500,000 cells/well of a non-tissue culture treated 6 well plate in 2 ml DMEM F12 MCSF growth media on Day 0 (Figure 4.2). Cells were cultured for 7 days and fed with addition of 1 ml DMEM F12 MCSF growth media containing MCSF (50 ng/ml) on Day 5 of culture, and addition of GMCSF (50 ng/ml) on Day 6. On Day 7 cells were washed with warm PBS to remove unadhered cells and media

was replaced with DMEM F12 containing L-glutamine (2 mM), penicillin (100 units/ml), streptomycin (0.1 mg/ml), 2% FBS, MCSF (25 ng/ml) and GMCSF (50ng/ml). Cells were either left unstimulated or were stimulated with LPS (100 ng/ml) and IFNγ (10 ng/ml) overnight (16 hours).

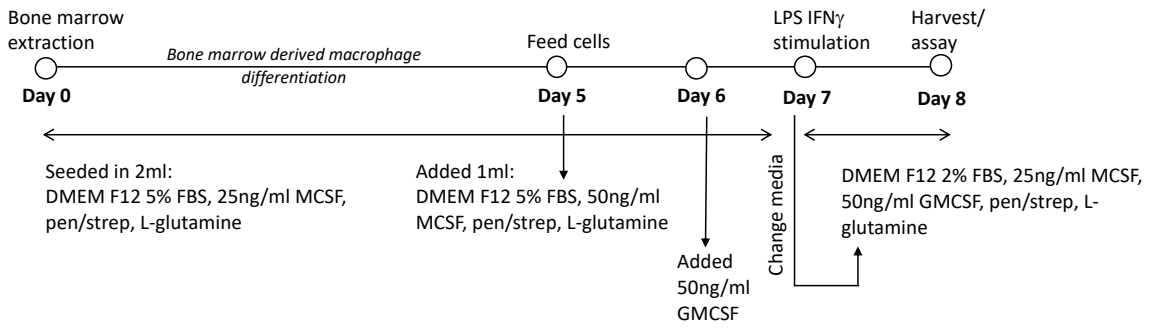


Figure 4.2 Optimised protocol for growing BMDMs in recombinant MCSF and GMCSF

4.3.4 Imaging of cells

Cells in Figure 4.4 were imaged using a Leica DMRBE microscope, but this had the disadvantage of exposing cells to unsterile air. All subsequent images were taken using the camera on a Huawei P9 Lite through the eye pieces of a Nikon TMS microscope as the images were clearer and the cells could remain sterile. The scale bars on images acquired using a Huawei P9 Lite were estimated by comparison with images of BMDMs (acquired with accurate scale bars) taken at the same time point using a microscope. These images were suitable for the purpose of demonstrating cellular adherence but higher quality images and accurate scale bars would be preferable for publication or more detailed analyses.

4.3.5 FACS

Fluorescence-activated cell sorting (FACS) analysis was carried out with Dr Jyoti Patel (a postdoctoral researcher within the group). On Day 7 of culture BMDMs were washed once in PBS before harvesting into PBS containing 5mM EDTA by flushing with a pipette. 500,000 cells were transferred into FACS tubes, centrifuged at 250 x g for 5 minutes at 4 °C and the supernatants discard. Cells were resuspended in 100 µl of FACS buffer (PBS containing BSA (0.2%) and EDTA (2 mM)) containing anti-mouse FcγRII/III CD16/32 (5 µg/ml; BD Bioscience) for 15 minutes on ice to block Fc receptors and non-specific antibody binding. Cells were then stained with fluorochrome conjugated antibodies specific for cell surface markers by incubation for 30 minutes on ice covered in foil. The antibody mixture of macrophage markers consisted of anti-CD45-PE-Cy7 (1 µg/ml), anti-CD11b-PerCP (1 µg/ml), anti-MHCII-PE (1 µg/ml) and anti-F4/80-APC (1 µg/ml). In control samples, parallel unstained and isotype control antibodies were included at the same concentration as the antigen-specific conjugates. Cells were washed in FACS buffer and centrifuged at 250 x g for 5 minutes at 4 °C and then fixed in 250 µl formaldehyde (2%). FACS was carried out using a CyAn Analyser flow cytometer (Dako) and data were analysed by Dr Jyoti Patel using FlowJo (Tree Star Inc.).

4.3.6 Cytokine array

A Proteome Profiler Mouse Cytokine Array Kit (Panel A, R&D systems) containing nitrocellulose membranes spotted with capture antibodies in duplicate was used to measure cytokines in 1 ml of media following the manufacturer's protocol in a method similar to Western blotting.

4.4 Results

4.4.1 Characterising Gch$^{fl/fl}$Tie2cre bone marrow derived macrophages grown using the established protocol

Before carrying out experiments to investigate the effects of BH_4 deficiency on macrophage mitochondrial function and redox signalling, bone marrow from Gch$^{fl/fl}$Tie2cre mice was cultured using the protocol previously used by our laboratory to generate macrophages (Section 4.3.2) (McNeill et al., 2015) and GTPCH and BH_4 levels were checked. As expected there was a small amount of GTPCH in control Gch$^{fl/fl}$ macrophages when unstimulated, and stimulation with LPS/IFNγ led to a greater abundance in control cells, whereas GTPCH was absent in Gch$^{fl/fl}$Tie2cre macrophages (Figure 4.3A). iNOS protein was found in all cells stimulated with LPS/IFNγ regardless of genotype apart from iNOS knockout (iNOS KO) negative controls (Figure 4.3A). Biopterin measurements revealed dramatically lower amounts of BH_4, BH_2 and biopterin in Gch$^{fl/fl}$Tie2cre macrophages compared with Gch$^{fl/fl}$ cells (Figure 4.3B-D) and this led to significantly lower total biopterin content (Figure 4.3E). The ratio of BH_4:BH_2+biopterin was also decreased due to the higher proportion of oxidised biopterins in Gch$^{fl/fl}$Tie2cre macrophages (Figure 4.3F). Analysis of media supernatants revealed that although production of iNOS was induced by LPS/IFNγ in both Gch$^{fl/fl}$ and Gch$^{fl/fl}$Tie2cre macrophages, only Gch$^{fl/fl}$ cells produced NO as indicated by nitrite secretion (Figure 4.3G). As these results confirmed the expected decreases in GTPCH, BH_4 and NO generation in Gch$^{fl/fl}$Tie2cre macrophages, experiments into mitochondrial function and ROS generation began.

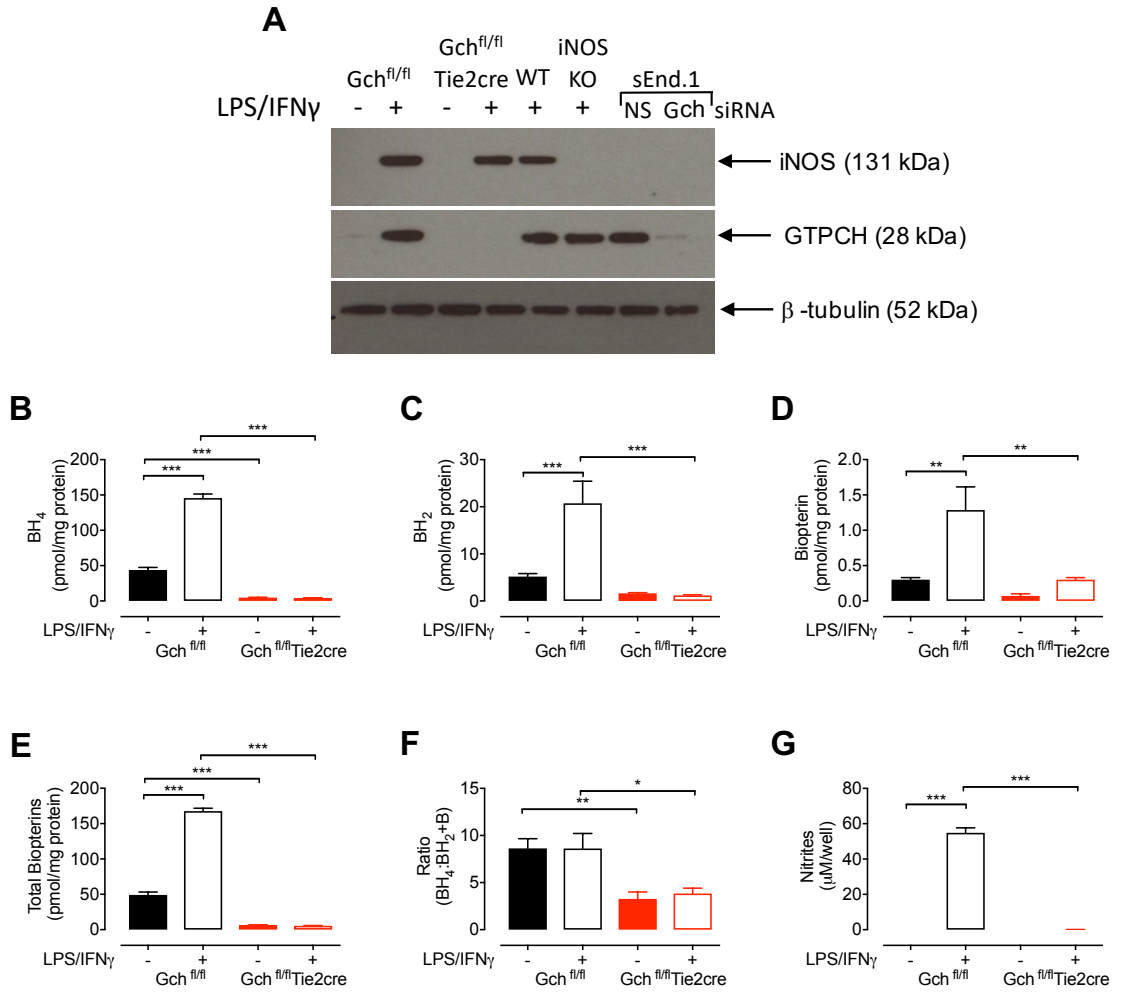


Figure 4.3 Characterisation of Gch$^{fl/fl}$Tie2cre BMDMs grown in media containing L-cell conditioned media

(A) Western blot analysis of GTPCH and iNOS in Gch$^{fl/fl}$ and Gch$^{fl/fl}$Tie2cre macrophages following overnight stimulation with LPS and IFNγ. Stimulated wild type (WT) and iNOS knock out (iNOS KO) macrophages were used as positive and negative controls for iNOS, and NS and Gch siRNA sEnd.1 cells were used as positive and negative controls for GTPCH. Anti-β-tubulin was used as the loading control (n=3). (B-F) HPLC was used to quantify (B) BH_4, (C) BH_2 and (D) biopterin and the results were used to calculate (E) total biopterins (BH_4+BH_2+biopterin) and (F) the ratio BH_4:BH_2+biopterin (n=7). (G) Nitrite was measured in media supernatants using the Griess assay (n=7). All data are presented as means ± SEM. Statistics were calculated using 2-way ANOVA and Tukey's post-test (* P<0.05, ** P<0.01, *** P<0.001).

4.4.2 Macrophages grown in very low serum media overnight are unhealthy

After becoming accustomed to growing BMDMs using the previously established protocol (Figure 4.4A) detachment of unstimulated cells on Day 8 of culture was consistently noted, and this became particularly apparent while using them for assays which took place over a number of hours. Overnight stimulation was considered to be 16 hours, and by 19 hours – which included the length required in many assays – a large number of cells became visibly rounded and detached in unstimulated but not stimulated cells (Figure 4.4B and C). It was therefore hypothesised that these cells were dying due to serum starvation, which was reduced to 0.2% BSA in OptiMEM on Day 7 (Figure 4.4A) and is known to trigger apoptosis in cells (Messam and Pittman, 1998). Healthy unstimulated cells were a vital control for all experiments, and furthermore led to concerns that although $M^{LPS/IFN\gamma}$ cells appeared healthy they may be similarly affected, as it is known that apoptotic changes and commitment to cell death occur hours before morphological changes become apparent (Brunet et al., 1998; Messam and Pittman, 1998). The cell culture protocol was modified, and the media changed to fresh DMEM F12 containing 10% FBS rather than low serum OptiMEM on Day 7 (Figure 4.4D), which resulted in cells that appeared attached and healthy on Day 8 in unstimulated and stimulated conditions (Figure 4.4E and F). This seemed to have solved the problem, but before continuing with experiments it was important to first re-characterise the properties of stimulated $Gch^{fl/fl}$ and $Gch^{fl/fl}$Tie2cre macrophages.

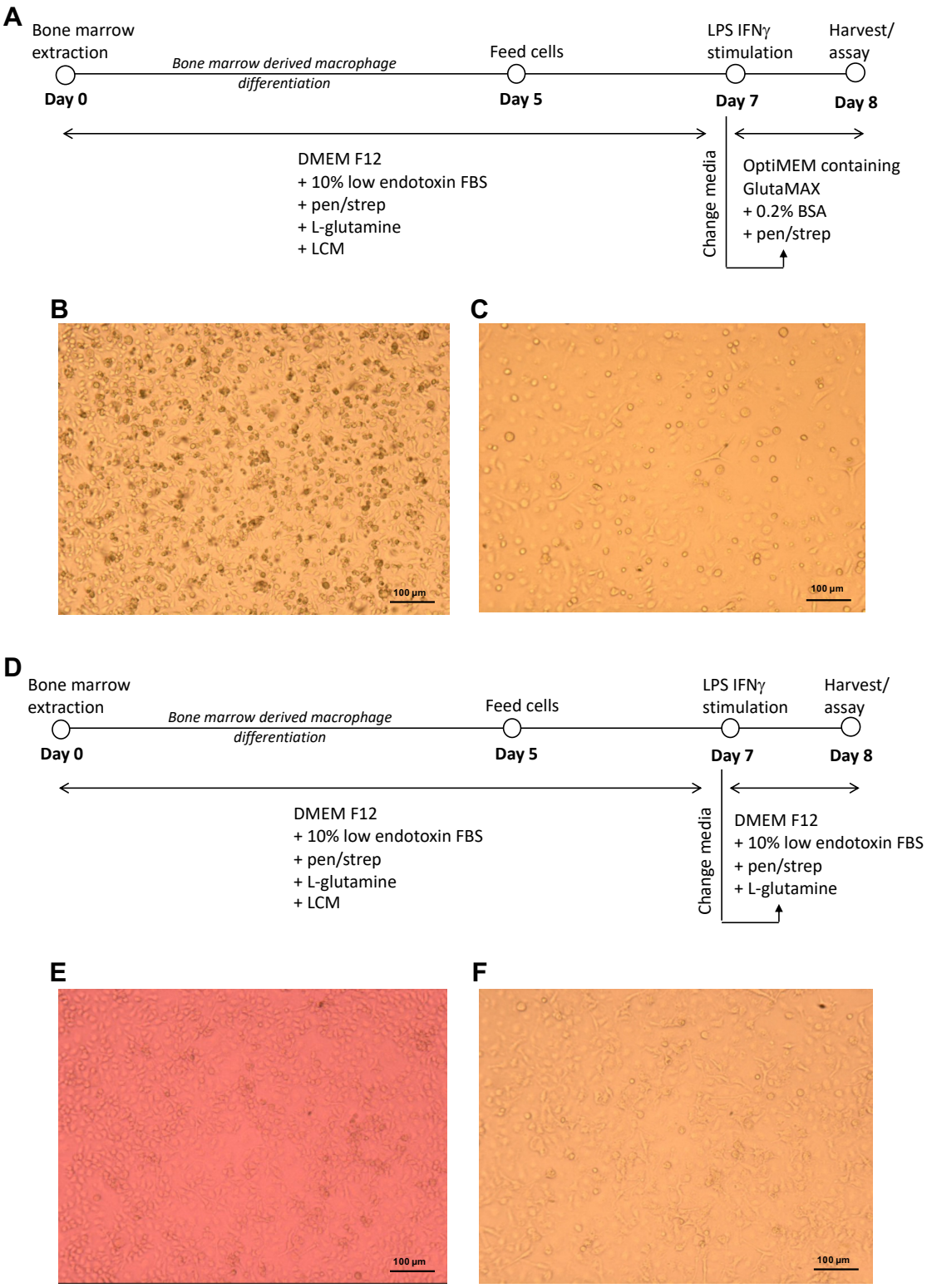


Figure 4.4 Macrophages grown in very low serum media overnight detach

(A) Outline of the protocol previously used by our laboratory to grow bone marrow derived macrophages using LCM for differentiation and OptiMEM containing very low serum (0.2% BSA) during overnight stimulation with LPS/IFNγ. (B - C) Representative images of $Gch^{fl/fl}$ cells on Day 8 following 19 hours in OptiMEM low serum media and either (B)

unstimulated or (C) simulated with LPS/IFNγ (n=1 in duplicate, but observed multiple times). (D) Outline of a protocol for culturing bone marrow derived macrophages using LCM for differentiation but maintaining cells in DMEM F12 containing 10% FBS during overnight stimulation with LPS/IFNγ. (E – F) Representative images of $Gch^{fl/fl}$ cells on Day 8 following 19 hours in DMEM F12 media containing 10% FBS and either (E) unstimulated or (F) simulated with LPS/IFNγ (n=1 in duplicate).

4.4.3 FBS and L-cell conditioned media contain BH_4 and BH_2

Nitrites were measured in media supernatants collected from macrophages following overnight stimulation with LPS/IFNγ and revealed that large amounts of nitrite were secreted from $M^{LPS/IFN\gamma}$ WT and $Gch^{fl/fl}$ cells when incubated in OptiMEM containing 0.2% BSA and DMEM F12 containing 10% FBS media (Figure 4.5A and B). However, whereas no nitrites were detected in media from stimulated $Gch^{fl/fl}$Tie2cre macrophages incubated in OptiMEM containing 0.2% BSA, 11.617 μM ±0.987 SD were found in media from $Gch^{fl/fl}$Tie2cre macrophages incubated in DMEM F12 containing 10% FBS (Figure 4.5B). This was probably due to functional iNOS in $Gch^{fl/fl}$Tie2cre macrophages incubated in DMEM F12 containing 10% FBS despite *Gch1* knockout because these data were corrected for any measurable nitrites in fresh media used as blank samples, and nitrites were undetectable in media from stimulated iNOS KO cells in both media types (Figure 4.5A and B). Hypothesising that BH_4 was supplemented by a component of DMEM F12 media containing 10% FBS at a sufficient levels to allow iNOS to produce NO, experiments were carried out to identify the source.

HPLC was used to quantify levels of biopterin species in constituents of macrophage cell culture media. This showed that DMEM F12, OptiMEM and DMEM base media alone contained detectable but very low levels of BH_4 and BH_2, and although biopterin measurements were much higher the inability of cells to convert this into BH_4 means that this is unlikely to supplement cells (Figure 4.6A). Much higher levels of BH_4 and BH_2 were found in 2 batches of low endotoxin FBS diluted to 10% working concentrations (Figure

4.6B), and the majority comprised of BH_2 which can be converted into BH_4 intracellularly by the DHFR salvage pathway (Crabtree et al., 2009b). This suggests that FBS was predominantly supplementing $Gch^{fl/fl}$Tie2cre macrophages incubated in DMEM F12 containing 10% FBS with BH_2, and this was converted into BH_4 allowing iNOS to produce NO. Interestingly similarly substantial levels of BH_4 and BH_2 were present in 10% LCM but not preparations of recombinant MCSF growth factor (Figure 4.6C). Thus the presence of both FBS and LCM in media during the first 7 days of BMDM culture were providing cells with BH_2 and BH_4, and it was fortuitous that eliminating LCM and serum starvation removed both sources during the overnight stimulation in the established laboratory protocol. The next aim was to minimise the biopterin content of the media throughout the BMDM cell culture protocol.

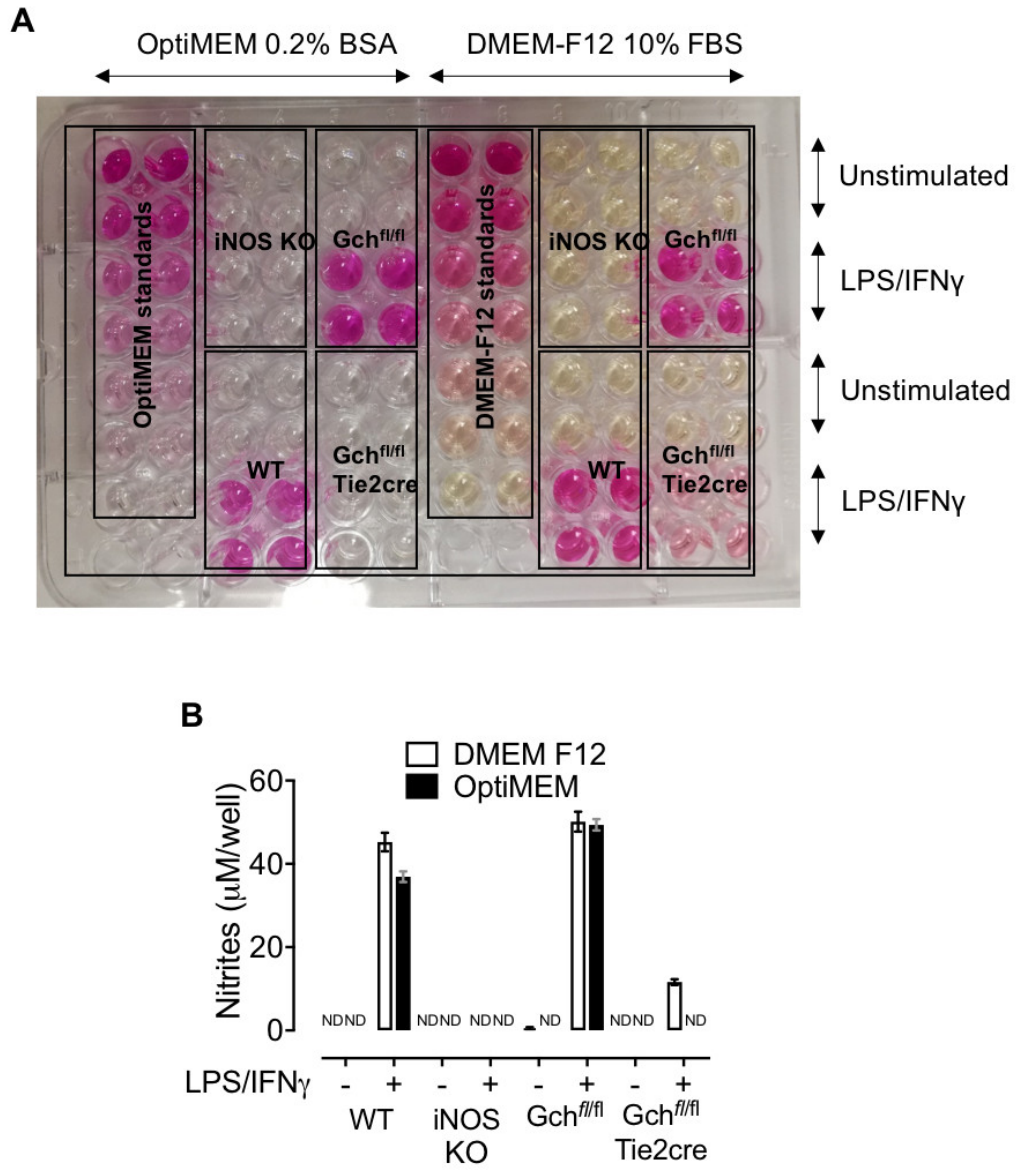


Figure 4.5 Gch$^{fl/fl}$Tie2cre macrophages stimulated with LPS/IFNγ in DMEM F12 media containing 10% FBS produce NO

(A) Image showing the results of a Griess assay carried out on media supernatants from wild type (WT), iNOS knockout (iNOS KO), Gch$^{fl/fl}$ and Gch$^{fl/fl}$Tie2cre macrophages following overnight incubation in OptiMEM containing 0.2% BSA or DMEM F12 media containing 10% FBS and stimulation with LPS/IFNγ. The intensity of pink colouring correlates with nitrite levels (n=2 in duplicate). (B) A plate reader (absorbance 550 nm) was used to quantify the concentration of nitrites in media on the plate shown above (n=2 in duplicate). All data are presented as means ± range. ND – not detectable.

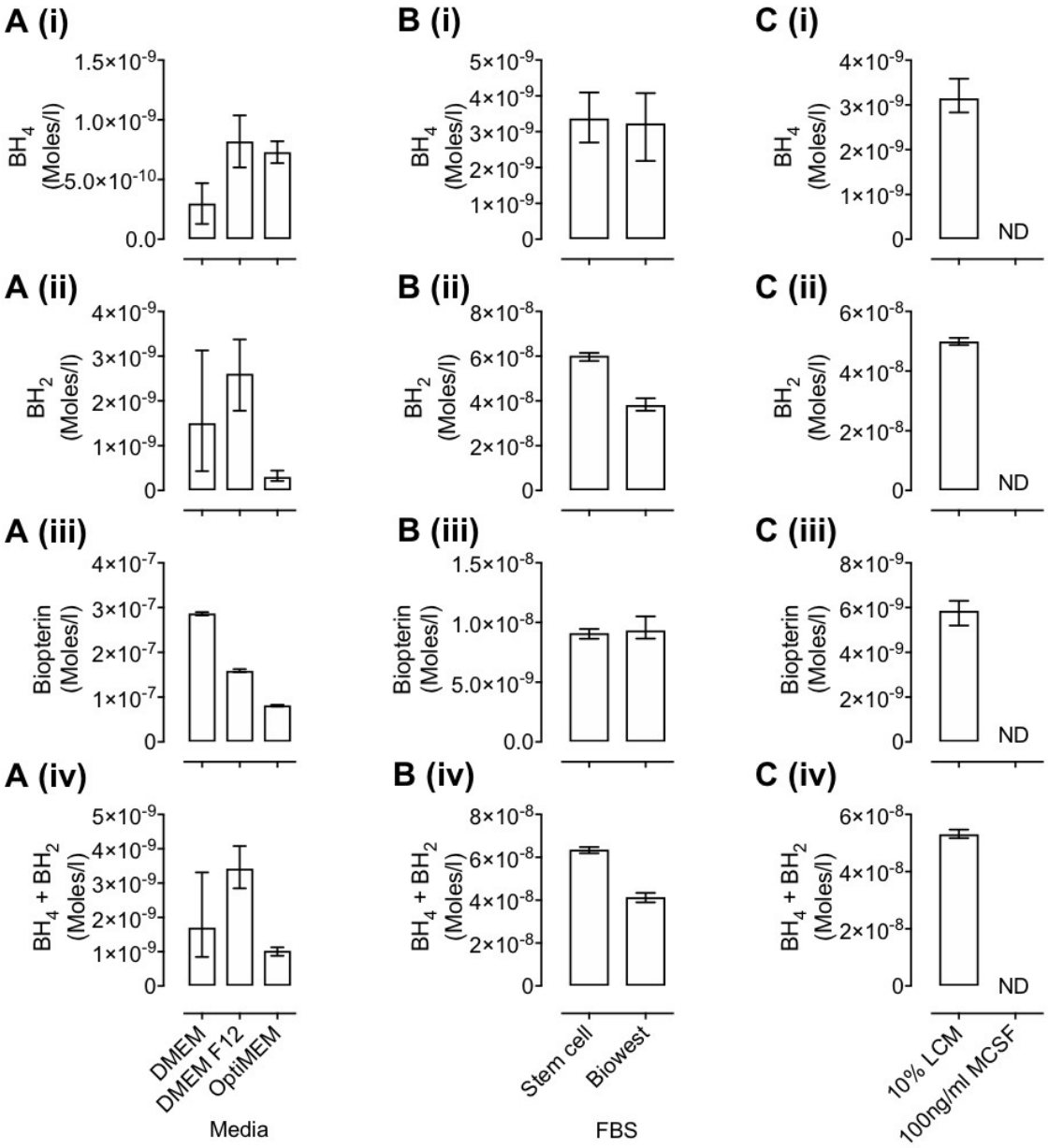


Figure 4.6 FBS and L-cell conditioned media contain substantial amounts of biopterins

The biopterin content of base media, LCM and FBS were measured using HPLC. (A i) BH_4, (A ii) BH_2 and (A iii) biopterin were measured in fresh DMEM, DMEM F12 and OptiMEM media without supplements. (A iv) Total concentrations BH_4+BH_2 were calculated. (B i) BH_4, (B ii) BH_2 and (B iii) biopterin were measured in 10% LCM and 100 ng/ml recombinant macrophage colony stimulating factor (MCSF). (B iv) Total concentrations BH_4+BH_2 were calculated. (C i) BH_4, (C ii) BH_2 and (C iii) biopterin were measured in 10% Stem cell grade and Ultralow endotoxin (Biowest) FBS. (C iv) Total concentrations BH_4 + BH_2 were calculated. (n=1 in triplicate). All data are presented as means ± range.

4.4.4 Optimising BMDM cell culture in low biopterin conditions

As one prominent source of biopterins, FBS concentrations were optimised to the lowest level possible in cell culture media while maintaining healthy cells. Bone marrow grown for 7 days in DMEM F12 containing 10% LCM and 10, 5 or 2% FBS revealed adherent cells indicative of differentiated macrophages in all instances on Day 7 (Figure 4.7). Cells grown in 5 or 10% FBS conditions were equally confluent (by eye), however when grown in 2% FBS cells grew much slower. This led to a protocol culturing cells for 7 Days in 5% FBS and switching to 2% FBS during overnight stimulation to minimise biopterins.

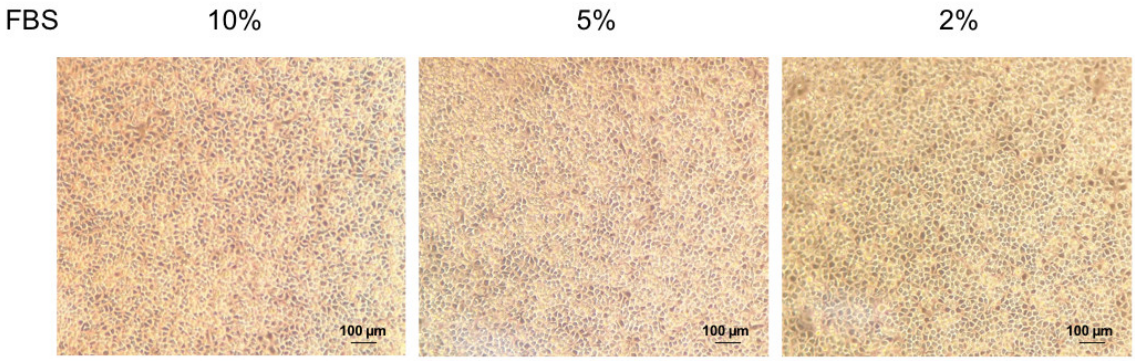


Figure 4.7 Bone marrow derived macrophages can be cultured in 5% FBS

Bone marrow from $Gch^{fl/fl}$ mice was cultured for 7 days in DMEM F12 containing LCM and either 10, 5 or 2% FBS. Images of bone marrow derived macrophages were taken on Day 7 of culture and representative images demonstrate health of cells within a confluent area (n=1 in duplicate).

Next conditions were optimised to culture BMDMs using recombinant MCSF – which had proven biopterin free (Figure 4.6C) – rather than biopterin rich LCM as the source of growth factor. The previous literature consisted of a range of protocols using between 6 and 50 ng/ml MCSF in BMDM growth media, and a similarly large number of feeding protocols (Anzinger et al., 2012; Fleetwood et al., 2007; Lacey et al., 2012; Turnbull et al., 2006). Culturing macrophages using a range of seeding densities and feeding protocols (not shown) revealed that bone marrow seeded at 500,000 cells/well of a 6 well plate in DMEM F12 media containing 5% FBS and 25 ng/ml MCSF for 7 Days, with addition of 50 ng/ml MCSF media on Day 5, was optimal to produce confluent macrophages on Day 7 (Figure 4.8A and B). Removing MCSF from media overnight between Day 7 and 8 resulted in detachment of cells (Figure 4.8C), but with MCSF in the media cells were adherent in both 5 and 2% FBS media (Figure 4.8C), so DMEM F12 media containing 2% FBS and 25 ng/ml MCSF was chosen for overnight stimulation (Figure 4.8A).

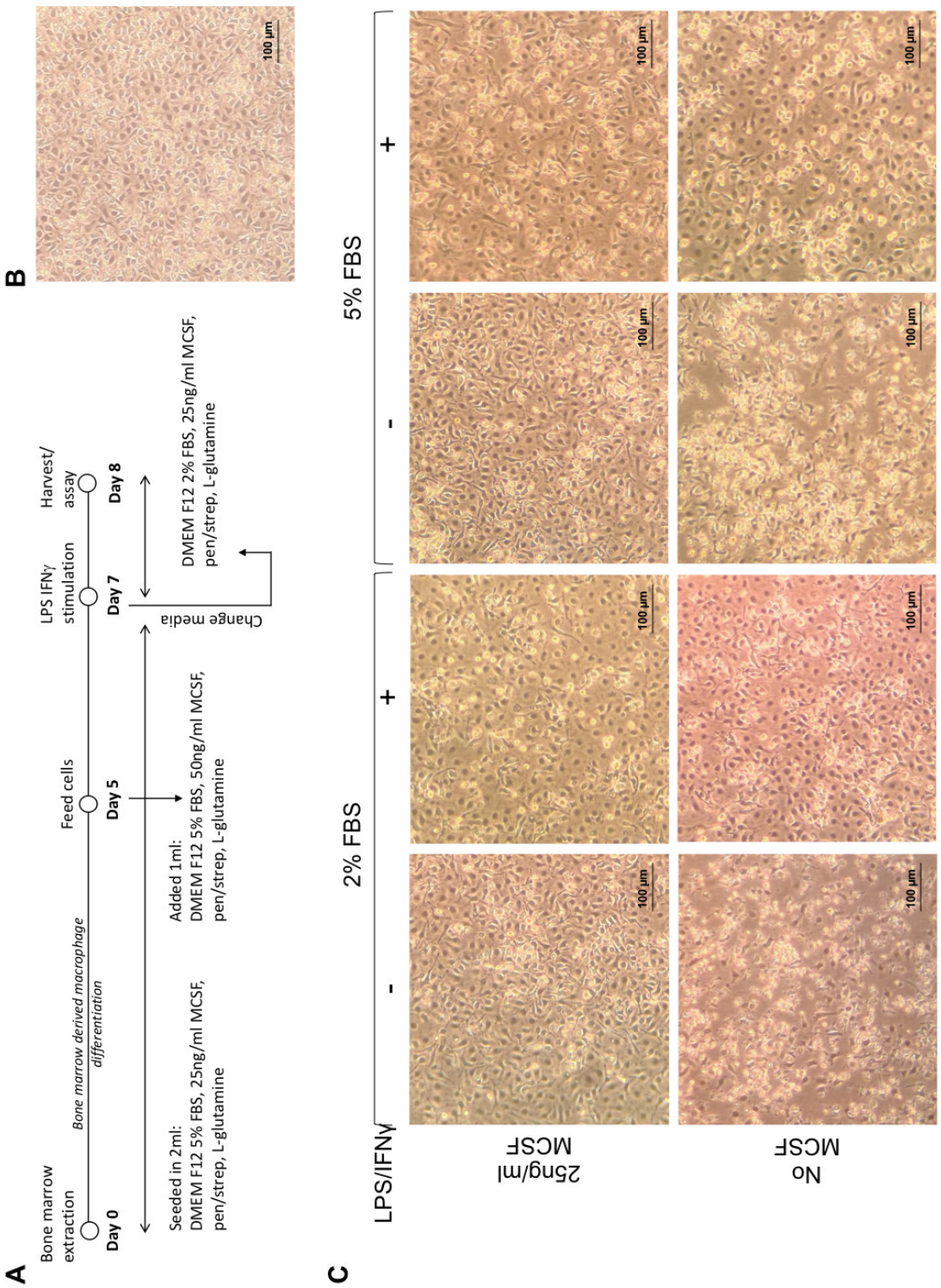


Figure 4.8 Protocol for culturing bone marrow derived macrophages using recombinant MCSF and low FBS concentrations

(A) Outline of the optimised protocol for culturing bone marrow derived macrophages using DMEM F12 media containing recombinant MCSF and 5% FBS over 7 days, before stimulating in fresh media containing MCSF and 2 % FBS overnight. (B) Representative image of $Gch^{fl/fl}$ macrophages on Day 7. (C) Representative images of $Gch^{fl/fl}$ macrophages on Day 8 following overnight incubation in DMEM F12 media containing either 5 or 2% FBS, with or without MCSF, unstimulated or stimulated with LPS/IFNγ (n=1).

4.4.5 Treating macrophages with GMCSF leads to increased LPS/IFNγ induced production of NO

It has been shown that 'priming' macrophages grown in MCSF with GMCSF prior to stimulation with inflammatory cytokines such as LPS led to an enhanced inflammatory phenotype including increased cytokine and NO production (Lacey et al., 2012; Sorgi et al., 2012). To confirm the effect of GMCSF treatment on NO generation, cells grown in LCM, MCSF alone and MCSF cells treated with GMCSF (Figure 4.9A) were compared. After demonstrating that cells in all conditions were confluent and adherent on Day 8 (Figure 4.9B) nitrites were measured in media supernatants from $Gch^{fl/fl}$ and $Gch^{fl/fl}$Tie2cre macrophages using the Griess assay. Nitrite measurements showed that LPS/IFNγ induced NO synthesis in $Gch^{fl/fl}$ cells from the 3 cell culture protocols with indications of greater amounts in GMCSF treated MCSF cells, and there were no detectable nitrites in media from $Gch^{fl/fl}$Tie2cre macrophages (Figure 4.9C). This was an important confirmation that lowering FBS levels to 2% during stimulation had sufficiently decreased biopterin content of the media to maintain BH_4 deficiency in $Gch^{fl/fl}$Tie2cre macrophages. However, the effect of GMCSF treatment on NO generation in $Gch^{fl/fl}$ cells was less clear and a more thorough investigation was carried out.

NO generated by NOS may be oxidised to nitrite but also further to form nitrate, and to measure the abundance of both (termed NO_x) an NO analyser was used. NO_x levels were almost undetectable in unstimulated cells and elevated in all $M^{LPS/IFN\gamma}$ $Gch^{fl/fl}$ macrophages, and were around 2 fold higher in GMCSF treated $M^{LPS/IFN\gamma}$ cells compared with those cultured in MCSF or LCM only (Figure 4.10A). The same pattern was observed when the NO analyser method was modified to measure nitrites (Figure 4.10B), but the proportion of nitrites remained consistent at 35-39% in all stimulated macrophages regardless of media composition (Figure 4.10C).

The NOS enzymes use arginine and oxygen to form citrulline as a product along with NO, and conversion of arginine into citrulline was used to determine iNOS activity in stimulated $Gch^{fl/fl}$ macrophages. This NOS activity assay revealed that iNOS was more active in stimulated macrophages grown in MCSF than LCM, but was highest in GMCSF treated cells (Figure 8D). Interestingly Western blotting showed that the abundance of iNOS protein was not significantly different between stimulated macrophages grown in different media types (Figure 4.10E and F). Together these results indicated that increased NO production in GMCSF treated $M^{LPS/IFN\gamma}$ macrophages did not result from increased iNOS protein abundance but from increased enzyme activity. The mechanism is unclear, but BH_4 levels were not a limiting factor in cells that were not treated with GMCSF, as measurements showed similar levels between stimulated GMCSF treated and untreated MCSF cells, and were significantly elevated in cells grown in LCM (Figure 4.11A). GMCSF affected BH_4 production in unstimulated MCSF cells, as levels were significantly higher than those measured in MCSF cells not treated with GMCSF (Figure 4.11A). Total biopterin levels were similarly affected, but BH_2, biopterin and the ratio of BH_4 to oxidised biopterins were unchanged (Figure 4.11B-E).

These results confirmed that BMDM culture using recombinant MCSF and reduced FBS concentrations produced macrophages that induced NO production by $Gch^{fl/fl}$ but not $Gch^{fl/fl}$Tie2cre cells upon stimulation with LPS/IFNγ. GMCSF treatement was also shown to increase NO generation, however a more thorough evaluation validating macrophage differentiation and inflammatory response was required.

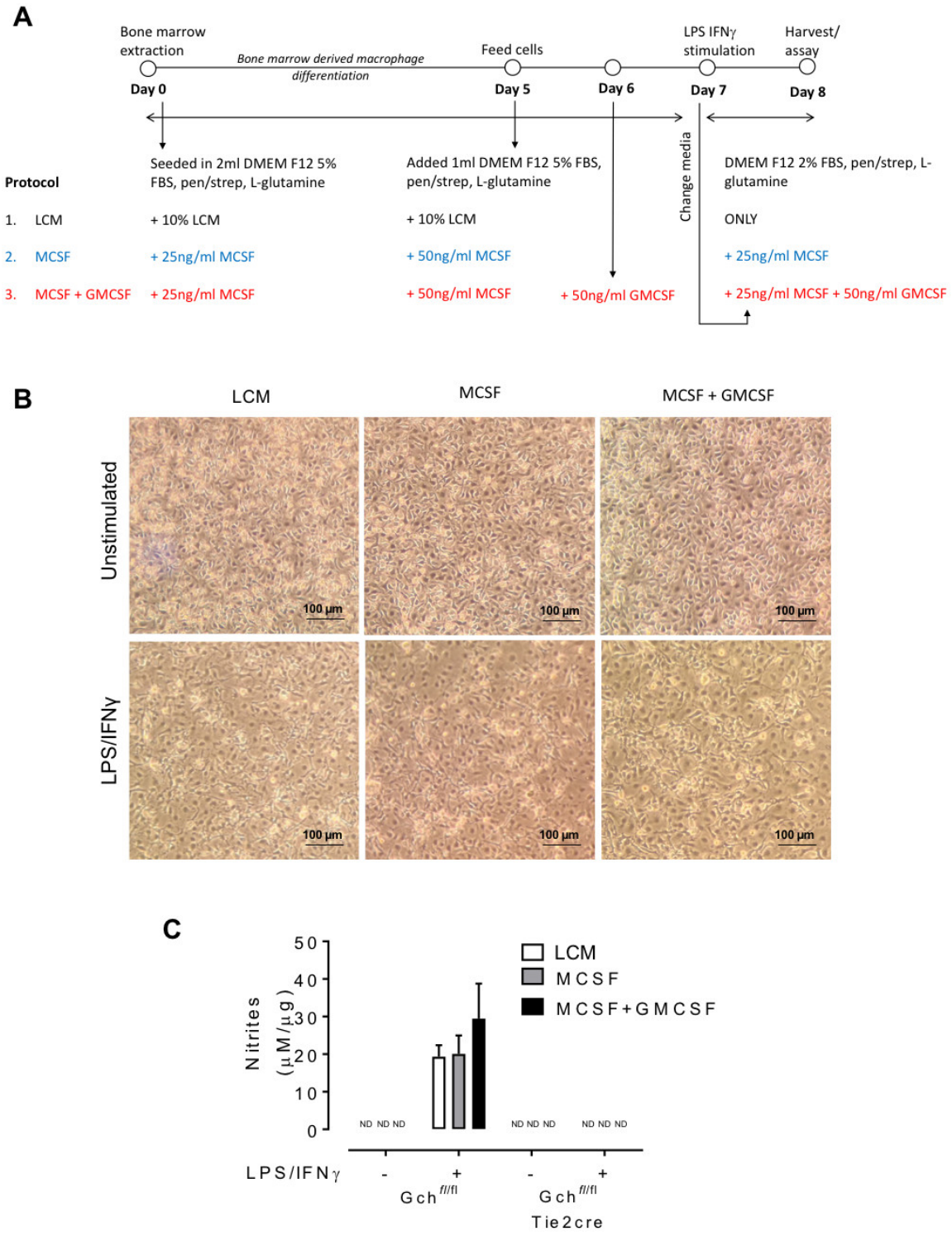


Figure 4.9 Protocols designed to compare LCM, MCSF and MCSF+GMCSF culture of bone marrow derived macrophages

(A) Outline of the protocols used to compare culture of bone marrow derived macrophages grown using LCM or MCSF ± GMCSF treatment. (B) Representative images of $Gch^{fl/fl}$ cells on Day 8. (C) Griess assay measurements of nitrites in media supernatants from $Gch^{fl/fl}$ and $Gch^{fl/fl}$Tie2cre macrophages (n=2, in duplicate). All data are presented as means ± range.

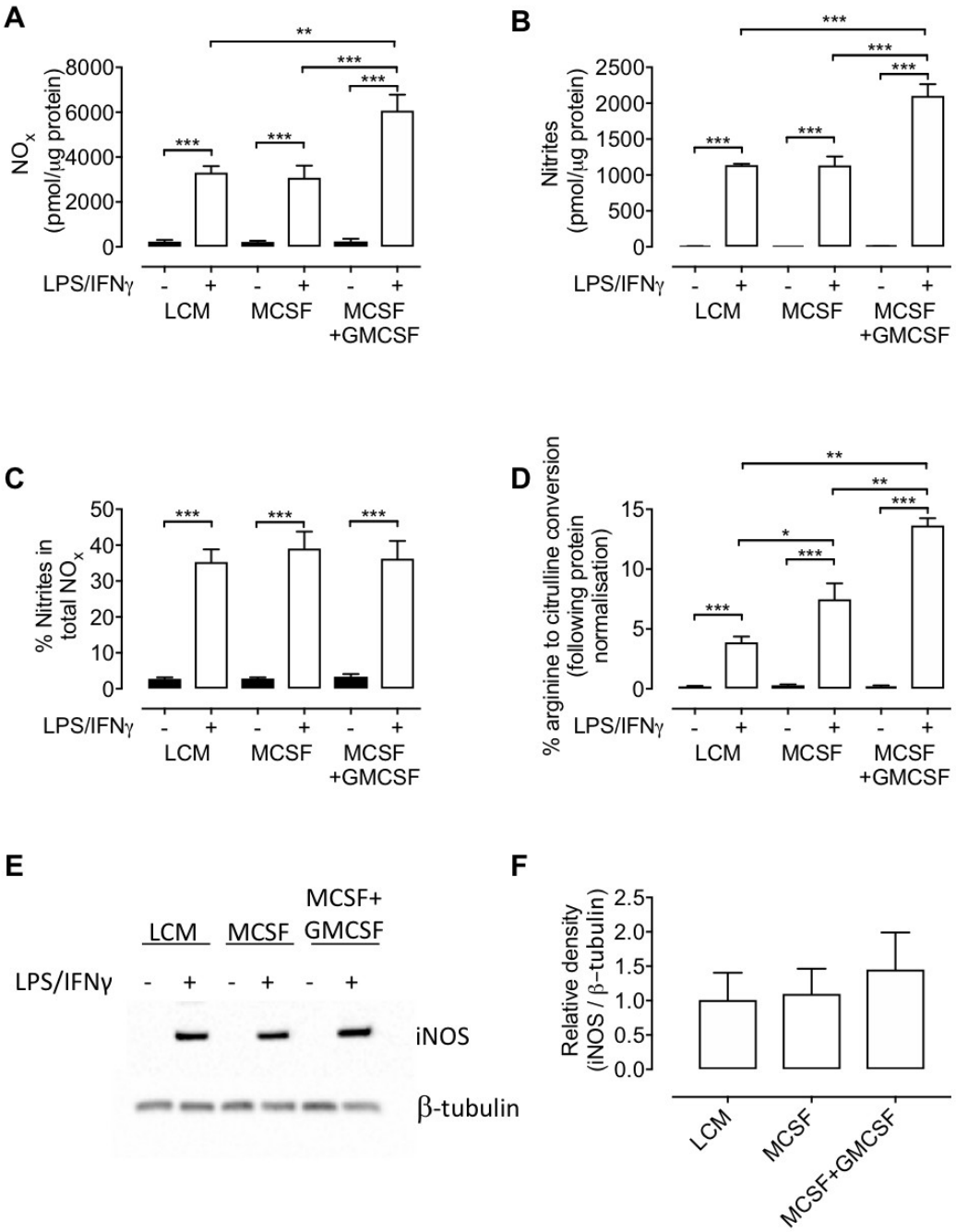


Figure 4.10 Macrophages cultured in MCSF and treated with GMCSF produce more nitric oxide upon stimulation with LPS/IFNγ

(A) NO_x (nitrite + nitrate) and (B) nitrites were measured in media supernatants from LPS/IFNγ $Gch^{fl/fl}$ macrophages grown in different growth media (n=4). (C) The proportion of nitrite as a percentage of NO_x in media. (D) Nitric oxide synthase activity was determined as a percentage of radiolabelled arginine converted into radiolabelled citrulline (n=4). (E) Western blot analysis of iNOS protein using β-tubulin as a loading control (n=4). (F) Quantification of the abundance of iNOS protein relative to β-tubulin (n=4). All data are presented as means ± SEM. Statistics were calculated using 2-way ANOVA and Tukey's post-test (* P<0.05, ** P<0.01, *** P<0.001).

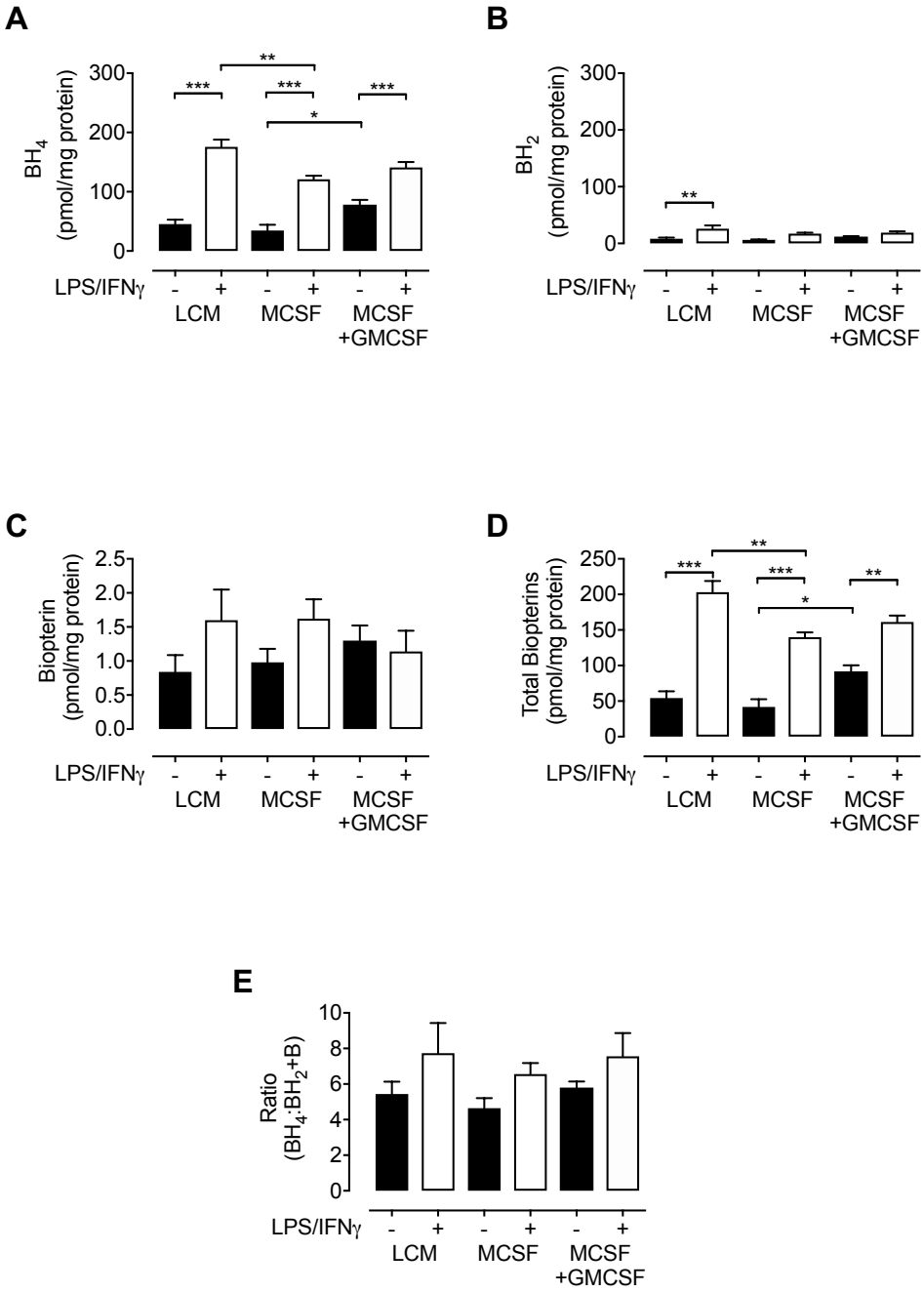


Figure 4.11 Biopterin measurements in macrophages cultured in LCM, MCSF and MCSF+GMCSF media

(A) BH_4, (B) BH_2 and (C) biopterin were measured in $Gch^{fl/fl}$ macrophages grown in different growth media (n=5). (D) Total biopterins and (E) the ratio BH_4:BH_2+B were calculated (n=5). All data are presented as means ± SEM. Statistics were calculated using 2-way ANOVA and Tukey's post-test (* P<0.05, ** P<0.01, *** P<0.001).

4.4.6 Characterising macrophages grown in MCSF media and treated with GMCSF

Macrophages grown in LCM, MCSF and MCSF+GMCSF were at least 95% positive for the leukocyte cell surface receptor CD45, as well as macrophage markers F4/80, CD11b and MHC II on Day 7 of culture (Figure 4.12), confirming their purity and maturation into macrophages. $Gch^{fl/fl}$Tie2cre macrophages showed the same profile as $Gch^{fl/fl}$ cells grown in MCSF media and treated with GMCSF, showing that knocking out *Gch1* did not affect macrophage differentiation according to these markers (Figure 4.12).

A major part of the macrophage inflammatory response is the production of pro-inflammatory cytokines, and a cytokine array was used to confirm production of inflammatory mediators by $M^{LPS/IFN\gamma}$ $Gch^{fl/fl}$ macrophages grown using the 3 cell culture protocols (Figure 4.13A and B). Although less accurate than ELISA measurements, quantification of these blots showed secretion of many pro-inflammatory cytokines from stimulated cells grown using all three types of media (Figure 4.13C). In particular, TNFα and IL-6 – commonly used to confirm the phenotype of inflammatory macrophages – were secreted by all cells, and the fact that MCSF was only detected in media from MCSF and MCSF+GMCSF cells and GMCSF only in media from MCSF+GMCSF cells confirms the robustness of the experiment. There were variations such as increased IL-1β and IL-1α in MCSF and MCSF+GMCSF cells compared with LCM, and decreased CCL2 in MCSF+GMCSF cells, however a more accurate method would be required to validate these changes. Of note, IL-10 – a key anti-inflammatory cytokine – appeared to be elevated in MCSF cells compared with GMCF treated cells or those grown in LCM, which would indicate a more anti-inflammatory phenotype in these cells than the other macrophages.

As BMDMs grown in MCSF and treated with GMCSF were confirmed to be pure macrophages that had an inflammatory profile when stimulated with LPS/IFNγ as well as producing enhanced amounts of NO, this cell culture protocol was used for further studies.

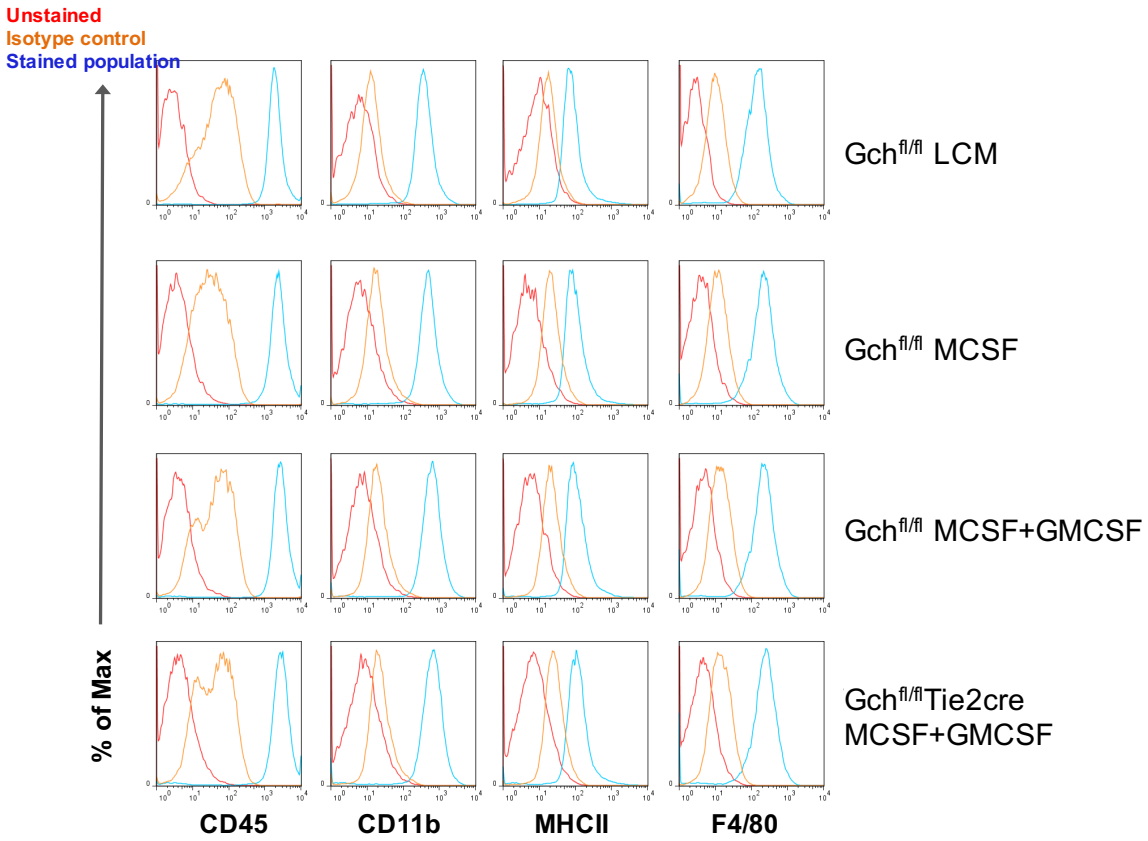


Figure 4.12 Characterisation of bone marrow derived macrophage markers on Day 7 of culture

$Gch^{fl/fl}$ and $Gch^{fl/fl}$Tie2cre macrophages cultured in LCM or MCSF media ± treatment with GMCSF were analysed on Day 7 of culture using flow cytometry. Fluorescence assisted cell sorting (FACS) of CD45, CD11b, MHC II and F4/80 cell surface markers was used. Cells were stained with anti-CD45-PE Cy7, anti-CD11b-PerCP Cy5, anti-MHCII-PE and anti-F4/80-APC. The red curves represent the unstained controls and orange curves represent the isotype controls. The blue curves represent the fluorescent intensity of the stained positive population. The purity was greater than 95% on day 7. This experiment was carried out with and analysis was carried out by Dr Jyoti Patel (Postdoctoral researcher within the Channon group).

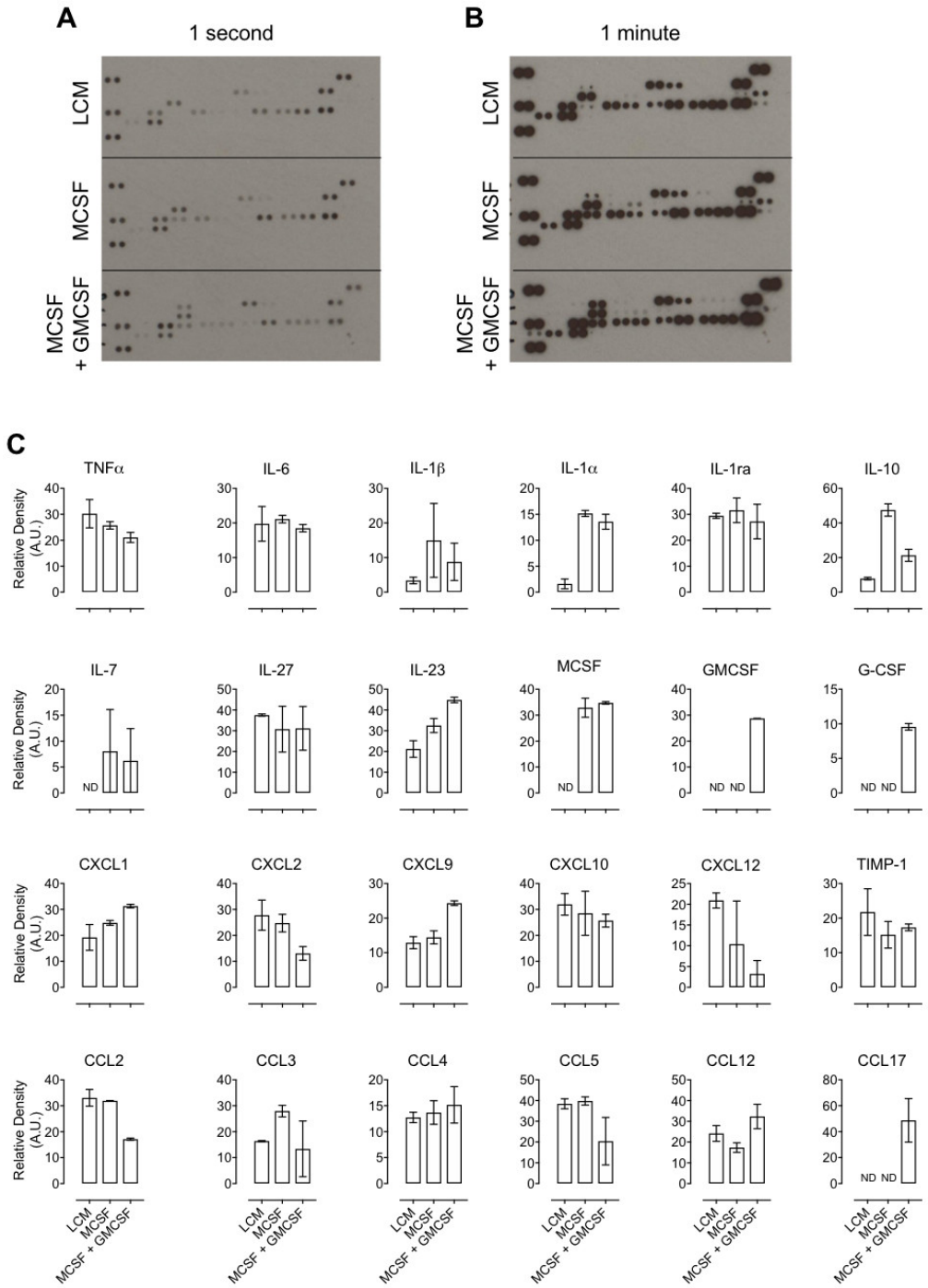


Figure 4.13 Measurement of cytokines secreted by LPS/IFNγ stimulated macrophages grown in LCM, MCSF and MCSF+GMCSF media

Cytokines were measured in media supernatants from LPS/IFNγ treated $Gch^{fl/fl}$ macrophages grown in different culture media using a cytokine profiler spotted with specific capture antibodies (n=2). Following incubation with biotinylated detection antibodies, blots were visualised for varying times using chemiluminescence and representative blots exposed for (A) 1 second and (B) 1 minute are shown. (C) Relative densities of duplicate spots were quantified (n=2). Data are presented as means ± range.

4.4.7 Defining the composition of cytokines in L-cell conditioned media

LCM contains MCSF and an undefined mixture of everything present in media from L929 cells. To further define the composition of the current batch used within our laboratory DMEM F12 media containing 10% LCM was incubated with a cytokine profiler array and revealed that in addition to MCSF this media contained TNFα, CXCL1, CCL2 and tissue inhibitor of metalloproteinases-1 (TIMP1), whereas MCSF+GMCSF media only contained MCSF and GMCSF (Figure 4.14A- C).

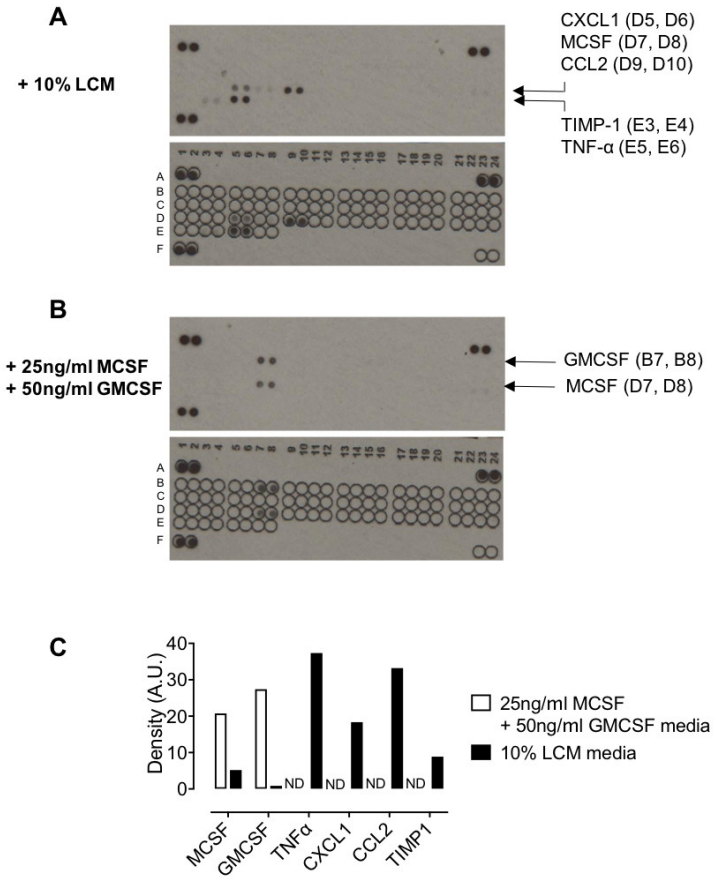


Figure 4.14 Measurement of cytokines in L-cell conditioned media

Cytokines were measured in DMEM F12 media containing 5% FBS and (A) 10% LCM or (B) MCSF and GMCSF using a cytokine profiler spotted with specific capture antibodies (n=1). Following incubation with biotinylated detection antibodies, blots were visualised using chemiluminescence and spots were quantified using the guide overlays as demonstrated. A1, A2, A23, A24, F1 and F2 were Streptavidin-HRP positive control reference spots and F23 and F24 were PBS negative control spots. (C) Relative densities of duplicate spots were quantified (n=1). ND – not detectable.

4.4.8 Characterising Gch$^{fl/fl}$Tie2cre BMDMs grown in MCSF media and treated with GMCSF

BMDMs grown from Gch$^{fl/fl}$Tie2cre mice using the newly optimised protocol – recombinant MCSF, GMCSF treatment and low FBS concentrations (**Section 4.3.3**) – were characterised. As expected, there was a small amount of GTPCH in control Gch$^{fl/fl}$ macrophages when unstimulated, and stimulation with LPS/IFNγ led to a greater abundance in control cells, whereas GTPCH was absent in Gch$^{fl/fl}$Tie2cre macrophages (Figure 4.15A). iNOS protein was found in all cells stimulated with LPS/IFNγ regardless of genotype apart from iNOS KO negative controls (Figure 4.15A). Biopterin measurements revealed dramatically lower amounts of BH_4, BH_2 and biopterin in Gch$^{fl/fl}$Tie2cre macrophages compared with Gch$^{fl/fl}$ cells (Figure 4.15B-D) and this led to significantly lower total biopterin content (Figure 4.15E). The ratio of BH_4:BH_2+biopterin was unchanged between Gch$^{fl/fl}$ and Gch$^{fl/fl}$Tie2cre macrophages (Figure 4.15F). Analysis of media supernatants revealed that although production of iNOS was induced by LPS/IFNγ in both Gch$^{fl/fl}$ and Gch$^{fl/fl}$Tie2cre macrophages, only Gch$^{fl/fl}$ cells produced NO as indicated by NO_x secretion (Figure 4.15G). As these results confirmed the expected decreased GTPCH, BH_4 and NO generation by Gch$^{fl/fl}$Tie2cre macrophages, this model was used for subsequent experiments.

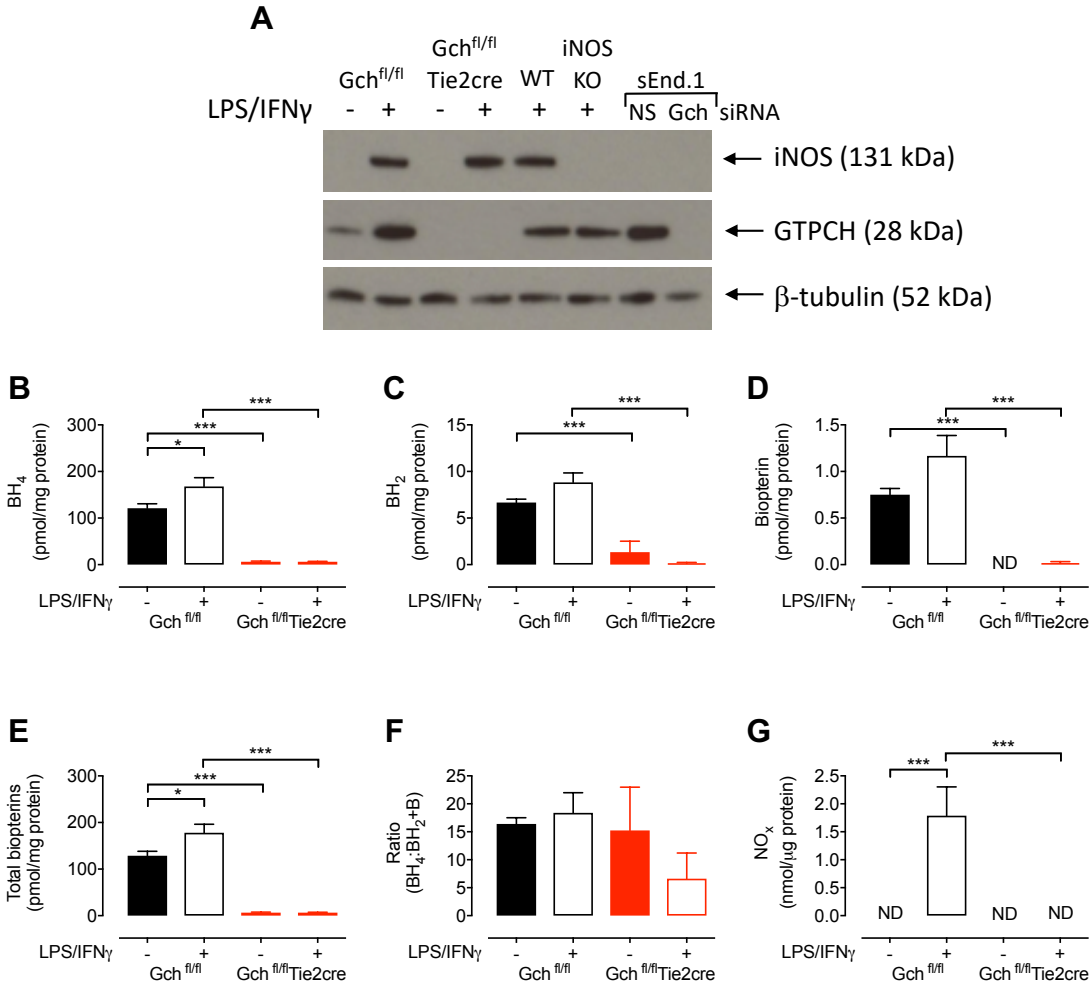


Figure 4.15 Characterisation of Gch$^{fl/fl}$Tie2cre bone marrow derived macrophages grown in media containing recombinant MCSF and treated with GMCSF

(A) Western blot analysis of GTPCH and iNOS in Gch$^{fl/fl}$ and Gch$^{fl/fl}$Tie2cre macrophages following overnight stimulation with LPS and IFNγ. Stimulated wild type (WT) and iNOS knock out (iNOS KO) macrophages were used as positive and negative controls for iNOS, and NS and Gch siRNA sEnd.1 cells were used as positive and negative controls for GTPCH. Anti-β-tubulin was used as the loading control (n=3). (B-F) HPLC was used to quantify (B) BH_4, (C) BH_2 and (D) biopterin and the results were used to calculate (E) total biopterins (BH_4+BH_2+biopterin) and (F) the ratio BH_4:BH_2+biopterin (n=6). (G) NO_x was measured in media supernatants using an NO analyser (n=6). All data are presented as means ± SEM. Statistics were calculated using 2-way ANOVA and Tukey's post-test (* P<0.05, ** P<0.01, *** P<0.001).

4.4.9 Characterising iNOS$^{-/-}$ BMDMs grown in MCSF media and treated with GMCSF

Chapter 3 provided evidence of a NOS-independent role for BH_4 in endothelial redox signalling and previous work from our laboratory indicated elevated ROS in Gch$^{fl/fl}$Tie2cre macrophages from a NOS-independent source (McNeill et al., 2015). For these reasons *Nos2*$^{-/-}$ (iNOS KO) BMDMs were used to distinguish the potential NO-independent effects of BH_4 deficiency in activated macrophages. GTPCH was detected in unstimulated WT and iNOS KO macrophages and was increased upon stimulation, and although stimulated WT cells contained iNOS it was absent in iNOS KO cells (Figure 4.16A). WT and iNOS KO macrophages contained comparable levels of BH_4, BH_2 and biopterin (Figure 4.16B-D). BH_4, total biopterins and the ratio of BH_4:BH_2+biopterin were significantly increased upon stimulation (Figure 4.16B, E and F). Analysis of media supernatants showed that unlike WT cells iNOS KO macrophages were unable to produce NO as indicated by NO_x secretion (Figure 4.16G).

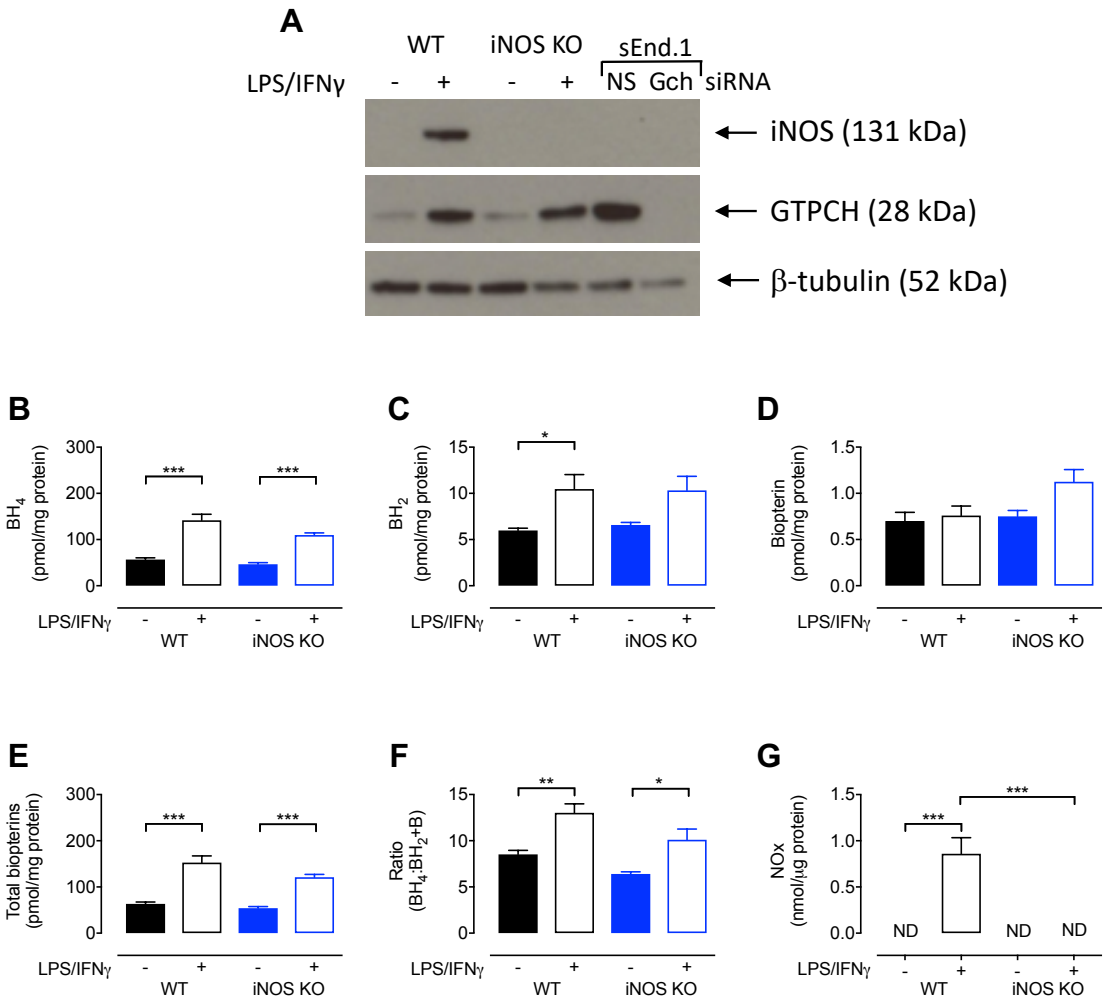


Figure 4.16 Characterisation of iNOS knockout bone marrow derived macrophages grown in media containing recombinant MCSF and treated with GMCSF

(A) Western blot analysis of GTPCH and iNOS in wild type (WT) and iNOS knockout (iNOS KO) macrophages following overnight stimulation with LPS and IFNγ. NS and Gch siRNA sEnd.1 cells were used as positive and negative controls for GTPCH. Anti-β-tubulin was used as the loading control (n=3). (B-F) HPLC was used to quantify (B) BH_4, (C) BH_2 and (D) biopterin and the results were used to calculate (E) total biopterins (BH_4+BH_2+biopterin) and (F) the ratio BH_4:BH_2+biopterin (n=5). (G) NO_x was measured in media supernatants using an NO analyser (n=6). All data are presented as means ± SEM. Statistics were calculated using 2-way ANOVA and Tukey's post-test (* P<0.05, ** P<0.01, *** P<0.001).

4.5 Discussion

4.5.1 Overview

The results presented in this chapter led to the development of an optimised protocol for culturing BMDMs using a more defined media that minimised biopterin content while maintaining adherent cells. The primary observation that serum starvation during the final stages of the laboratory's established protocol caused cells to detach was easily rectified by the inclusion of FBS in cell culture media. However, following this amendment $M^{LPS/IFN\gamma}$ $Gch^{fl/fl}$Tie2cre macrophages that were unable to synthesise BH_4 and NO using the established protocol, became capable of producing NO. This led to the revelation that FBS contained sufficient biopterins to supplement these cells, and characterisation of other media constituents demonstrated a similar biopterin content in LCM – which was the source of the growth factor MCSF. Determined to minimise biopterin supplementation of $Gch^{fl/fl}$Tie2cre macrophages through cell culture media while maintaining adherent cells, a new protocol using decreased FBS concentrations and recombinant MCSF was optimised. In addition, treating macrophages with GMCSF prior to and during stimulation was found to enhance NO generation and was included in a refined protocol. The new protocol was used to culture $Gch^{fl/fl}$Tie2cre and iNOS KO BMDMs and it was shown that BH_4 deficiency was a feature of $Gch^{fl/fl}$Tie2cre but not iNOS KO macrophages, while both were unable to generate NO. Thus confirming that this new protocol would be suitable for future experiments investigating the effects of BH_4 and NO deficiency on macrophage metabolism.

4.5.2 Serum starvation and cell culture

Serum starvation or reduction is very commonly used in cell culture systems prior to carrying out certain assays. As an abundant source of growth factors, removal of serum has become an important step in synchronising cells to effectively study the cell cycle (Langan et al., 2017; Pardee, 1974), and removal of the variety of extracellular signalling molecules

in serum has become a routine way of reducing interfering signals in a range of assays (Chen et al., 2003; Sancak et al., 2008). However, serum starvation or reduction is also known to induce signalling pathways, including apoptosis, at time points that vary between cell types and potentially interfere with experimental procedures and interpretation of results (González-Polo et al., 2005; Lu et al., 2008; Messam and Pittman, 1998; Pirkmajer and Chibalin, 2011). In this study, unstimulated macrophages detached after overnight incubation in very low serum media (0.2% BSA), which was inadequate for assays requiring adherent cells and indicated cell death. Interestingly, $M^{LPS/IFN\gamma}$ macrophages remained attached, suggesting a resistance to the effects of reduced serum or perhaps a different time course. The inclusion of 10% FBS in media during overnight stimulation maintained adherence of unstimulated and stimulated cells, however the unexpected production of NO by stimulated $Gch^{fl/fl}$Tie2cre cells unable to produce BH_4 led to the discovery of notable BH_4 and BH_2 levels in FBS. It is appreciated that FBS contains a vast mixture of incompletely defined molecules that will vary between batches, and identification of substantial biopterin levels highlights this. It is perhaps unsurprising, as although the presence of biopterin in commercial FBS is not reported, it is extensively described in blood plasma samples from multiple species (Fiege et al., 2004; Shintaku et al., 2005; Zhao et al., 2009). The biopterins in media containing 10% FBS were sufficient to supplement BH_4 deficient cells and allowed NO generation. FBS levels were therefore reduced to 5% throughout the 7 day differentiation of bone marrow into macrophages and to 2% during overnight stimulation, as these concentrations minimised biopterins whilst maintaining cell growth and adherence. Bone marrow incubated in 2% FBS media for 7 days were shown to grow slower but with normal morphology, therefore alleviating major concerns about apoptosis, although short-term effects of a switch from 5% to 2% were not tested. These results demonstrate the need to define cell culture media where possible and to adapt serum levels to minimise interference with the experimental model and hypothesis.

4.5.3 Replacing L-cell conditioned media with recombinant MCSF

During this report LCM was found to contain BH_4 and BH_2 thus showing that L929 cells produce and secrete biopterins into their media. Growing BMDMs in LCM was therefore supplementing BH_4-deficient $Gch^{fl/fl}$Tie2cre cells with biopterins. LCM is used as a convenient source of MCSF, which is required for differentiation and maintenance of macrophages (Stanley and Heard, 1977; Stanley et al., 1978), however – similar to FBS – it is not well defined and varies between batches. Measurement of cytokines revealed that, in addition to MCSF, our current batch of LCM contained TNFα, CXCL1, CCL2 and TIMP1, and although it was not measurable on this array L929 cells have also been shown to produce IFNβ (Warren and Vogel, 1985). These molecules are likely to affect differentiation and the 'unstimulated' state of BMDMs as TNFα is a potent inflammatory mediator, CCL2 (also known as monocyte chemoattractant protein-1) plays a key role in macrophage/monocyte migration and infiltration, CXCL1 is a neutrophil chemoattractant and TIMP-1 is a metalloproteinase inhibitor. To eliminate these uncertain effects as well as biopterin supplementation, LCM was replaced with a protocol using recombinant MCSF. The concentration of MCSF in culture media was optimised to 25 ng/ml, and interestingly although MCSF levels appeared relatively much lower in media containing 10% LCM, the cells in LCM grew at least as rapidly (not shown). This is possibly a consequence of the additional cytokines in LCM.

It is preferable to culture cells in a system that is defined, as experimental outcomes are more easily interpreted and reproducibility is higher, and replacing LCM with recombinant MCSF achieves this on top of removing an external source of BH_4. Although LCM is still commonly used – because it is cheaper and easy to self-produce – replacement with pure growth factors is increasingly recommended by experts in the field (Murray et al., 2014). Purchase of recombinant proteins has been prohibitively expensive in the past but is

becoming more affordable and so more accessible, and seems to be the logical way forward for culturing BMDMs in the future.

4.5.4 MCSF and GMCSF in BMDM culture

MCSF has been used to generate *in vitro* BMDMs from bone marrow progenitor cells for decades (Stanley and Heard, 1977), as it is a cytokine which causes differentiation of haematopoietic stem cells into macrophages and is involved in their proliferation and survival (Wiktor-Jedrzejczak et al., 1990). GMCSF in another growth factor commonly used in cell culture systems to generate bone marrow derived dendritic cells, however evidence suggests that these cells display macrophage markers and are transcriptionally more similar to macrophages than dendritic cells (Lacey et al., 2012; Mabbott et al., 2010; Na et al., 2016). Thus GMCSF derived macrophages have become another commonly used but distinct BMDM model. In this study, GMCSF was used to treat macrophages differentiated using the better understood MCSF cell culture system, as GMCSF has been shown to have a 'priming' effect leading to enhanced inflammatory cytokine and NO production when added prior to stimulation (Lacey et al., 2012; Sorgi et al., 2012). Differences in cytokine levels and increased NO generation were observed in GMCSF treated macrophages compared with untreated cells in this report, and will be discussed further below.

4.5.5 Measurement of cytokines in GMCSF treated BMDMs

Although cytokines were measured in this study, it was primarily to ensure that LPS/IFNγ stimulation activated an inflammatory response in BMDMs rather than to draw accurate comparisons between cells. A cytokine blot array was used to confirm the induced secretion of the inflammatory cytokines TNFα and members of the interleukin, CCL and CXCL families by cells grown in all media types. Quantification using this technique is only of relative abundance and is far less accurate than ELISA, and experiments were only carried out on two samples due to expense, so conclusive comparisons between cells from different

media were avoided although potentially hinted. In particular, it was interesting to note indications of higher anti-inflammatory IL-10 in cells grown in MCSF alone than either those grown in LCM or treated with GMCSF. Notable IL-10 secretion by MCSF derived BMDMs compared with GMCSF treated cells has been described previously (Sorgi et al., 2012), but this additionally highlights a possible difference compared with BMDMs grown in LCM as the source of MCSF. These results show that the 3 types of media produce BMDMs which respond by secreting pro-inflammatory cytokines upon stimulation, but un-primed MCSF cells possibly also produce the highest amount of anti-inflammatory IL-10.

4.5.6 GMCSF treatment increases NO production in stimulated BMDMs

In accordance with a previous report (Sorgi et al., 2012), GMCSF treatment of MCSF macrophages led to higher NO production by stimulated macrophages compared with un-primed cells (LCM or recombinant MCSF derived). The mechanisms involved are unknown, but equal abundance of iNOS protein in stimulated macrophages grown in different media, accompanied by increased iNOS activity in GMCSF treated cells in this study, strongly suggests that up-regulation of enzyme activity is the cause. The regulatory mechanisms controlling iNOS activity are not outlined as thoroughly as they are for the other NOS isoforms, and focus has been on transcriptional induction of the encoding gene. It is known that iNOS is limited by availability of arginine as a substrate and NADPH and BH_4 cofactors, but it seemed unlikely that either arginine or NADPH were limiting in LCM conditions and MCSF derived cells not treated with GMCSF although confirmatory tests should be carried out. Interestingly, biopterin measurements showed that GMCSF treatment led to increased BH_4 synthesis in unstimulated cells, however BH_4 was of equal abundance in stimulated untreated MCSF and GMCSF treated macrophages, and significantly higher in stimulated LCM derived cells and therefore was not limiting iNOS activity. Post-translation modifications might also determine iNOS function, as there has been one report

of inhibitory tyrosine phosphorylation in intestinal epithelial cells (Hausel et al., 2005). It would be prudent to follow up the mechanisms involved in regulating the differences seen in iNOS activity in these cells, as it could demonstrate that tyrosine phosphorylation occurs in macrophages or may identify novel regulatory mechanisms in a poorly understood area of NOS biology.

4.5.7 Advantages and disadvantages of the new BMDM cell culture protocol

There are many advantages of using the newly optimised protocol for culturing BMDMs in comparison with the protocol previously used in our laboratory. These are the maintenance of adherent cells during overnight stimulation, lower biopterin content in media throughout culture and more defined conditions. Restoration of serum to maintain cells during stimulation also potentially allows for extended experiments to be carried out – such as investigations into plasticity (Van den Bossche et al., 2016) – which would previously have been prohibited by cells detaching. Defined media should be strived for to aid reproducibility and interpretation of different studies as discussed, and replacing LCM with MCSF would be broadly beneficial in all BMDM studies. On the other hand, optimising biopterin content of cell culture media was uniquely relevant to avoid biopterin supplementation in experiments using a model of BH_4 deficiency. The main disadvantage is the greater expense required to grow BMDMs using a combination of commercially available recombinant MCSF and GMCSF than self-producing LCM as the MCSF source. However, costs can be halved by choosing to grow cells in MCSF alone without GMCSF treatment. GMCSF priming has the advantage of enhancing NO secretion upon stimulation of MCSF macrophages, which was considered advantageous for studies into the effects of NO signalling and was the reason for the inclusion in the new protocol, but it could be omitted.

4.5.8 Conclusions

In this chapter a protocol was optimised to culture BMDMs in more defined media containing minimal biopterins compared with the laboratory's previous protocol. The main biopterin rich media components were identified as FBS and LCM. FBS levels were therefore decreased to levels which maintained cell growth and adherence, while LCM was replaced with recombinant MCSF. In addition, GMCSF was included as a cytokine to 'prime' or co-stimulate macrophages differentiated in MCSF, as this increased NO generation by LPS/IFNγ treated cells. $Gch^{fl/fl}$Tie2cre BMDMs grown using the optimised protocol were deficient in BH_4 and unable to produce NO, while iNOS KO cells maintained BH_4 synthesis but similarly lacked NO generation. The new protocol was therefore deemed suitable for generation of BMDMs to be used in future experiments investigating the roles of BH_4 and NO signalling on macrophage mitochondrial function and metabolism.

Chapter 5:
Investigating the role of BH_4 in mitochondrial function and metabolism in inflammatory macrophages

Chapter 5: Investigating the role of BH_4 in mitochondrial function and metabolism in inflammatory macrophages

5.1 Introduction

Inflammation is an important part of the innate immune response to infections and macrophages play an integral role in this process by recognising and eliminating pathogens as well as producing cytokines to recruit other leukocytes. However, inflammatory macrophages are also involved in atherogenesis and sepsis (Farley et al., 2006; Frostegård et al., 1999) and may present a potential therapeutic target. The mechanisms regulating macrophage polarisation are still being elucidated; however, recently studies have highlighted the importance of metabolic remodelling in inflammatory cells.

Macrophages classically activated by pro-inflammatory stimuli, such as LPS and IFNγ ($M^{LPS/IFN\gamma}$), undergo a metabolic switch that includes the upregulation of glycolysis, remodelling of the TCA cycle, and the inhibition of mitochondrial respiration. Central to the pro-inflammatory switch is the expression of iNOS, which generates large quantities of NO and requires BH_4 as a cofactor (Tayeh and Marletta, 1989). The NO generated is responsible for inhibiting mitochondrial respiration via nitrosation of Complex I of the ETC and reversible inhibition of Complex IV (Cleeter et al., 1994; Clementi et al., 1998; Van den Bossche et al., 2016). However, it is unknown whether NO regulates changes in glycolysis and the TCA cycle in activated macrophages. Crucially, the up-regulation of glycolysis and changes in TCA cycle metabolic intermediates are pivotal determinants of the macrophage inflammatory phenotype (Arts et al., 2016; Infantino et al., 2011; Mills et al., 2018; Palsson-McDermott et al., 2015; Tannahill et al., 2013). Succinate accumulation, for example, directs HIF1α-mediated up-regulation of glycolysis and IL-1β production, as well as driving ROS generation (Mills et al., 2016; Tannahill et al., 2013). Elevation in succinate has been attributed to the citrate-derived metabolite itaconate inhibiting SDH

(Cordes et al., 2016; Lampropoulou et al., 2016). Furthermore, itaconate has recently been shown to be a potent anti-inflammatory mediator, limiting inflammation through KEAP1-NRF2 signalling (Mills et al., 2018). It is clear that elucidating the mechanisms regulating metabolic pathways and the balance of metabolites is vital for understanding macrophage function.

In addition to its requirement in NOS-derived NO production, a novel non-cofactor role for BH_4 in modulating mitochondrial superoxide generation in endothelial cells was identified in Chapter 3 and an unidentified NOS-independent source of elevated ROS was reported in BH_4-deficient macrophages (McNeill et al., 2015). Therefore, in this chapter BMDMs from two complementary knockout models (*Gch1* (encoding the BH_4 synthetic enzyme GTPCH) and *Nos2* (encoding iNOS)) that lacked the capacity to generate inducible NO were used to investigate the effects of NO deficiency on the biology of activated macrophages and also address potential NO-independent effects of BH_4 depletion. This included investigating the production of ROS in BH_4-deficient macrophages and a multi-'omics' approach to identify novel pathways modulated by BH_4 and NO. This highlighted changes in mitochondrial proteins and metabolic pathways, which were subsequently explored.

5.2 Aims and hypotheses

5.2.1 Hypotheses

Due to observations of elevated ROS from a source other than NOS in $Gch^{fl/fl}$Tie2cre macrophages (McNeill et al., 2015), and identification of elevated mitochondrial superoxide from BH_4 deficient endothelial cells in Chapter 3 of this thesis, it was hypothesised that mitochondria were the site of increased ROS generation in BH_4-deficient macrophages. Next, it was proposed that a whole-cell proteomics study would highlight novel pathways modulated by BH_4 levels. Upon finding changes in proteins involved in cytokine production, mitochondrial function, and metabolism during the proteomics analysis, it was hypothesised that BH_4 modulated these changes independent from NO signalling.

5.2.2 Aims

This study used $Gch^{fl/fl}$Tie2cre macrophages, which lacked BH_4, to investigate the effects of BH_4 deficiency on redox signalling, mitochondrial function, metabolism, and cytokine production. To determine whether NO signalling drove BH_4-dependent changes, $Gch^{fl/fl}$Tie2cre macrophages were compared with iNOS KO cells. The specific aims were:

- To determine whether elevated ROS from BH_4 deficient macrophages was mitochondrial in origin.
- To identify novel pathways modulated by BH_4 using proteomics and metabolomics.
- To investigate whether BH_4 deficiency induced changes in mitochondrial function, metabolism and cytokine production resulted from loss of NO signalling.

5.3 Methods

General methods were outlined in Chapter 2. Chapter specific methods and optimisation are outlined below.

5.3.1 ROS measurements using DHE and HPLC with UV detection

To identify differences in cellular DHE uptake and calculate the portion of oxidised intracellular DHE, accurate DHE measurements were optimised using a newly purchased UV detector. Several wavelengths have been reported as optimal for DHE detection including 210, 350 and 245 nm (Fernandes et al., 2006; Zhao et al., 2003) and an experiment was carried out to decide which one was optimal with our detector. 50 μM DHE standards made up in 1:1 mixtures of 0.1 M HCl to methanol were injected (50 μl). 2-hydroxyethidium and ethidium peaks were detected using fluorescence detection (as described in **Section 2.7**) to confirm that the HPLC system was working as expected while the UV detector was set to the various wavelengths. Peaks were detected at around 6 minutes in all cases and 245 nm was considered optimal due to a large clear peak without interference (Figure 5.1A) – unlike a small clear peak at 350 nm and a peak merged with a preceding peak at 210 nm (Figure 5.1B and C). It still remained to be confirmed that these peaks corresponded with the concentration of DHE, and as these were clean standard samples it was important to confirm that these conditions would be suitable for analysis of cell samples. Firstly, 245 and 350 nm UV detection were tested in DHE treated sEnd.1 cell samples, and the peaks at 6 minutes were still clearly identifiable by both wavelengths but as 245 nm produced a larger peak it was considered more sensitive (Figure 5.2A and B). To confirm that the UV detector set to 245 nm was detecting DHE, increasing amounts of DHE standard were injected and the area of the peak at 6 minutes increased in proportion to the concentration (Figure 5.3A). In addition, 50 μM DHE standards were incubated in the presence of increasing amounts of potassium superoxide to oxidise DHE as a control. As expected this led to decreased UV

detectable peak areas at 6 minutes and increased peak areas of the DHE oxidation products 2-hydroxyethidium and ethidium as detected by the fluorescence detector (Figure 5.3B-D). Together this confirmed the validity of using the UV detector set to 245 nm to measure relative amounts of DHE in samples. This method was therefore used in combination with the previous DHE assay protocol (**Section 2.7**) to measure DHE and its oxidation products in this chapter. BMDMs grown in 6 well plates were incubated with 25 μM DHE for 15 minutes at 37 °C and the protocol proceeded as described (**Section 2.7**). Cell were harvested into PBS by flushing with a pipette.

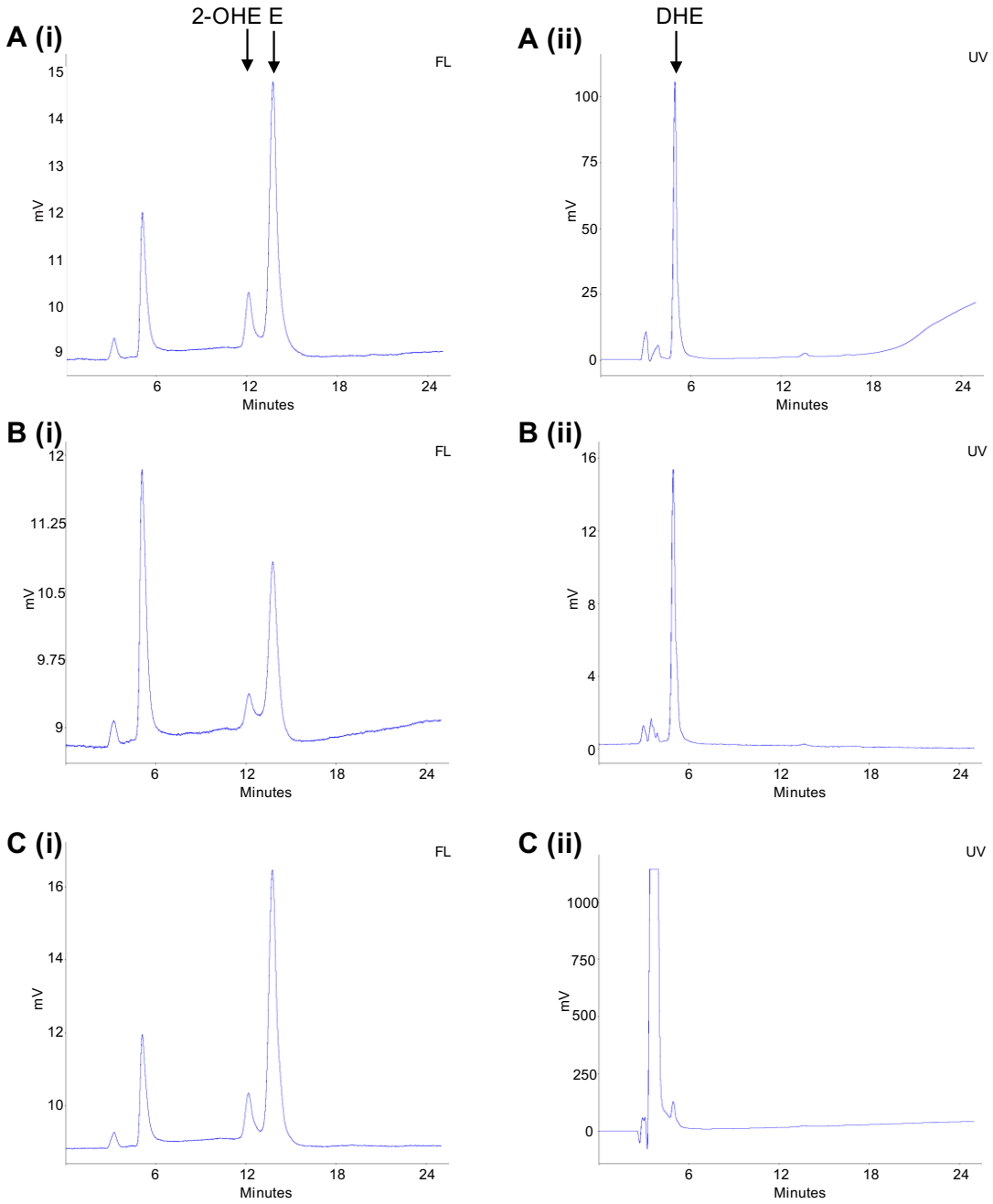


Figure 5.1 Detection of DHE using HPLC and a UV detector set to various wavelengths

Chromatograms from 50 µM DHE standards separated using HPLC. A fluorescence detector was used to measure 2-hydroxyethidium (2-OHE) and ethidium (E), while a UV detector set to (A) 245, (B) 350 and (C) 210 nm was used to measure DHE. FL – fluorescent detection, UV – ultra violet detection.

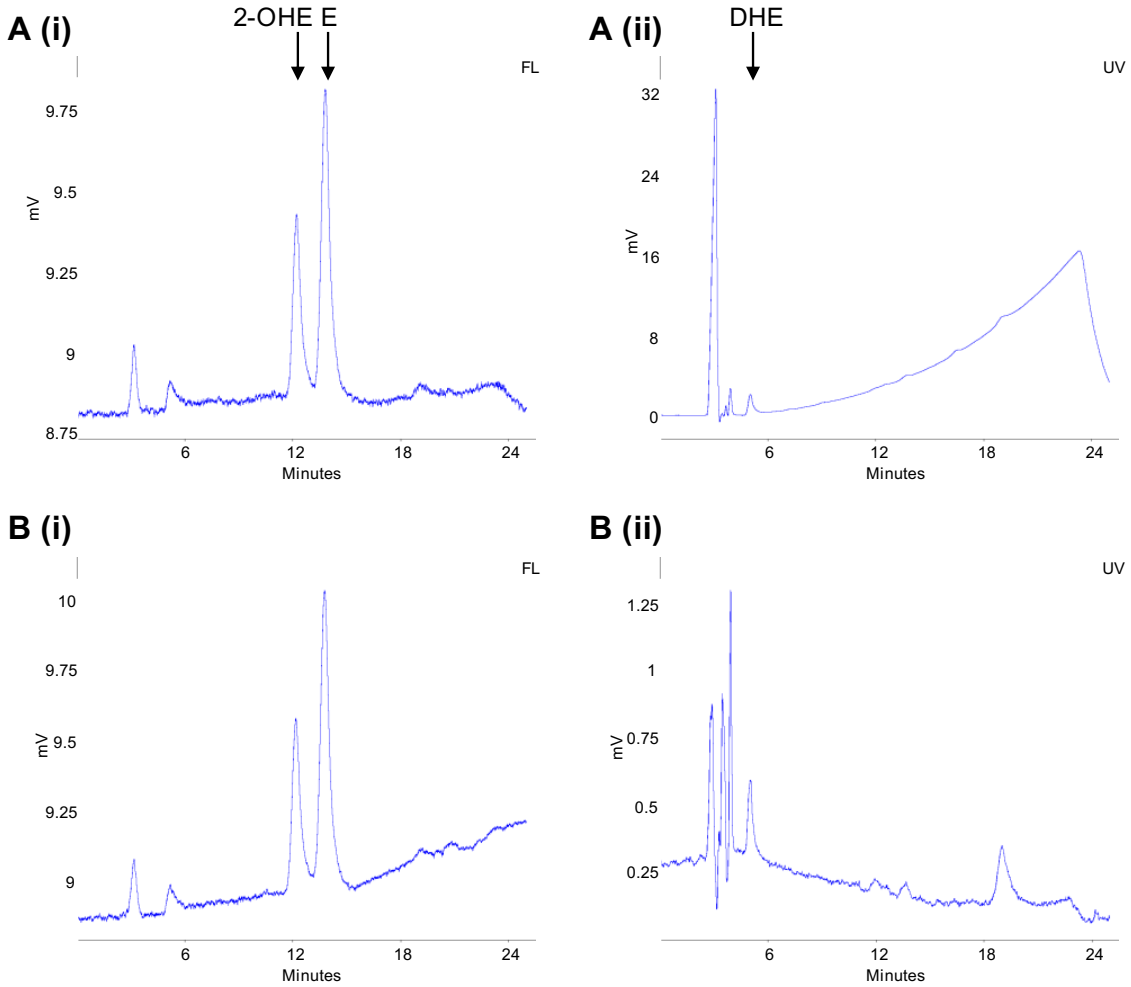


Figure 5.2 Detection of DHE in sEnd.1 cells using a UV detector set to 245 and 350 nm

Chromatograms measuring DHE and its oxidation products in sEnd.1 cells treated with DHE. HPLC separation and a fluorescence detector were used to measure 2-hydroxyethidium (2-OHE) and ethidium (E), while a UV detector set to (A) 245 and (B) 350 nm was used to measure DHE. FL – fluorescent detection, UV – ultra violet detection.

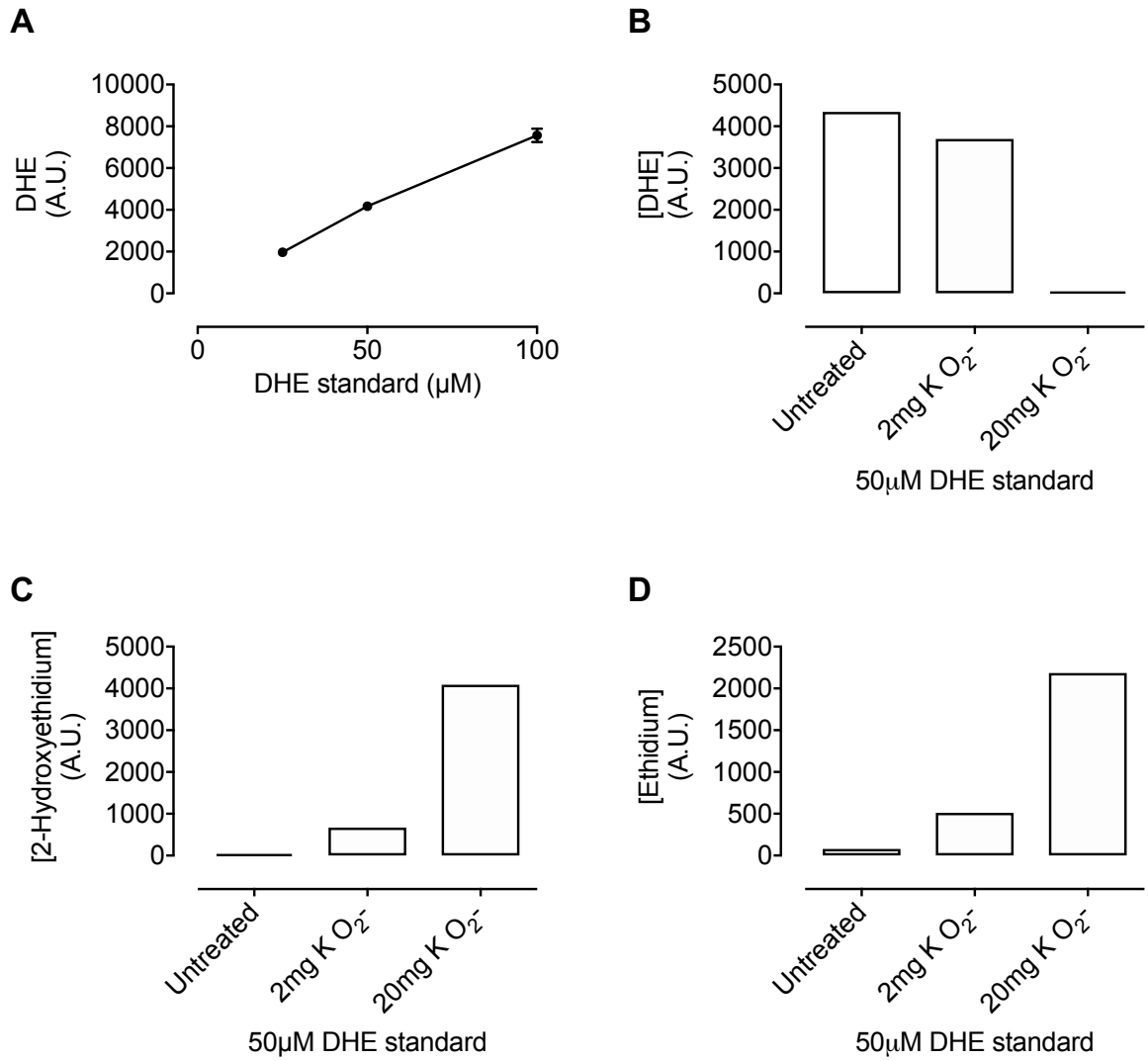


Figure 5.3 DHE standard curve and oxidation by potassium superoxide

(A) Increasing concentrations of DHE standards were measured using HPLC with UV detection (245 nm). (B-D) 50 μM DHE standards and their oxidation products were measured following treatment with potassium superoxide (K O_2^-). Samples were separated by HPLC and (B) DHE was quantified using a UV detector (245 nm), while (C) 2-hydroxyethidium and (D) ethidium were quantified using a fluorescence detector. The area under the curve of the DHE, 2-hyroxyethidium and ethidium peaks were quantified and presented in arbitrary units (A.U.).

5.3.2 Hydrogen peroxide measurements

Culture medium from cultured and stimulated BM macrophages ($1x10^6$ cells, seeded in a 6 well plate), was collected and centrifuged at 500 x g for 5 minutes. The hydrogen peroxide concentration was then measured by plunging an amperometric Hydrogen Peroxide Microsensor electrode connected to a Free Radical Analyser system (WPI, UK) into a PBS solution in which 100 µl of cleared media was added. The output current resultant to the hydrogen peroxide concentration detected was recorded and analysed using LabTrax 2 software. This measurement was carried out by Dr Marina Diotallevi (a research assistant within the laboratory).

5.3.3 Proteomics

5.3.3.1 Protein extraction and digestion

Cell pellets were lysed in RIPA buffer by freeze thawing on dry ice and centrifuged at 17,000 x g for 10 minutes at 4 °C. Extraction, digestion, and labelling of proteins were carried out using solutions prepared in triethylammonium bicarbonate buffer (TEAB, 1 mol/litre). Dithiothreitol (DTT, 5 mmol/litre) was added to supernatants and incubated for 30 minutes at room temperature in order to reduce samples. Iodoacetamide (20 mmol/litre) was added and incubated for 30 minutes at room temperature to alkylate cysteines in samples before protein was precipitated out using a methanol/chloroform extraction method. In brief, relative to sample volumes, 3 volumes of methanol and 0.5 volumes of chloroform were added to samples and vortexed, before adding a further 2.25 volumes of water and vortexing again. Samples were centrifuged at 17,000 x g for 1 minute and the upper aqueous phase was removed. More methanol was added and samples were vortexed and centrifuged at 17,000 x g for 2 minutes. Supernatants were discarded and the resulting protein pellet was resuspended in urea (6 mol/litre) and subsequently diluted to 1 mol/litre urea with water. Sequencing-grade modified trypsin (Promega) was added at a ratio of 1:50, relative to

protein content, and samples were digested overnight at 37 °C. The following day, formic acid (< 1%) was added to stop trypsinolysis, before samples were desalted using C18 Sep-Pack cartridges (Waters), vacuum dried (Speedvac, ThermoFisher Scientific), and stored at -80 °C.

5.3.3.2 Tandem Mass Tag (TMT)-labelling of peptides

Digested proteins were resuspended in TEAB (50 mM). Peptide concentrations were determined using a Pierce^{TM} Quantitative Colorimetric Peptide Assay kit (ThermoFisher Scientific) and calculated against a standard curve of known peptide concentrations with a plate reader set at an absorbance of 490 nm. 100 µg of each sample was taken, made up to 100 µg/µl in TEAB (50 mM) and labelled using Tandem Mass Tag^{TM} (TMT^{TM}) 10plex Isobaric Label Reagent Sets (ThermoFisher Scientific) following the manufacturer's protocol. TMT labels were resuspended in acetonitrile, added to samples, and incubated at room temperature for 1 hour. Hydroxylamine (5%) was added for 15 minutes to quench the labelling reactions. The experimental design required 16 samples (4 each of untreated Gch$^{fl/fl}$, untreated Gch$^{fl/fl}$Tie2cre, M$^{LPS/IFN\gamma}$ Gch$^{fl/fl}$, and M$^{LPS/IFN\gamma}$ Gch$^{fl/fl}$Tie2cre), which were therefore split over 2 TMT10plex^{TM} kits (8 samples in each), with 2 labels used to link the sample sets and formed of identical pools containing equal quantities of all samples. Samples labelled using kit 1 and kit 2 were pooled separately and desalted using C18 Sep-Pack cartridges (Waters), vacuum dried and stored at -80 °C.

5.3.3.3 Mass spectrometric analysis of proteins

Samples were run on a mass spectrometer by Mr Simon Davis in the Discovery Proteomics Facility, University of Oxford. TMT-labelled peptides resuspended in 2% acetonitrile 0.1% trifluoroacetic acid (TFA) were fractionated through an XBridge BEH C18 2.5um XP column (Waters) using HPLC and a high pH fractionation protocol. Mobile phases consisted of water (pH 10, Buffer A) and acetonitrile (90%, pH 10, Buffer B) and ran at 1% Buffer B

for 12 mins, followed by a linear gradient to 35% Buffer B over 72 minutes and finally 95% Buffer B for 10 minutes. Eluted peptides were collected every 2 minutes and concatenated at the end to form 8 fractions, which were vacuum dried and then resuspended in 2% acetonitrile and 0.1% TFA. Fractions were analysed by LC-MS/MS using a Dionex Ultimate 3000 nanoUPLC coupled to an Orbitrap Fusion Lumos mass spectrometer (Thermo Scientific). Peptides were separated on a 50 cm EASY-Spray C18 column (75 µm x 500 mm, 2 µm particle size; Thermo Scientific) over a 120-minute gradient, from 2% to 35% acetonitrile in 0.1% formic acid, 5% DMSO. The mass spectrometer was set to perform data-dependant acquisition in SPS-MS^3 mode, with a cycle time of 4 seconds. Detailed mass spectrometer settings are listed in Table 5.1.

MS1	
Detector	Orbitrap, 120k
Scan range	380 - 1500 m/z
AGC target	200000
Injection time	50 ms
MS2	
Detector	IonTrap, Rapid
First mass	120
AGC target	10000
Injection time	50 ms
Isolation width	0.7 m/z
Fragmentation	CID 35%
MS3	
Detector	Orbitrap, 60k
Scan range	120 - 500 m/z
AGC target	100000
Injection time	120 ms
SPS notches	3
Fragmentation	HCD 65%

Table 5.1 Mass spectrometry settings used for proteomic analysis

5.3.3.4 Proteomic data analysis

The data were analysed in R using the default "stats" package for Analysis of Variance (ANOVA) and Tukey's 'Honest Significant Different' (TukeyHSD) package for post-hoc test on all the proteins by the statistician Dr Anuj Goel. The data comprised of 5,704 different proteins measured on primary macrophages (N=4) from $Gch^{fl/fl}$ and $Gch^{fl/fl}$Tie2cre mice that were unstimulated or harvested following activation with LPS/IFNγ. A two-way ANOVA was performed, comparing a panel of proteins in $Gch^{fl/fl}$Tie2cre against the $Gch^{fl/fl}$ samples, followed by TukeyHSD method to create a set of confidence intervals based on the sample means. The proteins having a *P*-value < $9x10^{-6}$ (based on Bonferroni correction = 0.05/5704) were considered significant. Fold change calculations were determined as a ratio of A/B as specified in the figure legends as A vs B (eg. $Gch^{fl/fl}$Tie2cre vs $Gch^{fl/fl}$), such that a doubling in abundance is considered a fold change of 2 and a halving of abundance is considered a fold change of 0.5.

Enrichment analysis was carried out (by myself) using the ClueGO plugin in Cytoscape (Bindea et al., 2009; Shannon et al., 2003), by searching gene names encoding proteins that were considered statistically significant and changed abundance ≥20%, against 4 data bases: Gene ontology (GO) Biological Process (GO-BP), GO Cellular Component (GO-CC), GO Molecular Function (GO-MF) and Kyoto Encyclopaedia of Genes and Genomes (KEGG) pathways. Significantly enriched terms (P<0.05) containing ≥3 genes covering ≥4% of genes in that term were used to create ClueGO Layouts, where each node represents a term (GO-BP, -CC and -MF are circular and KEGG are hexagonal) and the size depends on the *P* value (whereby lower *P* is indicated by a bigger node). GO term fusion was applied to merge nodes containing highly similar genes and terms were grouped into networks based on their kappa score level (≥0.3). Nodes of the same colour have overlapping functional

networks and the most significant term in each group was labelled with all others hidden for simplicity. All node/term information was downloaded together with names of the genes identified in our data set that led to enrichment and these were used to create heat maps showing the scaled abundance of proteins encoded by these genes using GraphPad Prism 7.

5.3.4 Cytokine measurements by ELISA

DuoSet enzyme-linked immunosorbent assays (ELISAs) (R&D Systems) were used to measure TNF-α, IL-6, IL-10, and IL-1β in condition media supernatants collected from macrophages re-plated at $1x10^6$ cells per well of a 6 well plate on day 7 of culture and stimulated with LPS/IFNγ for 16 hours. To measure cytokines neat supernatants were used for IL-10 and IL-1β, and supernatants were diluted 1:100 and 1:400 for TNFα and IL-6 respectively to allow comparison with standard curves. The day before the assay Nunc-immuno 96 well plates (ThermoFisher Scientific) were pre-coated overnight at room temperature with Capture antibodies (DuoSet) resuspended in PBS according to the manufacturer's instructions. On the day of the assay, plates were washed in Wash Buffer (0.05% Tween20 in PBS) and blocked in Reagent Diluent (1% fatty acid free BSA (Sigma) in PBS) for 1 hour. After further washing, samples and standards were added in duplicate (made up in Reagent Diluent/media as appropriate), and incubated for 2 hours before additional wash steps. Detection antibodies (DuoSet) were added to wells and incubated for 2 hours before additional wash steps. Wells were incubated with Streptavidin-HRP (DuoSet) for 20 minutes protected from light, and then washed again. Substrate Solution (Substrate Reagent Pack, R&D Systems) was added, comprised of 1:1 mixture of Colour Reagent A and B, for 20 minutes protected from light. Stop Solution was added (0.67 N H_2SO_4) and plates were read on a BMG microplate reader at 450 and 540 nm. For data analysis, 540 nm readings were subtracted from 450 nm values to correct for optical imperfections in the plates, duplicate readings were averaged and blank optical densities subtracted from

standards and samples. Sample concentrations were calculated against standard curves generated using a four parameter logistic curve-fit, and multiplied by dilution factors if appropriate.

5.3.5 Metabolomics

Cell were harvested and pellets immediately frozen on dry ice and stored at -80 °C prior to shipping to Metabolon on dry ice. Metabolon measured metabolites using mass spectrometry and carried out statistical analysis, as outlined below from the Metabolon analysis information.

5.3.5.1 Sample Preparation

Samples were prepared using the automated MicroLab STAR® system from Hamilton Company. Several recovery standards were added prior to the first step in the extraction process for quality control purposes. To remove protein, dissociate small molecules bound to protein or trapped in the precipitated protein matrix and, to recover chemically diverse metabolites, proteins were precipitated with methanol under vigorous shaking for 2 min (Glen Mills GenoGrinder 2000), followed by centrifugation. The resulting extract was divided into five fractions: two for analysis by two separate reverse phase (RP)/UPLC-MS/MS methods with positive ion mode electrospray ionization (ESI), one for analysis by RP/UPLC-MS/MS with negative ion mode ESI, one for analysis by HILIC/UPLC-MS/MS with negative ion mode ESI, and one sample was reserved for backup. Samples were placed briefly on a TurboVap® (Zymark) to remove the organic solvent. The sample extracts were stored overnight under nitrogen before preparation for analysis.

5.3.5.2 Ultrahigh-Performance Liquid Chromatography-Tandem Mass Spectroscopy (UPLC-MS/MS)

All methods utilised a Waters ACQUITY ultra-performance liquid chromatography (UPLC) and a Thermo Scientific Q-Exactive high resolution/accurate mass spectrometer interfaced with a heated electrospray ionization (HESI-II) source and Orbitrap mass analyzer operated at 35,000 mass resolution. The sample extract was dried then reconstituted in solvents compatible to each of the four methods. Each reconstitution solvent contained a series of standards at fixed concentrations to ensure injection and chromatographic consistency. One aliquot was analyzed using acidic positive ion conditions, chromatographically optimized for more hydrophilic compounds. In this method, the extract was gradient eluted from a C18 column (Waters UPLC BEH C18-2.1x100 mm, 1.7 µm) using water and methanol, containing 0.05% perfluoropentanoic acid (PFPA) and 0.1% formic acid (FA). Another aliquot was also analyzed using acidic positive ion conditions, however it was chromatographically optimized for more hydrophobic compounds. In this method, the extract was gradient eluted from the same afore mentioned C18 column using methanol, acetonitrile, water, 0.05% PFPA and 0.01% FA and was operated at an overall higher organic content. Another aliquot was analyzed using basic negative ion optimized conditions using a separate dedicated C18 column. The basic extracts were gradient eluted from the column using methanol and water, however with 6.5mM Ammonium Bicarbonate at pH 8. The fourth aliquot was analyzed via negative ionization following elution from a HILIC column (Waters UPLC BEH Amide 2.1x150 mm, 1.7 µm) using a gradient consisting of water and acetonitrile with 10mM Ammonium Formate, pH 10.8. The MS analysis alternated between MS and data-dependent MS^n scans using dynamic exclusion. The scan range varied slighted between methods but covered 70-1000 m/z.

5.3.5.3 Bioinformatics:

Raw data was extracted, peak-identified and QC processed using Metabolon's hardware and software built on a web-service platform using Microsoft's .NET technologies. Compounds

were identified by comparison to library entries of purified standards or recurrent unknown entities. Metabolon maintains a library based on authenticated standards that contains the retention time/index (RI), mass to charge ratio (*m/z)*, and chromatographic data (including MS/MS spectral data). Furthermore, biochemical identifications are based on three criteria: retention index within a narrow RI window of the proposed identification, accurate mass match to the library +/- 10 ppm, and the MS/MS forward and reverse scores between the experimental data and authentic standards. Peaks were quantified using area-under-the-curve. Data were normalised to protein concentration and log transformed. 2-way ANOVA contrasts were used to identify metabolites that differed significantly ($P \leq 0.05$) between experimental groups. An estimate of the false discovery rate (q-value) was calculated with a low q-value ($q<0.10$) indicating high confidence in a result.

5.3.6 Complex I activity assay

Dr Thomas Nicol (a post-doc within the laboratory) measured Complex I activity in mitochondria isolated using the Qproteome mitochondrial isolation kit (Qiagen). 25 µg of mitochondrial protein was resuspended in 1x native sample buffer (Invitrogen), 2% digitonin (supercomplexes) or 2% DDM (n-dodecyl-β-D-maltoside) (isolated complex I), and 1x protease inhibitors (Roche) followed by 1 hour incubation on ice before final addition of 0.5% G-250 sample additive. Prepared samples were run on 3-12% bis-tris native gels under native conditions at 150 volts for 30 minutes in 1x native cathode buffer followed by 90 minutes at 150 volts in 0.1x native cathode buffer. Following electrophoresis, gels were incubated in 150 µM NADH, 3 mM nitro blue tetrazolium and 2 mM Tris at pH 7.4 for 3 hours.

5.3.7 Seahorse extracellular flux assays

5.3.7.1 MitoStress test

On day 7 of culture macrophages were plated at a density of 80,000 cells per well into XF^{e}96 microplates following optimization of seeding density. Cells were left to attach for 2 hours before stimulation with LPS/IFNγ if required, for 16 hours. Extracellular flux analysis was then performed as described for MitoStress test assays in **Section 2.12**. Sequential injection of the following compounds from the XF Cell Mito Stress Test Kit (Agilent): oligomycin (2 μmol/L, injection port A), FCCP (2 μmol/L, injection port B), and combined antimycin A (0.5 μmol/L), and rotenone (0.5 μmol/L) (injection port C). Cells were measured in 10 replicate wells and all Seahorse data was normalised to cell number using representative plates (n=4) analysed using an Operreta High-Content Imaging System (PerkinElmer) to image and count wells to generate a normalisation factor.

5.3.7.2 Glycolysis rate assay

Glycolytic activity was determined using the simultaneous ECAR readings generated during the above XF Cell Mito Stress Test, and included the subsequent addition of 2-deoxyglucose (100 mM, Sigma) injected through port D. The third ECAR measurement following the 2-deoxyglucose injection was subtracted from the third base-line ECAR reading to calculate 'basal glycolysis'.

Secondly, the Seahorse XF Glycolytic Rate Assay protocol was used to generate a more robust measurement of glycolysis that takes into account acidification by CO_2 generated through the TCA cycle (Mookerjee et al., 2015). Cells were plated and stimulated as above for the XF Cell Mito Stress Test. One hour prior to the assay, cells were washed and the culture medium was replaced with Seahorse XF Base Medium without Phenol Red (modified DMEM, pH 7.4; Agilent), supplemented with glucose (10 mM, Sigma), glutamine

(2 mM, Sigma), sodium pyruvate (1 mM, Sigma), and HEPES (5 mM, Agilent) before being incubated at 37 °C, at atmospheric CO_2 levels. Immediately prior to the assay this media was again replaced. 3 base-line OCR and ECAR measurements were taken followed by 3 measurements after injection of combined antimycin A (0.5 μM), and rotenone (0.5 μM) (injection port A, Mito Stress Test Kit), and 5 measurements after injection of 2-deoxyglucose (50 mM, Sigma). ECAR measurements were converted into proton efflux rates (PER) and mitochondrial OCR (base-line OCR – rotenone/antimycin A) was used to determine the PER attributed to glycolysis (glycoPER) and mitochondrial (mitoPER) acidification using the Agilent Seahorse XF Glycolytic Rate Assay Report Generator and the Buffer (BF; 2.2) and CO_2 contribution factors (CCF; 0.61) predetermined by Agilent for this media composition.

5.3.8 Isocitrate dehydrogenase activity assay

Isocitrate dehydrogenase (IDH) activity was determined for $NADP^+$ dependent isoforms, IDH1 and IDH2, using a colorimetric IDH Assay Kit (Abcam). In duplicate, cell lysates (7.5μg) and NADPH standards were loaded into 96 well clear plates and incubated with $NADP^+$ and Isocitrate Substrate. NADPH production was recorded on a BMG microplate reader measuring optical density (OD) OD_{450nm} in an kinetic assay with an Endpoint of 20 minutes. Endpoint results were used to calculate the amount of NADP in each well from a standard curve, after averaging duplicates and subtracting blank values. IDH activity was determined using the following equation:

IDH activity = (Amount of NADP / (Time of reaction x Volume in well)) x dilution factor

This assay was carried out by Dr Marina Diotallevi (a research assistant within the laboratory).

5.3.9 Aconitase activity assay

The cytosolic aconitase activity was determined using an enzyme activity assay kit (Abcam, ab109712). Cell pellets were lysed into 200 µl of cold assay buffer. After protein concentration determination, 70µg of each cell lysate was assayed in duplicate into a 96-well UV plate provided and incubated with isocitrate and manganese. The conversion of isocitrate to cis-aconitate was immediately recorded by kinetic measurement at OD_{240nm} for 30 min with 60 seconds interval and 3 seconds shaking between readings at room temperature. As recommended by the manual, the resulting aconitase activity was determined by picking two points in a linear increasing interval:

Rate (OD/min) = (Absorbance 1 - Absorbance 2) / Time (min).

This assay was carried out by Dr Marina Diotallevi (a research assistant within the laboratory).

5.4 Results

5.4.1 Characterisation of Gch$^{fl/fl}$Tie2cre and iNOS KO BMDMs

To investigate ROS production and the molecular pathways modulated by NO and BH_4 in $M^{LPS/IFN\gamma}$ macrophages, *Gch1*-deficient BMDMs from Gch$^{fl/fl}$Tie2cre mice were used following their characterisation in Chapter 4. In the absence of GTPCH protein (Figure 5.4A), resultant BH_4 deficiency (Figure 5.4B) led to macrophages that were unable to produce NO (Figure 5.4C), despite cytokine-induced expression of iNOS protein (Figure 5.4A). Due to evidence supporting a NOS-independent role for BH_4 in redox signalling in endothelial cells (presented in Chapter 3) and Gch$^{fl/fl}$Tie2cre macrophages (McNeill et al., 2015), *Nos2*$^{-/-}$ (iNOS KO) BMDMs – which have normal BH_4 levels but were unable to generate NO (Figure 5.4D and E) – were also used to distinguish potential NO-independent effects of BH_4 deficiency on macrophage activation.

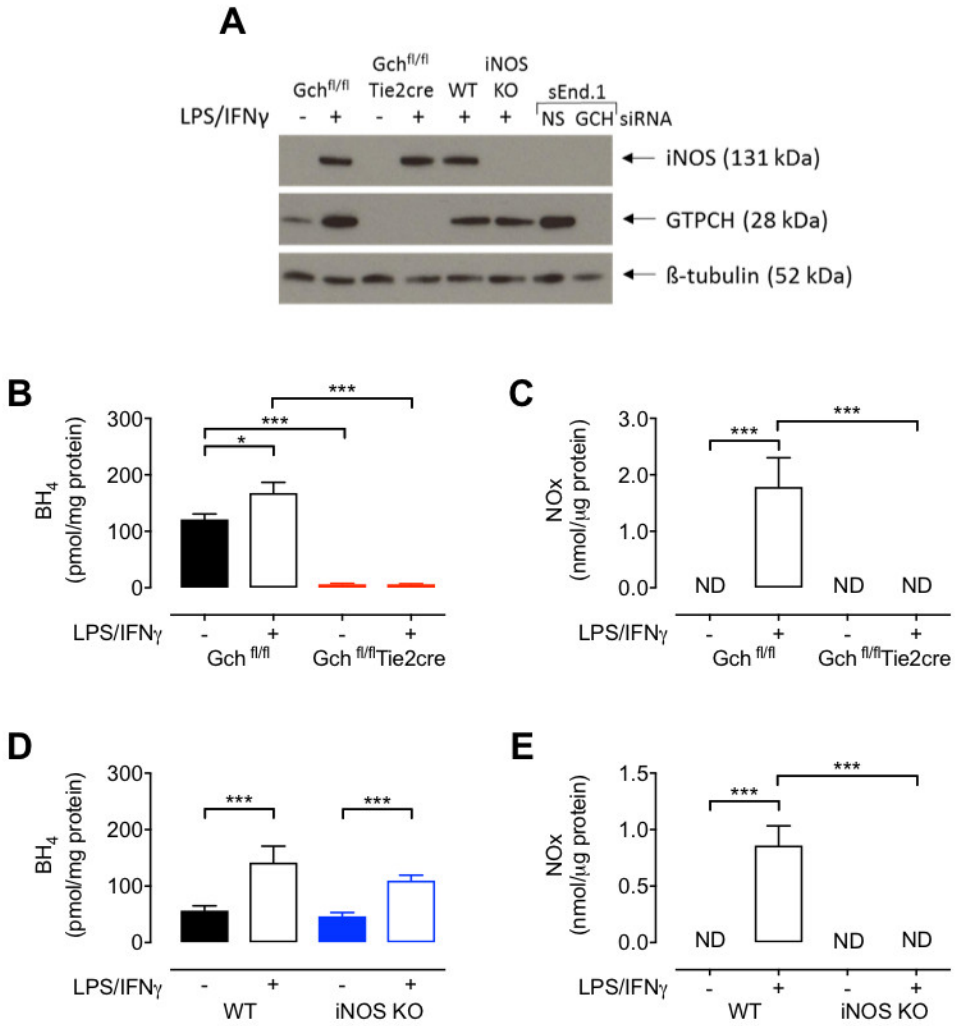


Figure 5.4 Characterisation of Gch$^{fl/fl}$Tie2cre and iNOS KO BMDMs

(A) Western blot analysis of GTPCH and iNOS in Gch$^{fl/fl}$, Gch$^{fl/fl}$Tie2cre, wild type (WT) and iNOS knockout (iNOS KO) macrophages following overnight stimulation with LPS and IFNγ. Stimulated WT and iNOS KO macrophages were used as positive and negative controls for iNOS, and NS and Gch siRNA sEnd.1 cells were used as positive and negative controls for GTPCH. Anti-β-tubulin was used as the loading control (n=3). (B) HPLC was used to quantify BH_4 in Gch$^{fl/fl}$Tie2cre cells (n=7). (C) NO_x was measured in media supernatants from Gch$^{fl/fl}$Tie2cre cells using an NO analyser (n=7). (D) HPLC was used to quantify BH_4 in iNOS KO cells (n=5). (E) NO_x was measured in media supernatants from iNOS KO cells using an NO analyser (n=6). All data are presented as means ± SEM Statistics were calculated using 2-way ANOVA and Tukey's post-test (* P<0.05, ** P<0.01, *** P<0.001).

5.4.2 Measuring ROS produced by BMDMs

DHE was used to determine intracellular superoxide production in BMDMs by measuring the superoxide-specific oxidation product 2-hydroxyethidium using HPLC. Ethidium was also measured as an indicator of other ROS, although its precise specificity is uncertain. Quantification of the peak areas of 2-hydroxyethidium from macrophages incubated with DHE showed no difference in 2-hydroxyethidium levels between unstimulated and $M^{LPS/IFN\gamma}$ $Gch^{fl/fl}$ cells but significantly elevated amounts in $M^{LPS/IFN\gamma}$ $Gch^{fl/fl}$Tie2cre cells (Figure 5.5A). Levels of ethidium were significantly decreased in unstimulated $Gch^{fl/fl}$ macrophages compared with stimulated cells; however, levels were significantly higher in unstimulated and $M^{LPS/IFN\gamma}$ $Gch^{fl/fl}$Tie2cre macrophages (Figure 5.5B). These results were comparable with previous reports from our lab (McNeill et al., 2015) and presumably indicated elevated ROS production from BH_4-deficient macrophages. However, following optimisation of a method to measure DHE using a UV detector (**Section 5.3.1**), differences in cellular uptake were observed, such as a trend towards (although not significantly) decreased DHE levels in $M^{LPS/IFN\gamma}$ $Gch^{fl/fl}$ cells (Figure 5.5C). To account for variations in probe uptake, ratios of 2-hydroxyethidium or ethidium relative to DHE were calculated to present the proportion of oxidised DHE. This revealed strikingly different results compared with peak areas alone, such as significantly elevated 2-hydroxyethidium:DHE ratio in $M^{LPS/IFN\gamma}$ $Gch^{fl/fl}$ macrophages compared with unstumulated cells – suggesting increased superoxide production (Figure 5.5D). Interestingly, the ratio of 2-hydroxyethidium:DHE in $M^{LPS/IFN\gamma}$ $Gch^{fl/fl}$Tie2cre macrophages compared with $Gch^{fl/fl}$ cells was significantly decreased (similar to unstimulated cells), suggesting that superoxide production is not induced in these cells (Figure 5.5D). In contrast, the ethidium:DHE ratio was unchanged between unstimulated and stimulated $Gch^{fl/fl}$ cells, but was comparatively increased in stimulated $Gch^{fl/fl}$Tie2cre macrophages (Figure 5.5E), which may indicate increased oxidation by other

mechanisms in BH_4-deficient $M^{LPS/IFN\gamma}$ macrophages. However, the relative oxidation of varying amounts of cellular DHE does not conclusively answer the question of whether BH_4 deficiency alters macrophage ROS production and more studies are required.

Similarly, the DHE assay was carried out in iNOS KO macrophages to determine whether changes observed in BH_4-deficient cells were due to loss of NO production. There were no significant changes in the levels of 2-hydroxyethidium or ethidium in unstimulated or $M^{LPS/IFN\gamma}$ WT and iNOS KO macrophages, apart from significantly less ethidium in stimulated WT cells (Figure 5.6A and B). There were variable levels of DHE including significantly less in $M^{LPS/IFN\gamma}$ WT macrophages (Figure 5.6C). The ratio of 2-hydroxyethidium:DHE was elevated in $M^{LPS/IFN\gamma}$ WT and iNOS KO macrophages, compared with unstimulated cells (Figure 5.6D), indicating elevated superoxide production in stimulated NO-synthesising and NO-deficient cells. This result differs from the decreased superoxide levels in stimulated $Gch^{fl/fl}$Tie2cre macrophages, suggesting a BH_4-dependent effect. However, the ethidium:DHE ratio is similarly elevated in stimulated iNOS KO and BH_4-deficient cells and is thus more likely to result from loss of NO (Figure 5.6E).

As an alternative indicator of ROS production, extracellular H_2O_2 secretion was measured in media supernatants from $Gch^{fl/fl}$Tie2cre and iNOS KO macrophages. H_2O_2 was undetectable in unstimulated macrophages but at least 400 nM in $M^{LPS/IFN\gamma}$ $Gch^{fl/fl}$ and WT cells (Figure 5.7A and B). It was undetectable in BH_4 deficient $M^{LPS/IFN\gamma}$ macrophages and all but one sample (which had low levels [41 nM]) from iNOS KO cells (Figure 5.7A and B). This corresponds with the observed decrease in 2-hydroxyethidium:DHE ratio and thus intracellular superoxide produced by $Gch^{fl/fl}$Tie2cre macrophages, but not the increase in the iNOS KO cells.

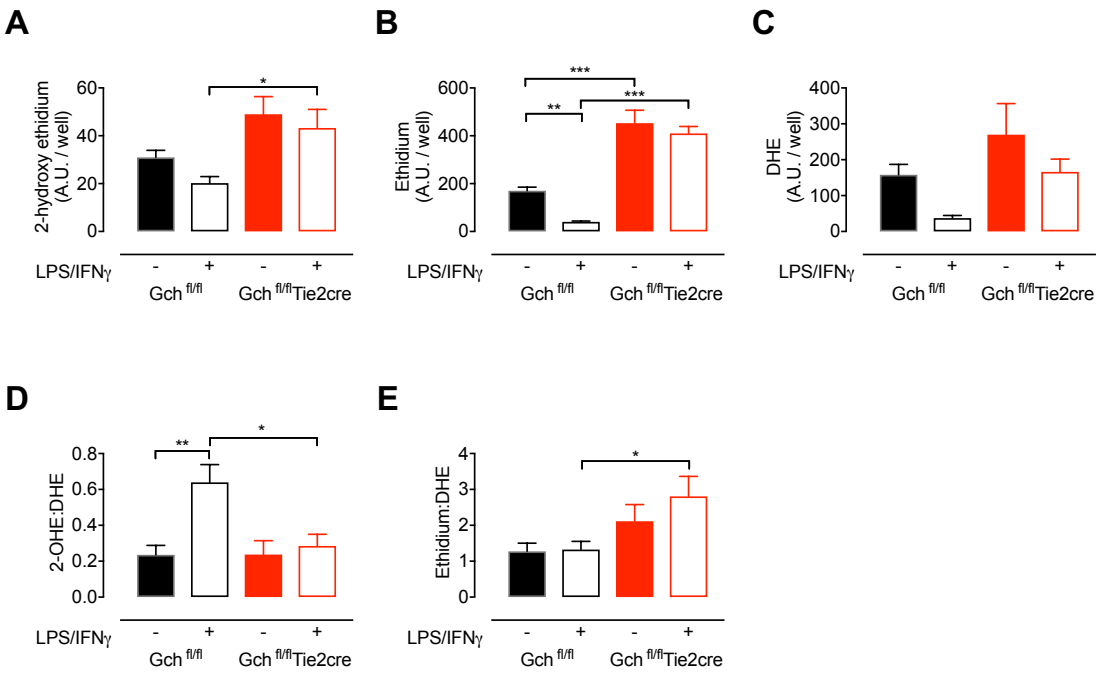


Figure 5.5 ROS measurements in Gch$^{fl/fl}$Tie2cre macrophages using DHE

Oxidation of DHE into (A) 2-hydroxyethidium (2-OHE) and (B) ethidium was measured by HPLC and used to determine ROS production in BH_4 deficient Gch$^{fl/fl}$Tie2cre cells stimulated with LPS/IFNγ. (C) DHE was measured by HPLC using a UV detector. The ratios of DHE oxidised to (D) 2-hydroxyethidium or (E) ethidium were calculated to determine the proportion oxidised to these species. All data are n=6 presented as means ± SEM Statistics were calculated using 2-way ANOVA and Tukey's post-test (* P<0.05, ** P<0.01, *** P<0.001).

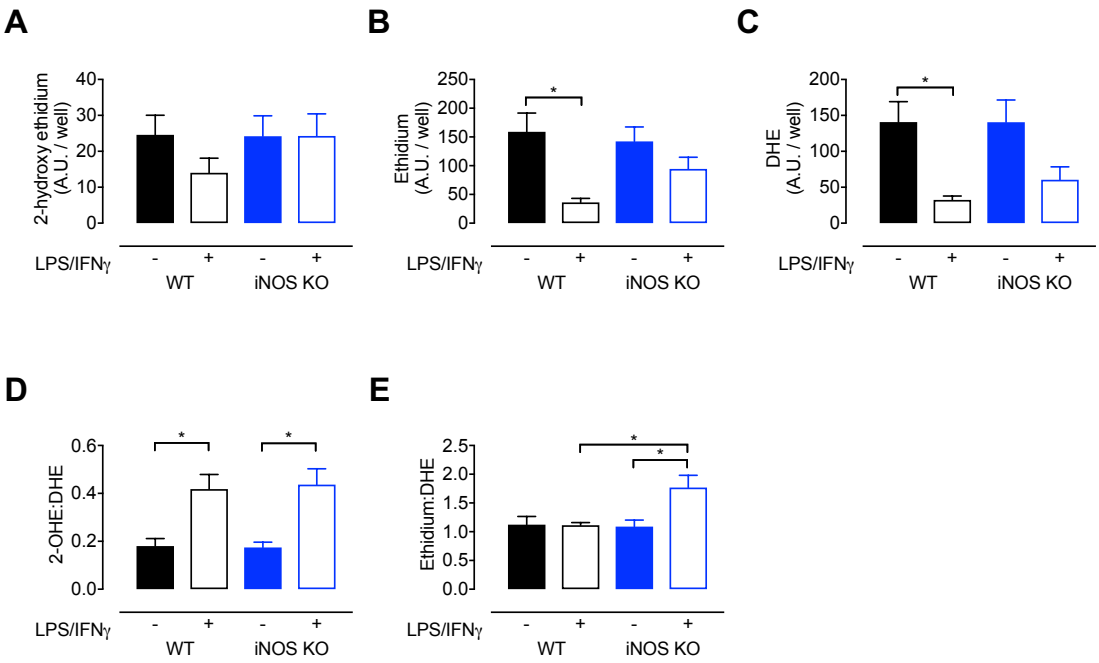


Figure 5.6 ROS measurements in iNOS KO macrophages using DHE

Oxidation of DHE into (A) 2-hydroxyethidium (2-OHE) and (B) ethidium was measured by HPLC and used to determine ROS production in iNOS KO cells stimulated with LPS/IFNγ. (C) DHE was measured by HPLC using a UV detector. The ratios of DHE oxidised to (D) 2-hydroxyethidium or (E) ethidium were calculated to determine the proportion oxidised to these species. All data are n=4-5 presented as means ± SEM Statistics were calculated using 2-way ANOVA and Tukey's post-test (* $P<0.05$, ** $P<0.01$, *** $P<0.001$).

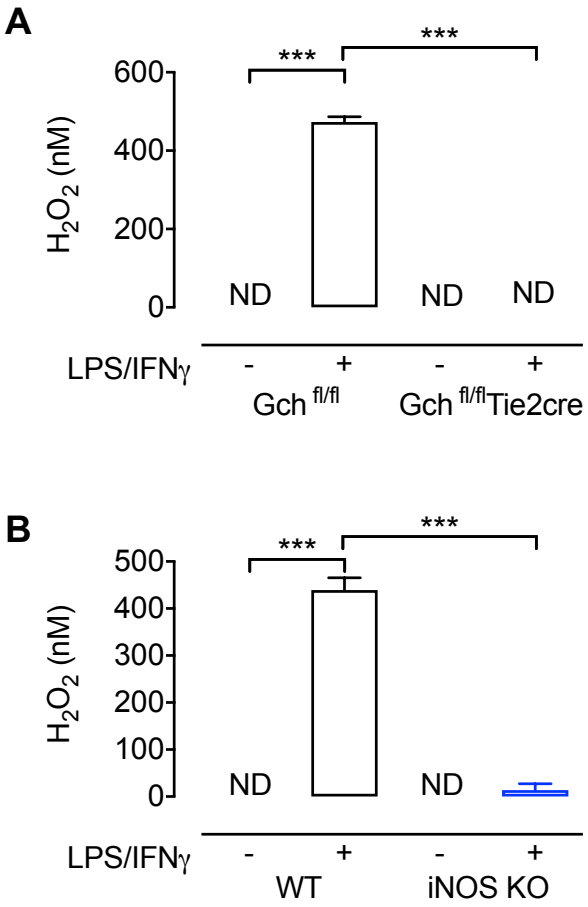


Figure 5.7 H_2O_2 secreted from Gch$^{fl/fl}$Tie2cre and iNOS KO macrophages

H_2O_2 was measured in media supernatants from (A) Gch$^{fl/fl}$Tie2cre (n=3-4) and (B) iNOS KO (n=3) macrophages stimulated with LPS/IFNγ. All data are presented as means ± SEM Statistics were calculated using 2-way ANOVA and Tukey's post-test (*** P<0.001).

5.4.3 Proteomic analysis of Gch$^{fl/fl}$Tie2cre macrophages

Previous work in our laboratory used transcriptomic analysis to investigate pathways modulated by BH_4 in $M^{LPS/IFN\gamma}$ Gch$^{fl/fl}$Tie2cre macrophages (McNeill et al., 2015). As transcriptomic studies often assume that changes reflect protein levels – which is not necessarily the case due to post-transcriptional and post-translational processing as well as protein turnover (Ghazalpour et al., 2011) – the work in this thesis used proteomic analysis to overcome these issues.

To identify novel pathways modulated by BH_4, TMT-labelling and whole-cell proteomic analysis of Gch$^{fl/fl}$Tie2cre macrophages and Gch$^{fl/fl}$ controls was used to quantify the relative abundance of proteins in unstimulated and LPS/IFNγ-activated cells. This approach measured 5704 proteins present in all samples, which were taken forward for analysis. The expected changes in GTPCH and iNOS abundance were observed (Figure 5.8A and B) and comparable with results from Western blots (Figure 5.4A), demonstrating the robustness and validity of the experimental model. In addition, it was reassuring to note that GTPCH was the significantly decreased protein with the greatest fold change in both unstimulated and $M^{LPS/IFN\gamma}$ Gch$^{fl/fl}$Tie2cre macrophages compared with Gch$^{fl/fl}$ cells (Table 5.2 and 5.3). Arsenite methyltransferase was similarly one of the most significantly decreased proteins in Gch$^{fl/fl}$Tie2cre macrophages (Table 5.2 and 5.3) and this change was predicted by a transcriptomics study indicating decreased *As3mt* transcript in unstimulated and $M^{LPS/IFN\gamma}$ cells (McNeill et al., 2015). It is also of note that several of the significantly altered proteins with the greatest fold change between genotypes are mitochondrial, such as adenylate kinase, NDUFA12, NDUFS6, or metabolic proteins such as squalene synthase, fatty acid desaturase 2 and GLUT-1 (Tables 5.2 and 5.3; Figure 5.9A-E). Interestingly, only a select number of proteins differed significantly according to genotype (Table 5.4) and enrichment analysis was carried out to identify the molecular functions and pathways affected.

Additional analysis showing the proteomic data in a Volcano plot would be useful to show all data points in a way that represents both fold change and *P* values . This scatter plot of fold change (x-axis) vs significance (y-axis) would also allow easy visualisation of proteins with large magnitude changes that were also statistically significant.

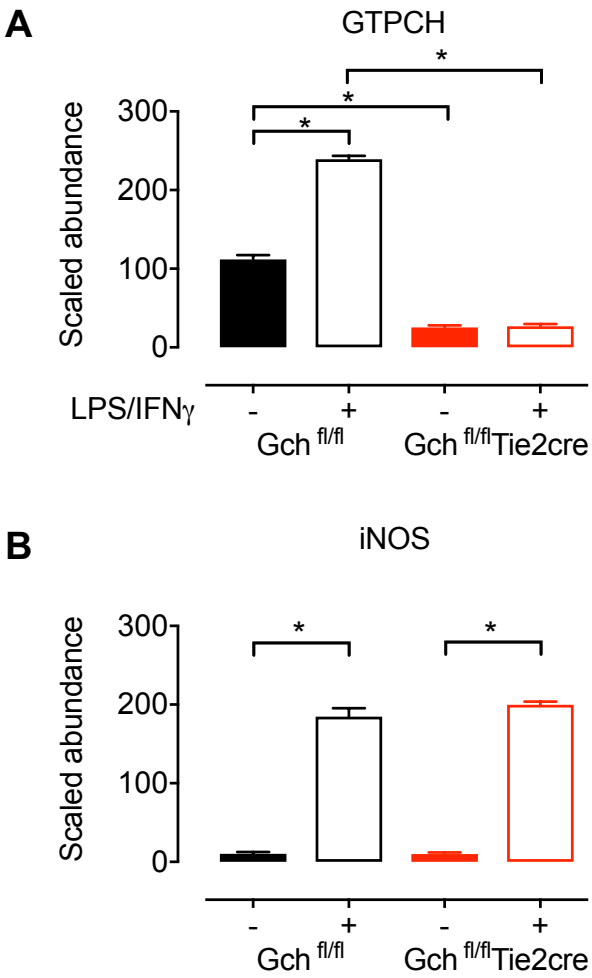


Figure 5.8 GTPCH and iNOS protein abundance

Scaled abundance of GTPCH and iNOS protein in Gch$^{fl/fl}$Tie2cre macrophages quantified using proteomic analysis of TMT-labelled samples (n=4). Data are mean ± SEM. *P* values calculated using 2-way ANOVA ($P<9x10^{-6}$) with Tukey's HSD (*$P<0.05$).

Protein	Fold change (Ratio $Gch^{fl/fl}Tie2cre/Gch^{fl/fl}$)
Squalene synthase	2.69
Adenylate kinase 4, mitochondrial	2.25
Thioredoxin interacting protein	1.59
C5a anaphylatoxin chemotactic receptor 1	1.54
Extracellular serine/threonine protein kinase FAM20C	1.49
PTB-containing, cubilin and LRP1-interacting protein	1.42
Beta-1,4 N-acetylgalactosaminyltransferase 1	1.41
6-phosphofructokinase, liver type	1.37
Class II histocompatibility antigen, M alpha chain	0.74
C-type lectin domain family 6 member A	0.74
Urokinase-type plasminogen activator	0.72
MCG21506	0.71
Interferon regulatory factor 4	0.71
Methylcytosine dioxygenase TET2	0.70
Catenin beta-1	0.61
Peroxisomal acyl-coenzyme A oxidase 3	0.52
Placenta-expressed transcript 1 protein	0.45
Cytochrome P450 2S1	0.42
Arsenite methyltransferase	0.27
GTP cyclohydrolase 1 (GTPCH)	0.23

Table 5.2 The 20 significantly altered proteins with the greatest fold change between unstimulated $Gch^{fl/fl}Tie2cre$ versus $Gch^{fl/fl}$ macrophages measured using mass spectrometry

Protein	Fold change (Ratio $Gch^{fl/fl}Tie2cre/Gch^{fl/fl}$)
R3H and coiled-coil domain-containing protein 1	4.95
Protein Ms4a7	2.90
Serum amyloid A-3 protein	2.30
NADH dehydrogenase [ubiquinone] 1 alpha subcomplex subunit 12 (NDUFA12)	1.96
Fatty acid desaturase 2	1.89
Protein Gm20547	1.79
Cytochrome P450 4V2	1.77
NADH dehydrogenase [ubiquinone] iron-sulfur protein 6, mitochondrial (NDUFS6)	1.73
Radical S-adenosyl methionine domain-containing protein 2	0.54
Peroxisomal acyl-coenzyme A oxidase 3	0.53
DEP domain-containing mTOR-interacting protein	0.53
Solute carrier family 2, facilitated glucose transporter member 1 (GLUT-1)	0.51
Platelet-activating factor acetyl hydrolase	0.50
OX-2 membrane glycoprotein	0.47
Cytochrome P450 2S1	0.46
Stearoyl-CoA desaturase-3	0.41
BCL2/adenovirus E1B 19 kDa protein-interacting protein 3	0.35
Arsenite methyltransferase	0.33
Isoform 2 of sphingosine kinase 1	0.21
GTP cyclohydrolase 1 (GTPCH)	0.11

Table 5.3 The 20 significantly altered proteins with the greatest fold change between LPS/IFNγ stimulated $Gch^{fl/fl}Tie2cre$ versus $Gch^{fl/fl}$ macrophages measured using mass spectrometry

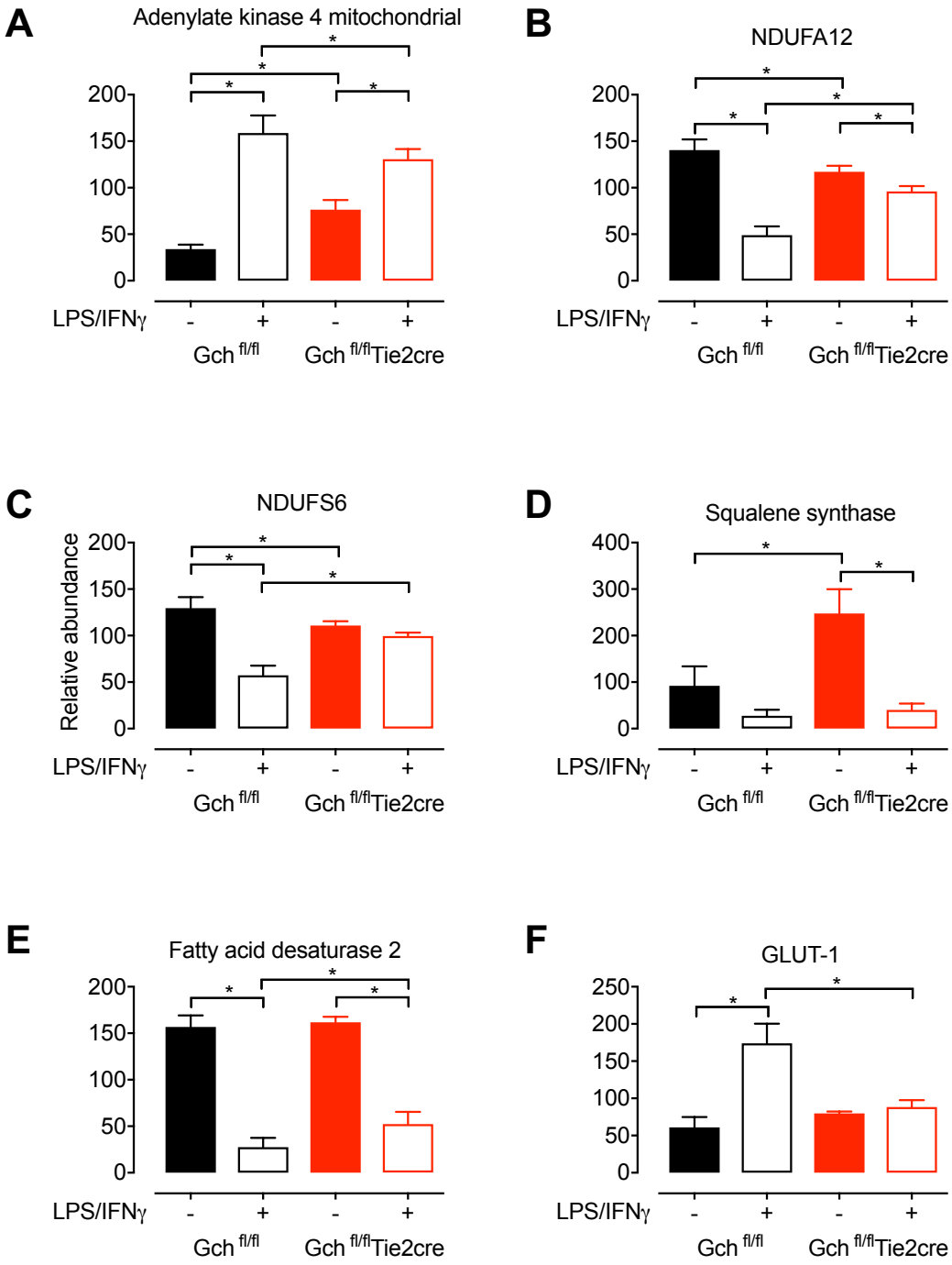


Figure 5.9 Scaled abundance of selected proteins with the greatest fold change between Gch$^{fl/fl}$Tie2cre and Gch$^{fl/fl}$ macrophages

Scaled abundance of selected proteins from the tables of 20 most significantly altered proteins with the greatest fold change between Gch$^{fl/fl}$Tie2cre and Gch$^{fl/fl}$ macrophages (n=4). Data are mean ± SEM. *P* values calculated using 2-way ANOVA ($P<9x10^{-6}$) with Tukey's HSD (*$P<0.05$).

$Gch^{fl/fl}Tie2cre$ vs $Gch^{fl/fl}$	Proteins (ANOVA $P < 0.05$, Fold Change 20%)	
	Increased	Decreased
Unstimulated	24	38
LPS/IFNγ	94	55

Table 5.4 Number of proteins significantly changed in abundance between $Gch^{fl/fl}Tie2cre$ and $Gch^{fl/fl}$ macrophages as determined by mass spectrometric analysis
The number of proteins significantly changed ≥20% between $Gch^{fl/fl}Tie2cre$ and $Gch^{fl/fl}$ macrophages analysed using mass spectrometry (n=4). (ANOVA $P<9x10^{-6}$, Tukey's HSD $*P<0.05$)

5.4.3.1 Proteomic analysis reveals BH_4-mediated modulation of glycolysis, macrophage activation, DNA binding and protein folding in unstimulated macrophages

GO term enrichment analysis of the 24 proteins that were significantly increased in unstimulated $Gch^{fl/fl}Tie2cre$ versus $Gch^{fl/fl}$ macrophages showed elevated levels of proteins involved in nucleoside phosphorylation, glycolysis/gluconeogenesis and regulation of macrophage activation (Figure 5.10A and B). Analysis of the 38 decreased proteins identified lower levels of proteins involved in the regulation of DNA binding and chaperone mediated protein folding (Figure 5.11A and B). It also highlighted neuroblast proliferation, and although this category name is not relevant to macrophage development it encompassed α- and β-catenin proteins involved in cell adhesion. These changes must be due to BH_4 deficiency independent from NOS as iNOS is not induced in these cells.

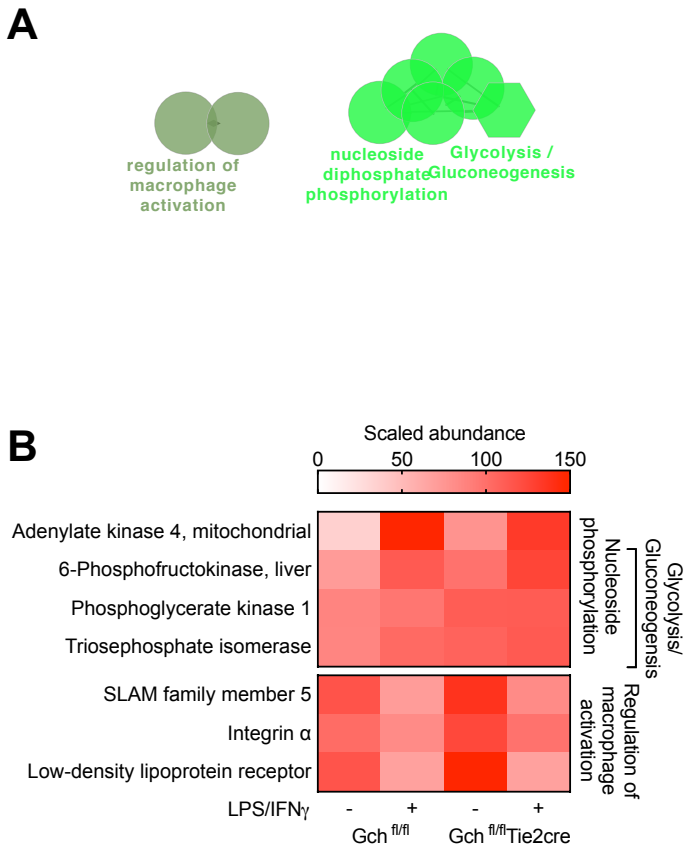


Figure 5.10 Enrichment analysis of proteins elevated in unstimulated Gch$^{fl/fl}$Tie2cre macrophages

(A) GO term enrichment analysis of significantly increased proteins in unstimulated Gch$^{fl/fl}$Tie2cre BMDMs. The most significant term in each cluster is annotated with the manual addition of 'Glycolysis/gluconeogenesis' which is relevant to the study. (B) Heat map showing the mean scaled abundance of proteins identified in the most significantly enriched GO terms from the analysis of elevated proteins (n=4). (ANOVA $P<9x10^{-6}$, Tukey's HSD $P<0.05$)

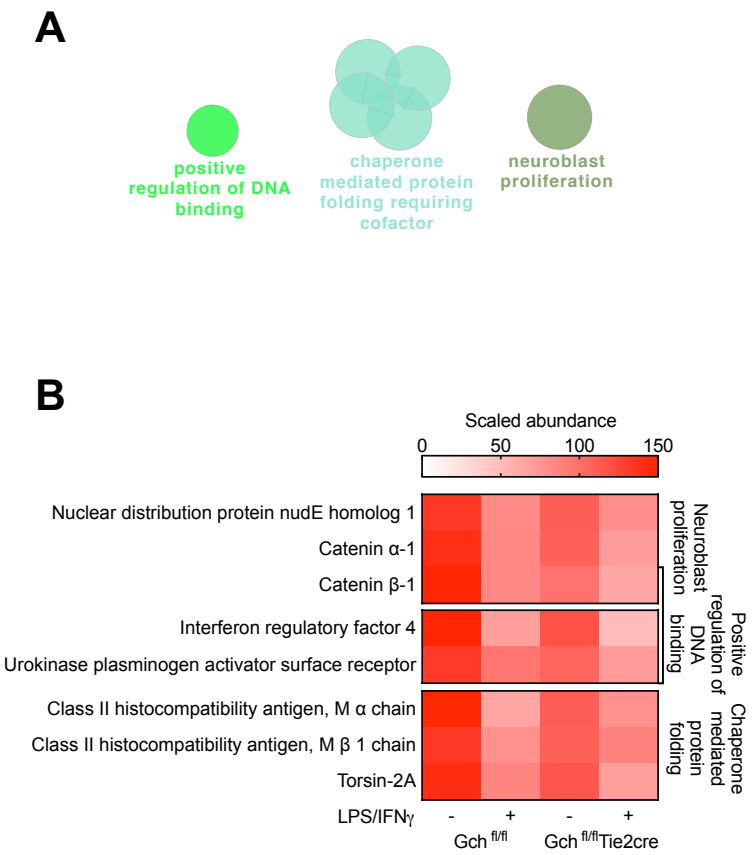


Figure 5.11 Enrichment analysis of proteins decreased in unstimulated Gch$^{fl/fl}$Tie2cre macrophages

(A) GO term enrichment analysis of significantly decreased proteins in unstimulated Gch$^{fl/fl}$Tie2cre BMDMs. The most significant term in each cluster is annotated. (B) Heat map showing the mean scaled abundance of proteins identified in the most significantly enriched GO terms from the analysis of decreased proteins (n=4). (ANOVA $P<9x10^{-6}$, Tukey's HSD $P<0.05$)

5.4.3.2 Proteomic analysis reveals BH_4-mediated modulation of inflammation, mitochondrial function, and metabolism in stimulated macrophages

GO term enrichment analysis of the 94 proteins that were significantly increased in stimulated $Gch^{fl/fl}$Tie2cre versus $Gch^{fl/fl}$ macrophages identified elevated levels of proteins involved in the response to interferon-β (IFNβ), production of IL-1β, antigen presentation, and subunits of mitochondrial respiratory chain Complex I (Figure 5.12A and B). These results suggested both an enhanced response to – and synthesis of – specific inflammatory cytokines in BH_4-deficient macrophages and a potential mechanism linking absence of BH_4 and NO to the maintenance of Complex I function.

Enrichment analysis of the 55 decreased proteins highlighted additional mitochondrial and metabolic changes and showed lower levels of proteins involved in the mitochondrial ribosome, mitochondrial gene expression, and carbohydrate metabolism (Figure 5.13A and B). Furthermore, metabolic enzymes such as the GLUT-1, squalene synthase, fatty acid desaturase-2, and Complex I subunits (NDUFS6 and NDUFA12) were amongst the 20 most significantly changed proteins in this data set (Table 5.2 and 5.3; Figure 5.9). Taken together, these results implicated BH_4 in the modulation of several novel aspects of metabolism, mitochondrial function, and inflammation, but whether mitochondrial and metabolic changes resulted from loss of NO signalling remained to be confirmed and became the focus of further investigation.

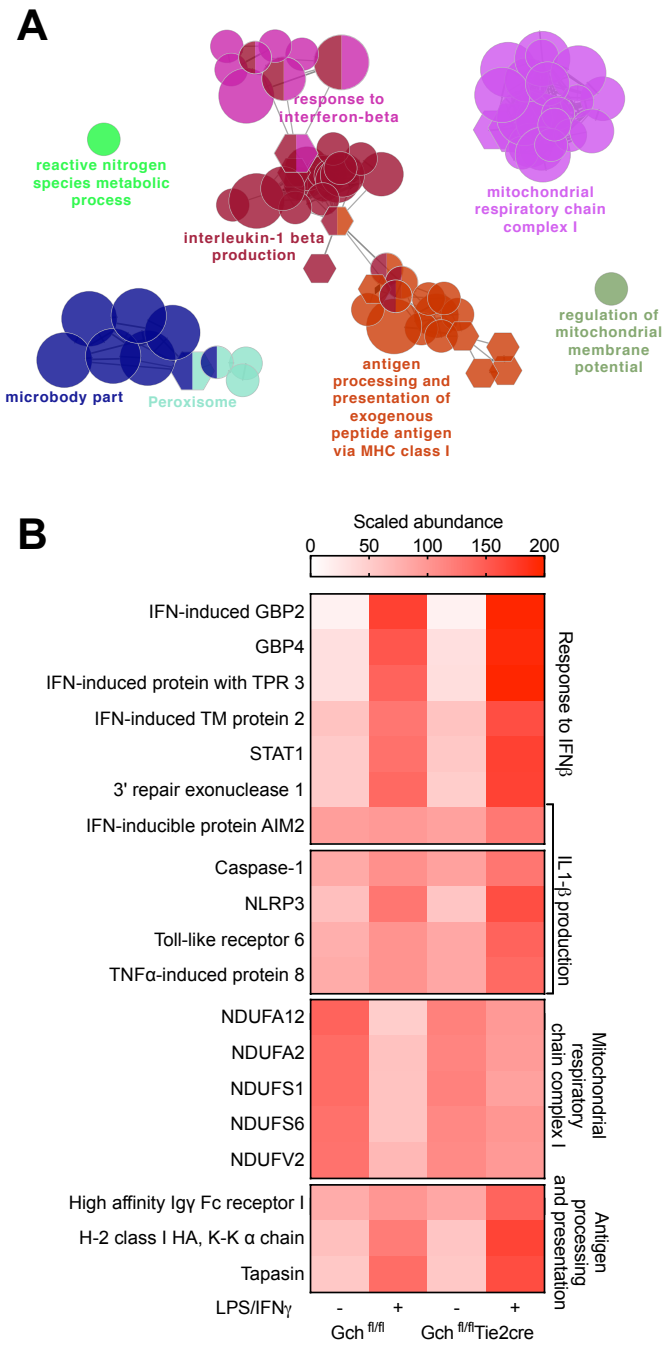


Figure 5.12 Enrichment analysis of proteins elevated in Gch$^{fl/fl}$Tie2cre macrophages stimulated with LPS/IFNγ

(A) GO term enrichment analysis of significantly increased proteins in Gch$^{fl/fl}$Tie2cre BMDMs stimulated with LPS/IFNγ. The most significant term in each cluster is annotated. (B) Heat map showing the mean scaled abundance of proteins identified in the most significantly enriched GO terms from the analysis of elevated proteins (n=4). (ANOVA $P<9x10^{-6}$, Tukey's HSD $P<0.05$)

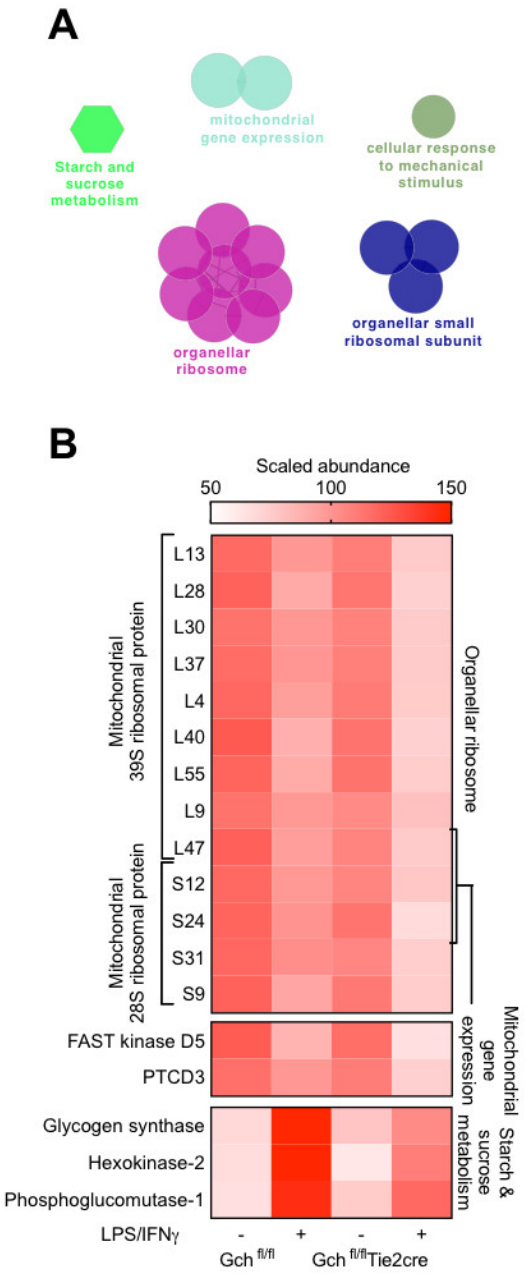


Figure 5.13 Enrichment analysis of proteins decreased in Gch$^{fl/fl}$Tie2cre macrophages stimulated with LPS/IFNγ

(A) GO term enrichment analysis of significantly decreased proteins in Gch$^{fl/fl}$Tie2cre BMDMs stimulated with LPS/IFNγ. The most significant term in each cluster is annotated. (B) Heat map showing the mean scaled abundance of proteins identified in the most significantly enriched GO terms from the analysis of decreased proteins (n=4). (ANOVA $P<9x10^{-6}$, Tukey's HSD $P<0.05$)

5.4.4 IL-1β secretion is elevated due to loss of NO signalling

To confirm that stimulated BH_4-deficient macrophages were producing more IL-1β as predicted by the enrichment analysis, *Il1b* mRNA and IL-1β secretion were measured and revealed striking elevations in both (Figure 5.14A and B). These increases in *Il1b* mRNA and IL-1β secretion were also found in $M^{LPS/IFN\gamma}$ iNOS KO cells, indicating that it occurred due to loss of NO signalling (Figure 5.14C and D). On the other hand, LPS/IFNγ induced levels of TNFα, IL-6 and IL-10 secretion were maintained in NO-deficient cells (apart from a small decrease in IL-6 in stimulated $Gch^{fl/fl}$Tie2cre as previously reported (McNeill et al., 2015)) (Figure 5.14E-J).

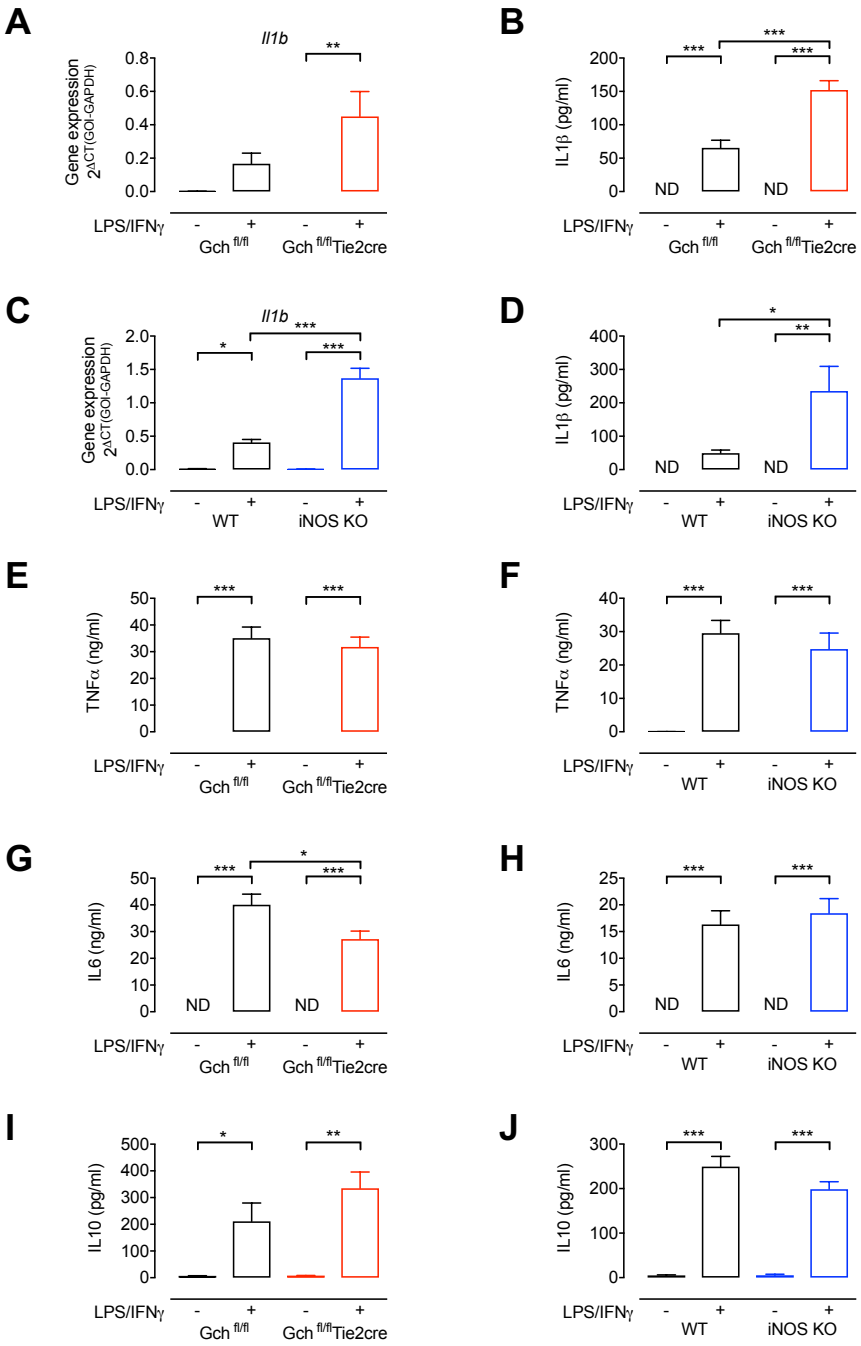


Figure 5.14 Cytokine measurements in Gch$^{fl/fl}$Tie2cre and iNOS KO macrophages

(A) *Il1b* gene expression in Gch$^{fl/fl}$Tie2cre cells measured using qRT-PCR. (B) Levels of IL-1β in supernatants from Gch$^{fl/fl}$Tie2cre cells measured by ELISA. (C) *Il1b* gene expression in iNOS KO cells. (D) Levels of IL-1β in supernatants from iNOS KO cells. ELISA measurements of TNFα in (E) Gch$^{fl/fl}$Tie2cre and (F) iNOS KO cells, IL-6 in (G) Gch$^{fl/fl}$Tie2cre and (H) iNOS KO cells and IL-10 in (I) Gch$^{fl/fl}$Tie2cre and (J) iNOS KO cells. Data are n=5 mean ± SEM. *P* values calculated using 2-way ANOVA with Tukey's post-test (* $P<0.05$, ** $P<0.01$, *** $P<0.001$).

5.4.5 NO regulates levels of Complex I subunits and function

One of the most striking changes highlighted by the proteomic analysis were changes in several subunits of Complex I, which is situated in the mitochondrial inner membrane. It is an intricate protein of almost 1000 kDa and comprising 45 subunits (Guerrero-Castillo et al., 2017), of which 35 were measured in this study. Complex I is formed of 4 distinct modules (Figure 5.15A) and the abundance of subunits making up the P and Q modules were not significantly different upon stimulation or genotype variations, apart from a significant decrease in NDUFS2 in $M^{LPS/IFN\gamma}$ $Gch^{fl/fl}$ macrophages compared with unstimulated cells (Figure 5.15C). Interestingly, there were significant co-ordinated decreases in 5 out of 8 subunits making up the catalytic NADH binding module (N-module) in stimulated $Gch^{fl/fl}$ cells, with another 2 subunits (NDUFS4 and NDUFV1) showing a similar pattern but not statistically significant (Figure 5.15C). Upon activation, these decreases were largely attenuated by the absence of BH_4 and NO in $Gch^{fl/fl}$Tie2cre cells – including in the 3 subunits (NDUFV1, NDUFV2, NDUFS1) thought to be essential for catalysis. Western blot analysis of NDUFV2 in $Gch^{fl/fl}$ and WT cells confirmed depletion of this protein upon stimulation, and the fact that both $Gch^{fl/fl}$Tie2cre and iNOS KO $M^{LPS/IFN\gamma}$ cells retained much greater levels indicated that this was driven by NO (Figure 5.15D). Significantly reduced expression of *Ndufv2* in stimulated $Gch^{fl/fl}$ and WT cells suggested that changes in protein levels resulted from transcriptional regulation, and restored gene expression in $M^{LPS/IFN\gamma}$ iNOS KO would indicate that this was NO-dependent (Figure 5.15E and F). However, gene expression in $M^{LPS/IFN\gamma}$ $Gch^{fl/fl}$Tie2cre cells was repressed (Figure 5.15E), suggesting involvement of other mechanisms and highlighting a difference between BH_4-replete and -deficient cells. An in-gel activity assay confirmed that Complex I activity was decreased in $Gch^{fl/fl}$ $M^{LPS/IFN\gamma}$ cells but maintained in $Gch^{fl/fl}$Tie2cre $M^{LPS/IFN\gamma}$ cells and also showed that stimulated $Gch^{fl/fl}$ cells had a reduction in complex I containing

supercomplexes (Figure 5.15G). These results demonstrate a novel and important role for NO in modulating Complex I subunit abundance and activity in activated macrophages, in addition to the established inhibitory nitrosation of Complex I (Figure 5.15B).

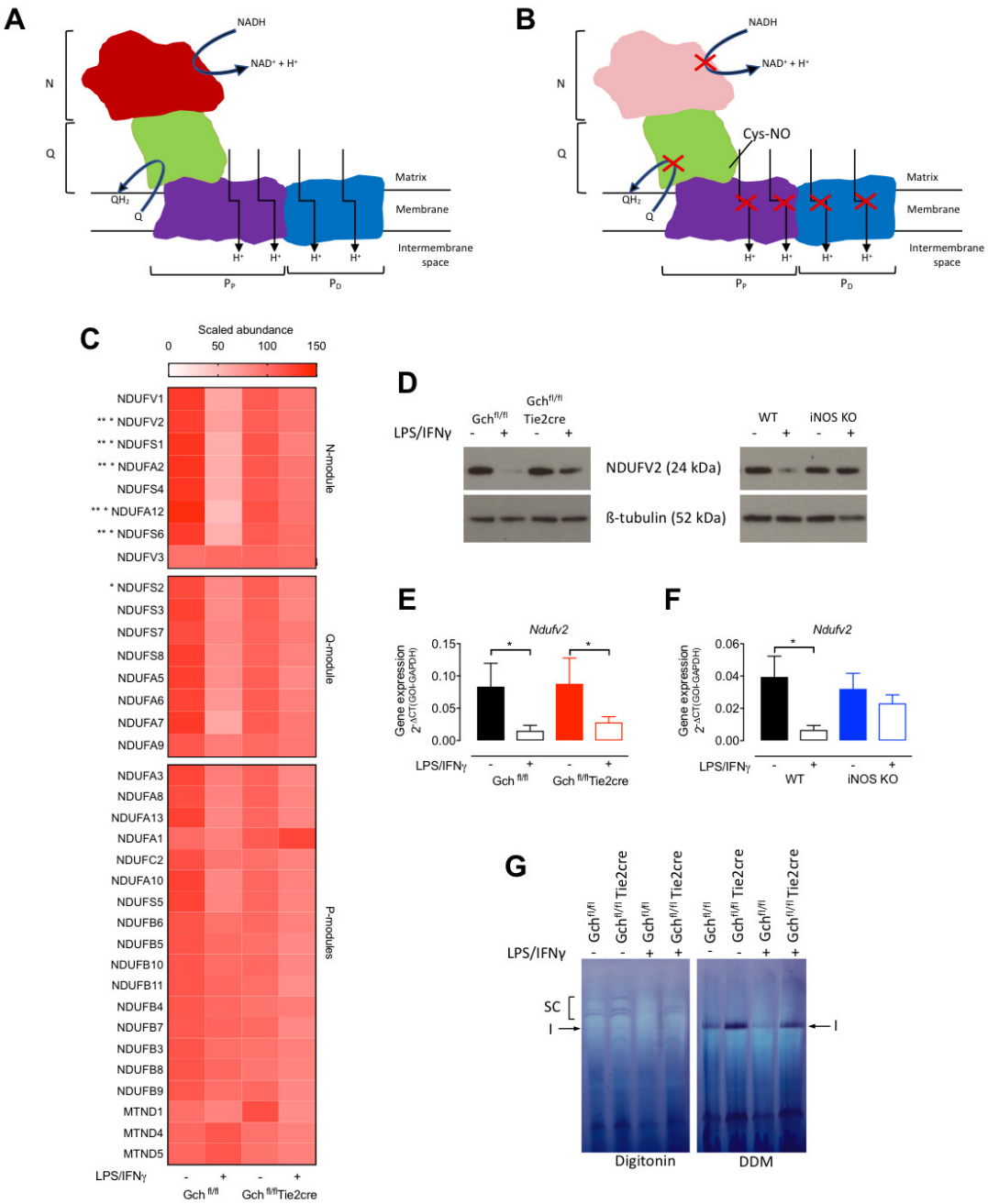


Figure 5.15 NO-dependent regulation of Complex I N-module subunits and activity

(A) Structure of the modules (N, Q, P_P and P_D) making up NADH dehydrogenase (Complex I) and (B) proposed NO mediated mechanisms leading to inhibition upon stimulation of BMDMs with LPS/IFNγ. (C) Heatmap showing mean scaled abundance of N, Q and P module subunits detected using mass spectrometry in $Gch^{fl/fl}$Tie2cre macrophages (n=4, *

significant difference unstimulated $Gch^{fl/fl}$ versus $M^{LPS/IFN\gamma}$ $Gch^{fl/fl}$, ** significant difference between $M^{LPS/IFN\gamma}$ $Gch^{fl/fl}$ versus $M^{LPS/IFN\gamma}$ $Gch^{fl/fl}$Tie2cre). (D) NDUFV2 protein levels determined by Western blotting in $Gch^{fl/fl}$Tie2cre and iNOS KO cells (n=4). (E-F) *Ndufv2* mRNA measured using qRT-PCR in (E) $Gch^{fl/fl}$Tie2cre and (F) iNOS KO cells (n=5). (G) Complex I (labelled I) in gel activity assay with digitonin, to demonstrate supercomplex (SC) abundance, and DDM (n-dodecyl-β-D-maltoside) to demonstrate isolated Complex I activity in $Gch^{fl/fl}$Tie2cre cells. Data are mean ± SEM. *P* values calculated using 2-way ANOVA with Tukey's post-test (*P<0.05).

5.4.6 NO regulates mitochondrial respiration

Decreased Complex I subunits and activity were paralleled by changes in OCR (Figure 5.16 and 5.17), as basal and ATP-linked respiration were largely maintained in activated cells unable to produce NO in $Gch^{fl/fl}$Tie2cre and iNOS KO, in contrast to the well-established NO-induced inhibition of respiration in $Gch^{fl/fl}$ and WT cells (Figure 5.16B-C and 5.17B-C). Interestingly, although maximum respiration is also significantly higher in stimulated NO-deficient cells, this remained no higher than basal levels and significantly lower than unstimulated cells (Figure 5.16D and 5.17D), indicating changes in respiratory capacity which occur after stimulation but via NO-independent mechanisms. Additionally, proton leak was decreased in $M^{LPS/IFN\gamma}$ $Gch^{fl/fl}$ and WT cells but comparatively higher in NO-deficient cells (Figure 5.16F and 5.17F), and non-mitochondrial OCR was significantly increased in stimulated NO synthesising macrophages but not $Gch^{fl/fl}$Tie2cre and iNOS KO cells (Figure 5.16G and 5.17G). Overall these results were remarkably similar in $Gch^{fl/fl}$Tie2cre and iNOS KO cells, with the main differences seen in unstimulated cells which were unchanged between $Gch^{fl/fl}$ and $Gch^{fl/fl}$Tie2cre macrophages but showed significantly higher basal, ATP-linked and maximum OCR in iNOS KO compared with WT cells. These results demonstrate the important role for NO in modulating the metabolic switch away from oxidative metabolism in activated macrophages.

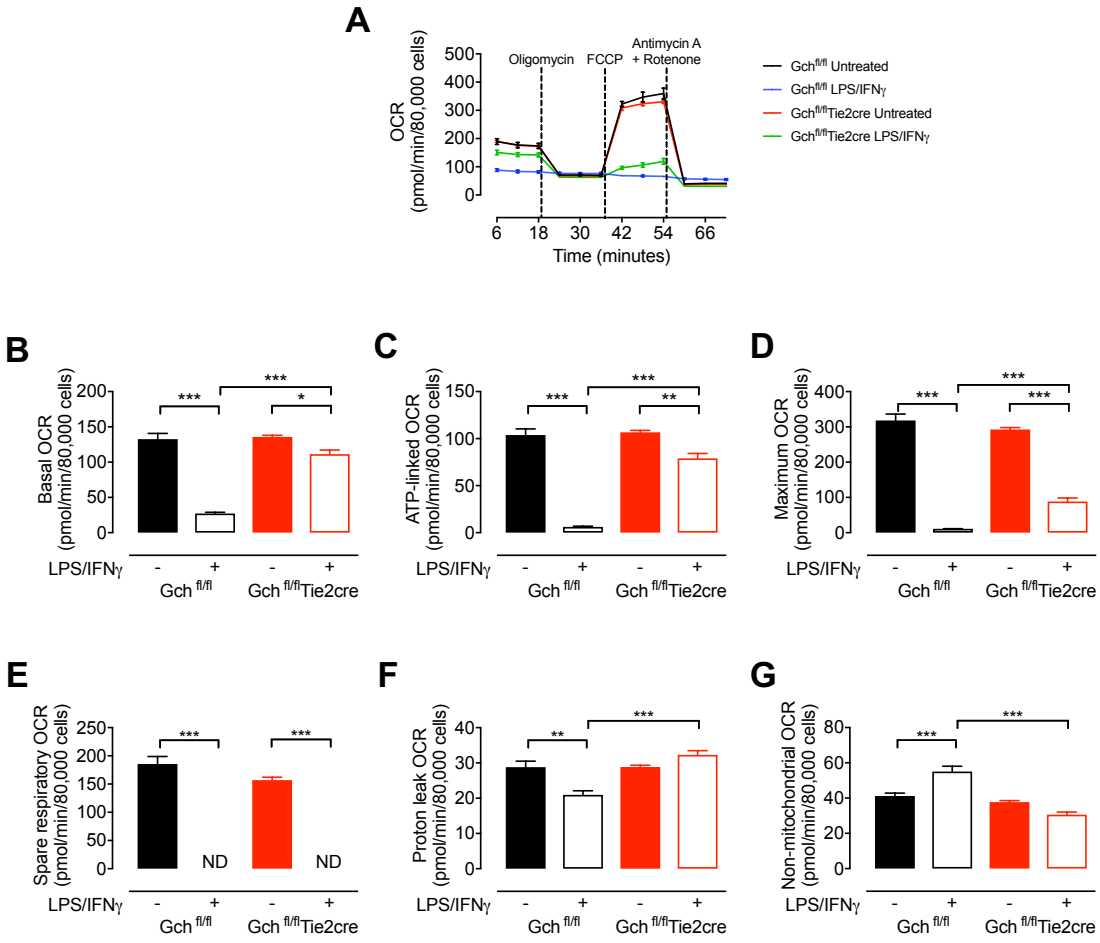


Figure 5.16 BH_4-dependent inhibition of mitochondrial respiration

(A) Oxygen consumption rate (OCR) was measured using an XF^{e}96 Seahorse bioanalyzer with sequential injection of oligomycin, FCCP, and combined rotenone and antimycin A in Gch$^{fl/fl}$Tie2cre macrophages. Measurements were used to determine (B) basal, (C) ATP-linked, (D) maximum, (E) spare respiratory capacity, (F) proton leak and (G) non-mitochondrial respiration. Data are n=5-6 mean ± SEM. *P* values calculated using 2-way ANOVA with Tukey's post-test (* $P<0.05$, ** $P<0.01$, *** $P<0.001$).

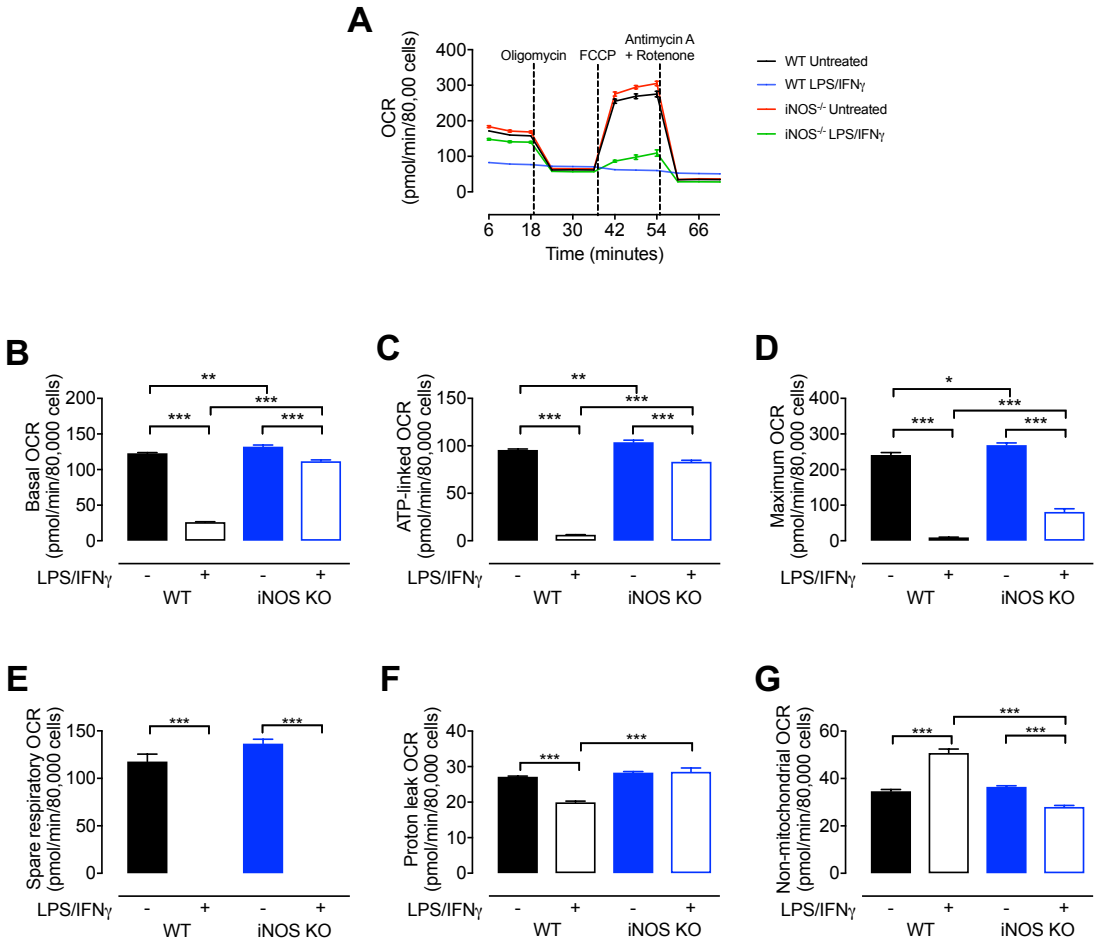


Figure 5.17 NO-dependent inhibition of mitochondrial respiration

(A) Oxygen consumption rate (OCR) was measured using an XF^{e}96 Seahorse bioanalyzer with sequential injection of oligomycin, FCCP, and combined rotenone and antimycin A in iNOS KO macrophages. Measurements were used to determine (B) basal, (C) ATP-linked, (D) maximum, (E) spare respiratory capacity, (F) proton leak and (G) non-mitochondrial respiration. Data are n=5-6 mean ± SEM. *P* values calculated using 2-way ANOVA with Tukey's post-test (* $P<0.05$, ** $P<0.01$, *** $P<0.001$).

5.4.7 Metabolomic analysis of Gch$^{fl/fl}$Tie2cre and iNOS KO macrophages

To explore the consequences of changes in the abundance of proteins involved in metabolism highlighted in the proteomic data and whether they were dependent on changes in NO signalling, mass spectrometry was used to measure metabolites in cells from the Gch$^{fl/fl}$Tie2cre and iNOS KO systems. Of the 290 metabolites detected in Gch$^{fl/fl}$ and Gch$^{fl/fl}$Tie2cre macrophages, 49 were significantly different according to genotype in unstimulated cells, and 39 in M$^{LPS/IFN\gamma}$ cells (Table 5.5). This was higher in WT and iNOS KO macrophages – prepared and analysed in a separate experiment – with 336 metabolites detected, of which 32 were significantly different according to genotype in unstimulated cells, and 123 in M$^{LPS/IFN\gamma}$ cells (Table 5.6). A large proportion of metabolites were significantly altered in all cell types upon stimulation with LPS/IFNγ (Table 5.5 and 5.6). The data were used to create network maps with pathway clustering and nodes representing the fold change of specific metabolites in M$^{LPS/IFN\gamma}$ cells compared with unstimulated cells (Figure 5.18 and 5.19). The 8 major groups were lipids, amino acids, nucleotides, carbohydrates, peptides, cofactors and vitamins, xenobiotics and energy. Changes between genotypes can be observed in all groups, including the glycolysis pathway highlighted in the carbohydrate category and the TCA cycle in the energy group, and both of these were investigated further due to their importance in macrophage metabolic remodelling.

Citrulline was the most altered metabolite between NO-deficient and -synthesising cells (Figure 5.20A and B). This indicated changes in arginine metabolism as levels of arginine were significantly decreased and citrulline were dramatically elevated in Gch$^{fl/fl}$ and WT cells upon stimulation but not in Gch$^{fl/fl}$Tie2cre and iNOS KO cells (Figure 5.20A-D). NOS enzymes metabolise arginine into citrulline and NO, so this reflects the expected loss of iNOS activity in Gch$^{fl/fl}$Tie2cre and iNOS KO cells and these expected changes confirm the robustness of the model. In iNOS KO (but not Gch$^{fl/fl}$Tie2cre) macrophages ornithine was

also measured, and was significantly elevated upon stimulation of WT cells and further increased in iNOS KO cells, possibly indicating changes in metabolism of arginine by arginase (Figure 5.20F). In addition, levels of biopterin and pterin were elevated in stimulated $Gch^{fl/fl}$ macrophages but decreased as expected in $Gch^{fl/fl}$Tie2cre cells (Figure 5.20E and G). Surprisingly pterin was also diminished in $M^{LPS/IFN\gamma}$ iNOS KO cells, although biopterin was not measured (Figure 5.20H). As the $Gch^{fl/fl}$Tie2cre and iNOS KO samples were analysed separately, different metabolites were detected in each set and the data are not directly comparable. The absence of certain metabolites in one data set does not necessarily confirm that levels were relatively decreased or lacking.

		Metabolites (ANOVA $P < 0.05$)	
Comparison		**Increased**	**Decreased**
$Gch^{fl/fl}$Tie2cre vs $Gch^{fl/fl}$	Unstimulated	27	22
	LPS/IFNγ	11	28
LPS/IFNγ vs Unstimulated	$Gch^{fl/fl}$	100	43
	$Gch^{fl/fl}$Tie2cre	67	39

Table 5.5 Number of metabolites significantly changed in abundance between $Gch^{fl/fl}$Tie2cre and $Gch^{fl/fl}$, and LPS/IFNγ and Unstimulated macrophages as determined by mass spectrometric analysis

		Metabolites (ANOVA $P < 0.05$)	
Comparison		**Increased**	**Decreased**
iNOS KO vs WT	Unstimulated	10	22
	LPS/IFNγ	33	90
LPS/IFNγ vs Unstimulated	WT	97	61
	iNOS KO	83	84

Table 5.6 Number of proteins significantly changed in abundance between iNOS KO and WT, and LPS/IFNγ and Unstimulated macrophages as determined by mass spectrometric analysis

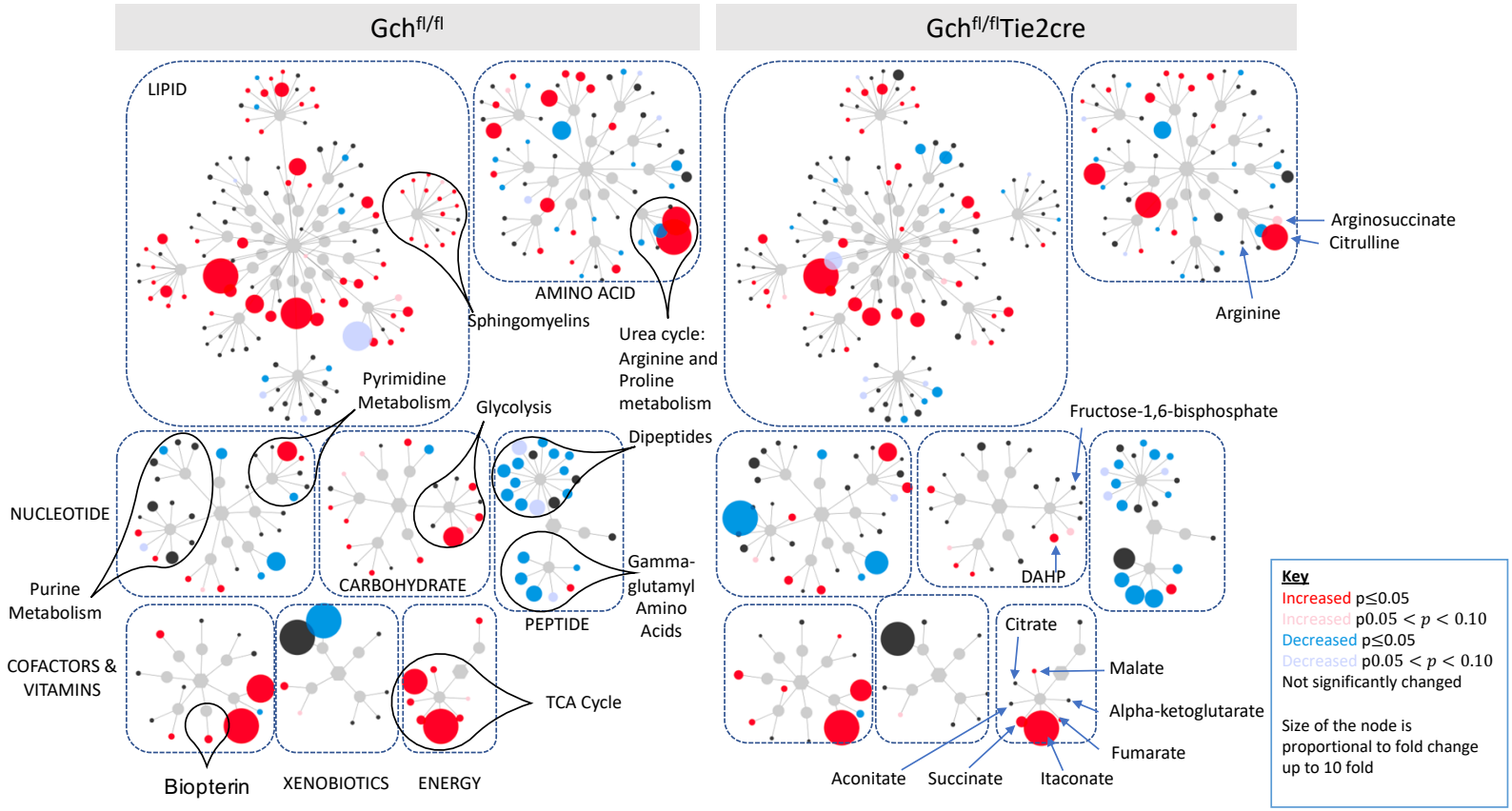


Figure 5.18 Metabolomic analysis of Gch$^{fl/fl}$Tie2cre macrophages

Network map with pathway clustering presenting the 290 metabolites identified by mass spectrometry. Outer nodes represent specific metabolites of sizes proportional to the fold change difference between unstimulated and M$^{LPS/IFN\gamma}$ macrophages. (Black – not significantly different (P<0.05), Red – significantly increased (P<0.05), Blue – significantly decreased (P<0.05), Pink – increased (0.05<P<0.1), Light blue – decreased (0.05<P<0.1)). Selected clusters and metabolites are labelled.

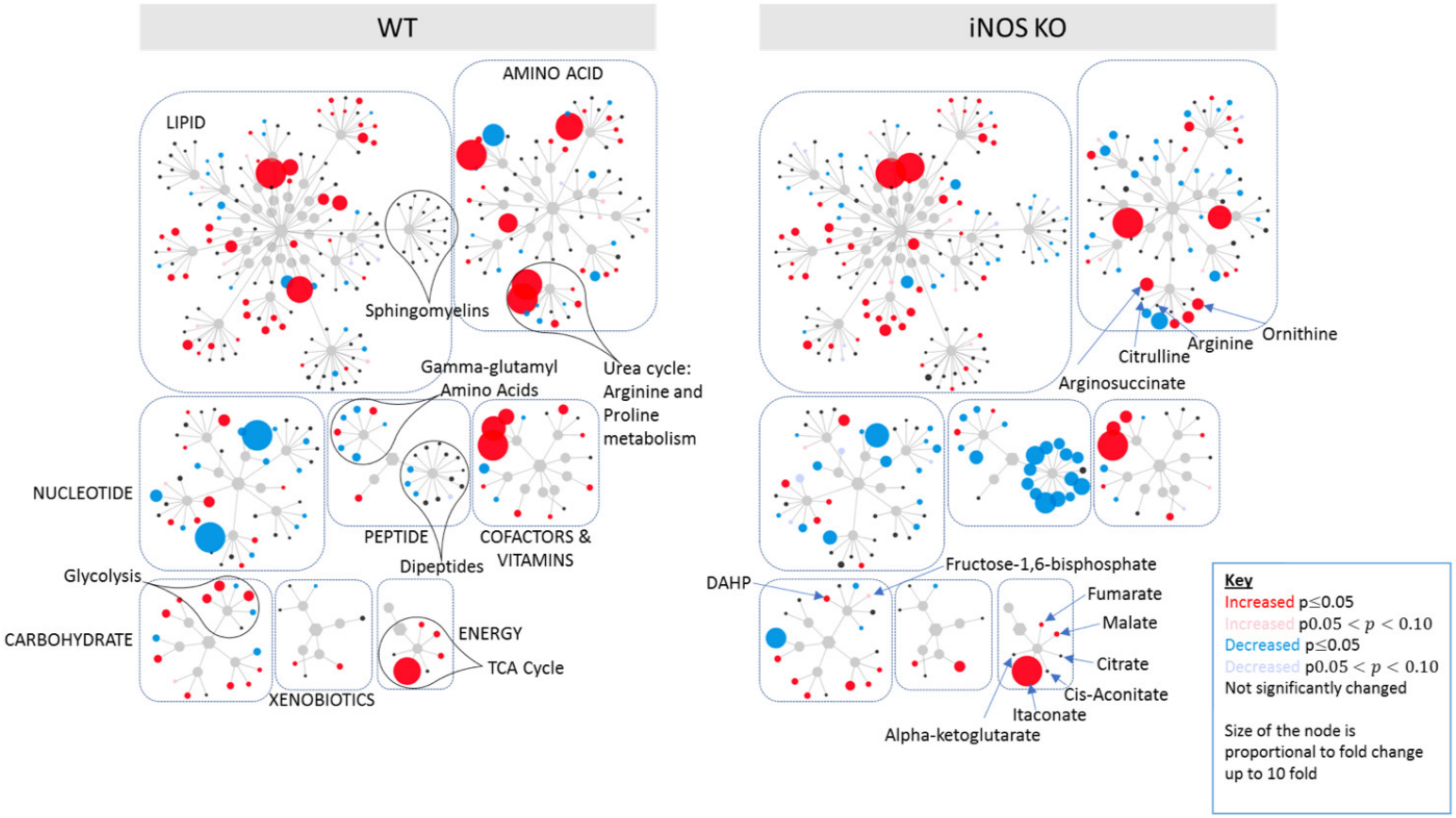


Figure 5.19 Metabolomic analysis of iNOS KO macrophages

Network map with pathway clustering presenting the 336 metabolites identified by mass spectrometry. Outer nodes represent specific metabolites of sizes proportional to the fold change difference between unstimulated and $M^{LPS/IFN\gamma}$ macrophages. (Black – not significantly different (P<0.05), Red – significantly increased (P<0.05), Blue – significantly decreased (P<0.05), Pink – increased (0.05<P<0.1), Light blue – decreased (0.05<P<0.1)). Selected clusters and metabolites are labelled.

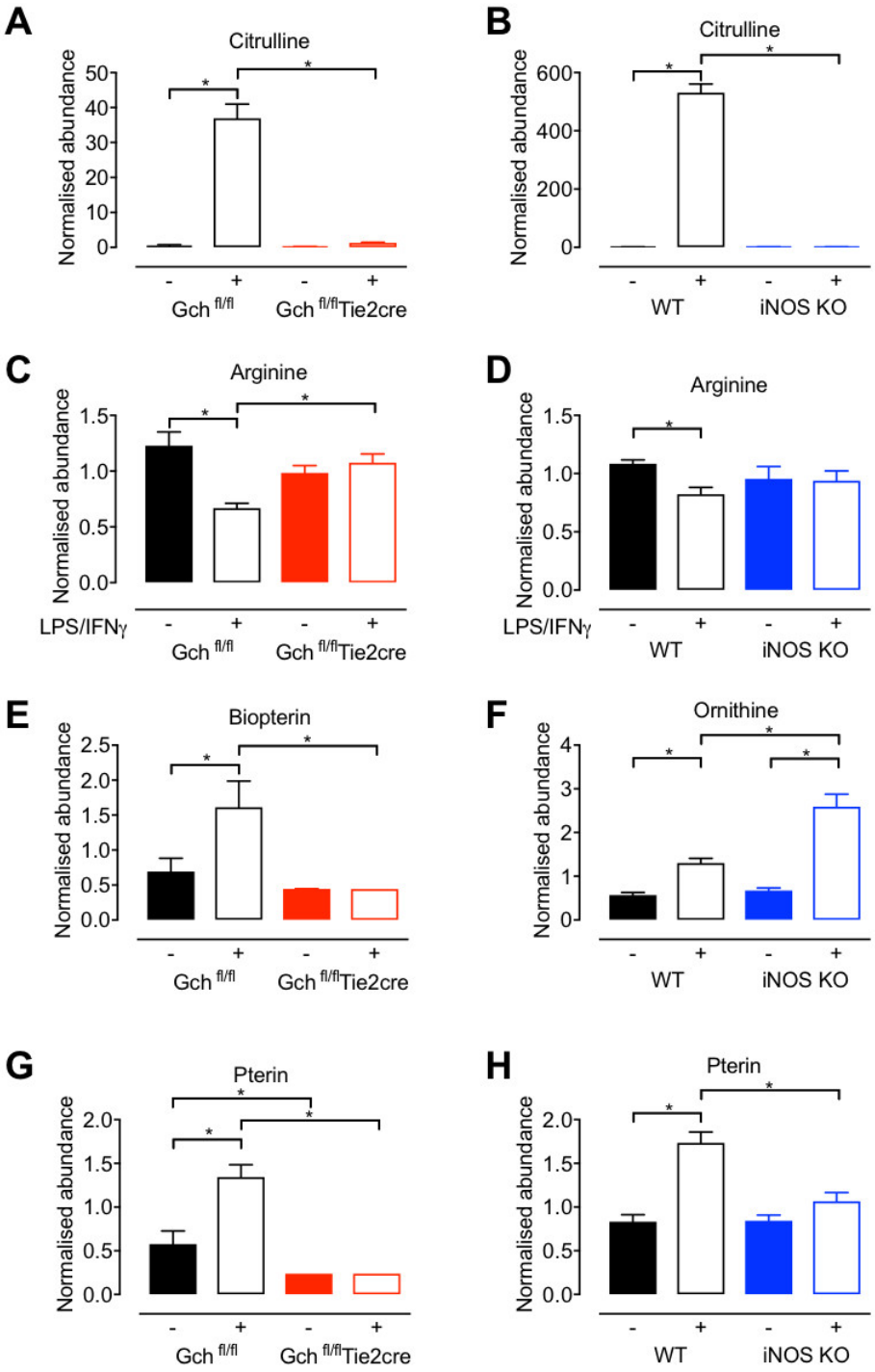


Figure 5.20 Abundance of metabolites involved in arginine and biopterin metabolism

Normalised abundance of (A and B) citrulline, (C and D) arginine, (E) biopterin, (F) ornithine and (G and H) pterin from Gch$^{fl/fl}$Tie2cre and iNOS KO macrophages measured using mass spectrometry. Data are n=6 mean ± SEM. *P* values calculated using 2-way ANOVA with Tukey's post-test (* $P<0.05$)

5.4.8 NO modulates HIF1α-mediated regulation of glycolysis

The switch from oxidative phosphorylation to glycolysis-mediated ATP synthesis is a characteristic of macrophages stimulated with LPS/IFNγ (Kelly and O'Neill, 2015) and is directed by increased levels of key proteins under the transcriptional control of HIF1α, including GLUT-1, hexokinase-2, and 6-phosphofructo-2-kinase/fructose-2,6-bisphosphatase 3 (PFKFB3) (Liu et al., 2016; Wang et al., 2017). These established changes were reproduced in activated NO-producing macrophages in this study (Figure 5.21A and B). However, GO term enrichment analysis highlighted comparatively less of the enzymes related to 'starch and sucrose metabolism' in stimulated $Gch^{fl/fl}$Tie2cre cells, including glycolytic enzyme hexokinase-2 and proteins directing glycogen storage and release (Figure 5.13A and B). Furthermore, a refined search of the data showed apparent changes in several more proteins involved in glucose metabolism and glycolysis between $M^{LPS/IFN\gamma}$ $Gch^{fl/fl}$ and $Gch^{fl/fl}$Tie2cre cells (Figure 5.21A and B), with significant decreases in GLUT-1, hexokinase-1, and PFKFB3, and increases in hexokinase-3, triose phosphate isomerase, phosphoglycerate kinase, and glycerol-catabolising enzymes. Furthermore, metabolomics revealed marked changes in the abundance of glycolytic intermediates in NO-deficient versus -replete $M^{LPS/IFN\gamma}$ cells (Figures 5.21C and D), as well as the glycerol metabolite glycerol-3-phosphate (significantly decreased in iNOS KO but not $Gch^{fl/fl}$Tie2cre) which feeds into this pathway (Figures 5.22). The relative changes in metabolite abundance were very similar in stimulated $Gch^{fl/fl}$ versus $Gch^{fl/fl}$Tie2cre and WT versus iNOS KO cells, indicating that they resulted from loss of NO. In earlier parts of the glycolysis pathway there was less fructose-1,6-bisphosphate and dihyroxyacetone-phosphate in NO-deficient cells; however, in later steps there was slightly increased 3-phosphoglycerate (only in $Gch^{fl/fl}$Tie2cre) and no difference in levels of the final products of glycolysis, phosphoenolpyruvate and pyruvate (Figure 5.21E).

The product of glycolysis, pyruvate, is converted into lactate or oxidised in the TCA cycle, and both lead to acidification of the media through proton extrusion which can be used to estimate glycolytic activity. Intracellular lactate was increased in NO-replete $M^{LPS/IFN\gamma}$ cells but to a lesser extent in the absence of NO (Figure 5.21C- E). Interestingly the extracellular acidification rate (ECAR) resulting from glucose oxidation was elevated in all $M^{LPS/IFN\gamma}$ cells regardless of BH_4 or NO levels (Figure 5.23A and B), and so to investigate the proportional effects of lactate versus TCA acidification the glycolytic proton efflux rate (glycoPER) and percentage PER attributed to glycolysis were calculated in $Gch^{fl/fl}$ versus $Gch^{fl/fl}$Tie2cre cells. This confirmed that glycoPER – and thus glycolytic rate – was equally elevated in NO-synthesising and NO-deficient $M^{LPS/IFN\gamma}$ cells (Figure 5.23C) and that glycolysis was the major contributor to PER at >90% in $M^{LPS/IFN\gamma}$ cells, which was significantly higher than in non-stimulated cells (Figure 5.23D).

To further validate the proteomic changes observed in $M^{LPS/IFN\gamma}$ $Gch^{fl/fl}$Tie2cre cells, and their dependence on NO, expression of the gene encoding GLUT-1 (*Slc2a1*) was measured and the amount of hexokinase-2 protein in $Gch^{fl/fl}$Tie2cre and iNOS KO cells. This showed a failure to induce transcription of *Slc2a1* (Figure 5.24A and B) and decreased levels of hexokinase-2 protein (Figure 5.24C) in both $Gch^{fl/fl}$Tie2cre and iNOS KO cells. Interestingly, several proteins of lower abundance in activated cells unable to produce BH_4 and NO were those that were previously reported to be transcriptionally regulated by HIF1α (Table 5.7). Western blot analysis was therefore used to determine whether previously reported LPS-stimulated HIF1α stabilisation was disrupted in the absence of BH_4 and NO and found a lower abundance of HIF1α in $Gch^{fl/fl}$Tie2cre cells (Figure 5.24C). HIF1α was similarly decreased in iNOS KO cells, proving that this was due to loss of NO signalling (Figure 5.24C). HIF1α mediated glycolytic remodelling is therefore disrupted by loss of NO

signalling, however glycolysis is sufficiently upregulated in $M^{LPS/IFN\gamma}$ cells irrespective of BH_4 or NO levels.

Proteins encoded by genes induced by HIF1α	References
GLUT-1	(Chen et al., 2001; Liu et al., 2016; Wang et al., 2017)
Hexokinase-1	(Luo et al., 2006)
Hexokinase-2	(Mathupala et al., 2001; Riddle et al., 2000)
PFKFB3	(Liu et al., 2016; Obach et al., 2004)
Phosphoglucomutase-1	(Hu et al., 2003; Pelletier et al., 2012)
Glycogen synthase	(Pescador et al., 2010)

Table 5.7 Glycolytic and glycogen metabolising proteins encoded by genes transcriptionally regulated by HIF1α

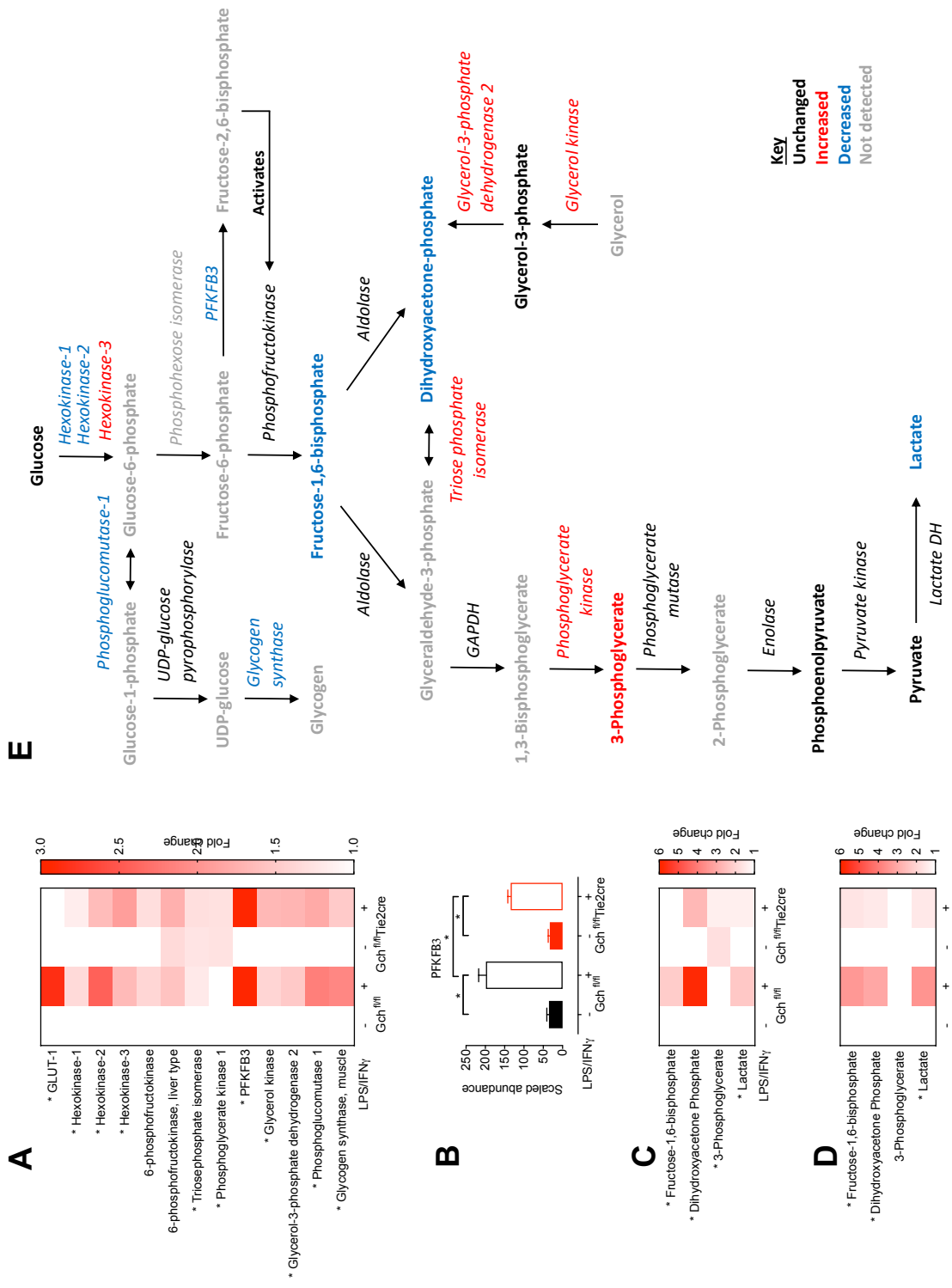


Figure 5.21 BH_4 and NO modulate levels of glycolytic proteins and metabolites

(A) Heat map showing fold changes in abundance of enzymes significantly changed ($P<0.05$) relative to $Gch^{fl/fl}$ unstimulated cells (n=4, * significant difference ($P<0.05$) between $M^{LPS/IFN\gamma}$ $Gch^{fl/fl}$ versus $Gch^{fl/fl}$Tie2cre, Note: PFKB3 = fold change >3). (B) Abundance of PFKFB3 protein (n=4). (C) Fold change heat maps of significantly changed ($P<0.05$) metabolites relative to unstimulated $Gch^{fl/fl}$ (n=6, * significant difference ($P<0.05$) between $M^{LPS/IFN\gamma}$ $Gch^{fl/fl}$ versus $Gch^{fl/fl}$Tie2cre) (D) Fold change heat maps of significantly

changed (P<0.05) metabolites relative to unstimulated WT cells (n=6, * significant difference (P<0.05) between $M^{LPS/IFN\gamma}$ WT versus iNOS KO). (E) Glucose metabolism pathway representing changes (>20%) in abundance of enzymes and metabolites in LPS/IFNγ stimulated $Gch^{fl/fl}$Tie2cre versus $Gch^{fl/fl}$ macrophages (Black – not significantly changed, Red – significantly increased, Blue – significantly decreased, Grey – not detected). Data are mean ± SEM. *P* values calculated using 2-way ANOVA with Tukey's post-test (*P<0.05).

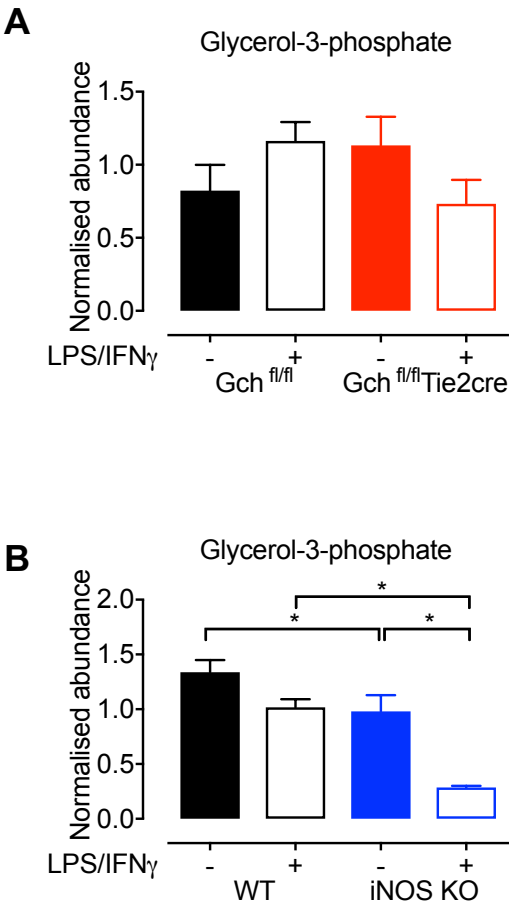


Figure 5.22 Abundance of glycerol-3-phosphate

Abundance of glycerol-3-phosphate in (A) $Gch^{fl/fl}$Tie2cre and (B) iNOS KO macrophages measured using mass spectrometry. Data are n=6 mean ± SEM. *P* values calculated using 2-way ANOVA with Tukey's post-test (*P<0.05).

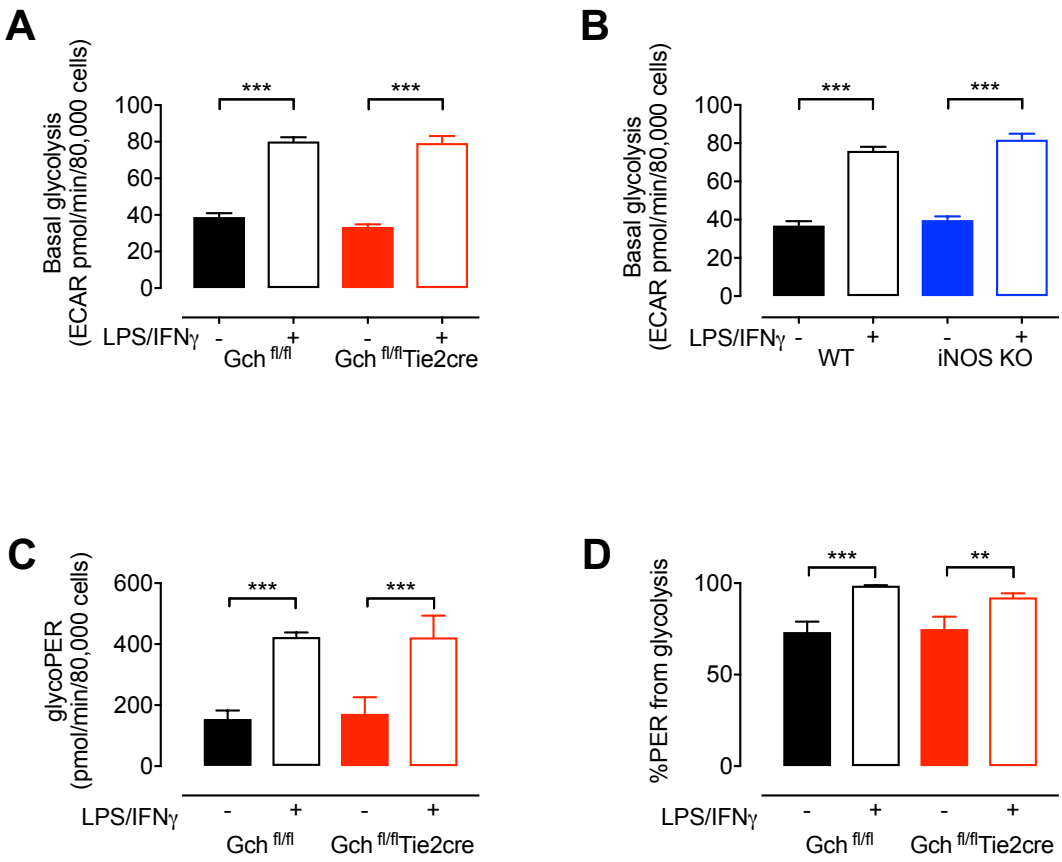


Figure 5.23 Glycolytic rate is unaffected by loss of BH_4 and NO

(A-B) Basal glycolysis determined using 2-deoxyglucose inhibitable ECAR measured using XF^e96 Seahorse bioanalyzer in (A) $Gch^{fl/fl}$Tie2cre and (B) iNOS KO cells (n=5-6). (C) Basal glycolytic rate determined in $Gch^{fl/fl}$Tie2cre cells by calculating glycolytic proton efflux rate (glycoPER) (n=3). (D) The contribution of glycolysis to acidification of media in $Gch^{fl/fl}$Tie2cre cells (n=3). Data are mean ± SEM. *P* values calculated using 2-way ANOVA with Tukey's post-test (*P<0.05).

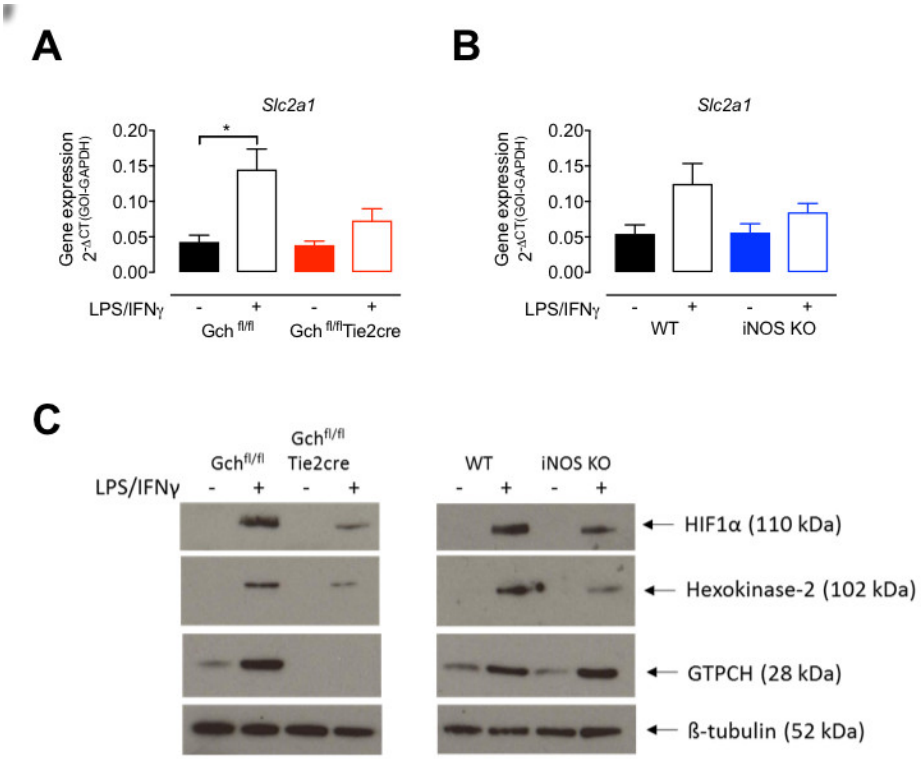


Figure 5.24 NO-signalling disrupts HIF1α mediated up-regulation of proteins

(A-B) qRT-PCR mRNA measurement of *Slc2a1* (gene encoding GLUT-1 protein) in (A) Gch$^{fl/fl}$Tie2cre and (B) iNOS KO cells (n=5). (C) Western blot analysis of HIF1α and hexokinase 2 proteins in Gch$^{fl/fl}$Tie2cre and iNOS KO cells (n=4). Antibodies against GTPCH protein were used to confirm its presence or absence. β-tubulin was used as a loading control. Data are mean ± SEM. *P* values calculated using 2-way ANOVA with Tukey's post-test (*P<0.05).

5.4.9 NO regulates levels of critical TCA cycle metabolites

Accumulation of TCA cycle metabolites citrate, succinate, fumarate, and itaconate are fundamental to metabolic reprogramming of inflammatory macrophages (Arts et al., 2016; Infantino et al., 2011; Mills et al., 2018; Tannahill et al., 2013). Using metabolomic analysis, these predicted elevations were observed in stimulated NO-producing ($Gch^{fl/fl}$ and WT) macrophages (Figure 5.25A and B). However, stimulated $Gch^{fl/fl}$Tie2cre cells had 1.6-fold more succinate (not detected in iNOS KO), and stimulated cells lacking NO ($Gch^{fl/fl}$Tie2cre and iNOS KO) even in the presence of BH_4 (iNOS KO) had dramatically less citrate, revealing an important effect of NO on citrate levels (Figure 5.25A-C). Itaconate was also elevated 2.5-fold more in $M^{LPS/IFN\gamma}$ NO-deficient cells (Figure 5.26A and B), and is synthesised from citrate through the intermediate cis-aconitate by the enzyme cis-aconitate decarboxylase encoded by *Irg1* (Michelucci et al., 2013). To investigate whether increased levels of cis-aconitate decarboxylase could underlie the elevated itaconate, the abundance of the enzyme and transcript were examined. There was no difference in protein levels in $M^{LPS/IFN\gamma}$ $Gch^{fl/fl}$ versus $Gch^{fl/fl}$Tie2cre cells by mass spectrometry (Figure 5.26C), despite finding increased induction of *Irg1* transcript in stimulated $Gch^{fl/fl}$Tie2cre and iNOS KO cells (Figure 5.26D and E).

Also of interest was the NO-dependent change in accumulation of citrate. Elevated citrate has previously been attributed to transcriptional repression of *Idh1* (Jha et al., 2015) and disruption of this 'break point' was therefore considered as a potential cause for the lower amount of citrate in the absence of NO. In accordance with previous reports (Jha et al., 2015; Tannahill et al., 2013), *Idh1* and *Idh2* gene expression were repressed in stimulated NO-synthesising cells and also observed in stimulated $Gch^{fl/fl}$Tie2cre and iNOS KO cells (Figure 25A - D). However, the proteomic data revealed that IDH 1 and IDH2 protein levels were unchanged by LPS/IFNγ stimulation (Figure 5.27E and F) – irrespective of BH_4 or NO

production – and this was confirmed by Western blotting for IDH1 (Figure 25G). IDH protein levels do not therefore explain changes in citrate in these models, nor underlie this 'break point'. In fact, no differences were found in the abundance of any TCA cycle enzymes in $M^{LPS/IFN\gamma}$ cells in the absence of BH_4 and NO (Figure 5.28), leading to the conclusion that changes in their activity must account for the observed impact on metabolite levels. Selected enzyme activities were therefore measured, which revealed significantly decreased IDH1 and 2 activity in stimulated $Gch^{fl/fl}$ but not $Gch^{fl/fl}$Tie2cre cells compared with unstimulated $Gch^{fl/fl}$ macrophages, and also a notable repression in unstimulated $Gch^{fl/fl}$Tie2cre cells (Figure 5.27H). Furthermore, proteomic data showed small but significantly decreased aconitase 1 protein (Figure 5.29A) (but not aconitase 2 Figure 5.28C) in $M^{LPS/IFN\gamma}$ cells, and dramatically decreased aconitase 1 and 2 activity was apparent in stimulated cells (Figure 5.29B), but these results were irrespective of BH_4 and NO production. This suggests that IDH but not aconitase activity is a key determinant of NO-dependent changes in TCA metabolites.

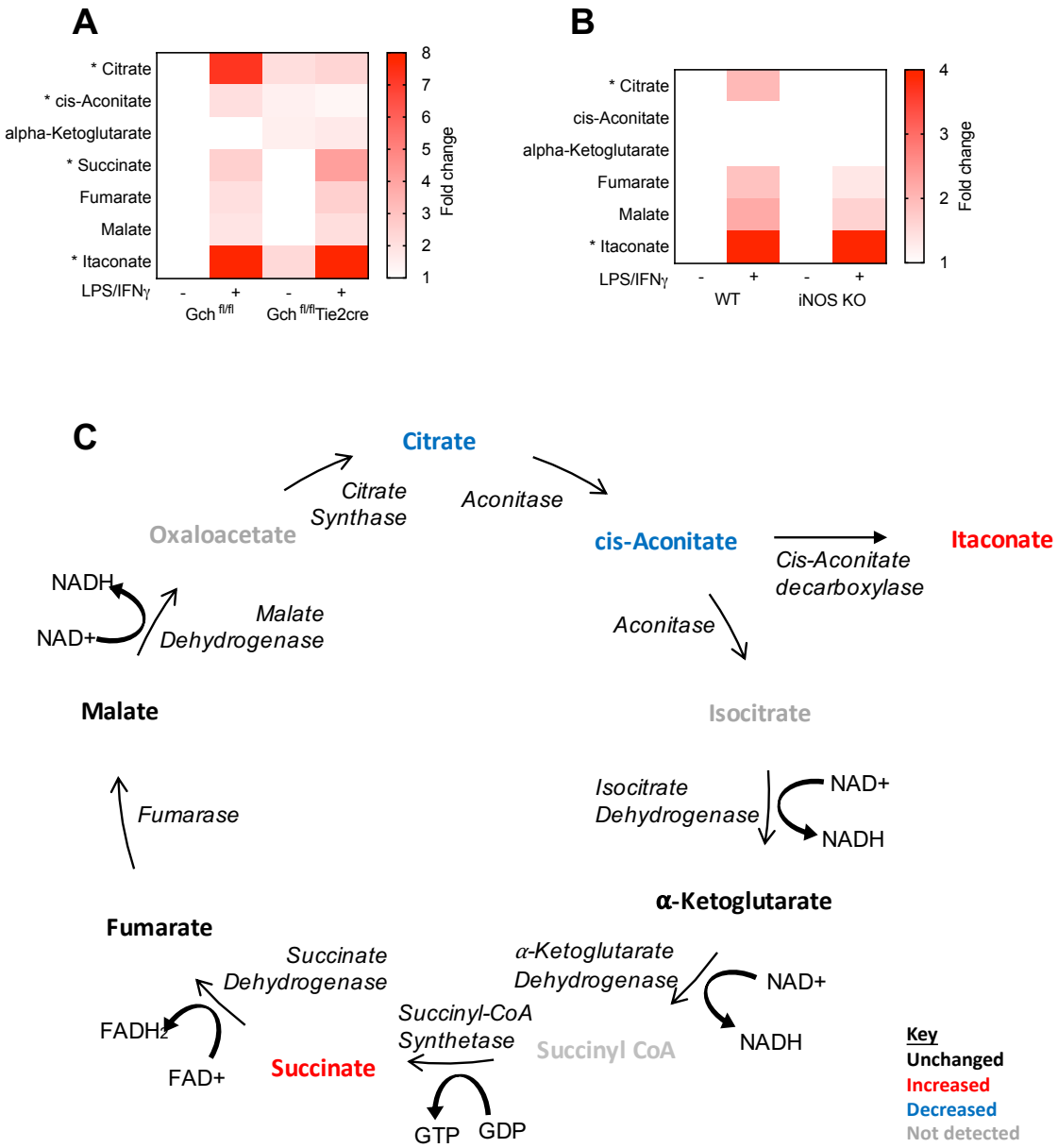


Figure 5.25 NO modulates levels of TCA cycle metabolites

(A) Fold change heat map of significantly changed (P<0.05) metabolites relative to $Gch^{fl/fl}$ (n=6, * significant difference (P<0.05) between $M^{LPS/IFN\gamma}$ $Gch^{fl/fl}$ versus $Gch^{fl/fl}$Tie2cre, Note: itaconate fold change>8). (B) Fold change heat map of significantly changed (P<0.05) metabolites relative to WT (n=6, * significant difference (P<0.05) between $M^{LPS/IFN\gamma}$ WT versus iNOS KO, Note: itaconate fold change >8). (C) TCA cycle pathway showing changes (>20%) in abundance of enzymes and metabolites in LPS/IFNγ stimulated $Gch^{fl/fl}$Tie2cre versus $Gch^{fl/fl}$ macrophages. Data are mean ± SEM. *P* values calculated using 2-way ANOVA with Tukey's post-test (*P<0.05).

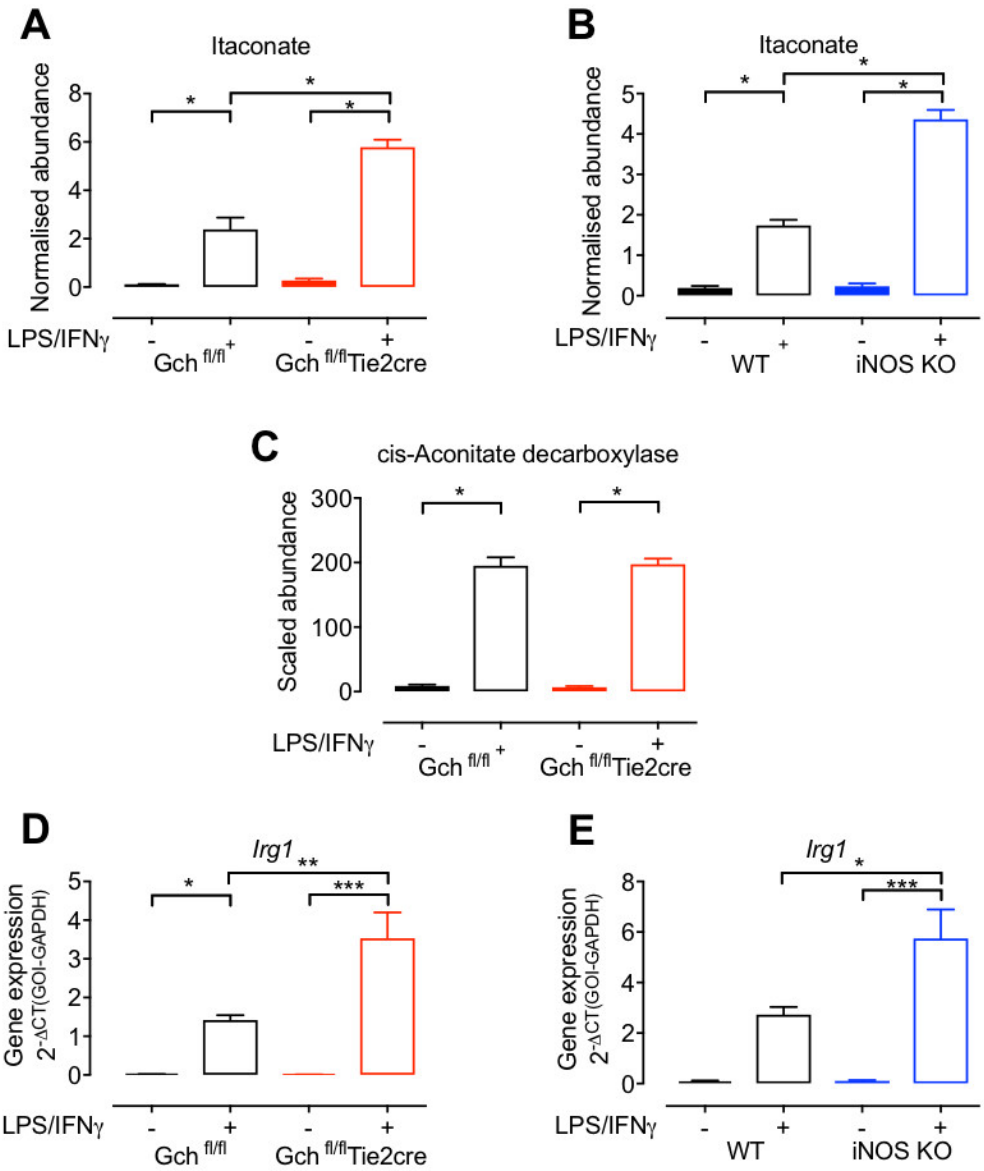


Figure 5.26 NO modulates itaconate production

(A-B) Itaconate metabolite abundance in (A) Gch$^{fl/fl}$Tie2cre and (B) iNOS KO cells (n=6). (C) Abundance of cis-aconitate decarboxylase protein in Gch$^{fl/fl}$Tie2cre cells (n=4). (D-E) *Irg1* gene expression in (D) Gch$^{fl/fl}$Tie2cre and (E) iNOS KO cells (n=5). Data are mean ± SEM. *P* values calculated using 2-way ANOVA with Tukey's post-test (* $P<0.05$, ** $P<0.01$, *** $P<0.001$).

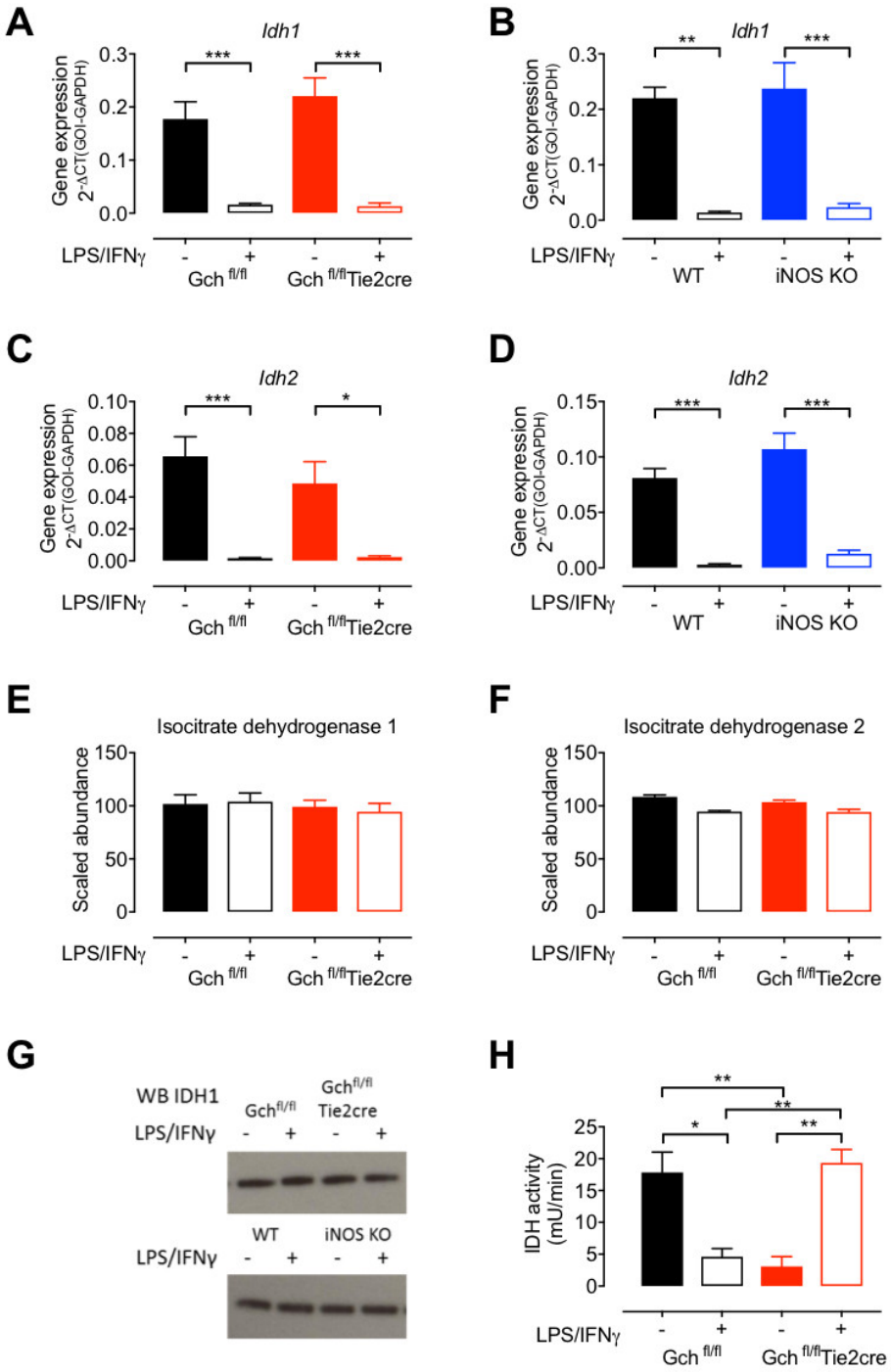


Figure 5.27 NO modulates IDH activity in macrophages stimulated with LPS/IFNγ

(A-B) *Idh1* gene expression in (A) Gch$^{fl/fl}$Tie2cre and (B) iNOS KO cells (n=5). (C-D) *Idh2* gene expression in (C) Gch$^{fl/fl}$Tie2cre and (D) iNOS KO cells (n=5). (E) IDH1 and (F) IDH2 protein abundance in Gch$^{fl/fl}$Tie2cre cells (n=4). (G) Western blot analysis of IDH1 protein in Gch$^{fl/fl}$Tie2cre and iNOS KO cells (n=3). (H) IDH1 and IDH2 combined activity in Gch$^{fl/fl}$Tie2cre cells (n=3). Data are mean ± SEM. *P* values calculated using 2-way ANOVA with Tukey's post-test (* $P<0.05$, ** $P<0.01$, *** $P<0.001$).

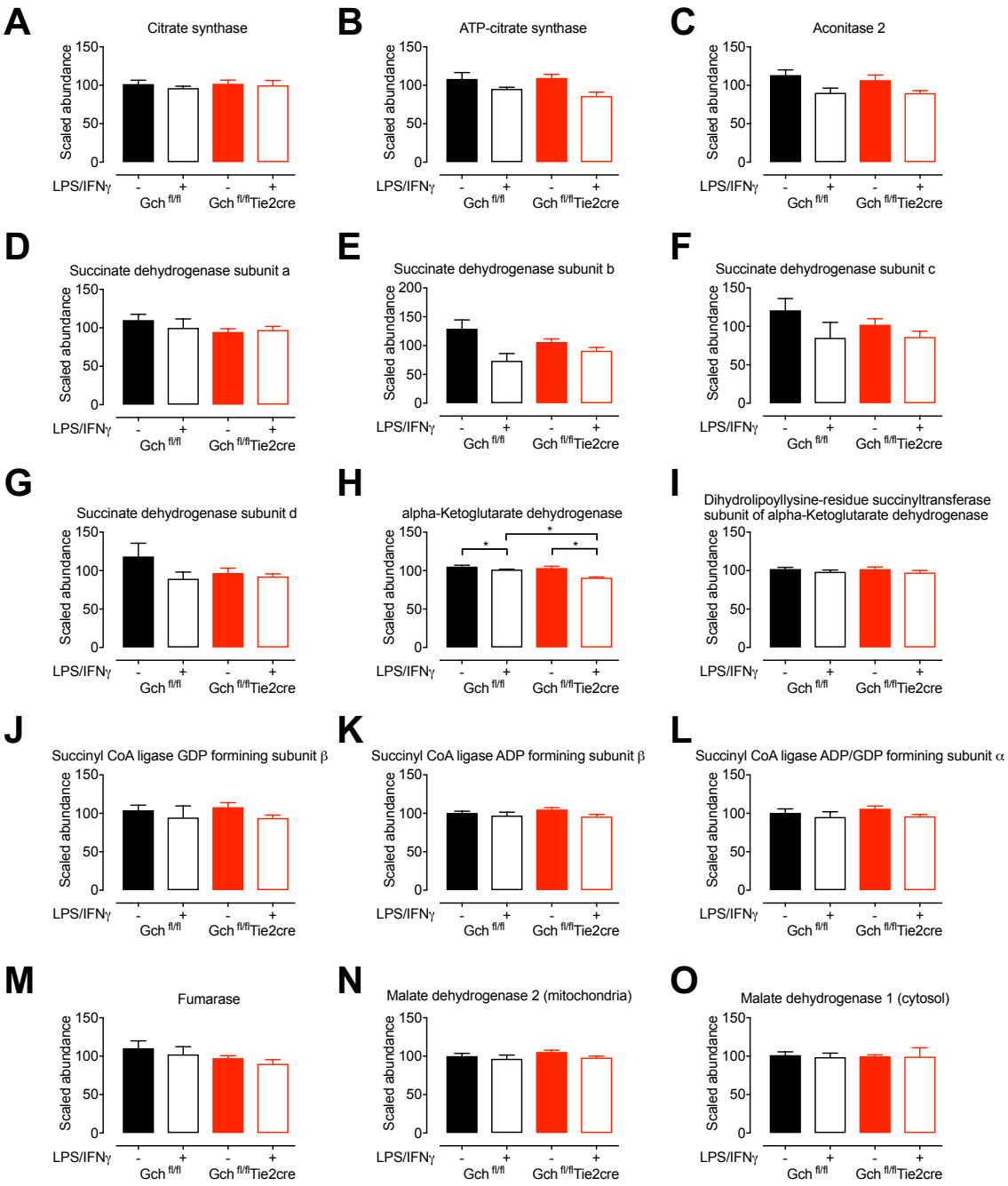


Figure 5.28 Abundance of TCA cycle enzymes in Gch$^{fl/fl}$Tie2cre macrophages

Abundance of TCA cycle enzymes measured using mass spectrometry. Data are n=4 ± SEM. *P* values calculated using 2-way ANOVA with Tukey's post-test (* $P<0.05$).

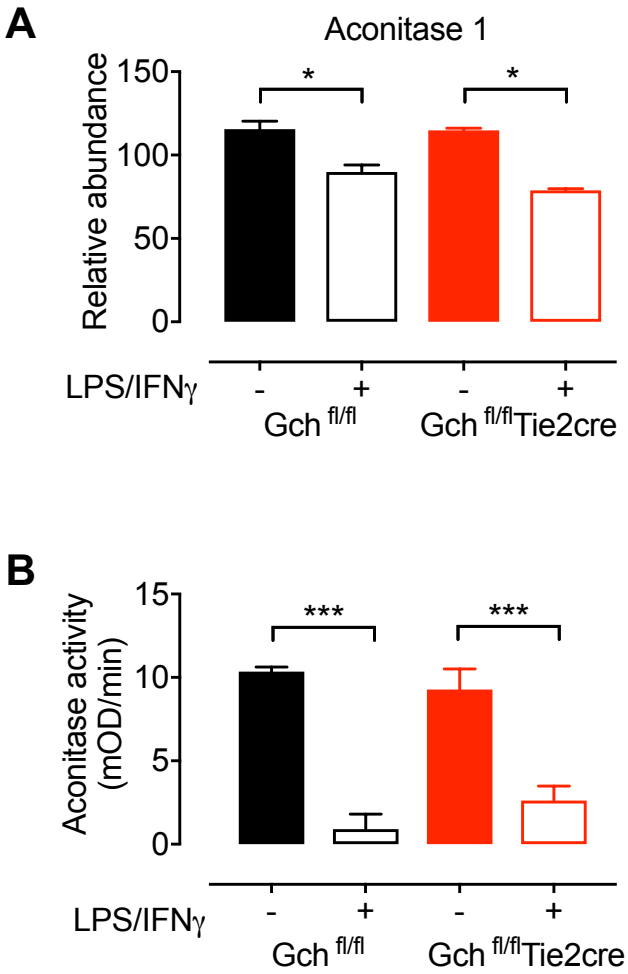


Figure 5.29 Aconitase activity is decreased in LPS/IFNγ stimulated macrophages

(A) Abundance of aconitase 1 measured in Gch$^{fl/fl}$Tie2cre cells using mass spectrometry (n=4). (B) Aconitase 1 and 2 activity assay in Gch$^{fl/fl}$Tie2cre cells (n=3-5). Data are mean ± SEM. *P* values calculated using 2-way ANOVA with Tukey's post-test (* $P<0.05$, *** $P<0.001$).

5.5 Discussion

5.5.1 Overview

It is well established that BH_4 is required for generation of NO by iNOS in macrophages responding to inflammatory stimuli and this is important for the destruction of pathogens, as part of the innate immune response. In addition, previous work from our lab indicated that BH_4 deficiency led to elevated ROS production by macrophages from a NOS-independent source. In the current study, experiments were carried out to identify the origin of the elevated ROS, however new methods of analysis suggested that both superoxide and hydrogen peroxide production were in fact decreased.

More recently, metabolic remodelling in macrophages has been recognised as a pivotal part of the pro-inflammatory switch, including the NO-mediated inhibition of mitochondrial oxidative phosphorylation. In the current study, proteomic and metabolomic analyses showed that BH_4 modulates specific metabolic changes in inflammatory macrophages through NO production and signalling. These include regulating respiratory function via changes in the abundance of critical N-module subunits in Complex I, HIF1α-mediated glycolytic remodelling, and changes in levels of the important TCA cycle metabolites (and inflammatory mediators) citrate, succinate, and itaconate. Taken together, these results demonstrated that inducible NO has a fundamental role in metabolic remodelling upon activation of macrophages.

5.5.2 BH_4-deficient macrophages produce less ROS?

It was originally hypothesised that BH_4-deficient macrophages produce elevated levels of ROS from the mitochondria. This was based on the previous report of increased ROS from a source other than NOS in these cells (McNeill et al., 2015), and the finding in Chapter 3 of this thesis showing that BH_4-deficient endothelial cells produced mitochondrial

superoxide. The previous report indicating elevated ROS in macrophages lacking BH_4 used HPLC to quantify peak areas of the oxidation products of DHE. In this report, using this method of analysis similarly increased peak areas of 2-hydroxyethidium and ethidium were observed, however the additional quantification of DHE revealed variations in cellular uptake. In particular, lower DHE levels were measured in stimulated BH_4-synthesising macrophages but not deficient cells, which may have influenced absolute amounts of the oxidation products. To account for these variations the proportions of DHE oxidised to 2-hyrdoxyethidium and ethidium were determined and suggested a very different interpretation of the data. Whereas the peak area of 2-hydroxyethidium was unchanged upon LPS/IFNγ stimulation in BH_4-synthesising cells, the ratio of 2-hydroxyethidium:DHE was increased (including iNOS KO cells), suggesting that superoxide production was elevated and oxidised a greater proportion of DHE. This is consistent with literature showing that inflammatory macrophages produce more ROS (Babior et al., 1973; Sanlioglu et al., 2001). Conversely, the ratio indicates no stimulation of superoxide production in activated BH_4-deficient cells. Furthermore, H_2O_2 was detected in media from stimulated BH_4-replete ($Gch^{fl/fl}$ and WT) but not BH_4-deficient cells, thus also providing evidence that ROS production was decreased. However, while the ratio of 2-hydroxyethidium:DHE indicated induced superoxide production in iNOS KO cells, H_2O_2 was undetectable in media. This suggests that the change in H_2O_2 secretion was NO-dependent and the change in intracellular superoxide production was BH_4 dependent. Superoxide is rapidly dismutated to H_2O_2 but intracellular superoxide and H_2O_2 may also react with various other molecules within the cell rather than diffusing extracellularly, which may in part explain this discordance. In addition, ethidium was measured, and the proportion of DHE converted into ethidium was elevated in stimulated NO-deficient cells suggesting that this occurs due to lack of NO signalling. Ethidium formation is proposed to involve various processes including reactive molecules, oxidases and cytochromes (Zhao et al., 2005; Zielonka and Kalyanaraman, 2010)

but these are not well verified, so conclusions as to the cause would require further investigation.

Overall, these findings do not provide evidence of increased ROS production from stimulated BH_4-deficient macrophages and instead suggest that superoxide and H_2O_2 production were decreased. It would be prudent to carry out further experiments using alternative approaches quantifying intracellular ROS to verify this result, such as electron paramagnetic resonance spin trapping (Finkelstein et al., 1980) and recently developed probes (Kaur et al., 2016; Robinson et al., 2006). Recent literature highlights elevated mitochondrial superoxide production by inflammatory macrophages (Mills et al., 2016; West et al., 2011), so it would be interesting to investigate whether this is decreased. Probes targeted to specific loci such as mitochondria, and measurements of antioxidant systems would not only be important to understand the redox environment but also the discordant superoxide and H_2O_2 measurements in iNOS KO cells.

5.5.3 NO regulates oxidative phosphorylation and the abundance of Complex I subunits

Metabolic changes are intricately linked with the switch to a pro-inflammatory phenotype in macrophages, including the critical 'Warburg'-like shift from oxidative metabolism to glycolytic ATP generation. NO is known to modulate ETC activity through nitrosation of Complex I and competitive inhibition of O_2-consuming Complex IV (Cleeter et al., 1994; Clementi et al., 1998) and is responsible for inhibiting oxidative phosphorylation in both activated macrophages and dendritic cells (Everts et al., 2012; Van den Bossche et al., 2016). In accordance with these studies, NO-dependent inhibition of mitochondrial respiration was observed in stimulated macrophages, with basal and ATP-linked respiration largely maintained in NO-deficient cells in contrast to inhibition in NO-synthesising cells. Inhibition of the ETC by NO was recently shown to limit macrophage plasticity, rendering inflammatory macrophages unable to remodel to an anti-inflammatory phenotype due to

irreversible repression of oxidation phosphorylation (Van den Bossche et al., 2016). Loss of NO signalling and maintaining mitochondrial respiration produced macrophages capable of remodelling (Van den Bossche et al., 2016), and the BH_4- and NO-deficient macrophages used in this study are likely to be similarly plastic.

The fact that respiration was marginally inhibited and uncoupled respiration (although elevated) remained below basal levels in NO-deficient cells, suggested that other mechanisms regulate changes in ETC activity in stimulated macrophages and this would be interesting to explore further. Several factors have been shown to affect the respiratory capacity of cells, including uncoupling proteins, ROS and variations in substrates (Dranka et al., 2010; Pfleger et al., 2015). ROS has been shown to decrease mitochondrial spare respiratory capacity in endothelial cells (Dranka et al., 2010); however, the evidence presented in this chapter indicates decreased superoxide generation from BH_4-deficient macrophages. A study has shown that different cell types require different substrates to achieve maximum respiratory capacity (Pfleger et al., 2015) and fatty acid oxidation is known to be crucial for spare respiratory capacity in memory T cells (van der Windt et al., 2012), so identifying the substrates fuelling mitochondrial respiration may be of interest. Uncoupling protein-2 is found in macrophages and has been linked with modulating immunity and is rapidly decreased in LPS stimulated macrophages (Arsenijevic et al., 2000; Emre et al., 2007). Uncoupling proteins were not measured in this study, but may be of interest as they are also linked with proton-leak which was elevated in stimulated NO-deficient cells.

Non-mitochondrial respiration was elevated in stimulated NO-synthesising cells, but not NO-deficient cells. Several enzymes consume oxygen, which could be contributing to non-mitochondrial OCR, such as lipoxygenases and NOX, and it is possible that decreased ROS generation is one reason for decreased non-mitochondrial OCR in BH_4- and NO-deficient

cells. On the other hand, as iNOS consumes oxygen to generate NO, changes in iNOS activity determine non-mitochondrial OCR and may explain these results, and iNOS was previously shown to be responsible for non-mitochondrial OCR in stimulated dendritic cells (Everts et al., 2012).

In addition, the data presented expands the repertoire of NO-dependent mechanisms governing the ETC to include regulating the abundance of proteins making up the NADH-binding catalytic module (N-module) of Complex I. It is therefore possible that, upon stimulation, loss of essential N-module subunits renders Complex I incapable of binding and accepting electrons from NADH – thereby providing an additional mechanism to modulate the metabolic switch away from oxidative metabolism in activated macrophages. To support this, Complex I activity was found to be reduced upon stimulation of NO-synthesising cells, as well as a reduction in detectable supercomplexes, which are known to form with Complexes III and IV and are thought to be important for electron transfer (Davies et al., 2018; Schagger and Pfeiffer, 2000). It is possible that NO transcriptionally regulates N-module subunit abundance as levels of *Ndufv2* transcript were significantly decreased in stimulated NO-synthesising macrophages. Lack of repression in iNOS KO cells would support this hypothesis, however significantly less *Ndufv2* was recorded in stimulated *Gch1* deficient cells, indicating that additional mechanisms are involved and perhaps the time course for transcriptional repression varies between genotypes.

5.5.4 NO regulates glycolytic remodelling

Inhibition of mitochondrial respiration is not essential for macrophages to maintain their inflammatory polarisation (Van den Bossche et al., 2016), in contrast with glycolysis which is up-regulated and required for inflammatory cell survival and cytokine production (Krawczyk et al., 2010; Tannahill et al., 2013). Up-regulation of glycolysis, following

LPS/IFNγ stimulation, is orchestrated by HIF1α transcriptionally regulating the production of several proteins involved in glucose metabolism (Liu et al., 2016; Wang et al., 2017). In NO-deficient activated macrophages, this study found the expected elevation of glycolytic rates despite inefficient induction of HIF1α and several of its transcriptionally regulated protein targets (GLUT-1, hexokinase-1 and -2, PFKFB3). NO is known to increase HIF1α activity through nitrosation and stabilisation under non-hypoxic conditions (Kasuno et al., 2004; Sandau et al., 2001; Sumbayev et al., 2003), therefore perhaps explaining why loss of NO signalling resulted in less HIF1α. LPS induced succinate accumulation is also known to promote stabilisation of HIF1α (Selak et al., 2005; Tannahill et al., 2013), which may account for the small amount of HIF1α protein that was observed. Moreoever, enhanced succinate levels in the metabolomic data might indicate that both succinate and NO are required for optimal HIF1α stabilisation. Overall, disruption of HIF1α mediated glycolytic remodelling led to lower levels of fructose-1,6-bisphate and lactate and highlighted the importance of NO signalling in regulating glycolysis in activated macrophages. Interestingly, and in accordance with our results, NO has previously been reported to increase glycolysis through fructose-1,6-bisphosphate production and elevated PFK2 activity in astrocytes following inhibition of respiration by NO (Almeida et al., 2004). This suggests that the mechanisms observed in macrophages could have a wider relevance to other NO-producing cell types.

It is important to consider alternate mechanisms up-regulating glycolysis in NO-deficient stimulated cells. Although disrupted HIF1α mediated protein changes appear to have inhibited the earlier part of glucose oxidation causing decreased fructose-1,6-bisphosphate, increased abundance of triose phosphate isomerase, phosphoglycerate kinase and 3-phosphoglycerate may indicate compensatory increased metabolism further along the pathway. In support of this, it is possible for metabolites from the pentose phosphate

pathway and glycerol catabolism to feed in through dihydroxyacetone phosphate and glycerol-3-phosphate, and there are indications of increased glycerol metabolism through increased abundance of catabolic enzymes and decreased levels of glycerol-3-phosphate. Overall, it is clear that whilst NO is critical for the HIF1α mediated upregulation of glycolysis, macrophages are capable of inducing glycolysis by other mechanisms in its absence and this warrants further investigation.

5.5.5 NO regulates levels of TCA cycle metabolites

Accumulation of specific TCA cycle metabolites in activated macrophages has led to the discovery of their functions in modulating inflammation (Arts et al., 2016; Infantino et al., 2011; Tannahill et al., 2013). Carbon flux analyses have identified two 'breaks' in the cycle, at IDH and SDH (Jha et al., 2015), leading to elevations in citrate and succinate respectively, and this was reproduced in activated NO-synthesising cells in this report. A study identifying transcriptional repression of *Idh1* has suggested this as the reason for redirection of citrate into lipid and itaconate synthesis rather than isocitrate metabolism (Jha et al., 2015). Here marked decreases in transcription of *Idh1* as well as *Idh2* were also measured, but analysis revealed no subsequent changes in IDH protein levels, and showed that decreased IDH and aconitase enzyme activity were dramatically decreased and therefore more likely to be responsible for accumulation of citrate. Furthermore, results in this chapter showed that citrate levels were modulated by NO, as citrate was no longer elevated in macrophages incapable of producing NO. Although aconitase activity was decreased, IDH activity was maintained in NO-deficient $M^{LPS/IFN\gamma}$ cells and provides a possible avenue utilising citrate in addition to increased itaconate production. This potentially explains lack of citrate accumulation, and is plausible as NO was previously shown to inhibit IDH activity through nitrosation (Lee et al., 2003; Yang et al., 2002).

Itaconate is one of the most highly induced metabolites following activation of BMDMs (Lampropoulou et al., 2016; Mills et al., 2018) and 2.5-fold greater levels were observed in NO-deficient $M^{LPS/IFN\gamma}$ cells compared to NO-replete cells. This suggests that NO can modulate inflammatory signalling by regulating itaconate levels, as itaconate is proven to be bactericidal, but also an anti-inflammatory mediator (Bambouskova et al., 2018; Mills et al., 2018). Unchanged levels of the synthetic enzyme cis-aconitate decarboxylase indicated that increased itaconate resulted from changes in enzyme activity and it is possible that the elevated protein response to IFNβ highlighted by our proteomic data is directing this in NO-deficient cells, as Type I IFNs were shown to stimulate itaconate production in several studies (Mills et al., 2018; Naujoks et al., 2016; Tallam et al., 2016). Itaconate may also account for elevated succinate levels in BH_4 and NO-deficient cells, as it is a proven inhibitor of SDH and leads to accumulation of succinate in stimulated macrophages (Cordes et al., 2016; Lampropoulou et al., 2016). This is another mechanism by which itaconate directs inflammatory signalling as succinate modulates HIF1α mediated IL-1β production and drives mitochondrial ROS generation (Mills et al., 2016; Tannahill et al., 2013).

5.5.6 NO limits production of IL-1β

The key pro-inflammatory mediators TNFα, IL-6 and IL-1β were all induced in activated NO-deficient as well as NO-synthesising cells; however, IL-1β secretion was elevated alongside the abundance of proteins making up the inflammasome complex (NLRP3, AIM2 and caspase-1). The inflammasome cleaves pro-IL-1β into its mature secreted form and NO is known to inhibit this complex through nitrosation (Hernandez-Cuellar et al., 2012; Mao et al., 2013; Mishra et al., 2013); thus, loss of NO signalling and decreased nitrosation of the inflammasome is likely to contribute to up-regulated IL-1β secretion. In addition, the observed increased abundance of inflammasome proteins and transcription of *Il1b* must occur through NO-dependent unidentified mechanisms. HIF1α transcriptionally regulates

Il1b in stimulated macrophages (Tannahill et al., 2013); however, as discussed, this is decreased in BH_4- and NO-deficient models and so does not explain this finding. More recently NRF2 signalling was shown to repress IL-1β production in macrophages (Mills et al., 2018) and our lab has demonstrated disrupted NRF2 signalling in stimulated macrophages devoid of NO due to BH_4 deficiency (Douglas et al., 2018; McNeill et al., 2015), so NO-dependent changes in this pathway potentially determine increased *Il1b* transcription.

5.5.7 NOS-independent role for BH_4 in macrophages

This chapter aimed to investigate roles of BH_4 in regulating ROS production, mitochondrial function and metabolism in inflammatory macrophages; it was also hypothesised that changes would occur independent from its NOS cofactor function.

The hypothesis that BH_4 deficiency would lead to elevated mitochondrial ROS in stimulated macrophages was rejected and evidence instead indicated that superoxide and H_2O_2 production were decreased. The change in H_2O_2 secretion was also observed in iNOS KO cells with replete BH_4 levels, indicating that this change was due to loss of functional NOS. However superoxide measurements were contrastingly increased in iNOS KO cells and so NOS-independent.

The proteomic data analysis highlighted BH_4-dependent regulation of proteins involved in mitochondrial function and metabolism in inflammatory macrophages. These were followed up with metabolomic analysis and biochemical assays in *Gch1* and iNOS KO cells to explore the functional consequences and confirm whether observed changes were due to loss of NO-signalling. As discussed, NO was shown to modulate IL-1β production, mitochondrial aerobic respiration, Complex I subunit abundance, HIF1α-mediated glycolytic remodelling and levels of TCA cycle metabolites. Thus, all of the areas investigated were regulated

through the NOS cofactor function of BH_4. Several other enriched GO terms were not followed up – such as the response to IFNβ and changes in proteins making up the mitochondrial ribosome – as well as individual proteins not highlighted by enrichment analysis, and so it is still not known whether NO signalling directs these.

Inflammatory macrophages, which are implicated in various pathologies, were the focus of this study; however, changes in protein and metabolite abundance in unstimulated BH_4-replete and -deficient cells were reported, therefore indicating a NOS-independent role for BH_4 (as these cell lacked iNOS). This includes proteins such as arsenite methyltransferase, squalene synthase, and those involved in protein folding and regulation of macrophage activation.

Overall, the data presented in this chapter provides many avenues that remain to be followed up and which have been alluded to throughout this discussion. These will be discussed in further detail in Chapter 6.

Chapter 6:
Final discussion

Chapter 6: Final Discussion

6.1 Original hypotheses and aims

It is well known that BH_4 is required for the production of NO by the NOS enzymes, and deficiency - due to oxidation or decreased synthesis - leads to increased superoxide production from uncoupled NOS. BH_4 is thus sensitive to changes in the redox environment and is also a key determinant of cellular NO-redox balance through modulation of NOS activity. Previous evidence from our laboratory indicated that in addition, BH_4 modulates redox signalling independent from NOS due the presence of elevated ROS in both BH_4-deficient endothelial cells and macrophages from an alternate but unidentified source. This thesis aimed to explore novel pathways modulated by BH_4 including identifying this ROS source. Previous literature provided evidence of BH_4 inside mitochondria, and BH_4 was shown to act as a mitochondrial superoxide scavenger in fibroblasts and to decrease respiratory function at high levels in cardiomyocytes, in both cases acting via NO-independent mechanisms. It was therefore hypothesised that BH_4 has roles in regulating mitochondrial redox signalling and function in endothelial cells and macrophages, and that this can occur independent from – as well as through – its NOS cofactor function.

6.2 Key findings and future directions

This thesis has described the role of BH_4 in the regulation of mitochondrial function and metabolism via NOS-dependent and -independent signalling, in both endothelial cells and macrophages. The key findings are described below:

1. BH_4 regulates mitochondrial redox signalling. Mitochondria were the major source of elevated superoxide produced by endothelial cells and fibroblasts following BH_4 depletion. This was independent from its NOS cofactor function.

2. BH_4 regulates mitochondrial morphology and TCA cycle metabolism in endothelial cells. Increased inhibitory phosphorylation of fission regulatory protein, DRP1, at serine 616 led to larger mitochondria in BH_4-deficient endothelial cells. In addition, there were increased succinate and decreased isocitrate levels in BH_4-deficient endothelial cells, as well as elevated fructose-1,6-bisphosphate.
3. BH_4 modulates metabolic remodelling of macrophages responding to inflammatory stimuli (LPS/IFNγ) via NO signalling.
    a. Proteomic analysis revealed a co-ordinated decrease in catalytic N-module Complex I subunits in inflammatory macrophages capable of producing BH_4 and NO. In BH_4-deficient macrophages this decrease was attenuated and similarly observed in the case of NDUFV2 in iNOS KO cells. This presents a plausible mechanism by which NO signalling modulates inhibition of Complex I activity and mitochondrial respiration in inflammatory macrophages.
    b. BH_4 modulates HIF1α mediated glycolytic remodelling through NO signalling. Levels of HIF1α and proteins encoded by HIF1α regulated genes were substantially increased in NO replete stimulated macrophages, but less so in BH_4-deficient and iNOS KO cells. Despite this, glycolysis was up-regulated in inflammatory macrophages regardless of NO production, indicating compensatory or alternative remodelling mechanisms in the absence of NO.
    c. BH_4 modulates the TCA cycle through NO signalling. Characteristic citrate, succinate and itaconate accumulation were observed in BH_4 and NO synthesising inflammatory macrophages using metabolomic analysis. In stimulated BH_4-deficient and iNOS KO cells citrate levels were significantly lower but itaconate levels were significantly increased. Succinate levels were

also elevated in BH_4-deficient cells. Interestingly, proteomic analysis indicated no changes in the abundance of TCA cycle enzymes or cis-aconitate decarboxylase, suggesting that NO-dependent regulation of enzyme activity was responsible.

Cells differentiate to carry out specific functions which may vary dramatically. Endothelial cells and macrophages have specialised and unique functions, so it was perhaps unsurprising that as well as certain commonalities, the results presented in this thesis highlighted many differences in the way BH_4 regulated mitochondrial redox signalling and metabolism in these cell types. These aspects as well as future directions and hypotheses that stem from this work are discussed below.

6.2.1 Investigating the role of BH_4 in different cell types

Although previous data from our laboratory indicated that elevated ROS from a NOS-independent source was common to both BH_4-deficient endothelial cells and macrophages, incorporation of additional methods to analyse ROS in this report suggested a different interpretation. In endothelial cells depleted of BH_4 the predominant source of elevated superoxide was revealed to be mitochondrial, whereas evidence indicated that ROS production from BH_4-deficient macrophages was unchanged in unstimulated cells and decreased in stimulated cells. Increased endothelial ROS generation – including that of mitochondrial origin – is associated with endothelial dysfunction and vascular pathologies, whereas induction of mitochondrial superoxide generation upon stimulation of BMDMs is a recognised signalling modality involved in host defence. The mechanisms regulating ROS generation are therefore almost certainly going to differ. The fact that BH_4 was largely oxidised within endothelial mitochondria may indicate a direct and important role in regulating redox balance within this organelle, but it is possible that this is not the case in macrophages as this was not tested and ROS levels were contrastingly diminished in

deficient conditions. Overall, the exact mechanisms through which BH_4 regulates ROS production and mitochondrial redox signalling remain to be characterised, and while these data indicated that BH_4 levels are influential the mechanisms are likely to vary between cell types.

In many respects endothelial cells and inflammatory macrophages are incomparable, particularly when investigating metabolism. Although endothelial cells are known to be highly glycolytic they maintain mitochondrial respiration despite NO generation, whereas inflammatory macrophages undergo dramatic metabolic reprogramming that includes NO-mediated inhibition of oxidative phosphorylation. iNOS is known to produce particularly high levels of NO compared with eNOS and may explain this difference and why BH_4 deficiency and loss of NO signalling had a profound effect allowing maintenance of respiration in macrophages but no observable effect in endothelial cells. A striking similarity between BH_4-deficient endothelial cells and inflammatory macrophages was increased accumulation of succinate. Although perhaps circumstantial, this finding may indicate a common BH_4-dependent mechanism regulating succinate metabolism that would be interesting to investigate.

Many cell types synthesise BH_4, including neurons, cardiomyocytes and hepatocytes, and – similar to endothelial cells – studies have focussed on the role of BH_4 as an enzymatic cofactor for NOS and AAH in these cells. Considering the evidence of a non-cofactor role for BH_4 in endothelial cells in this study it may be interesting to similarly explore this possibility in these other cell types.

6.2.2 Future studies into the role of BH_4 in endothelial cells

This study highlighted that BH_4 depletion led to elevated mitochondrial superoxide production in an endothelial cell line. Primary *Gch1* KO endothelial cells, rather than a transformed line, could be used to confirm this finding in a model that is more reflective of

in vivo cells. These cells can be acquired from the $Gch^{fl/fl}$Tie2cre mouse described in this thesis and would allow assessment of the long term implications of endothelial BH_4 deficiency. Furthermore, these mice can be used to determine the viability of targeting excessive endothelial mitochondrial ROS *in vivo* with mitochondria-targeted antioxidants to improve endothelial function caused by endothelial BH_4 deficiency. However, *Gch1* is excised in myeloid cells as well as endothelial cells in $Gch^{fl/fl}$Tie2cre mice, so generation of an endothelial specific conditional KO expressing Cre-recombinase under control of a vascular endothelial-cadherin promotor would be more suitable for *in vivo* studies to distinguish cell-type specific effects.

6.2.3 Future studies into the role of BH_4 and NO in macrophages

In this study many changes in mitochondrial function and metabolic pathways were observed in inflammatory BH_4-deficient $Gch^{fl/fl}$Tie2cre macrophages compared with $Gch^{fl/fl}$ control cells. To distinguish whether these changes were due to loss of NO signalling or NOS-independent effects of BH_4, iNOS KO macrophages were used. Of the pathways and proteins interrogated, all changes were observable in both $Gch^{fl/fl}$Tie2cre and iNOS KO models, and the importance of NO signalling was inferred. However, addition of an NO donor to these conditions would allow this theory to become more conclusive, as it must be remembered that in addition to loss of NO signalling both models showed changes in levels of other molecules such as arginine and citrulline. The potential presence of uncoupled iNOS and its contribution to redox changes should also be considered in any differences observed between iNOS KO and $Gch^{fl/fl}$Tie2cre cells, and BMDMs lacking both *Gch1* and *Nos2* would eliminate this ambiguity – although evidence in this thesis would suggest uncoupled iNOS is improbable.

Metabolomic analyses showed that BH_4 modulates the accumulation of citrate and itaconate (and potentially succinate) through NO, but this only provided a snap-shot of the chosen

time point and lacked information regarding metabolic flux. The fact that proteomic data showed unchanged levels of metabolic enzymes between genotypes indicated modulation of their activity, and this was confirmed in the case of IDH. IDH activity was increased in NO-deficient inflammatory macrophages, and together with elevated itaconate production may account for decreased levels of citrate in these cells. Additional enzyme activity assays and analysis of metabolic flux using metabolomic analyses to track the fate of substrates labelled with heavy carbon or nitrogen isotopes would provide a much greater insight. This would include investigating how NO regulates the TCA cycle 'break points' in inflammatory macrophages and the contributions of metabolic networks such as glycolysis and anaplerosis feeding into the TCA cycle. Combining this with approaches designed to investigate mechanisms modulating metabolic enzyme activity would help to reveal how NO regulates metabolic remodelling in stimulated macrophages. PTM of proteins are a probable regulatory step, and nitrosation is already known to modulate a range of metabolic enzymes, thus mass spectrometric analysis of nitrosation is a good starting point. These investigations into metabolic flux and enzyme activity may also prove an insightful follow-up to understanding how glycolysis is up-regulated in inflammatory macrophages in the absence of NO when HIF1α mediated changes are disrupted.

This report showed that BH_4 modulated the abundance of catalytic subunits in the N-module of Complex I via NO signalling, and has led to the hypothesis that this is a mechanism regulating Complex I activity and respiratory function in macrophages responding to inflammatory stimuli. It remains unclear how NO co-ordinated this change, and while *Ndufv2* mRNA levels were decreased upon stimulation of NO-synthesising cells, this transcript was also significantly decreased in BH_4-deficient cells. Therefore while transcriptional regulation may be responsible a time course would be useful to see whether BH_4-deficient cells are responding at a different rate. A transcriptional regulator selectively modulating N-module subunits is so far unreported and is one possible NO-dependent

regulatory mechanism. However, it is also possible that N-module subunits are selectively degraded in the stimulated NO-synthesising macrophages and exploring whether this process is defective in NO-deficient cells would be of interest.

There were many changes observed between genotypes in the proteomic and metabolomic data sets that remain to be followed-up, including IFNβ signalling, antigen presentation, cholesterol, purine and sphingolipid metabolism. In particular, there were indicators of decreased mitochondrial gene expression and protein synthesis in BH_4-deficient inflammatory macrophages, that warrant further investigation. The proteomic analysis highlighted significantly decreased mitochondrial ribosomal proteins, FASTKD5 and pentatricopeptide repeat domain containing protein 3, which are involved in translation and post-transcriptionally processing of mitochondrial mRNA (Antonicka and Shoubridge, 2015; Davies et al., 2009). As well as investigating how NO may regulate levels of these proteins, it would be interesting to examine whether BH_4 and NO deficiency affect mitochondrial biogenesis and content in these cells.

It is important to consider the consequences of altered metabolic remodelling, ROS and NO generation in BH_4-deficient inflammatory macrophage function. It has become increasingly clear in the literature that metabolic changes are linked with inflammatory signalling, and this thesis reports surprising changes in levels of metabolites – citrate, succinate and itaconate – that are key mediators. In this study, the effect of these changes on the ability of macrophages to fight infection was not explored and will form an important part of future studies both *in vitro* and *in vivo*. Furthermore, replicating these metabolic analyses in isolated inflammatory (such as zymosan-stimulated) peritoneal macrophages would be an interesting extension to these studies to assess the reproducibility of these results *in vivo*. Rather than using the $Gch^{fl/fl}$Tie2cre model – which also has endothelial BH_4 deficiency –

the *in vivo* effects of BH_4 deficient myeloid cells in infection could be more effectively studied with generation of a myeloid specific conditional KO such as LysMcre.

The use of BH_4- and NO-deficient murine BMDMs to investigate novel pathways regulated by these molecules in the switch to an inflammatory phenotype has provided novel insights into NO-dependent modulation of metabolic remodelling. However, as with all *in vitro* and murine systems it is necessary to consider the translational impact in human cells. This is particularly intriguing in this case, as synthesis of both NO and BH_4 are reportedly much lower and induced by different signals in human versus murine macrophages (Schroder et al., 2012; Weinberg et al., 1995). Future work, should therefore include investigating the roles of BH_4 and NO in human monocyte/macrophage metabolism using isolated human cells.

References

References

Abu-Soud, H.M., and Stuehr, D.J. (1993). Nitric oxide synthases reveal a role for calmodulin in controlling electron transfer. Proc. Natl. Acad. Sci. U. S. A. *90*, 10769–10772.

Abu-Soud, H.M., Gachhui, R., Raushel, F.M., and Stuehr, D.J. (1997). The ferrous-dioxy complex of neuronal nitric oxide synthase. Divergent effects of L-arginine and tetrahydrobiopterin on its stability. J. Biol. Chem. *272*, 17349–17353.

Aksenov, M.Y., and Markesbery, W.R. (2001). Changes in thiol content and expression of glutathione redox system genes in the hippocampus and cerebellum in Alzheimer's disease. Neurosci. Lett. *302*, 141–145.

Al-Mehdi, A.-B., Pastukh, V.M., Swiger, B.M., Reed, D.J., Patel, M.R., Bardwell, G.C., Pastukh, V. V., Alexeyev, M.F., and Gillespie, M.N. (2012). Perinuclear Mitochondrial Clustering Creates an Oxidant-Rich Nuclear Domain Required for Hypoxia-Induced Transcription. Sci. Signal. *5*, ra47-ra47.

Almeida, A., Moncada, S., and Bolaños, J.P. (2004). Nitric oxide switches on glycolysis through the AMP protein kinase and 6-phosphofructo-2-kinase pathway. Nat. Cell Biol. *6*, 45–51.

Alp, N.J., Mussa, S., Khoo, J., Cai, S., Guzik, T., Jefferson, A., Goh, N., Rockett, K.A., and Channon, K.M. (2003). Tetrahydrobiopterin-dependent preservation of nitric oxide-mediated endothelial function in diabetes by targeted transgenic GTP-cyclohydrolase I overexpression. J. Clin. Invest. *112*, 725–735.

Alp, N.J., McAteer, M.A., Khoo, J., Choudhury, R.P., and Channon, K.M. (2004). Increased endothelial tetrahydrobiopterin synthesis by targeted transgenic GTP-cyclohydrolase I overexpression reduces endothelial dysfunction and atherosclerosis in ApoE-knockout mice. Arterioscler. Thromb. Vasc. Biol. *24*, 445–450.

Antoniades, C., Shirodaria, C., Crabtree, M., Rinze, R., Alp, N., Cunnington, C., Diesch, J., Tousoulis, D., Stefanadis, C., Leeson, P., et al. (2007). Altered plasma versus vascular biopterins in human atherosclerosis reveal relationships between endothelial nitric oxide synthase coupling, endothelial function, and inflammation. Circulation *116*, 2851–2859.

Antonicka, H., and Shoubridge, E.A. (2015). Mitochondrial RNA Granules Are Centers for Posttranscriptional RNA Processing and Ribosome Biogenesis. Cell Rep. *10*, 920–932.

Anzinger, J.J., Chang, J., Xu, Q., Barthwal, M.K., Bohnacker, T., Wymann, M.P., and Kruth, H.S. (2012). Murine bone marrow-derived macrophages differentiated with GM-CSF become foam cells by PI3Kγ-dependent fluid-phase pinocytosis of native LDL. J. Lipid Res. *53*, 34–42.

Arsenijevic, D., Onuma, H., Pecqueur, C., Raimbault, S., Manning, B.S., Miroux, B., Couplan, E., Alves-Guerra, M.-C., Goubern, M., Surwit, R., et al. (2000). Disruption of the uncoupling protein-2 gene in mice reveals a role in immunity and reactive oxygen species production. Nat. Genet. *26*, 435–439.

Arts, R.J.W., Novakovic, B., ter Horst, R., Carvalho, A., Bekkering, S., Lachmandas, E., Rodrigues, F., Silvestre, R., Cheng, S.-C., Wang, S.-Y., et al. (2016). Glutaminolysis and Fumarate Accumulation Integrate Immunometabolic and Epigenetic Programs in Trained Immunity. Cell Metab. *24*, 807–819.

Ashor, A.W., Siervo, M., Lara, J., Oggioni, C., Afshar, S., and Mathers, J.C. (2015). Effect

of vitamin C and vitamin E supplementation on endothelial function: a systematic review and meta-analysis of randomised controlled trials. Br. J. Nutr. *113*, 1182–1194.

Babior, B.M., Kipnes, R.S., and Curnutte, J.T. (1973). Biological defense mechanisms. The production by leukocytes of superoxide, a potential bactericidal agent. J. Clin. Invest. *52*, 741–744.

Baek, K.J., Thiel, B.A., Lucas, S., and Stuehr, D.J. (1993). Macrophage nitric oxide synthase subunits. Purification, characterization, and role of prosthetic groups and substrate in regulating their association into a dimeric enzyme. J. Biol. Chem. *268*, 21120–21129.

Bahra, M., Kapil, V., Pearl, V., Ghosh, S., and Ahluwalia, A. (2012). Inorganic nitrate ingestion improves vascular compliance but does not alter flow-mediated dilatation in healthy volunteers. Nitric Oxide *26*, 197–202.

Balligand, J.L., Ungureanu-Longrois, D., Simmons, W.W., Pimental, D., Malinski, T.A., Kapturczak, M., Taha, Z., Lowenstein, C.J., Davidoff, A.J., and Kelly, R.A. (1994). Cytokine-inducible nitric oxide synthase (iNOS) expression in cardiac myocytes. Characterization and regulation of iNOS expression and detection of iNOS activity in single cardiac myocytes in vitro. J. Biol. Chem. *269*, 27580–27588.

Balligand, J.L., Kobzik, L., Han, X., Kaye, D.M., Belhassen, L., O'Hara, D.S., Kelly, R.A., Smith, T.W., and Michel, T. (1995). Nitric oxide-dependent parasympathetic signaling is due to activation of constitutive endothelial (type III) nitric oxide synthase in cardiac myocytes. J. Biol. Chem. *270*, 14582–14586.

Bambouskova, M., Gorvel, L., Lampropoulou, V., Sergushichev, A., Loginicheva, E., Johnson, K., Korenfeld, D., Mathyer, M.E., Kim, H., Huang, L.H., et al. (2018). Electrophilic properties of itaconate and derivatives regulate the IκBζ-ATF3 inflammatory axis. Nature *556*, 501–504.

Barth, E., Stämmler, G., Speiser, B., and Schaper, J. (1992). Ultrastructural quantitation of mitochondria and myofilaments in cardiac muscle from 10 different animal species including man. J. Mol. Cell. Cardiol. *24*, 669–681.

Bates, T.E., Loesch, A., Burnstock, G., and Clark, J.B. (1995). Immunocytochemical evidence for a mitochondrially located nitric oxide synthase in brain and liver. Biochem. Biophys. Res. Commun. *213*, 896–900.

Bates, T.E., Loesch, A., Burnstock, G., and Clark, J.B. (1996). Mitochondrial nitric oxide synthase: a ubiquitous regulator of oxidative phosphorylation? Biochem. Biophys. Res. Commun. *218*, 40–44.

Benjamin, N., O'Driscoll, F., Dougall, H., Duncan, C., Smith, L., Golden, M., and McKenzie, H. (1994). Stomach NO synthesis. Nature *368*, 502–502.

Berka, V., Yeh, H.C., Gao, D., Kiran, F., and Tsai, A.L. (2004). Redox function of tetrahydrobiopterin and effect of L-arginine on oxygen binding in endothelial nitric oxide synthase. Biochemistry *43*, 13137–13148.

Bindea, G., Mlecnik, B., Hackl, H., Charoentong, P., Tosolini, M., Kirilovsky, A., Fridman, W.-H., Pagès, F., Trajanoski, Z., and Galon, J. (2009). ClueGO: a Cytoscape plug-in to decipher functionally grouped gene ontology and pathway annotation networks. Bioinformatics *25*, 1091–1093.

Biteau, B., Labarre, J., and Toledano, M.B. (2003). ATP-dependent reduction of cysteine–sulphinic acid by S. cerevisiae sulphiredoxin. Nature *425*, 980–984.

Blouin, A., Bolender, R.P., and Weibel, E.R. (1977). Distribution of organelles and membranes between hepatocytes and nonhepatocytes in the rat liver parenchyma. A stereological study. J. Cell Biol. *72*, 441–455.

Bogdan, C. (2002). Response to "Species differences in macrophage NO production are important." Nat. Immunol. *3*, 102–102.

de Bono, J.P., Warrick, N., Bendall, J.K., Channon, K.M., and Alp, N.J. (2007). Radiochemical HPLC detection of arginine metabolism: Measurement of nitric oxide synthesis and arginase activity in vascular tissue. Nitric Oxide *16*, 1–9.

Boring, L., Gosling, J., Cleary, M., and Charo, I.F. (1998). Decreased lesion formation in CCR2-/- mice reveals a role for chemokines in the initiation of atherosclerosis. Nature *394*, 894–897.

Bossy, B., Petrilli, A., Klinglmayr, E., Chen, J., Lütz-Meindl, U., Knott, A.B., Masliah, E., Schwarzenbacher, R., and Bossy-Wetzel, E. (2010). S-nitrosylation of DRP1 does not affect enzymatic activity and is not specific to Alzheimer's disease. J. Alzheimer's Dis. *20*, S513–S526.

Boveris, A., and Chance, B. (1973). The mitochondrial generation of hydrogen peroxide. General properties and effect of hyperbaric oxygen. Biochem. J. *134*, 707–716.

Bozza, F.A., Salluh, J.I., Japiassu, A.M., Soares, M., Assis, E.F., Gomes, R.N., Bozza, M.T., Castro-Faria-Neto, H.C., and Bozza, P.T. (2007). Cytokine profiles as markers of disease severity in sepsis: a multiplex analysis. Crit. Care *11*, R49.

Brown, G.C., and Cooper, C.E. (1994). Nanomolar concentrations of nitric oxide reversibly inhibit synaptosomal respiration by competing with oxygen at cytochrome oxidase. FEBS Lett. *356*, 295–298.

Brunelle, J.K., Bell, E.L., Quesada, N.M., Vercauteren, K., Tiranti, V., Zeviani, M., Scarpulla, R.C., and Chandel, N.S. (2005). Oxygen sensing requires mitochondrial ROS but not oxidative phosphorylation. Cell Metab. *1*, 409–414.

Brunet, C.L., Gunby, R.H., Benson, R.S., Hickman, J.A., Watson, A.J., and Brady, G. (1998). Commitment to cell death measured by loss of clonogenicity is separable from the appearance of apoptotic markers. Cell Death Differ. *5*, 107–115.

Bult, H., Boeckxstaens, G.E., Pelckmans, P.A., Jordaens, F.H., Maercke, Y.M. Van, and Herman, A.G. (1990). Nitric oxide as an inhibitory non-adrenergic non-cholinergic neurotransmitter. Nature *345*, 346–347.

Burwell, L.S., Nadtochiy, S.M., Tompkins, A.J., Young, S., and Brookes, P.S. (2006). Direct evidence for S-nitrosation of mitochondrial complex I. Biochem. J. *394*, 627–634.

Buttery, L.D., Springall, D.R., Chester, A.H., Evans, T.J., Standfield, E.N., Parums, D. V, Yacoub, M.H., and Polak, J.M. (1996). Inducible nitric oxide synthase is present within human atherosclerotic lesions and promotes the formation and activity of peroxynitrite. Lab. Invest. *75*, 77–85.

Caramori, P.R.., Adelman, A.G., Azevedo, E.R., Newton, G.E., Parker, A.B., and Parker, J.D. (1998). Therapy with nitroglycerin increases coronary vasoconstriction in response to acetylcholine. J. Am. Coll. Cardiol. *32*, 1969–1974.

Castro, L., Rodriguez, M., and Radi, R. (1994). Aconitase is readily inactivated by peroxynitrite, but not by its precursor, nitric oxide. J. Biol. Chem. *269*, 29409–29415.

Celermajer, D.S., Sorensen, K.E., Bull, C., Robinson, J., and Deanfield, J.E. (1994). Endothelium-dependent dilation in the systemic arteries of asymptomatic subjects relates to coronary risk factors and their interaction. J. Am. Coll. Cardiol. *24*, 1468–1474.

Ceylan-Isik, A.F., Guo, K.K., Carlson, E.C., Privratsky, J.R., Liao, S.-J., Cai, L., Chen, A.F., and Ren, J. (2009). Metallothionein abrogates GTP cyclohydrolase I inhibition-induced cardiac contractile and morphological defects: role of mitochondrial biogenesis. Hypertension *53*, 1023–1031.

Chang, C.-R., and Blackstone, C. (2007). Cyclic AMP-dependent Protein Kinase Phosphorylation of Drp1 Regulates Its GTPase Activity and Mitochondrial Morphology. J. Biol. Chem. *282*, 21583–21587.

Chang, C.-H., Curtis, J.D., Maggi, L.B., Faubert, B., Villarino, A. V, O'Sullivan, D., Huang, S.C.-C., van der Windt, G.J.W., Blagih, J., Qiu, J., et al. (2013). Posttranscriptional control of T cell effector function by aerobic glycolysis. Cell *153*, 1239–1251.

Chang, T.-S., Cho, C.-S., Park, S., Yu, S., Kang, S.W., and Rhee, S.G. (2004). Peroxiredoxin III, a Mitochondrion-specific Peroxidase, Regulates Apoptotic Signaling by Mitochondria. J. Biol. Chem. *279*, 41975–41984.

Channon, K.M., Qian, H., Neplioueva, V., Blazing, M.A., Olmez, E., Shetty, G.A., Youngblood, S.A., Pawloski, J., McMahon, T., Stamler, J.S., et al. (1998). In vivo gene transfer of nitric oxide synthase enhances vasomotor function in carotid arteries from normal and cholesterol-Fed rabbits. Circulation *98*, 1905–1911.

Charles, I.G., Palmer, R.M., Hickery, M.S., Bayliss, M.T., Chubb, A.P., Hall, V.S., Moss, D.W., and Moncada, S. (1993). Cloning, characterization, and expression of a cDNA encoding an inducible nitric oxide synthase from the human chondrocyte. Proc. Natl. Acad. Sci. U. S. A. *90*, 11419–11423.

Charoensin, S., Eroglu, E., Opelt, M., Bischof, H., Madreiter-Sokolowski, C.T., Kirsch, A., Depaoli, M.R., Frank, S., Schrammel, A., Mayer, B., et al. (2017). Intact mitochondrial Ca 2+ uniport is essential for agonist-induced activation of endothelial nitric oxide synthase (eNOS). Free Radic. Biol. Med. *102*, 248–259.

Chatzispyrou, I.A., Held, N.M., Mouchiroud, L., Auwerx, J., and Houtkooper, R.H. (2015). Tetracycline antibiotics impair mitochondrial function and its experimental use confounds research. Cancer Res. *75*, 4446–4449.

Chávez-Sánchez, L., Garza-Reyes, M.G., Espinosa-Luna, J.E., Chávez-Rueda, K., Legorreta-Haquet, M.V., and Blanco-Favela, F. (2014). The role of TLR2, TLR4 and CD36 in macrophage activation and foam cell formation in response to oxLDL in humans. Hum. Immunol. *75*, 322–329.

Chen, C.-A., Wang, T.-Y., Varadharaj, S., Reyes, L.A., Hemann, C., Talukder, M.A.H., Chen, Y.-R., Druhan, L.J., and Zweier, J.L. (2010). S-glutathionylation uncouples eNOS and regulates its cellular and vascular function. Nature *468*, 1115–1118.

Chen, C., Pore, N., Behrooz, A., Ismail-Beigi, F., and Maity, A. (2001). Regulation of *glut1* mRNA by Hypoxia-inducible Factor-1. J. Biol. Chem. *276*, 9519–9525.

Chen, H., Montagnani, M., Funahashi, T., Shimomura, I., and Quon, M.J. (2003). Adiponectin stimulates production of nitric oxide in vascular endothelial cells. J. Biol. Chem. *278*, 45021–45026.

Chen, P.F., Tsai, A.L., Berka, V., and Wu, K.K. (1996). Endothelial nitric-oxide synthase.

Evidence for bidomain structure and successful reconstitution of catalytic activity from two separate domains generated by a baculovirus expression system. J. Biol. Chem. *271*, 14631–14635.

Chen, Z.-P., Mitchelhill, K.I., Michell, B.J., Stapleton, D., Rodriguez-Crespo, I., Witters, L.A., Power, D.A., Ortiz de Montellano, P.R., and Kemp, B.E. (1999). AMP-activated protein kinase phosphorylation of endothelial NO synthase. FEBS Lett. *443*, 285–289.

Cho, D.H., Nakamura, T., Fang, J., Cieplak, P., Godzik, A., Gu, Z., and Lipton, S.A. (2009). β-Amyloid-related mitochondrial fission and neuronal injury. Science (80-.). *324*, 102–105.

Cho, H.J., Xie, Q.W., Calaycay, J., Mumford, R.A., Swiderek, K.M., Lee, T.D., and Nathan, C. (1992). Calmodulin is a subunit of nitric oxide synthase from macrophages. J. Exp. Med. *176*, 599–604.

Choi, H.J., Lee, S.Y., Cho, Y., No, H., Kim, S.W., and Hwang, O. (2006). Tetrahydrobiopterin causes mitochondrial dysfunction in dopaminergic cells: implications for Parkinson's disease. Neurochem. Int. *48*, 255–262.

Choi, M.S., Jung, J.-Y., Kim, H.-J., Ham, M.R., Lee, T.R., and Shin, D.W. (2016). S-nitrosylation of fatty acid synthase regulates its activity through dimerization. J. Lipid Res. *57*, 607–615.

Chouchani, E.T., Methner, C., Nadtochiy, S.M., Logan, A., Pell, V.R., Ding, S., James, A.M., Cochemé, H.M., Reinhold, J., Lilley, K.S., et al. (2013). Cardioprotection by S-nitrosation of a cysteine switch on mitochondrial complex I. Nat. Med. *19*, 753–759.

Chouchani, E.T., Pell, V.R., Gaude, E., Aksentijević, D., Sundier, S.Y., Robb, E.L., Logan, A., Nadtochiy, S.M., Ord, E.N.J., Smith, A.C., et al. (2014). Ischaemic accumulation of succinate controls reperfusion injury through mitochondrial ROS. Nature *515*, 431–435.

Chuaiphichai, S., McNeill, E., Douglas, G., Crabtree, M.J., Bendall, J.K., Hale, A.B., Alp, N.J., and Channon, K.M. (2014). Cell-autonomous role of endothelial GTP cyclohydrolase 1 and tetrahydrobiopterin in blood pressure regulation. Hypertension.

Citron, B.A., Kaufman, S., Milstien, S., Naylor, E.W., Greene, C.L., and Davis, M.D. (1993). Mutation in the 4a-carbinolamine dehydratase gene leads to mild hyperphenylalaninemia with defective cofactor metabolism. Am. J. Hum. Genet. *53*, 768–774.

Cleeter, M.W., Cooper, J.M., Darley-Usmar, V.M., Moncada, S., and Schapira, A.H. (1994). Reversible inhibition of cytochrome c oxidase, the terminal enzyme of the mitochondrial respiratory chain, by nitric oxide. Implications for neurodegenerative diseases. FEBS Lett. *345*, 50–54.

Clementi, E., Brown, G.C., Feelisch, M., and Moncada, S. (1998). Persistent inhibition of cell respiration by nitric oxide: crucial role of S-nitrosylation of mitochondrial complex I and protective action of glutathione. Proc. Natl. Acad. Sci. U. S. A. *95*, 7631–7636.

Clementi, E., Brown, G.C., Foxwell, N., and Moncada, S. (1999). On the mechanism by which vascular endothelial cells regulate their oxygen consumption. Proc. Natl. Acad. Sci. U. S. A. *96*, 1559–1562.

Cordes, T., Wallace, M., Michelucci, A., Divakaruni, A.S., Sapcariu, S.C., Sousa, C., Koseki, H., Cabrales, P., Murphy, A.N., Hiller, K., et al. (2016). Immunoresponsive Gene 1 and Itaconate Inhibit Succinate Dehydrogenase to Modulate Intracellular Succinate Levels. J. Biol. Chem. *291*, 14274–14284.

Corraliza, I.M., Soler, G., Eichmann, K., and Modolell, M. (1995). Arginase Induction by Suppressors of Nitric Oxide Synthesis (IL-4, IL-10 and PGE2) in Murine Bone-Marrow-Derived Macrophages. Biochem. Biophys. Res. Commun. *206*, 667–673.

Cosby, K., Partovi, K.S., Crawford, J.H., Patel, R.P., Reiter, C.D., Martyr, S., Yang, B.K., Waclawiw, M.A., Zalos, G., Xu, X., et al. (2003). Nitrite reduction to nitric oxide by deoxyhemoglobin vasodilates the human circulation. Nat. Med. *9*, 1498–1505.

Crabtree, M.J., Smith, C.L., Lam, G., Goligorsky, M.S., and Gross, S.S. (2008). Ratio of 5,6,7,8-tetrahydrobiopterin to 7,8-dihydrobiopterin in endothelial cells determines glucose-elicited changes in NO vs. superoxide production by eNOS. Am. J. Physiol. Heart Circ. Physiol. *294*, H1530-40.

Crabtree, M.J., Tatham, A.L., Al-Wakeel, Y., Warrick, N., Hale, A.B., Cai, S., Channon, K.M., and Alp, N.J. (2009a). Quantitative regulation of intracellular endothelial nitric-oxide synthase (eNOS) coupling by both tetrahydrobiopterin-eNOS stoichiometry and biopterin redox status: insights from cells with tet-regulated GTP cyclohydrolase I expression. J. Biol. Chem. *284*, 1136–1144.

Crabtree, M.J., Tatham, A.L., Hale, A.B., Alp, N.J., and Channon, K.M. (2009b). Critical role for tetrahydrobiopterin recycling by dihydrofolate reductase in regulation of endothelial nitric-oxide synthase coupling: relative importance of the de novo biopterin synthesis versus salvage pathways. J. Biol. Chem. *284*, 28128–28136.

Crabtree, M.J., Brixey, R., Batchelor, H., Hale, A.B., and Channon, K.M. (2013). Integrated redox sensor and effector functions for tetrahydrobiopterin- and glutathionylation-dependent endothelial nitric-oxide synthase uncoupling. J. Biol. Chem. *288*, 561–569.

Craven, P.A., and DeRubertis, F.R. (1978). Restoration of the responsiveness of purified guanylate cyclase to nitrosoguanidine, nitric oxide, and related activators by heme and hemeproteins. Evidence for involvement of the paramagnetic nitrosyl-heme complex in enzyme activation. J. Biol. Chem. *253*, 8433–8443.

Culic, O., Gruwel, M.L., and Schrader, J. (1997). Energy turnover of vascular endothelial cells. Am. J. Physiol. Physiol. *273*, C205–C213.

Cunnington, C., Van Assche, T., Shirodaria, C., Kylintireas, I., Lindsay, A.C., Lee, J.M., Antoniades, C., Margaritis, M., Lee, R., Cerrato, R., et al. (2012). Systemic and vascular oxidation limits the efficacy of oral tetrahydrobiopterin treatment in patients with coronary artery disease. Circulation *125*, 1356–1366.

Cybulsky, M.I., and Gimbrone, M.A. (1991). Endothelial expression of a mononuclear leukocyte adhesion molecule during atherogenesis. Science *251*, 788–791.

Davies, K.M., Blum, T.B., and Kühlbrandt, W. (2018). Conserved in situ arrangement of complex I and III2 in mitochondrial respiratory chain supercomplexes of mammals, yeast, and plants. Proc. Natl. Acad. Sci. U. S. A. *115*, 3024–3029.

Davies, S.M.K., Rackham, O., Shearwood, A.-M.J., Hamilton, K.L., Narsai, R., Whelan, J., and Filipovska, A. (2009). Pentatricopeptide repeat domain protein 3 associates with the mitochondrial small ribosomal subunit and regulates translation. FEBS Lett. *583*, 1853–1858.

De Bock, K., Georgiadou, M., Schoors, S., Kuchnio, A., Wong, B.W., Cantelmo, A.R., Quaegebeur, A., Ghesquière, B., Cauwenberghs, S., Eelen, G., et al. (2013). Role of PFKFB3-Driven Glycolysis in Vessel Sprouting. Cell *154*, 651–663.

Detmers, P.A., Hernandez, M., Mudgett, J., Hassing, H., Burton, C., Mundt, S., Chun, S., Fletcher, D., Card, D.J., Lisnock, J., et al. (2000). Deficiency in inducible nitric oxide synthase results in reduced atherosclerosis in apolipoprotein E-deficient mice. J. Immunol. *165*, 3430–3435.

Dianzani, I., de Sanctis, L., Smooker, P.M., Gough, T.J., Alliaudi, C., Brusco, A., Spada, M., Blau, N., Dobos, M., Zhang, H.P., et al. (1998). Dihydropteridine reductase deficiency: physical structure of the QDPR gene, identification of two new mutations and genotype-phenotype correlations. Hum. Mutat. *12*, 267–273.

Dikalov, S.I., Nazarewicz, R.R., Bikineyeva, A., Hilenski, L., Lassègue, B., Griendling, K.K., Harrison, D.G., and Dikalova, A.E. (2014). Nox2-induced production of mitochondrial superoxide in angiotensin II-mediated endothelial oxidative stress and hypertension. Antioxid. Redox Signal. *20*, 281–294.

Dikalova, A.E., Bikineyeva, A.T., Budzyn, K., Nazarewicz, R.R., McCann, L., Lewis, W., Harrison, D.G., and Dikalov, S.I. (2010). Therapeutic targeting of mitochondrial superoxide in hypertension. Circ. Res. *107*, 106–116.

Dimmeler, S., Fleming, I., Fisslthaler, B., Hermann, C., Busse, R., and Zeiher, A.M. (1999). Activation of nitric oxide synthase in endothelial cells by Akt-dependent phosphorylation. Nature *399*, 601–605.

Douglas, G., Hale, A.B., Crabtree, M.J., Ryan, B.J., Hansler, A., Watschinger, K., Gross, S.S., Lygate, C.A., Alp, N.J., and Channon, K.M. (2014). A requirement for Gch1 and tetrahydrobiopterin in embryonic development. Dev. Biol.

Douglas, G., Hale, A.B., Patel, J., Chuaiphichai, S., Al Haj Zen, A., Rashbrook, V.S., Trelfa, L., Crabtree, M.J., McNeill, E., and Channon, K.M. (2018). Roles for endothelial cell and macrophage Gch1 and tetrahydrobiopterin in atherosclerosis progression. Cardiovasc. Res.

Doulias, P.-T., Tenopoulou, M., Greene, J.L., Raju, K., and Ischiropoulos, H. (2013). Nitric oxide regulates mitochondrial fatty acid metabolism through reversible protein S-nitrosylation. Sci. Signal. *6*, rs1.

Dranka, B.P., Hill, B.G., and Darley-Usmar, V.M. (2010). Mitochondrial reserve capacity in endothelial cells: The impact of nitric oxide and reactive oxygen species. Free Radic. Biol. Med. *48*, 905–914.

Du, J., Teng, R.-J., Lawrence, M., Guan, T., Xu, H., Ge, Y., and Shi, Y. (2012). The protein partners of GTP cyclohydrolase I in rat organs. PLoS One *7*, e33991.

Duan, X., Yang, J., Ren, B., Tan, G., and Ding, H. (2009). Reactivity of nitric oxide with the [4Fe–4S] cluster of dihydroxyacid dehydratase from *Escherichia coli*. Biochem. J. *417*, 783–789.

Dweik, R.A., Laskowski, D., Abu-Soud, H.M., Kaneko, F., Hutte, R., Stuehr, D.J., and Erzurum, S.C. (1998). Nitric oxide synthesis in the lung. Regulation by oxygen through a kinetic mechanism. J. Clin. Invest. *101*, 660–666.

Elfering, S.L., Sarkela, T.M., and Giulivi, C. (2002). Biochemistry of Mitochondrial Nitric-oxide Synthase. J. Biol. Chem. *277*, 38079–38086.

Emre, Y., Hurtaud, C., Nübel, T., Criscuolo, F., Ricquier, D., and Cassard-Doulcier, A.-M. (2007). Mitochondria contribute to LPS-induced MAPK activation via uncoupling protein UCP2 in macrophages. Biochem. J. *402*, 271–278.

Endemann, G., Stanton, L.W., Madden, K.S., Bryant, C.M., White, R.T., and Protter, A.A. (1993). CD36 is a receptor for oxidized low density lipoprotein. J. Biol. Chem. *268*, 11811–11816.

Engler, M.M., Engler, M.B., Malloy, M.J., Chiu, E.Y., Schloetter, M.C., Paul, S.M., Stuehlinger, M., Lin, K.Y., Cooke, J.P., Morrow, J.D., et al. (2003). Antioxidant Vitamins C and E Improve Endothelial Function in Children With Hyperlipidemia: Endothelial Assessment of Risk from Lipids in Youth (EARLY) Trial. Circulation *108*, 1059–1063.

Everts, B., Amiel, E., van der Windt, G.J.W., Freitas, T.C., Chott, R., Yarasheski, K.E., Pearce, E.L., and Pearce, E.J. (2012). Commitment to glycolysis sustains survival of NO-producing inflammatory dendritic cells. Blood *120*, 1422–1431.

Fang, F.C., and Vazquez-Torres, A. (2002). Nitric oxide production by human macrophages: there's NO doubt about it. Am. J. Physiol. - Lung Cell. Mol. Physiol. *282*, L941–L943.

Farley, K.S., Wang, L.F., Razavi, H.M., Law, C., Rohan, M., McCormack, D.G., and Mehta, S. (2006). Effects of macrophage inducible nitric oxide synthase in murine septic lung injury. Am. J. Physiol. Cell. Mol. Physiol. *290*, L1164–L1172.

Febbraio, M., Podrez, E.A., Smith, J.D., Hajjar, D.P., Hazen, S.L., Hoff, H.F., Sharma, K., and Silverstein, R.L. (2000). Targeted disruption of the class B scavenger receptor CD36 protects against atherosclerotic lesion development in mice. J. Clin. Invest. *105*, 1049–1056.

Fernandes, D.C., Wosniak, J., Pescatore, L.A., Bertoline, M.A., Liberman, M., Laurindo, F.R.M., and Santos, C.X.C. (2006). Analysis of DHE-derived oxidation products by HPLC in the assessment of superoxide production and NADPH oxidase activity in vascular systems. AJP Cell Physiol. *292*, C413–C422.

Fernández-Agüera, M.C., Gao, L., González-Rodríguez, P., Pintado, C.O., Arias-Mayenco, I., García-Flores, P., García-Pergañeda, A., Pascual, A., Ortega-Sáenz, P., and López-Barneo, J. (2015). Oxygen Sensing by Arterial Chemoreceptors Depends on Mitochondrial Complex I Signaling. Cell Metab. *22*, 825–837.

Fernández-Vizarra, E., Ferrín, G., Pérez-Martos, A., Fernández-Silva, P., Zeviani, M., and Enríquez, J.A. (2010). Isolation of mitochondria for biogenetical studies: An update. Mitochondrion *10*, 253–262.

Fiege, B., Ballhausen, D., Kierat, L., Leimbacher, W., Goriounov, D., Schircks, B., Thöny, B., and Blau, N. (2004). Plasma tetrahydrobiopterin and its pharmacokinetic following oral administration. Mol. Genet. Metab. *81*, 45–51.

Finkelstein, E., Rosen, G.M., and Rauckman, E.J. (1980). Spin trapping. Kinetics of the reaction of superoxide and hydroxyl radicals with nitrones. J. Am. Chem. Soc. *102*, 4994–4999.

Fleetwood, A.J., Lawrence, T., Hamilton, J.A., and Cook, A.D. (2007). Granulocyte-macrophage colony-stimulating factor (CSF) and macrophage CSF-dependent macrophage phenotypes display differences in cytokine profiles and transcription factor activities: implications for CSF blockade in inflammation. J. Immunol. *178*, 5245–5252.

Fleming, I., Fisslthaler, B., Dimmeler, S., Kemp, B.E., and Busse, R. (2001). Phosphorylation of Thr(495) regulates Ca(2+)/calmodulin-dependent endothelial nitric oxide synthase activity. Circ. Res. *88*, E68-75.

Flint, D.H., Tuminello, J.F., and Emptage, M.H. (1993). The inactivation of Fe-S cluster containing hydro-lyases by superoxide. J. Biol. Chem. *268*, 22369–22376.

Forgione, M.A., Weiss, N., Heydrick, S., Cap, A., Klings, E.S., Bierl, C., Eberhardt, R.T., Farber, H.W., and Loscalzo, J. (2002). Cellular glutathione peroxidase deficiency and endothelial dysfunction. Am. J. Physiol. Circ. Physiol. *282*, H1255–H1261.

Forman, H.J., Zhang, H., and Rinna, A. (2009). Glutathione: overview of its protective roles, measurement, and biosynthesis. Mol. Aspects Med. *30*, 1–12.

Frank, M., Duvezin-Caubet, S., Koob, S., Occhipinti, A., Jagasia, R., Petcherski, A., Ruonala, M.O., Priault, M., Salin, B., and Reichert, A.S. (2012). Mitophagy is triggered by mild oxidative stress in a mitochondrial fission dependent manner. Biochim. Biophys. Acta *1823*, 2297–2310.

Frezza, C., Cipolat, S., and Scorrano, L. (2007). Organelle isolation: functional mitochondria from mouse liver, muscle and cultured fibroblasts. Nat. Protoc. *2*, 287–295.

Frostegård, J., Ulfgren, A.K., Nyberg, P., Hedin, U., Swedenborg, J., Andersson, U., and Hansson, G.K. (1999). Cytokine expression in advanced human atherosclerotic plaques: dominance of pro-inflammatory (Th1) and macrophage-stimulating cytokines. Atherosclerosis *145*, 33–43.

Furchgott, R.F., and Zawadzki, J. V (1980). The obligatory role of endothelial cells in the relaxation of arterial smooth muscle by acetylcholine. Nature *288*, 373–376.

Gao, S., Chen, J., Brodsky, S. V, Huang, H., Adler, S., Lee, J.H., Dhadwal, N., Cohen-Gould, L., Gross, S.S., and Goligorsky, M.S. (2004). Docking of endothelial nitric oxide synthase (eNOS) to the mitochondrial outer membrane: a pentabasic amino acid sequence in the autoinhibitory domain of eNOS targets a proteinase K-cleavable peptide on the cytoplasmic face of mitochondria. J. Biol. Chem. *279*, 15968–15974.

García-Cardeña, G., Oh, P., Liu, J., Schnitzer, J.E., and Sessa, W.C. (1996). Targeting of nitric oxide synthase to endothelial cell caveolae via palmitoylation: implications for nitric oxide signaling. Proc. Natl. Acad. Sci. U. S. A. *93*, 6448–6453.

Gardner, P.R., Costantino, G., Szabó, C., and Salzman, A.L. (1997). Nitric oxide sensitivity of the aconitases. J. Biol. Chem. *272*, 25071–25076.

Garg, U.C., and Hassid, A. (1989). Nitric oxide-generating vasodilators and 8-bromo-cyclic guanosine monophosphate inhibit mitogenesis and proliferation of cultured rat vascular smooth muscle cells. J. Clin. Invest. *83*, 1774–1777.

Ghazalpour, A., Bennett, B., Petyuk, V.A., Orozco, L., Hagopian, R., Mungrue, I.N., Farber, C.R., Sinsheimer, J., Kang, H.M., Furlotte, N., et al. (2011). Comparative analysis of proteome and transcriptome variation in mouse. PLoS Genet. *7*, e1001393.

Ghosh, D.K., and Stuehr, D.J. (1995). Macrophage NO synthase: characterization of isolated oxygenase and reductase domains reveals a head-to-head subunit interaction. Biochemistry *34*, 801–807.

Giedt, R.J., Yang, C., Zweier, J.L., Matzavinos, A., and Alevriadou, B.R. (2012). Mitochondrial fission in endothelial cells after simulated ischemia/reperfusion: role of nitric oxide and reactive oxygen species. Free Radic. Biol. Med. *52*, 348–356.

Gioscia-Ryan, R.A., LaRocca, T.J., Sindler, A.L., Zigler, M.C., Murphy, M.P., and Seals, D.R. (2014a). Mitochondria-targeted antioxidant (MitoQ) ameliorates age-related arterial endothelial dysfunction in mice. J. Physiol. *592*, 2549–2561.

Gioscia-Ryan, R.A., LaRocca, T.J., Sindler, A.L., Zigler, M.C., Murphy, M.P., and Seals,

D.R. (2014b). Mitochondria-targeted antioxidant (MitoQ) ameliorates age-related arterial endothelial dysfunction in mice. J. Physiol. *592*, 2549–2561.

Goetz, R.M., Thatte, H.S., Prabhakar, P., Cho, M.R., Michel, T., and Golan, D.E. (1999). Estradiol induces the calcium-dependent translocation of endothelial nitric oxide synthase. Proc. Natl. Acad. Sci. U. S. A. *96*, 2788–2793.

González-Polo, R.-A., Boya, P., Pauleau, A.-L., Jalil, A., Larochette, N., Souquère, S., Eskelinen, E.-L., Pierron, G., Saftig, P., and Kroemer, G. (2005). The apoptosis/autophagy paradox: autophagic vacuolization before apoptotic death. J. Cell Sci. *118*, 3091–3102.

Gori, T., Mak, S.S., Kelly, S., and Parker, J.D. (2001). Evidence supporting abnormalities in nitric oxide synthase function induced by nitroglycerin in humans. J. Am. Coll. Cardiol. *38*, 1096–1101.

Graham, D., Huynh, N.N., Hamilton, C.A., Beattie, E., Smith, R.A.J., Cocheme, H.M., Murphy, M.P., and Dominiczak, A.F. (2009a). Mitochondria-Targeted Antioxidant MitoQ10 Improves Endothelial Function and Attenuates Cardiac Hypertrophy. Hypertension *54*, 322–328.

Graham, D., Huynh, N.N., Hamilton, C.A., Beattie, E., Smith, R.A.J., Cochemé, H.M., Murphy, M.P., and Dominiczak, A.F. (2009b). Mitochondria-targeted antioxidant MitoQ10 improves endothelial function and attenuates cardiac hypertrophy. Hypertension *54*, 322–328.

Griffith, O.W., and Meister, A. (1985). Origin and turnover of mitochondrial glutathione. Proc. Natl. Acad. Sci. U. S. A. *82*, 4668–4672.

Gross, S.S., Jaffe, E.A., Levi, R., and Kilbourn, R.G. (1991). Cytokine-activated endothelial cells express an isotype of nitric oxide synthase which is tetrahydrobiopterin-dependent, calmodulin-independent and inhibited by arginine analogs with a rank-order of potency characteristic of activated macrophages. Biochem. Biophys. Res. Commun. *178*, 823–829.

Gross, T.J., Kremens, K., Powers, L.S., Brink, B., Knutson, T., Domann, F.E., Philibert, R.A., Milhem, M.M., and Monick, M.M. (2014). Epigenetic Silencing of the Human NOS2 Gene: Rethinking the Role of Nitric Oxide in Human Macrophage Inflammatory Responses. J. Immunol. *192*, 2326–2338.

Gryglewski, R.J., Palmer, R.M.J., and Moncada, S. (1986). Superoxide anion is involved in the breakdown of endothelium-derived vascular relaxing factor. Nature *320*, 454–456.

Gu, L., Okada, Y., Clinton, S.K., Gerard, C., Sukhova, G.K., Libby, P., and Rollins, B.J. (1998). Absence of monocyte chemoattractant protein-1 reduces atherosclerosis in low density lipoprotein receptor-deficient mice. Mol. Cell *2*, 275–281.

Guerrero-Castillo, S., Baertling, F., Kownatzki, D., Wessels, H.J., Arnold, S., Brandt, U., and Nijtmans, L. (2017). The Assembly Pathway of Mitochondrial Respiratory Chain Complex I. Cell Metab. *25*, 128–139.

Guiducci, C., Vicari, A.P., Sangaletti, S., Trinchieri, G., and Colombo, M.P. (2005). Redirecting in vivo elicited tumor infiltrating macrophages and dendritic cells towards tumor rejection. Cancer Res. *65*, 3437–3446.

Hara, M.R., Agrawal, N., Kim, S.F., Cascio, M.B., Fujimuro, M., Ozeki, Y., Takahashi, M., Cheah, J.H., Tankou, S.K., Hester, L.D., et al. (2005). S-nitrosylated GAPDH initiates apoptotic cell death by nuclear translocation following Siah1 binding. Nat. Cell Biol. *7*, 665–674.

Harada, T., Kagamiyama, H., and Hatakeyama, K. (1993). Feedback regulation mechanisms for the control of GTP cyclohydrolase I activity. Science *260*, 1507–1510.

Haschemi, A., Kosma, P., Gille, L., Evans, C.R., Burant, C.F., Starkl, P., Knapp, B., Haas, R., Schmid, J.A., Jandl, C., et al. (2012). The sedoheptulose kinase CARKL directs macrophage polarization through control of glucose metabolism. Cell Metab. *15*, 813–826.

Hashimoto, D., Chow, A., Noizat, C., Teo, P., Beasley, M.B., Leboeuf, M., Becker, C.D., See, P., Price, J., Lucas, D., et al. (2013). Tissue-Resident Macrophages Self-Maintain Locally throughout Adult Life with Minimal Contribution from Circulating Monocytes. Immunity *38*, 792–804.

Hattori, Y., Oka, M., Kasai, K., Nakanishi, N., and Shimoda, S.I. (1995). Lipopolysaccharide treatment in vivo induces tissue expression of GTP cyclohydrolase I mRNA. FEBS Lett. *368*, 336–338.

Hausel, P., Latado, H., Courjault-Gautier, F., and Felley-Bosco, E. (2005). Src-mediated phosphorylation regulates subcellular distribution and activity of human inducible nitric oxide synthase. Oncogene *25*, 198–206.

Hegyi, L., Skepper, J.N., Cary, N.R.B., and Mitchinson, M.J. (1996). Foam cell apoptosis and the development of the lipid core of human atherosclerosis. J. Pathol. *180*, 423–429.

Heiss, C., Meyer, C., Totzeck, M., Hendgen-Cotta, U.B., Heinen, Y., Luedike, P., Keymel, S., Ayoub, N., Lundberg, J.O., Weitzberg, E., et al. (2012). Dietary inorganic nitrate mobilizes circulating angiogenic cells. Free Radic. Biol. Med. *52*, 1767–1772.

Heitzer, T., Brockhoff, C., Mayer, B., Warnholtz, A., Mollnau, H., Henne, S., Meinertz, T., and Münzel, T. (2000). Tetrahydrobiopterin improves endothelium-dependent vasodilation in chronic smokers : evidence for a dysfunctional nitric oxide synthase. Circ. Res. *86*, E36-41.

Hernandez-Cuellar, E., Tsuchiya, K., Hara, H., Fang, R., Sakai, S., Kawamura, I., Akira, S., and Mitsuyama, M. (2012). Cutting Edge: Nitric Oxide Inhibits the NLRP3 Inflammasome. J. Immunol. *189*, 5113–5117.

Heusch, P., Aker, S., Boengler, K., Deindl, E., Sand, A., Klein, K., Rassaf, T., Konietzka, I., Sewell, A., Menazza, S., et al. (2010). Increased inducible nitric oxide synthase and arginase II expression in heart failure: no net nitrite/ nitrate production and protein S-nitrosylation. Am J Physiol Hear. Circ Physiol *299*, H446–H453.

Hibbs, J.B., Taintor, R.R., and Vavrin, Z. (1987). Macrophage cytotoxicity: role for L-arginine deiminase and imino nitrogen oxidation to nitrite. Science *235*, 473–476.

Higashi, Y., Sasaki, S., Nakagawa, K., Fukuda, Y., Matsuura, H., Oshima, T., and Chayama, K. (2002). Tetrahydrobiopterin enhances forearm vascular response to acetylcholine in both normotensive and hypertensive individuals. Am. J. Hypertens. *15*, 326–332.

Higashi, Y., Sasaki, S., Nakagawa, K., Kimura, M., Noma, K., Hara, K., Jitsuiki, D., Goto, C., Oshima, T., Chayama, K., et al. (2006). Tetrahydrobiopterin improves aging-related impairment of endothelium-dependent vasodilation through increase in nitric oxide production. Atherosclerosis *186*, 390–395.

Hill, H.D., and Straka, J.G. (1988). Protein determination using bicinchoninic acid in the presence of sulfhydryl reagents. Anal. Biochem. *170*, 203–208.

van Hinsbergh, V.W., Scheffer, M., Havekes, L., and Kempen, H.J. (1986). Role of

endothelial cells and their products in the modification of low-density lipoproteins. Biochim. Biophys. Acta *878*, 49–64.

Hu, C.-J., Wang, L.-Y., Chodosh, L.A., Keith, B., and Simon, M.C. (2003). Differential roles of hypoxia-inducible factor 1alpha (HIF-1alpha) and HIF-2alpha in hypoxic gene regulation. Mol. Cell. Biol. *23*, 9361–9374.

Huang, P.L., Huang, Z., Mashimo, H., Bloch, K.D., Moskowitz, M.A., Bevan, J.A., and Fishman, M.C. (1995). Hypertension in mice lacking the gene for endothelial nitric oxide synthase. Nature *377*, 239–242.

Huang, S.C.-C., Smith, A.M., Everts, B., Colonna, M., Pearce, E.L., Schilling, J.D., and Pearce, E.J. (2016). Metabolic Reprogramming Mediated by the mTORC2-IRF4 Signaling Axis Is Essential for Macrophage Alternative Activation. Immunity *45*, 817–830.

Huie, R.E., and Padmaja, S. (1993). The reaction of no with superoxide. Free Radic. Res. Commun. *18*, 195–199.

Hurshman, A.R., Krebs, C., Edmondson, D.E., and Marletta, M.A. (2003). Ability of Tetrahydrobiopterin Analogues to Support Catalysis by Inducible Nitric Oxide Synthase: Formation of a Pterin Radical is Required for Enzyme Activity. Biochemistry *42*, 13287–13303.

Ichinose, H., Ohye, T., Takahashi, E., Seki, N., Hori, T., Segawa, M., Nomura, Y., Endo, K., Tanaka, H., Tsuji, S., et al. (1994). Hereditary progressive dystonia with marked diurnal fluctuation caused by mutations in the GTP cyclohydrolase I gene. Nat. Genet. *8*, 236–242.

Ignarro, L.J., Buga, G.M., Wood, K.S., Byrns, R.E., and Chaudhuri, G. (1987). Endothelium-derived relaxing factor produced and released from artery and vein is nitric oxide. Proc. Natl. Acad. Sci. U. S. A. *84*, 9265–9269.

Infantino, V., Convertini, P., Cucci, L., Panaro, M.A., Di Noia, M.A., Calvello, R., Palmieri, F., and Iacobazzi, V. (2011). The mitochondrial citrate carrier: a new player in inflammation. Biochem. J. *438*, 433–436.

Iwakiri, Y., Satoh, A., Chatterjee, S., Toomre, D.K., Chalouni, C.M., Fulton, D., Groszmann, R.J., Shah, V.H., and Sessa, W.C. (2006). Nitric oxide synthase generates nitric oxide locally to regulate compartmentalized protein S-nitrosylation and protein trafficking. Proc. Natl. Acad. Sci. U. S. A. *103*, 19777–19782.

Jaffrey, S.R., Erdjument-Bromage, H., Ferris, C.D., Tempst, P., and Snyder, S.H. (2001). Protein S-nitrosylation: a physiological signal for neuronal nitric oxide. Nat. Cell Biol. *3*, 193–197.

Janssens, S.P., Shimouchi, A., Quertermous, T., Bloch, D.B., and Bloch, K.D. (1992). Cloning and expression of a cDNA encoding human endothelium-derived relaxing factor/nitric oxide synthase. J. Biol. Chem. *267*, 14519–14522.

Jha, A.K., Huang, S.C.-C., Sergushichev, A., Lampropoulou, V., Ivanova, Y., Loginicheva, E., Chmielewski, K., Stewart, K.M., Ashall, J., Everts, B., et al. (2015). Network Integration of Parallel Metabolic and Transcriptional Data Reveals Metabolic Modules that Regulate Macrophage Polarization. Immunity *42*, 419–430.

Jia, L., Bonaventura, C., Bonaventura, J., and Stamler, J.S. (1996). S-nitrosohaemoglobin: a dynamic activity of blood involved in vascular control. Nature *380*, 221–226.

Ju, H., Zou, R., Venema, V.J., and Venema, R.C. (1997). Direct interaction of endothelial

nitric-oxide synthase and caveolin-1 inhibits synthase activity. J. Biol. Chem. *272*, 18522–18525.

Judkins, C.P., Diep, H., Broughton, B.R.S., Mast, A.E., Hooker, E.U., Miller, A.A., Selemidis, S., Dusting, G.J., Sobey, C.G., and Drummond, G.R. (2010). Direct evidence of a role for Nox2 in superoxide production, reduced nitric oxide bioavailability, and early atherosclerotic plaque formation in ApoE-/- mice. AJP Hear. Circ. Physiol. *298*, H24–H32.

Kanai, A.J., Pearce, L.L., Clemens, P.R., Birder, L.A., VanBibber, M.M., Choi, S.Y., de Groat, W.C., and Peterson, J. (2001). Identification of a neuronal nitric oxide synthase in isolated cardiac mitochondria using electrochemical detection. Proc. Natl. Acad. Sci. U. S. A. *98*, 14126–14131.

Kashatus, J.A., Nascimento, A., Myers, L.J., Sher, A., Byrne, F.L., Hoehn, K.L., Counter, C.M., and Kashatus, D.F. (2015). Erk2 phosphorylation of Drp1 promotes mitochondrial fission and MAPK-driven tumor growth. Mol. Cell *57*, 537–551.

Kasuno, K., Takabuchi, S., Fukuda, K., Kizaka-Kondoh, S., Yodoi, J., Adachi, T., Semenza, G.L., and Hirota, K. (2004). Nitric Oxide Induces Hypoxia-inducible Factor 1 Activation That Is Dependent on MAPK and Phosphatidylinositol 3-Kinase Signaling. J. Biol. Chem. *279*, 2550–2558.

Kaufman, S. (1959). Studies on the mechanism of the enzymatic conversion of phenylalanine to tyrosine. J. Biol. Chem. *234*, 2677–2682.

Kaur, A., Jankowska, K., Pilgrim, C., Fraser, S.T., and New, E.J. (2016). Studies of Hematopoietic Cell Differentiation with a Ratiometric and Reversible Sensor of Mitochondrial Reactive Oxygen Species. Antioxid. Redox Signal. *24*, 667–679.

Kelly, B., and O'Neill, L.A.J. (2015). Metabolic reprogramming in macrophages and dendritic cells in innate immunity. Cell Res. *25*, 771–784.

Kelso, G.F., Porteous, C.M., Coulter, C. V, Hughes, G., Porteous, W.K., Ledgerwood, E.C., Smith, R.A.J., and Murphy, M.P. (2001). Selective targeting of a redox-active ubiquinone to mitochondria within cells: Antioxidant and antiapoptotic properties. J. Biol. Chem. *276*, 4588–4596.

Khallou-Laschet, J., Varthaman, A., Fornasa, G., Compain, C., Gaston, A.-T., Clement, M., Dussiot, M., Levillain, O., Graff-Dubois, S., Nicoletti, A., et al. (2010). Macrophage Plasticity in Experimental Atherosclerosis. PLoS One *5*, e8852.

Khan, B. V, Harrison, D.G., Olbrych, M.T., Alexander, R.W., and Medford, R.M. (1996). Nitric oxide regulates vascular cell adhesion molecule 1 gene expression and redox-sensitive transcriptional events in human vascular endothelial cells. Proc. Natl. Acad. Sci. U. S. A. *93*, 9114–9119.

Kharitonov, V.G., Sundquist, A.R., and Sharma, V.S. (1995). Kinetics of nitrosation of thiols by nitric oxide in the presence of oxygen. J. Biol. Chem. *270*, 28158–28164.

Khoo, N.K.H., Mo, L., Zharikov, S., Kamga-Pride, C., Quesnelle, K., Golin-Bisello, F., Li, L., Wang, Y., and Shiva, S. (2014). Nitrite augments glucose uptake in adipocytes through the protein kinase A-dependent stimulation of mitochondrial fusion. Free Radic. Biol. Med. *70*, 45–53.

Kilbourn, R.G., Gross, S.S., Jubran, A., Adams, J., Griffith, O.W., Levi, R., and Lodato, R.F. (1990a). NG-methyl-L-arginine inhibits tumor necrosis factor-induced hypotension: implications for the involvement of nitric oxide. Proc. Natl. Acad. Sci. U. S. A. *87*, 3629–

3632.

Kilbourn, R.G., Jubran, A., Gross, S.S., Griffith, O.W., Levi, R., Adams, J., and Lodato, R.F. (1990b). Reversal of endotoxin-mediated shock by NG-methyl-L-arginine, an inhibitor of nitric oxide synthesis. Biochem. Biophys. Res. Commun. *172*, 1132–1138.

Kilbourn, R.G., Gross, S.S., Lodato, R.F., Adams, J., Levi, R., Miller, L.L., Lachman, L.B., and Griffith, O.W. (1992). Inhibition of interleukin-1-alpha-induced nitric oxide synthase in vascular smooth muscle and full reversal of interleukin-1-alpha-induced hypotension by N omega-amino-L-arginine. J. Natl. Cancer Inst. *84*, 1008–1016.

Kinlay, S., Behrendt, D., Fang, J.C., Delagrange, D., Morrow, J., Witztum, J.L., Rifai, N., Selwyn, A.P., Creager, M.A., and Ganz, P. (2004). Long-term effect of combined vitamins E and C on coronary and peripheral endothelial function. J. Am. Coll. Cardiol. *43*, 629–634.

Kong, S.K., Yim, M.B., Stadtman, E.R., and Chock, P.B. (1996). Peroxynitrite disables the tyrosine phosphorylation regulatory mechanism: Lymphocyte-specific tyrosine kinase fails to phosphorylate nitrated cdc2(6-20)NH2 peptide. Proc. Natl. Acad. Sci. U. S. A. *93*, 3377–3382.

Kornberg, M.D., Sen, N., Hara, M.R., Juluri, K.R., Nguyen, J.V.K., Snowman, A.M., Law, L., Hester, L.D., and Snyder, S.H. (2010). GAPDH mediates nitrosylation of nuclear proteins. Nat. Cell Biol. *12*, 1094–1100.

Kotsonis, P., Fröhlich, L.G., Shutenko, Z. V, Horejsi, R., Pfleiderer, W., and Schmidt, H.H. (2000). Allosteric regulation of neuronal nitric oxide synthase by tetrahydrobiopterin and suppression of auto-damaging superoxide. Biochem. J. *346 Pt 3*, 767–776.

Koziel, A., and Jarmuszkiewicz, W. (2017). Hypoxia and aerobic metabolism adaptations of human endothelial cells. Pflügers Arch. - Eur. J. Physiol. *469*, 815–827.

Krawczyk, C.M., Holowka, T., Sun, J., Blagih, J., Amiel, E., DeBerardinis, R.J., Cross, J.R., Jung, E., Thompson, C.B., Jones, R.G., et al. (2010). Toll-like receptor-induced changes in glycolytic metabolism regulate dendritic cell activation. Blood *115*, 4742–4749.

Kujoth, G.C., Hiona, A., Pugh, T.D., Someya, S., Panzer, K., Wohlgemuth, S.E., Hofer, T., Seo, A.Y., Sullivan, R., Jobling, W.A., et al. (2005). Mitochondrial DNA mutations, oxidative stress, and apoptosis in mammalian aging. Science *309*, 481–484.

Kun, J.F., Mordmüller, B., Perkins, D.J., May, J., Mercereau-Puijalon, O., Alpers, M., Weinberg, J.B., and Kremsner, P.G. (2001). Nitric oxide synthase 2(Lambaréné) (G-954C), increased nitric oxide production, and protection against malaria. J. Infect. Dis. *184*, 330–336.

Kurahara, H., Shinchi, H., Mataki, Y., Maemura, K., Noma, H., Kubo, F., Sakoda, M., Ueno, S., Natsugoe, S., and Takao, S. (2011). Significance of M2-Polarized Tumor-Associated Macrophage in Pancreatic Cancer. J. Surg. Res. *167*, e211–e219.

Kussmaul, L., and Hirst, J. (2006). The mechanism of superoxide production by NADH:ubiquinone oxidoreductase (complex I) from bovine heart mitochondria. Proc. Natl. Acad. Sci. *103*, 7607–7612.

Kuzkaya, N., Weissmann, N., Harrison, D.G., and Dikalov, S. (2003). Interactions of peroxynitrite, tetrahydrobiopterin, ascorbic acid, and thiols: implications for uncoupling endothelial nitric-oxide synthase. J. Biol. Chem. *278*, 22546–22554.

Kwon, N.S., Nathan, C.F., and Stuehr, D.J. (1989). Reduced biopterin as a cofactor in the

generation of nitrogen oxides by murine macrophages. J. Biol. Chem. *264*, 20496–20501.

Lacey, D.C., Achuthan, A., Fleetwood, A.J., Dinh, H., Roiniotis, J., Scholz, G.M., Chang, M.W., Beckman, S.K., Cook, A.D., and Hamilton, J.A. (2012). Defining GM-CSF- and Macrophage-CSF-Dependent Macrophage Responses by In Vitro Models. J. Immunol. *188*, 5752–5765.

Lacza, Z., Snipes, J.A., Zhang, J., Horváth, E.M., Figueroa, J.P., Szabó, C., and Busija, D.W. (2003). Mitochondrial nitric oxide synthase is not eNOS, nNOS or iNOS. Free Radic. Biol. Med. *35*, 1217–1228.

Lampropoulou, V., Sergushichev, A., Bambouskova, M., Nair, S., Vincent, E.E., Loginicheva, E., Cervantes-Barragan, L., Ma, X., Huang, S.C.-C., Griss, T., et al. (2016). Itaconate Links Inhibition of Succinate Dehydrogenase with Macrophage Metabolic Remodeling and Regulation of Inflammation. Cell Metab. *24*, 158–166.

Landmesser, U., Dikalov, S., Price, S.R., McCann, L., Fukai, T., Holland, S.M., Mitch, W.E., and Harrison, D.G. (2003). Oxidation of tetrahydrobiopterin leads to uncoupling of endothelial cell nitric oxide synthase in hypertension. J. Clin. Invest. *111*, 1201–1209.

Langan, T.J., Rodgers, K.R., and Chou, R.C. (2017). Synchronization of Mammalian Cell Cultures by Serum Deprivation. In Methods in Molecular Biology (Clifton, N.J.), pp. 97–105.

Larsen, F.J., Ekblom, B., Sahlin, K., Lundberg, J.O., Weitzberg, E., Blackwell, J., DiMenna, F., Gilchrist, M., Benjamin, N., Jones, A., et al. (2006). Effects of dietary nitrate on blood pressure in healthy volunteers. N. Engl. J. Med. *355*, 2792–2793.

Laursen, J.B., Somers, M., Kurz, S., McCann, L., Warnholtz, A., Freeman, B.A., Tarpey, M., Fukai, T., and Harrison, D.G. (2001). Endothelial regulation of vasomotion in apoE-deficient mice: implications for interactions between peroxynitrite and tetrahydrobiopterin. Circulation *103*, 1282–1288.

Lee, J.H., Yang, E.S., and Park, J.-W. (2003). Inactivation of $NADP^+$-dependent Isocitrate Dehydrogenase by Peroxynitrite. J. Biol. Chem. *278*, 51360–51371.

Lee, S.M., Koh, H.-J., Park, D.-C., Song, B.J., Huh, T.-L., and Park, J.-W. (2002). Cytosolic NADP(+)-dependent isocitrate dehydrogenase status modulates oxidative damage to cells. Free Radic. Biol. Med. *32*, 1185–1196.

Levy, H.L., Milanowski, A., Chakrapani, A., Cleary, M., Lee, P., Trefz, F.K., Whitley, C.B., Feillet, F., Feigenbaum, A.S., Bebchuk, J.D., et al. (2007). Efficacy of sapropterin dihydrochloride (tetrahydrobiopterin, 6R-BH4) for reduction of phenylalanine concentration in patients with phenylketonuria: a phase III randomised placebo-controlled study. Lancet *370*, 504–510.

Li, F., Calingasan, N.Y., Yu, F., Mauck, W.M., Toidze, M., Almeida, C.G., Takahashi, R.H., Carlson, G.A., Flint Beal, M., Lin, M.T., et al. (2004). Increased plaque burden in brains of APP mutant MnSOD heterozygous knockout mice. J. Neurochem. *89*, 1308–1312.

Li, L., Zhu, L., Hao, B., Gao, W., Wang, Q., Li, K., Wang, M., Huang, M., Liu, Z., Yang, Q., et al. (2017). iNOS-derived nitric oxide promotes glycolysis by inducing pyruvate kinase M2 nuclear translocation in ovarian cancer. Oncotarget *8*, 33047–33063.

Liochev, S.I., and Fridovich, I. (1994). The role of O2.− in the production of HO.: in vitro and in vivo. Free Radic. Biol. Med. *16*, 29–33.

Liu, J., Hughes, T.E., and Sessa, W.C. (1997). The first 35 amino acids and fatty acylation sites determine the molecular targeting of endothelial nitric oxide synthase into the Golgi region of cells: a green fluorescent protein study. J. Cell Biol. *137*, 1525–1535.

Liu, L., Lu, Y., Martinez, J., Bi, Y., Lian, G., Wang, T., Milasta, S., Wang, J., Yang, M., Liu, G., et al. (2016). Proinflammatory signal suppresses proliferation and shifts macrophage metabolism from Myc-dependent to HIF1 **α** -dependent. Proc. Natl. Acad. Sci. *113*, 1564–1569.

Liu, Y., Zhao, H., Li, H., Kalyanaraman, B., Nicolosi, A.C., and Gutterman, D.D. (2003). Mitochondrial Sources of H2O2 Generation Play a Key Role in Flow-Mediated Dilation in Human Coronary Resistance Arteries. Circ. Res. *93*, 573–580.

Lu, C., Shi, Y., Wang, Z., Song, Z., Zhu, M., Cai, Q., and Chen, T. (2008). Serum starvation induces H2AX phosphorylation to regulate apoptosis via p38 MAPK pathway. FEBS Lett. *582*, 2703–2708.

Lundberg, J.O., Weitzberg, E., Lundberg, J.M., and Alving, K. (1994). Intragastric nitric oxide production in humans: measurements in expelled air. Gut *35*, 1543–1546.

Lundberg, M., Johansson, C., Chandra, J., Enoksson, M., Jacobsson, G., Ljung, J., Johansson, M., and Holmgren, A. (2001). Cloning and Expression of a Novel Human Glutaredoxin (Grx2) with Mitochondrial and Nuclear Isoforms. J. Biol. Chem. *276*, 26269–26275.

Luo, F., Liu, X., Yan, N., Li, S., Cao, G., Cheng, Q., Xia, Q., and Wang, H. (2006). Hypoxia-inducible transcription factor-1α promotes hypoxia-induced A549 apoptosis via a mechanism that involves the glycolysis pathway. BMC Cancer *6*, 26.

Mabbott, N.A., Kenneth Baillie, J., Hume, D.A., and Freeman, T.C. (2010). Meta-analysis of lineage-specific gene expression signatures in mouse leukocyte populations. Immunobiology *215*, 724–736.

MacMicking, J.D., Nathan, C., Hom, G., Chartrain, N., Fletcher, D.S., Trumbauer, M., Stevens, K., Xie, Q., Sokol, K., Hutchinson, N., et al. (1995). Altered responses to bacterial infection and endotoxic shock in mice lacking inducible nitric oxide synthase. Cell *81*, 641–650.

Maier, W., Cosentino, F., Lütolf, R.B., Fleisch, M., Seiler, C., Hess, O.M., Meier, B., and Lüscher, T.F. (2000). Tetrahydrobiopterin improves endothelial function in patients with coronary artery disease. J. Cardiovasc. Pharmacol. *35*, 173–178.

Manczak, M., Mao, P., Calkins, M.J., Cornea, A., Reddy, A.P., Murphy, M.P., Szeto, H.H., Park, B., and Reddy, P.H. (2010). Mitochondria-Targeted Antioxidants Protect Against Amyloid-β Toxicity in Alzheimer's Disease Neurons. J. Alzheimer's Dis. *20*, S609–S631.

Mao, K., Chen, S., Chen, M., Ma, Y., Wang, Y., Huang, B., He, Z., Zeng, Y., Hu, Y., Sun, S., et al. (2013). Nitric oxide suppresses NLRP3 inflammasome activation and protects against LPS-induced septic shock. Cell Res. *23*, 201–212.

Marks-Konczalik, J., Chu, S.C., and Moss, J. (1998). Cytokine-mediated transcriptional induction of the human inducible nitric oxide synthase gene requires both activator protein 1 and nuclear factor kappaB-binding sites. J. Biol. Chem. *273*, 22201–22208.

Marsden, P.A., Schappert, K.T., Chen, H.S., Flowers, M., Sundell, C.L., Wilcox, J.N., Lamas, S., and Michel, T. (1992). Molecular cloning and characterization of human endothelial nitric oxide synthase. FEBS Lett. *307*, 287–293.

Mathupala, S.P., Rempel, A., and Pedersen, P.L. (2001). Glucose catabolism in cancer cells: Identification and characterization of a marked activation response of the type II hexokinase gene to hypoxic conditions. J. Biol. Chem. *276*, 43407–43412.

McCord, J.M., and Fridovich, I. (1969). Superoxide dismutase. An enzymic function for erythrocuprein (hemocuprein). J. Biol. Chem. *244*, 6049–6055.

McNeill, E., Crabtree, M.J., Sahgal, N., Patel, J., Chuaiphichai, S., Iqbal, A.J., Hale, A.B., Greaves, D.R., and Channon, K.M. (2015). Regulation of iNOS function and cellular redox state by macrophage Gch1 reveals specific requirements for tetrahydrobiopterin in NRF2 activation. Free Radic. Biol. Med. *79*, 206–216.

Mencacci, N.E., Isaias, I.U., Reich, M.M., Ganos, C., Plagnol, V., Polke, J.M., Bras, J., Hersheson, J., Stamelou, M., Pittman, A.M., et al. (2014). Parkinson's disease in GTP cyclohydrolase 1 mutation carriers. Brain *137*, 2480–2492.

Mercuri, F., Tonutti, L., Taboga, C., Ceriello, A., Assaloni, R., Motz, E., and Quagliaro, L. (2001). Detection of nitrotyrosine in the diabetic plasma: evidence of oxidative stress. Diabetologia *44*, 834–838.

Messam, C.A., and Pittman, R.N. (1998). Asynchrony and Commitment to Die during Apoptosis. Exp. Cell Res. *238*, 389–398.

Michel, J.B., Feron, O., Sacks, D., and Michel, T. (1997). Reciprocal regulation of endothelial nitric-oxide synthase by Ca2+-calmodulin and caveolin. J. Biol. Chem. *272*, 15583–15586.

Michelucci, A., Cordes, T., Ghelfi, J., Pailot, A., Reiling, N., Goldmann, O., Binz, T., Wegner, A., Tallam, A., Rausell, A., et al. (2013). Immune-responsive gene 1 protein links metabolism to immunity by catalyzing itaconic acid production. Proc. Natl. Acad. Sci. *110*, 7820–7825.

Mills, E.L., Kelly, B., Logan, A., Costa, A.S.H., Varma, M., Bryant, C.E., Tourlomousis, P., Däbritz, J.H.M., Gottlieb, E., Latorre, I., et al. (2016). Succinate Dehydrogenase Supports Metabolic Repurposing of Mitochondria to Drive Inflammatory Macrophages. Cell *167*, 457–470.e13.

Mills, E.L., Ryan, D.G., Prag, H.A., Dikovskaya, D., Menon, D., Zaslona, Z., Jedrychowski, M.P., Costa, A.S.H., Higgins, M., Hams, E., et al. (2018). Itaconate is an anti-inflammatory metabolite that activates Nrf2 via alkylation of KEAP1. Nature *556*, 113–117.

Milstien, S., and Katusic, Z. (1999). Oxidation of Tetrahydrobiopterin by Peroxynitrite: Implications for Vascular Endothelial Function. Biochem. Biophys. Res. Commun. *263*, 681–684.

Milstien, S., Jaffe, H., Kowlessur, D., and Bonner, T.I. (1996). Purification and cloning of the GTP cyclohydrolase I feedback regulatory protein, GFRP. J. Biol. Chem. *271*, 19743–19751.

Mishra, B.B., Rathinam, V.A.K., Martens, G.W., Martinot, A.J., Kornfeld, H., Fitzgerald, K.A., and Sassetti, C.M. (2013). Nitric oxide controls the immunopathology of tuberculosis by inhibiting NLRP3 inflammasome–dependent processing of IL-1β. Nat. Immunol. *14*, 52–60.

Mohr, S., Stamler, J.S., and Brüne, B. (1996). Posttranslational modification of glyceraldehyde-3-phosphate dehydrogenase by S-nitrosylation and subsequent NADH attachment. J. Biol. Chem. *271*, 4209–4214.

Molina y Vedia, L., McDonald, B., Reep, B., Brüne, B., Di Silvio, M., Billiar, T.R., and Lapetina, E.G. (1992). Nitric oxide-induced S-nitrosylation of glyceraldehyde-3-phosphate dehydrogenase inhibits enzymatic activity and increases endogenous ADP-ribosylation. J. Biol. Chem. *267*, 24929–24932.

Mookerjee, S.A., Goncalves, R.L.S., Gerencser, A.A., Nicholls, D.G., and Brand, M.D. (2015). The contributions of respiration and glycolysis to extracellular acid production. Biochim. Biophys. Acta - Bioenerg. *1847*, 171–181.

Moullan, N., Mouchiroud, L., Wang, X., Ryu, D., Williams, E.G., Mottis, A., Jovaisaite, V., Frochaux, M.V., Quiros, P.M., Deplancke, B., et al. (2015). Tetracyclines Disturb Mitochondrial Function across Eukaryotic Models: A Call for Caution in Biomedical Research. Cell Rep. *10*, 1681–1691.

Murohara, T., Asahara, T., Silver, M., Bauters, C., Masuda, H., Kalka, C., Kearney, M., Chen, D., Symes, J.F., Fishman, M.C., et al. (1998). Nitric oxide synthase modulates angiogenesis in response to tissue ischemia. J. Clin. Invest. *101*, 2567–2578.

Murray, P.J., Allen, J.E., Biswas, S.K., Fisher, E.A., Gilroy, D.W., Goerdt, S., Gordon, S., Hamilton, J.A., Ivashkiv, L.B., Lawrence, T., et al. (2014). Macrophage Activation and Polarization: Nomenclature and Experimental Guidelines. Immunity *41*, 14–20.

Na, Y.R., Jung, D., Gu, G.J., and Seok, S.H. (2016). GM-CSF Grown Bone Marrow Derived Cells Are Composed of Phenotypically Different Dendritic Cells and Macrophages. Mol. Cells *39*, 734–741.

Nagatsu, T., Levitt, M., and Udenfriend, S. (1964). Conversion of L-tyrosine to 3,4-dihydroxyphenylalanine by cell-free preparations of brain and sympathetically innervated tissues. Biochem. Biophys. Res. Commun. *14*, 543–549.

Nakada, K., Inoue, K., Ono, T., Isobe, K., Ogura, A., Goto, Y.I., Nonaka, I., and Hayashi, J.I. (2001). Inter-mitochondrial complementation: Mitochondria-specific system preventing mice from expression of disease phenotypes by mutant mtDNA. Nat. Med. *7*, 934–940.

Nakamura, K., Bindokas, V.P., Kowlessur, D., Elas, M., Milstien, S., Marks, J.D., Halpern, H.J., and Kang, U.J. (2001). Tetrahydrobiopterin scavenges superoxide in dopaminergic neurons. J. Biol. Chem. *276*, 34402–34407.

Nakane, M., Schmidt, H.H., Pollock, J.S., Förstermann, U., and Murad, F. (1993). Cloned human brain nitric oxide synthase is highly expressed in skeletal muscle. FEBS Lett. *316*, 175–180.

Nakashima, Y., Raines, E.W., Plump, A.S., Breslow, J.L., and Ross, R. (1998). Upregulation of VCAM-1 and ICAM-1 at atherosclerosis-prone sites on the endothelium in the ApoE-deficient mouse. Arterioscler. Thromb. Vasc. Biol. *18*, 842–851.

Nakayama, D.K., Geller, D.A., Di Silvio, M., Bloomgarden, G., Davies, P., Pitt, B.R., Hatakeyama, K., Kagamiyama, H., Simmons, R.L., and Billiar, T.R. (1994). Tetrahydrobiopterin synthesis and inducible nitric oxide production in pulmonary artery smooth muscle. Am. J. Physiol. Cell. Mol. Physiol. *266*, L455–L460.

Nalls, M.A., Pankratz, N., Lill, C.M., Do, C.B., Hernandez, D.G., Saad, M., DeStefano, A.L., Kara, E., Bras, J., Sharma, M., et al. (2014). Large-scale meta-analysis of genome-wide association data identifies six new risk loci for Parkinson's disease. Nat. Genet. *46*, 989–993.

Nathan, C.F., Murray, H.W., Wiebe, M.E., and Rubin, B.Y. (1983). Identification of

interferon-gamma as the lymphokine that activates human macrophage oxidative metabolism and antimicrobial activity. J. Exp. Med. *158*, 670–689.

Naujoks, J., Tabeling, C., Dill, B.D., Hoffmann, C., Brown, A.S., Kunze, M., Kempa, S., Peter, A., Mollenkopf, H.-J., Dorhoi, A., et al. (2016). IFNs Modify the Proteome of Legionella-Containing Vacuoles and Restrict Infection Via IRG1-Derived Itaconic Acid. PLOS Pathog. *12*, e1005408.

Nichol, C.A., Lee, C.L., Edelstein, M.P., Chao, J.Y., and Duch, D.S. (1983). Biosynthesis of tetrahydrobiopterin by de novo and salvage pathways in adrenal medulla extracts, mammalian cell cultures, and rat brain in vivo. Proc. Natl. Acad. Sci. U. S. A. *80*, 1546–1550.

Nicholson, S., Bonecini-Almeida, M. da G., Lapa e Silva, J.R., Nathan, C., Xie, Q.W., Mumford, R., Weidner, J.R., Calaycay, J., Geng, J., Boechat, N., et al. (1996). Inducible nitric oxide synthase in pulmonary alveolar macrophages from patients with tuberculosis. J. Exp. Med. *183*, 2293–2302.

Nishikawa, T., Edelstein, D., Du, X.L., Yamagishi, S., Matsumura, T., Kaneda, Y., Yorek, M.A., Beebe, D., Oates, P.J., Hammes, H.-P., et al. (2000). Normalizing mitochondrial superoxide production blocks three pathways of hyperglycaemic damage. Nature *404*, 787–790.

Nishimura, S., Manabe, I., Nagasaki, M., Eto, K., Yamashita, H., Ohsugi, M., Otsu, M., Hara, K., Ueki, K., Sugiura, S., et al. (2009). CD8+ effector T cells contribute to macrophage recruitment and adipose tissue inflammation in obesity. Nat. Med. *15*, 914–920.

Obach, M., Navarro-Sabaté, À., Caro, J., Kong, X., Duran, J., Gómez, M., Perales, J.C., Ventura, F., Rosa, J.L., and Bartrons, R. (2004). 6-Phosphofructo-2-kinase (*pfkfb3*) Gene Promoter Contains Hypoxia-inducible Factor-1 Binding Sites Necessary for Transactivation in Response to Hypoxia. J. Biol. Chem. *279*, 53562–53570.

Odegaard, J.I., Ricardo-Gonzalez, R.R., Goforth, M.H., Morel, C.R., Subramanian, V., Mukundan, L., Eagle, A.R., Vats, D., Brombacher, F., Ferrante, A.W., et al. (2007). Macrophage-specific PPARγ controls alternative activation and improves insulin resistance. Nature *447*, 1116–1120.

Ohashi, A., Fukumuro, M., Sawabe, K., Mamada, K., Sugawara, Y., Matsuoka, H., and Hasegawa, H. (2009). Transcellular relocation of tetrahydrobiopterin across Caco-2 cells: A model study of tetrahydrobiopterin absorption through epithelial cells of intestinal mucosa. J. Inherit. Metab. Dis. *32*, 73–78.

Ohashi, A., Mamada, K., Harada, T., Naito, M., Takahashi, T., Aizawa, S., and Hasegawa, H. (2017). Organic anion transporters, OAT1 and OAT3, are crucial biopterin transporters involved in bodily distribution of tetrahydrobiopterin and exclusion of its excess. Mol. Cell. Biochem. *435*, 97–108.

Okazaki, T., Otani, H., Shimazu, T., Yoshioka, K., Fujita, M., Katano, T., Ito, S., and Iwasaka, T. (2011). Reversal of inducible nitric oxide synthase uncoupling unmasks tolerance to ischemia/reperfusion injury in the diabetic rat heart. J. Mol. Cell. Cardiol. *50*, 534–544.

Oldendorf, W.H., Cornford, M.E., and Brown, W.J. (1977). The large apparent work capability of the blood-brain barrier: A study of the mitochondrial content of capillary endothelial cells in brain and other tissues of the rat. Ann. Neurol. *1*, 409–417.

Ozaki, M., Kawashima, S., Yamashita, T., Hirase, T., Namiki, M., Inoue, N., Hirata, K., Yasui, H., Sakurai, H., Yoshida, Y., et al. (2002). Overexpression of endothelial nitric oxide synthase accelerates atherosclerotic lesion formation in apoE-deficient mice. J. Clin. Invest. *110*, 331–340.

Packer, M.A., Porteous, C.M., and Murphy, M.P. (1996). Superoxide production by mitochondria in the presence of nitric oxide forms peroxynitrite. Biochem. Mol. Biol. Int. *40*, 527–534.

Palmer, R.M., Ferrige, A.G., and Moncada, S. (1987). Nitric oxide release accounts for the biological activity of endothelium-derived relaxing factor. Nature *327*, 524–526.

Palsson-McDermott, E.M., Curtis, A.M., Goel, G., Lauterbach, M.A.R., Sheedy, F.J., Gleeson, L.E., van den Bosch, M.W.M., Quinn, S.R., Domingo-Fernandez, R., Johnston, D.G.W., et al. (2015). Pyruvate kinase M2 regulates Hif-1α activity and IL-1β induction and is a critical determinant of the warburg effect in LPS-activated macrophages. Cell Metab. *21*, 65–80.

Pardee, A.B. (1974). A restriction point for control of normal animal cell proliferation. Proc. Natl. Acad. Sci. U. S. A. *71*, 1286–1290.

Pelletier, J., Bellot, G., Gounon, P., Lacas-Gervais, S., Pouysségur, J., and Mazure, N.M. (2012). Glycogen Synthesis is Induced in Hypoxia by the Hypoxia-Inducible Factor and Promotes Cancer Cell Survival. Front. Oncol. *2*, 18.

Peralta, D., Bronowska, A.K., Morgan, B., Dóka, É., Van Laer, K., Nagy, P., Gräter, F., and Dick, T.P. (2015). A proton relay enhances H2O2 sensitivity of GAPDH to facilitate metabolic adaptation. Nat. Chem. Biol. *11*, 156–163.

Pescador, N., Villar, D., Cifuentes, D., Garcia-Rocha, M., Ortiz-Barahona, A., Vazquez, S., Ordoñez, A., Cuevas, Y., Saez-Morales, D., Garcia-Bermejo, M.L., et al. (2010). Hypoxia Promotes Glycogen Accumulation through Hypoxia Inducible Factor (HIF)-Mediated Induction of Glycogen Synthase 1. PLoS One *5*, e9644.

Pfleger, J., He, M., and Abdellatif, M. (2015). Mitochondrial complex II is a source of the reserve respiratory capacity that is regulated by metabolic sensors and promotes cell survival. Cell Death Dis. *6*, e1835.

Pirkmajer, S., and Chibalin, A. V. (2011). Serum starvation: caveat emptor. AJP Cell Physiol. *301*, C272–C279.

Plantinga, Y., Ghiadoni, L., Magagna, A., Giannarelli, C., Franzoni, F., Taddei, S., and Salvetti, A. (2007). Supplementation With Vitamins C and E Improves Arterial Stiffness and Endothelial Function in Essential Hypertensive Patients. Am. J. Hypertens. *20*, 392–397.

Prabhakar, P., Thatte, H.S., Goetz, R.M., Cho, M.R., Golan, D.E., and Michel, T. (1998). Receptor-regulated translocation of endothelial nitric-oxide synthase. J. Biol. Chem. *273*, 27383–27388.

Pritchard, K.A., Groszek, L., Smalley, D.M., Sessa, W.C., Wu, M., Villalon, P., Wolin, M.S., and Stemerman, M.B. (1995). Native low-density lipoprotein increases endothelial cell nitric oxide synthase generation of superoxide anion. Circ. Res. *77*, 510–518.

Pryde, K.R., and Hirst, J. (2011). Superoxide Is Produced by the Reduced Flavin in Mitochondrial Complex I. J. Biol. Chem. *286*, 18056–18065.

Quinn, M.T., Parthasarathy, S., Fong, L.G., and Steinberg, D. (1987). Oxidatively modified low density lipoproteins: a potential role in recruitment and retention of monocyte/macrophages during atherogenesis. Proc. Natl. Acad. Sci. U. S. A. *84*, 2995–2998.

Quintero, M., Colombo, S.L., Godfrey, A., and Moncada, S. (2006). Mitochondria as signaling organelles in the vascular endothelium. Proc. Natl. Acad. Sci. U. S. A. *103*, 5379–5384.

Radomski, M.W., Palmer, R.M.J., and Moncada, S. (1987). ENDOGENOUS NITRIC OXIDE INHIBITS HUMAN PLATELET ADHESION TO VASCULAR ENDOTHELIUM. Lancet *330*, 1057–1058.

Rahaman, S.O., Lennon, D.J., Febbraio, M., Podrez, E.A., Hazen, S.L., and Silverstein, R.L. (2006). A CD36-dependent signaling cascade is necessary for macrophage foam cell formation. Cell Metab. *4*, 211–221.

Raju, K., Doulias, P.-T., Evans, P., Krizman, E.N., Jackson, J.G., Horyn, O., Daikhin, Y., Nissim, I., Yudkoff, M., Nissim, I., et al. (2015). Regulation of brain glutamate metabolism by nitric oxide and S-nitrosylation. Sci. Signal. *8*, ra68-ra68.

Rapoport, R.M., Draznin, M.B., and Murad, F. (1983). Endothelium-dependent relaxation in rat aorta may be mediated through cyclic GMP-dependent protein phosphorylation. Nature *306*, 174–176.

Reiner, M., Bloch, W., and Addicks, K. (2001). Functional Interaction of Caveolin-1 and eNOS in Myocardial Capillary Endothelium Revealed by Immunoelectron Microscopy. J. Histochem. Cytochem. *49*, 1605–1609.

Rembold, H., and Buff, K. (1972a). Tetrahydrobiopterin, a cofactor in mitochondrial electron transfer. A soluble transfer system. Eur. J. Biochem. *28*, 586–591.

Rembold, H., and Buff, K. (1972b). Tetrahydrobiopterin, a cofactor in mitochondrial electron transfer. Effect of tetrahydropterins on intact rat-liver mitochondria. Eur. J. Biochem. *28*, 579–585.

Ribas, V., García-Ruiz, C., and Fernández-Checa, J.C. (2014). Glutathione and mitochondria. Front. Pharmacol. *5*, 151.

Riddle, S.R., Ahmad, A., Ahmad, S., Deeb, S.S., Malkki, M., Schneider, B.K., Allen, C.B., and White, C.W. (2000). Hypoxia induces hexokinase II gene expression in human lung cell line A549. Am. J. Physiol. Cell. Mol. Physiol. *278*, L407–L416.

Rizza, S., Cardaci, S., Montagna, C., Di Giacomo, G., De Zio, D., Bordi, M., Maiani, E., Campello, S., Borreca, A., Puca, A.A., et al. (2018). S -nitrosylation drives cell senescence and aging in mammals by controlling mitochondrial dynamics and mitophagy. Proc. Natl. Acad. Sci. *115*, 201722452.

Robb, E.L., Hall, A.R., Prime, T.A., Eaton, S., Szibor, M., Viscomi, C., James, A.M., and Murphy, M.P. (2018). Control of mitochondrial superoxide production by reverse electron transport at complex I. J. Biol. Chem. *293*, 9869–9879.

Robin, E.D., Murphy, B.J., and Theodore, J. (1984). Coordinate regulation of glycolysis by hypoxia in mammalian cells. J. Cell. Physiol. *118*, 287–290.

Robinson, K.M., Janes, M.S., Pehar, M., Monette, J.S., Ross, M.F., Hagen, T.M., Murphy, M.P., and Beckman, J.S. (2006). Selective fluorescent imaging of superoxide in vivo using

ethidium-based probes. Proc. Natl. Acad. Sci. U. S. A. *103*, 15038–15043.

Rossman, M.J., Santos-Parker, J.R., Steward, C.A.C., Bispham, N.Z., Cuevas, L.M., Rosenberg, H.L., Woodward, K.A., Chonchol, M., Gioscia-Ryan, R.A., Murphy, M.P., et al. (2018). Chronic Supplementation With a Mitochondrial Antioxidant (MitoQ) Improves Vascular Function in Healthy Older Adults. Hypertens. (Dallas, Tex. 1979) *71*, 1056–1063.

Sancak, Y., Peterson, T.R., Shaul, Y.D., Lindquist, R.A., Thoreen, C.C., Bar-Peled, L., and Sabatini, D.M. (2008). The rag GTPases bind raptor and mediate amino acid signaling to mTORC1. Science (80-.). *320*, 1496–1501.

Sánchez, F.A., Savalia, N.B., Durán, R.G., Lal, B.K., Boric, M.P., and Durán, W.N. (2006). Functional significance of differential eNOS translocation. Am. J. Physiol. Heart Circ. Physiol. *291*, H1058-64.

Sandau, K.B., Fandrey, J., and Brüne, B. (2001). Accumulation of HIF-1alpha under the influence of nitric oxide. Blood *97*, 1009–1015.

Sanlioglu, S., Williams, C.M., Samavati, L., Butler, N.S., Wang, G., McCray, P.B., Ritchie, T.C., Hunninghake, G.W., Zandi, E., and Engelhardt, J.F. (2001). Lipopolysaccharide Induces Rac1-dependent Reactive Oxygen Species Formation and Coordinates Tumor Necrosis Factor-α Secretion through IKK Regulation of NF-κB. J. Biol. Chem. *276*, 30188–30198.

Schafer, F.Q., and Buettner, G.R. (2001). Redox environment of the cell as viewed through the redox state of the glutathione disulfide/glutathione couple. Free Radic. Biol. Med. *30*, 1191–1212.

Van Schaftingen, E., Lederer, B., Bartrons, R., and Hers, H.G. (1982). A kinetic study of pyrophosphate: fructose-6-phosphate phosphotransferase from potato tubers. Application to a microassay of fructose 2,6-bisphosphate. Eur. J. Biochem. *129*, 191–195.

Schagger, H., and Pfeiffer, K. (2000). Supercomplexes in the respiratory chains of yeast and mammalian mitochondria. EMBO J. *19*, 1777–1783.

Scheitlin, C.G., Julian, J.A., Shanmughapriya, S., Madesh, M., Tsoukias, N.M., and Alevriadou, B.R. (2016). Endothelial mitochondria regulate the intracellular Ca 2+ response to fluid shear stress. Am. J. Physiol. - Cell Physiol. *310*, C479–C490.

Schmidt, T.S., and Alp, N.J. (2007). Mechanisms for the role of tetrahydrobiopterin in endothelial function and vascular disease. Clin. Sci. *113*, 47–63.

Schmidt, P.P., Lange, R., Gorren, A.C., Werner, E.R., Mayer, B., and Andersson, K.K. (2001). Formation of a protonated trihydrobiopterin radical cation in the first reaction cycle of neuronal and endothelial nitric oxide synthase detected by electron paramagnetic resonance spectroscopy. J. Biol. Inorg. Chem. *6*, 151–158.

Schneemann, M., and Schoedon, G. (2002). Species differences in macrophage NO production are important (multiple letters). Nat. Immunol. *3*, 102.

Schneemann, M., Schoedon, G., Hofer, S., Blau, N., Guerrero, L., and Schaffner, A. (1993). Nitric oxide synthase is not a constituent of the antimicrobian armature of human mononuclear phagocytes. J. Infect. Dis. *167*, 1358–1363.

Schoedon, G., Schneemann, M., Hofer, S., Guerrero, L., Blau, N., and Schaffner, A. (1993). Regulation of the L-arginine-dependent and tetrahydrobiopterin-dependent biosynthesis of nitric oxide in murine macrophages. Eur. J. Biochem. *213*, 833–839.

Schroder, K., Irvine, K.M., Taylor, M.S., Bokil, N.J., Le Cao, K.-A., Masterman, K.-A., Labzin, L.I., Semple, C.A., Kapetanovic, R., Fairbairn, L., et al. (2012). Conservation and divergence in Toll-like receptor 4-regulated gene expression in primary human versus mouse macrophages. Proc. Natl. Acad. Sci. U. S. A. *109*, E944-53.

Selak, M.A., Armour, S.M., MacKenzie, E.D., Boulahbel, H., Watson, D.G., Mansfield, K.D., Pan, Y., Simon, M.C., Thompson, C.B., and Gottlieb, E. (2005). Succinate links TCA cycle dysfunction to oncogenesis by inhibiting HIF-α prolyl hydroxylase. Cancer Cell *7*, 77–85.

Sethumadhavan, S., Whitsett, J., Bennett, B., Ionova, I.A., Pieper, G.M., and Vasquez-Vivar, J. (2016). Increasing tetrahydrobiopterin in cardiomyocytes adversely affects cardiac redox state and mitochondrial function independently of changes in NO production. Free Radic. Biol. Med. *93*, 1–11.

Shannon, P., Markiel, A., Ozier, O., Baliga, N.S., Wang, J.T., Ramage, D., Amin, N., Schwikowski, B., and Ideker, T. (2003). Cytoscape: A Software Environment for Integrated Models of Biomolecular Interaction Networks. Genome Res. *13*, 2498–2504.

Sharara, A.I., Perkins, D.J., Misukonis, M.A., Chan, S.U., Dominitz, J.A., and Weinberg, J.B. (1997). Interferon (IFN)-alpha activation of human blood mononuclear cells in vitro and in vivo for nitric oxide synthase (NOS) type 2 mRNA and protein expression: possible relationship of induced NOS2 to the anti-hepatitis C effects of IFN-alpha in vivo. J. Exp. Med. *186*, 1495–1502.

Shen, J., Luscinskas, F.W., Connolly, A., Dewey, C.F., and Gimbrone, M.A. (1992). Fluid shear stress modulates cytosolic free calcium in vascular endothelial cells. Am. J. Physiol. *262*, C384-90.

Shen, L., Li, H., Shi, Y., Wang, D., Gong, J., Xun, J., Zhou, S., Xiang, R., and Tan, X. (2016). M2 tumour-associated macrophages contribute to tumour progression via legumain remodelling the extracellular matrix in diffuse large B cell lymphoma. Sci. Rep. *6*, 30347.

Sheng, J., Ruedl, C., and Karjalainen, K. (2015). Most Tissue-Resident Macrophages Except Microglia Are Derived from Fetal Hematopoietic Stem Cells. Immunity *43*, 382–393.

Shenouda, S.M., Widlansky, M.E., Chen, K., Xu, G., Holbrook, M., Tabit, C.E., Hamburg, N.M., Frame, A.A., Caiano, T.L., Kluge, M.A., et al. (2011). Altered Mitochondrial Dynamics Contributes to Endothelial Dysfunction in Diabetes Mellitus. Circulation *124*, 444–453.

Sheta, E.A., McMillan, K., and Masters, B.S. (1994). Evidence for a bidomain structure of constitutive cerebellar nitric oxide synthase. J. Biol. Chem. *269*, 15147–15153.

Shimizu, H., Kiyohara, Y., Kato, I., Kitazono, T., Tanizaki, Y., Kubo, M., Ueno, H., Ibayashi, S., Fujishima, M., and Iida, M. (2004). Relationship Between Plasma Glutathione Levels and Cardiovascular Disease in a Defined Population: The Hisayama Study. Stroke *35*, 2072–2077.

Shimizu, S., Shiota, K., Yamamoto, S., Miyasaka, Y., Ishii, M., Watabe, T., Nishida, M., Mori, Y., Yamamoto, T., and Kiuchi, Y. (2003). Hydrogen peroxide stimulates tetrahydrobiopterin synthesis through the induction of GTP-cyclohydrolase I and increases nitric oxide synthase activity in vascular endothelial cells. Free Radic. Biol. Med. *34*, 1343–1352.

Shimizu, S., Ishibashi, M., Kumagai, S., Wajima, T., Hiroi, T., Kurihara, T., Ishii, M., and

Kiuchi, Y. (2013). Decreased cardiac mitochondrial tetrahydrobiopterin in a rat model of pressure overload. Int. J. Mol. Med. *31*, 589–596.

Shintaku, H., Fujioka, H., Sawada, Y., Asada, M., and Yamano, T. (2005). Plasma biopterin levels and tetrahydrobiopterin responsiveness. Mol. Genet. Metab. *86*, 104–106.

Singer, I., Kawka, D., Scott, S., Weidner, J., Mumford, R., Riehl, T., and Stenson, W. (1996). Expression of inducible nitric oxide synthase and nitrotyrosine in colonic epithelium in inflammatory bowel disease. Gastroenterology *111*, 871–885.

Skålén, K., Gustafsson, M., Rydberg, E.K., Hultén, L.M., Wiklund, O., Innerarity, T.L., and Borén, J. (2002). Subendothelial retention of atherogenic lipoproteins in early atherosclerosis. Nature *417*, 750–754.

Smirnova, E., Griparic, L., Shurland, D.L., and van der Bliek, A.M. (2001). Dynamin-related protein Drp1 is required for mitochondrial division in mammalian cells. Mol. Biol. Cell *12*, 2245–2256.

Smith, M.A., Richey Harris, P.L., Sayre, L.M., Beckman, J.S., and Perry, G. (1997). Widespread peroxynitrite-mediated damage in Alzheimer's disease. J. Neurosci. *17*, 2653–2657.

Smith, R.A.J., Porteous, C.M., Coulter, C. V, and Murphy, M.P. (1999). Selective targeting of an antioxidant to mitochondria. Eur. J. Biochem. *263*, 709–716.

Song, Z., Ghochani, M., McCaffery, J.M., Frey, T.G., and Chan, D.C. (2009). Mitofusins and OPA1 Mediate Sequential Steps in Mitochondrial Membrane Fusion. Mol. Biol. Cell *20*, 3525–3532.

Sorescu, D., Weiss, D., Lassègue, B., Clempus, R.E., Szöcs, K., Sorescu, G.P., Valppu, L., Quinn, M.T., Lambeth, J.D., Vega, J.D., et al. (2002). Superoxide production and expression of nox family proteins in human atherosclerosis. Circulation *105*, 1429–1435.

Sorgi, C.A., Rose, S., Court, N., Carlos, D., Paula-Silva, F.W.G., Assis, P.A., Frantz, F.G., Ryffel, B., Quesniaux, V., and Faccioli, L.H. (2012). GM-CSF Priming Drives Bone Marrow-Derived Macrophages to a Pro-Inflammatory Pattern and Downmodulates PGE2 in Response to TLR2 Ligands. PLoS One *7*, e40523.

Spahr, R., Krützfeldt, A., Mertens, S., Siegmund, B., and Piper, H.M. Fatty acids are not an important fuel for coronary microvascular endothelial cells. Mol. Cell. Biochem. *88*, 59–64.

Spratt, D.E., Taiakina, V., Palmer, M., and Guillemette, J.G. (2007). Differential Binding of Calmodulin Domains to Constitutive and Inducible Nitric Oxide Synthase Enzymes †. Biochemistry *46*, 8288–8300.

Spyrou, G., Enmark, E., Miranda-Vizuete, A., and Gustafsson, J. (1997). Cloning and expression of a novel mammalian thioredoxin. J. Biol. Chem. *272*, 2936–2941.

Stamler, J.S., Simon, D.I., Osborne, J.A., Mullins, M.E., Jaraki, O., Michel, T., Singel, D.J., and Loscalzo, J. (1992). S-nitrosylation of proteins with nitric oxide: synthesis and characterization of biologically active compounds. Proc. Natl. Acad. Sci. U. S. A. *89*, 444–448.

Stanley, E.R., and Heard, P.M. (1977). Factors regulating macrophage production and growth. Purification and some properties of the colony stimulating factor from medium conditioned by mouse L cells. J. Biol. Chem. *252*, 4305–4312.

Stanley, E.R., Chen, D.M., and Lin, H.S. (1978). Induction of macrophage production and proliferation by a purified colony stimulating factor [22]. Nature *274*, 168–170.

Starkov, A.A., Fiskum, G., Chinopoulos, C., Lorenzo, B.J., Browne, S.E., Patel, M.S., and Beal, M.F. (2004). Mitochondrial -Ketoglutarate Dehydrogenase Complex Generates Reactive Oxygen Species. J. Neurosci. *24*, 7779–7788.

Stein, M., Keshav, S., Harris, N., and Gordon, S. (1992). Interleukin 4 potently enhances murine macrophage mannose receptor activity: a marker of alternative immunologic macrophage activation. J. Exp. Med. *176*, 287–292.

Stroes, E., Kastelein, J., Cosentino, F., Erkelens, W., Wever, R., Koomans, H., Lüscher, T., and Rabelink, T. (1997). Tetrahydrobiopterin restores endothelial function in hypercholesterolemia. J. Clin. Invest. *99*, 41–46.

Stroes, E., Hijmering, M., van Zandvoort, M., Wever, R., Rabelink, T.J., and van Faassen, E.E. (1998). Origin of superoxide production by endothelial nitric oxide synthase. FEBS Lett. *438*, 161–164.

Stuehr, D.J., and Ikeda-Saito, M. (1992). Spectral characterization of brain and macrophage nitric oxide synthases. Cytochrome P-450-like hemeproteins that contain a flavin semiquinone radical. J. Biol. Chem. *267*, 20547–20550.

Stuehr, D.J., Gross, S.S., Sakuma, I., Levi, R., and Nathan, C.F. (1989). Activated murine macrophages secrete a metabolite of arginine with the bioactivity of endothelium-derived relaxing factor and the chemical reactivity of nitric oxide. J. Exp. Med. *169*, 1011–1020.

Sumbayev, V. V, Budde, A., Zhou, J., and Brüne, B. (2003). HIF-1 alpha protein as a target for S-nitrosation. FEBS Lett. *535*, 106–112.

Sundaresan, M., Yu, Z.X., Ferrans, V.J., Irani, K., and Finkel, T. (1995). Requirement for generation of H2O2 for platelet-derived growth factor signal transduction. Science *270*, 296–299.

Suzuki, H., Kurihara, Y., Takeya, M., Kamada, N., Kataoka, M., Jishage, K., Ueda, O., Sakaguchi, H., Higashi, T., Suzuki, T., et al. (1997). A role for macrophage scavenger receptors in atherosclerosis and susceptibility to infection. Nature *386*, 292–296.

Takaya, T., Hirata, K. -i., Yamashita, T., Shinohara, M., Sasaki, N., Inoue, N., Yada, T., Goto, M., Fukatsu, A., Hayashi, T., et al. (2007). A Specific Role for eNOS-Derived Reactive Oxygen Species in Atherosclerosis Progression. Arterioscler. Thromb. Vasc. Biol. *27*, 1632–1637.

Tallam, A., Perumal, T.M., Antony, P.M., Jäger, C., Fritz, J. V., Vallar, L., Balling, R., del Sol, A., and Michelucci, A. (2016). Gene Regulatory Network Inference of Immunoresponsive Gene 1 (IRG1) Identifies Interferon Regulatory Factor 1 (IRF1) as Its Transcriptional Regulator in Mammalian Macrophages. PLoS One *11*, e0149050.

Tannahill, G.M., Curtis, A.M., Adamik, J., Palsson-McDermott, E.M., McGettrick, A.F., Goel, G., Frezza, C., Bernard, N.J., Kelly, B., Foley, N.H., et al. (2013). Succinate is an inflammatory signal that induces IL-1β through HIF-1α. Nature *496*, 238–242.

Tay, Y.M.S., Lim, K.S., Sheu, F.-S., Jenner, A., Whiteman, M., Wong, K.P., and Halliwell, B. (2004). Do Mitochondria make Nitric Oxide? No? Free Radic. Res. *38*, 591–599.

Tayeh, M.A., and Marletta, M.A. (1989). Macrophage oxidation of L-arginine to nitric oxide, nitrite, and nitrate. Tetrahydrobiopterin is required as a cofactor. J. Biol. Chem. *264*,

19654–19658.

Taylor, B.S., de Vera, M.E., Ganster, R.W., Wang, Q., Shapiro, R.A., Morris, S.M., Billiar, T.R., and Geller, D.A. (1998). Multiple NF-kappaB enhancer elements regulate cytokine induction of the human inducible nitric oxide synthase gene. J. Biol. Chem. *273*, 15148–15156.

Thöny, B., Leimbacher, W., Blau, N., Harvie, A., and Heizmann, C.W. (1994). Hyperphenylalaninemia due to defects in tetrahydrobiopterin metabolism: molecular characterization of mutations in 6-pyruvoyl-tetrahydropterin synthase. Am. J. Hum. Genet. *54*, 782–792.

Tong, J.H., and Kaufman, S. (1975). Tryptophan hydroxylase. Purification and some properties of the enzyme from rabbit hindbrain. J. Biol. Chem. *250*, 4152–4158.

Tórtora, V., Quijano, C., Freeman, B., Radi, R., and Castro, L. (2007). Mitochondrial aconitase reaction with nitric oxide, S-nitrosoglutathione, and peroxynitrite: Mechanisms and relative contributions to aconitase inactivation. Free Radic. Biol. Med. *42*, 1075–1088.

Totzeck, M., Hendgen-Cotta, U.B., Luedike, P., Berenbrink, M., Klare, J.P., Steinhoff, H.-J., Semmler, D., Shiva, S., Williams, D., Kipar, A., et al. (2012). Nitrite Regulates Hypoxic Vasodilation via Myoglobin-Dependent Nitric Oxide Generation. Circulation *126*, 325–334.

Turnbull, I.R., Gilfillan, S., Cella, M., Aoshi, T., Miller, M., Piccio, L., Hernandez, M., and Colonna, M. (2006). Cutting edge: TREM-2 attenuates macrophage activation. J. Immunol. *177*, 3520–3524.

Turrens, J.F., Alexandre, A., and Lehninger, A.L. (1985). Ubisemiquinone is the electron donor for superoxide formation by complex III of heart mitochondria. Arch. Biochem. Biophys. *237*, 408–414.

Twig, G., Elorza, A., Molina, A.J.A., Mohamed, H., Wikstrom, J.D., Walzer, G., Stiles, L., Haigh, S.E., Katz, S., Las, G., et al. (2008). Fission and selective fusion govern mitochondrial segregation and elimination by autophagy. EMBO J. *27*, 433–446.

Valdez, L.B., Zaobornyj, T., Alvarez, S., Bustamante, J., Costa, L.E., and Boveris, A. (2004). Heart mitochondrial nitric oxide synthase. Effects of hypoxia and aging. Mol. Aspects Med. *25*, 49–59.

Van den Bossche, J., Baardman, J., Otto, N.A., van der Velden, S., Neele, A.E., van den Berg, S.M., Luque-Martin, R., Chen, H.-J., Boshuizen, M.C.S., Ahmed, M., et al. (2016). Mitochondrial Dysfunction Prevents Repolarization of Inflammatory Macrophages. Cell Rep. *17*, 684–696.

van der Windt, G.J.W., Everts, B., Chang, C.-H., Curtis, J.D., Freitas, T.C., Amiel, E., Pearce, E.J., and Pearce, E.L. (2012). Mitochondrial Respiratory Capacity Is a Critical Regulator of CD8+ T Cell Memory Development. Immunity *36*, 68–78.

Vásquez-Vivar, J., Kalyanaraman, B., Martásek, P., Hogg, N., Masters, B.S., Karoui, H., Tordo, P., and Pritchard, K.A. (1998). Superoxide generation by endothelial nitric oxide synthase: the influence of cofactors. Proc. Natl. Acad. Sci. U. S. A. *95*, 9220–9225.

Vásquez-Vivar, J., Whitsett, J., Martásek, P., Hogg, N., and Kalyanaraman, B. (2001). Reaction of tetrahydrobiopterin with superoxide: EPR-kinetic analysis and characterization of the pteridine radical. Free Radic. Biol. Med. *31*, 975–985.

Vásquez-Vivar, J., Martásek, P., Whitsett, J., Joseph, J., and Kalyanaraman, B. (2002). The

ratio between tetrahydrobiopterin and oxidized tetrahydrobiopterin analogues controls superoxide release from endothelial nitric oxide synthase: an EPR spin trapping study. Biochem. J. *362*, 733–739.

Vats, D., Mukundan, L., Odegaard, J.I., Zhang, L., Smith, K.L., Morel, C.R., Greaves, D.R., Murray, P.J., Chawla, A., and Chawla, A. (2006). Oxidative metabolism and PGC-1β attenuate macrophage-mediated inflammation. Cell Metab. *4*, 13–24.

Vazquez-Torres, A., Jones-Carson, J., Mastroeni, P., Ischiropoulos, H., and Fang, F.C. (2000). Antimicrobial Actions of the Nadph Phagocyte Oxidase and Inducible Nitric Oxide Synthase in Experimental Salmonellosis. I. Effects on Microbial Killing by Activated Peritoneal Macrophages in Vitro. J. Exp. Med. *192*, 227–236.

Vexler, Z.S., Wong, A., Francisco, C., Manabat, C., Christen, S., Täuber, M., Ferriero, D.M., and Gregory, G. (2003). Fructose-1,6-bisphosphate preserves intracellular glutathione and protects cortical neurons against oxidative stress. Brain Res. *960*, 90–98.

Villalta, F., Zhang, Y., Bibb, K.E., Kappes, J.C., and Lima, M.F. (1998). The cysteine-cysteine family of chemokines RANTES, MIP-1alpha, and MIP-1beta induce trypanocidal activity in human macrophages via nitric oxide. Infect. Immun. *66*, 4690–4695.

Vivekananthan, D.P., Penn, M.S., Sapp, S.K., Hsu, A., and Topol, E.J. (2003). Use of antioxidant vitamins for the prevention of cardiovascular disease: meta-analysis of randomised trials. Lancet (London, England) *361*, 2017–2023.

Vouldoukis, I., Riveros-Moreno, V., Dugas, B., Ouaaz, F., Bécherel, P., Debré, P., Moncada, S., and Mossalayi, M.D. (1995). The killing of Leishmania major by human macrophages is mediated by nitric oxide induced after ligation of the Fc epsilon RII/CD23 surface antigen. Proc. Natl. Acad. Sci. U. S. A. *92*, 7804–7808.

Wang, D.B., Garden, G.A., Kinoshita, C., Wyles, C., Babazadeh, N., Sopher, B., Kinoshita, Y., and Morrison, R.S. (2013). Declines in Drp1 and parkin expression underlie DNA damage-induced changes in mitochondrial length and neuronal death. J. Neurosci. *33*, 1357–1365.

Wang, T., Liu, H., Lian, G., Zhang, S.-Y., Wang, X., and Jiang, C. (2017). HIF1α-Induced Glycolysis Metabolism Is Essential to the Activation of Inflammatory Macrophages. Mediators Inflamm. *2017*, 9029327.

Warren, M.K., and Vogel, S.N. (1985). Bone marrow-derived macrophages: development and regulation of differentiation markers by colony-stimulating factor and interferons. J. Immunol. *134*, 982–989.

Watschinger, K., Keller, M.A., Golderer, G., Hermann, M., Maglione, M., Sarg, B., Lindner, H.H., Hermetter, A., Werner-Felmayer, G., Konrat, R., et al. (2010). Identification of the gene encoding alkylglycerol monooxygenase defines a third class of tetrahydrobiopterin-dependent enzymes. Proc. Natl. Acad. Sci. U. S. A. *107*, 13672–13677.

Webb, A., Bond, R., McLean, P., Uppal, R., Benjamin, N., and Ahluwalia, A. (2004). Reduction of nitrite to nitric oxide during ischemia protects against myocardial ischemia-reperfusion damage. Proc. Natl. Acad. Sci. *101*, 13683–13688.

Webb, A.J., Patel, N., Loukogeorgakis, S., Okorie, M., Aboud, Z., Misra, S., Rashid, R., Miall, P., Deanfield, J., Benjamin, N., et al. (2008). Acute Blood Pressure Lowering, Vasoprotective, and Antiplatelet Properties of Dietary Nitrate via Bioconversion to Nitrite. Hypertension *51*, 784–790.

Wei, C.-C., Wang, Z.-Q., Hemann, C., Hille, R., and Stuehr, D.J. (2003). A Tetrahydrobiopterin Radical Forms and then Becomes Reduced during *N* ω - Hydroxyarginine Oxidation by Nitric-oxide Synthase. J. Biol. Chem. *278*, 46668–46673.

Wei, X., Charles, I.G., Smith, A., Ure, J., Feng, G., Huang, F., Xu, D., Mullers, W., Moncada, S., and Liew, F.Y. (1995). Altered immune responses in mice lacking inducible nitric oxide synthase. Nature *375*, 408–411.

Weinberg, J.B., Misukonis, M.A., Shami, P.J., Mason, S.N., Sauls, D.L., Dittman, W.A., Wood, E.R., Smith, G.K., McDonald, B., and Bachus, K.E. (1995). Human mononuclear phagocyte inducible nitric oxide synthase (iNOS): analysis of iNOS mRNA, iNOS protein, biopterin, and nitric oxide production by blood monocytes and peritoneal macrophages. Blood *86*, 1184–1195.

Weisiger, R.A., and Fridovich, I. (1973). Superoxide dismutase. Organelle specificity. J. Biol. Chem. *248*, 3582–3592.

Werner, E.R., Werner-Felmayer, G., Fuchs, D., Hausen, A., Reibnegger, G., and Wachter, H. (1989). Parallel induction of tetrahydrobiopterin biosynthesis and indoleamine 2,3-dioxygenase activity in human cells and cell lines by interferon-gamma. Biochem. J. *262*, 861–866.

West, A.P., Brodsky, I.E., Rahner, C., Woo, D.K., Erdjument-Bromage, H., Tempst, P., Walsh, M.C., Choi, Y., Shadel, G.S., and Ghosh, S. (2011). TLR signalling augments macrophage bactericidal activity through mitochondrial ROS. Nature *472*, 476–480.

Widder, J.D., Chen, W., Li, L., Dikalov, S., Thony, B., Hatakeyama, K., and Harrison, D.G. (2007). Regulation of Tetrahydrobiopterin Biosynthesis by Shear Stress. Circ. Res. *101*, 830–838.

Wiktor-Jedrzejczak, W., Bartocci, A., Ferrante, A.W., Ahmed-Ansari, A., Sell, K.W., Pollard, J.W., and Stanley, E.R. (1990). Total absence of colony-stimulating factor 1 in the macrophage-deficient osteopetrotic (op/op) mouse. Proc. Natl. Acad. Sci. U. S. A. *87*, 4828–4832.

Williams, R.L., Courtneidge, S.A., and Wagner, E.F. (1988). Embryonic lethalities and endothelial tumors in chimeric mice expressing polyoma virus middle T oncogene. Cell *52*, 121–131.

Williamson, D.H., Lund, P., and Krebs, H.A. (1967). The redox state of free nicotinamide-adenine dinucleotide in the cytoplasm and mitochondria of rat liver. Biochem. J. *103*, 514–527.

Wilson, K.T., Fu, S., Ramanujam, K.S., and Meltzer, S.J. (1998). Increased expression of inducible nitric oxide synthase and cyclooxygenase-2 in Barrett's esophagus and associated adenocarcinomas. Cancer Res. *58*, 2929–2934.

Wolhuter, K., Whitwell, H.J., Switzer, C.H., Burgoyne, J.R., Timms, J.F., and Eaton, P. (2018). Evidence against Stable Protein S-Nitrosylation as a Widespread Mechanism of Post-translational Regulation. Mol. Cell *69*, 438–450.e5.

Xia, Y., and Zweier, J.L. (1997). Superoxide and peroxynitrite generation from inducible nitric oxide synthase in macrophages. Proc. Natl. Acad. Sci. *94*, 6954–6958.

Xia, Y., Roman, L.J., Masters, B.S.S., and Zweier, J.L. (1998). Inducible nitric-oxide synthase generates superoxide from the reductase domain. J. Biol. Chem. *273*, 22635–22639.

Xie, Q.W., Kashiwabara, Y., and Nathan, C. (1994). Role of transcription factor NF-kappa B/Rel in induction of nitric oxide synthase. J. Biol. Chem. *269*, 4705–4708.

Xu, H., Barnes, G.T., Yang, Q., Tan, G., Yang, D., Chou, C.J., Sole, J., Nichols, A., Ross, J.S., Tartaglia, L.A., et al. (2003). Chronic inflammation in fat plays a crucial role in the development of obesity-related insulin resistance. J. Clin. Invest. *112*, 1821–1830.

Xu, L., Eu, J.P., Meissner, G., and Stamler, J.S. (1998). Activation of the cardiac calcium release channel (ryanodine receptor) by poly-S-nitrosylation. Science *279*, 234–237.

Xue, J., Schmidt, S.V., Sander, J., Draffehn, A., Krebs, W., Quester, I., De Nardo, D., Gohel, T.D., Emde, M., Schmidleithner, L., et al. (2014). Transcriptome-Based Network Analysis Reveals a Spectrum Model of Human Macrophage Activation. Immunity *40*, 274–288.

Yang, E.S., Richter, C., Chun, J.-S., Huh, T.-L., Kang, S.-S., and Park, J.-W. (2002). Inactivation of NADP(+)-dependent isocitrate dehydrogenase by nitric oxide. Free Radic. Biol. Med. *33*, 927–937.

Ye, Y., Li, J., and Yuan, Z. (2013). Effect of Antioxidant Vitamin Supplementation on Cardiovascular Outcomes: A Meta-Analysis of Randomized Controlled Trials. PLoS One *8*, e56803.

Yona, S., Kim, K.-W., Wolf, Y., Mildner, A., Varol, D., Breker, M., Strauss-Ayali, D., Viukov, S., Guilliams, M., Misharin, A., et al. (2013). Fate mapping reveals origins and dynamics of monocytes and tissue macrophages under homeostasis. Immunity *38*, 79–91.

Zemojtel, T., Kolanczyk, M., Kossler, N., Stricker, S., Lurz, R., Mikula, I., Duchniewicz, M., Schuelke, M., Ghafourifar, P., Martasek, P., et al. (2006). Mammalian mitochondrial nitric oxide synthase: Characterization of a novel candidate. FEBS Lett. *580*, 455–462.

Zhang, H., Luo, Y., Zhang, W., He, Y., Dai, S., Zhang, R., Huang, Y., Bernatchez, P., Giordano, F.J., Shadel, G., et al. (2007a). Endothelial-Specific Expression of Mitochondrial Thioredoxin Improves Endothelial Cell Function and Reduces Atherosclerotic Lesions. Am. J. Pathol. *170*, 1108–1120.

Zhang, P., Xu, X., Hu, X., Van Deel, E.D., Zhu, G., and Chen, Y. (2007b). Inducible nitric oxide synthase deficiency protects the heart from systolic overload-induced ventricular hypertrophy and congestive heart failure. Circ. Res. *100*, 1089–1098.

Zhao, H., Kalivendi, S., Zhang, H., Joseph, J., Nithipatikom, K., Vásquez-Vivar, J., and Kalyanaraman, B. (2003). Superoxide reacts with hydroethidine but forms a fluorescent product that is distinctly different from ethidium: potential implications in intracellular fluorescence detection of superoxide. Free Radic. Biol. Med. *34*, 1359–1368.

Zhao, H., Joseph, J., Fales, H.M., Sokoloski, E.A., Levine, R.L., Vasquez-Vivar, J., and Kalyanaraman, B. (2005). Detection and characterization of the product of hydroethidine and intracellular superoxide by HPLC and limitations of fluorescence. Proc. Natl. Acad. Sci. U. S. A. *102*, 5727–5732.

Zhao, Y., Cao, J., Chen, Y.-S., Zhu, Y., Patrick, C., Chien, B., Cheng, A., and Foehr, E.D. (2009). Detection of tetrahydrobiopterin by LC–MS/MS in plasma from multiple species. Bioanalysis *1*, 895–903.

Zielonka, J., and Kalyanaraman, B. (2010). Hydroethidine- and MitoSOX-derived red fluorescence is not a reliable indicator of intracellular superoxide formation: another inconvenient truth. Free Radic. Biol. Med. *48*, 983–1001.

Zielonka, J., Vasquez-Vivar, J., and Kalyanaraman, B. (2008). Detection of 2-hydroxyethidium in cellular systems: a unique marker product of superoxide and hydroethidine. Nat. Protoc. *3*, 8–21.

Zweier, J.L., Wang, P., Samouilov, A., and Kuppusamy, P. (1995). Enzyme-independent formation of nitric oxide in biological tissues. Nat. Med. *1*, 804–809.

Appendices

Appendices

Timing and Venue of Research

The work described in this thesis was carried out between October 2014 and September 2018 in the laboratories of Prof Keith Channon and Dr Mark Crabtree situated in the British Heart Foundation (BHF) Molecular Cardiology and Functional Genetics Facility, Division of Cardiovascular Medicine, Radcliffe Department of Medicine, Wellcome Trust Centre for Human Genetics, University of Oxford, UK. Proteomics analysis were carried out in the laboratory of Prof Benedikt Kessler situated in the Target Discovery Institute, Nuffield Department of Medicine, NDM Research Building, University of Oxford, UK.

Research Funding

The author was funded by a BHF non-clinical PhD studentship as part of the 4-year PhD programme. The laboratory of Keith Channon was supported by a programme grant from the BHF and the laboratory of Dr Mark Crabtree was supported by an Intermediate BHF Fellowship awarded to Dr Crabtree.

Publications Arising Directly from this Thesis

Bailey, J., Shaw, A., McNeill, E., Diotallevi, M., Nicol, T., Chuaiphichai, S., Hale, A., Davis, S., Fischer, R., Kessler, B.M., McCullagh, J., Channon, K.M., and Crabtree, M.J. (2018) Nitric oxide modulates metabolic remodelling in inflammatory macrophages through TCA cycle regulation and itaconate accumulation (*Cell Rep.* Currently in review)

Bailey, J., Shaw, A., Fischer, R., Ryan, B.J., Kessler, B.M., McCullagh, J., Wade-Martins, R., Channon, K.M., and Crabtree, M.J. (2017). A novel role for endothelial tetrahydrobiopterin in mitochondrial redox balance. *Free Radic. Biol. Med.* 104, 214–225.

Other Publications

Bailey, J. D., Davis, S., Shaw, A., Fischer, R., Benson, M., Zhu, H., Brown, J., Bhattacharya, S., Kessler, B. M., Channon, K. M., Crabtree, M. J. (2018) Tetrahydrobiopterin modulates ubiquitin conjugation to UBC13/UBE2N and proteasome activity by S-nitrosation. *Sci. Rep. 8*, 14310

Presentations at International Meetings

Bailey, J., Shaw, A., McNeill, E., Hale, A., McCullagh, J., Channon, K.M., and Crabtree, M.J. A role for tetrahydrobiopterin in macrophage mitochondrial bioenergetics and redox signalling. *Gordon Research Conference on Biology and Pathobiology of Oxygen Radicals from Cell Signalling and Detection to Therapy in Ventura, USA,* February 2018 (Poster presentation)

Bailey, J., Shaw, A., Fischer, R., Ryan, B.J., Kessler, B.M., McCullagh, J., Wade-Martins, R., Channon, K.M., and Crabtree, M.J. BH_4-deficiency induced changes in endothelial cell NO-redox balance reveals a novel role for BH_4 in the mitochondria. *The Royal Society Meeting: Chemical Biology Approaches to Assesing and Modulating Mitochondria, Buckinghamshire, UK,* September 2016 (Poster presentation)

Bailey, J., Shaw, A., Fischer, R., Ryan, B.J., Kessler, B.M., McCullagh, J., Wade-Martins, R., Channon, K.M., and Crabtree, M.J. BH_4-deficiency induced changes in endothelial cell NO-redox balance reveals a novel role for BH_4 in the mitochondria. *9th International Conference on the Biology, Chemistry, and Therapeutic Applications of Nitric Oxide in Sendai, Japan,* May 2016 (Oral presentation)

Acknowledgements

Firstly, I would like to thank my supervisors Dr Mark Crabtree and Prof Keith Channon for giving me the opportunity to carry out my DPhil research within their groups and for their mentorship. I am especially grateful to Mark for his unwavering optimism and support throughout my time in the laboratory.

I would also like to thank Prof Benedikt Kessler and Dr Roman Fischer for allowing me to spend my rotation within their laboratory in the Proteomics Facility, along with Mr Simon Davis for all of his help and running my samples on their mass spectrometer.

My DPhil wouldn't have been possible without the support of the entire Channon/Crabtree group to whom I am extremely grateful. In particular, Andrew Shaw was a pleasure to work with during his time in the Crabtree group and has provided invaluable encouragement, wisdom and support. I would also like to thank Ashley Hale for his help with so many aspects of laboratory and animal experiments, as well as Surawee Chuaiphichai for assistance collecting bones for BMDM experiments and being my desk mate for the past few years. Thank you to Eileen McNeill for advice during the macrophage work, Jyoti Patel for her assistance with the FACS experiment, and Marina Diotallevi and Thomas Nicol for helping me through those final experiments. And a special thank you to all Channon/Crabtree members for making my experience in the lab so enjoyable!

I would like to highlight the funding that I have received from the BHF to support my studies and the generous travel grants from Jesus College.

Finally, I would like to thank my family and friends for supporting my studies. Especially my parents and Zobair Arya.